

The John A. Blume Earthquake Engineering Center

Department of Civil Engineering
Stanford University

MODEL TESTS ON EARTHQUAKE SIMULATORS DEVELOPMENT AND IMPLEMENTATION OF EXPERIMENTAL PROCEDURES



by

**Russell S. Mills
Helmut Krawinkler
James M. Gere**

A report on a research
project sponsored by the
National Science Foundation
Grants ENV75-20036 and ENV77-14444

Report No. 39
June 1979

The John A. Blume Earthquake Engineering Center was established to promote research and education in earthquake engineering. Through its activities our understanding of earthquakes and their effects on mankind's facilities and structures is improving. The Center conducts research, provides instruction, publishes reports and articles, conducts seminars and conferences, and provides financial support for students. The Center is named for Dr. John A. Blume, a well-known consulting engineer and Stanford alumnus.

Address

The John A. Blume Earthquake Engineering Center
Department of Civil Engineering
Stanford University
Stanford, California 94305

MODEL TESTS ON EARTHQUAKE SIMULATORS -- DEVELOPMENT
AND IMPLEMENTATION OF EXPERIMENTAL PROCEDURES

by

Russell S. Mills

Helmut Krawinkler

James M. Gere

The John A. Blume Earthquake Engineering Center
Department of Civil Engineering
Stanford University
Stanford, California 94305

A Report on a Research Project Sponsored by the
NATIONAL SCIENCE FOUNDATION
Grants ENV75-20036 and ENV77-14444

June 1979

ABSTRACT

For problems which involve complex structures with material and/or geometric non-linear behavior, such as are encountered in earthquake engineering, the practical capabilities of mathematical methods of analysis may be surpassed. In such cases, experimental analysis may serve as an alternative and as a means of extending the limits of theoretical knowledge.

Essential to accurate experimentation in earthquake engineering is an adequate dynamic test facility consisting of suitable excitation sources (e.g., an earthquake simulator), instrumentation and a minicomputer system for signal generation, data acquisition and data reduction. Due to size constraints, testing of complete structures in the laboratory will often be limited to small-scale models. The necessary capabilities of a test system for dynamic model studies is discussed and illustrated by reference to the facilities at the John A. Blume Earthquake Engineering Center at Stanford University.

An actual model test serves to illustrate the accuracy of replica modeling, to assist in the development of testing methodologies and to evaluate the adequacy of a dynamic test facility. In order to develop confidence in the ability of a small-scale model to replicate structural response to earthquakes it was desirable to have a well-defined prototype with documented dynamic properties for correlation of model response. Thus, a three-story, single bay steel frame structure previously tested on the shake table at the University of California, Berkeley was used as a prototype for a 1:6 scale model study.

The primary task in the development of a replica model is to simulate all aspects of the prototype structural system which may contribute to the earthquake response characteristics. One modeling method which is applicable to a great number of building structures where gravity effects must be included is artificial mass simulation. Such modeling involves the addition of structurally uncoupled mass to augment the density of the model structure, permitting the choice of a model structural material without regard for mass density scaling.

The model wide-flange sections were machined from A36 steel bar stock and primary structural connections were fully welded, utilizing the TIG heliarc process. Subsequent heat treatment of the finished model frames was performed to relieve high initial stresses and to satisfy construction tolerances which were derived from geometric scaling of standard tolerances for building structures.

A comprehensive test study, encompassing material, subassembly and earthquake simulator tests, was performed to enable an accurate comparison of model and prototype response. Earthquake simulator tests utilized the El Centro 1940 North-South component and an artificial earthquake composed of discrete spectral components to excite the structure both elastically and inelastically.

The results of the model test series are discussed in detail. Accurate simulation of the prototype structure in terms of global and local response parameters was achieved. The nature of prototype inelastic response was duplicated by the small-scale model as characterized by yielding of the joint panel zones in shear and by comparison of the ductility demand and energy distribution of the respective structures. Observed minor discrepancies in model-prototype correlation can be explained by the larger weld sizes of the model and by the influence of earthquake simulator reproduction capabilities on test structure response.

ACKNOWLEDGEMENTS

The research reported herein is part of the project "Scale Modeling and Testing of Structures for Reproducing Response to Earthquake Excitation" conducted under the sponsorship of the National Science Foundation. The authors are grateful for the financial support of NSF which made this project possible. The continued encouragement of Dr. S. C. Liu of NSF is especially acknowledged.

As the research extended over a period of several years, a number of people, including the laboratory staff and several graduate students of the John A. Blume Earthquake Engineering Center, have participated and made significant contributions. Especially the help of Professors Holt Ashley and Cedric W. Richards and of the graduate students Gregory P. Luth and Piotr D. Moncarz is gratefully acknowledged.

The use of experimental and computer facilities was provided by the John A. Blume Earthquake Engineering Center, Professors James M. Gere and Haresh C. Shah, Directors. Mr. Roy Stephen of the University of California kindly arranged for the use of data files containing information on the dynamic response of the prototype test structure.

TABLE OF CONTENTS

	Acknowledgment	iii
	Table of Contents	iv
	List of Tables	vi
	List of Illustrations	vii
Chapter 1	INTRODUCTION	1
Chapter 2	OBJECTIVES AND SCOPE	7
Chapter 3	EXPERIMENTAL FACILITIES FOR DYNAMIC MODEL STUDIES ..	9
3.1	General Discussion	9
3.2	Earthquake Simulation by Means of Shake Tables	14
3.2.1	Design and Performance Requirements for Shake Tables	14
3.2.2	Generation of Input Motion	23
3.2.3	Measures of Shake Table Performance	27
3.3	Material and Component Test System	43
3.3.1	Performance Requirements	43
3.3.2	Input Command Signal	44
3.4	Instrumentation	46
3.5	Data Acquisition	52
3.6	Data Reduction	64
Chapter 4	MODELS OF STEEL-FRAME STRUCTURES UTILIZING ARTIFICIAL MASS SIMULATION	67
4.1	General Discussion	67
4.2	Case Study -- Prototype and Model	71
4.2.1	Prototype Structure	71
4.2.2	Model Structure	74
4.3	Model Fabrication Techniques	79
4.3.1	Element Fabrication	80
4.3.2	Element Connection	82
4.3.3	AMS Model Fabrication	84

TABLE OF CONTENTS (Continued)

4.4	Material and Component Tests	90
4.4.1	Objectives	90
4.4.2	Material Tests	90
4.4.3	Component Tests	94
4.5	Earthquake Simulator Tests	100
4.5.1	Objectives	100
4.5.2	Instrumentation and Data Acquisition	101
4.5.3	Parameters for Correlation of Model and Prototype Response	105
4.5.4	Testing History	111
4.5.5	Evaluation of Preliminary Tests	114
4.5.6	Evaluation of Earthquake Simulator Tests ...	116
4.5.7	Summary -- Model vs. Prototype Response	127
Chapter 5	SUMMARY AND CONCLUSIONS	245
References	252
Appendix A	NUMERICAL METHODS	256
A.1	Interpolation	256
A.2	Integration and Differentiation	257
A.3	Smoothing	259
A.4	Examples	259
Appendix B	COMPUTER PROGRAMS RELATED TO THE JABEEC TEST SYSTEM	270

LIST OF TABLES

3.1	Methods for Supporting Shake Tables	17
3.2	Earthquake Simulator -- Performance Requirements	24
3.3	Computer System Test Schedule	63
4.1	Modeling Laws for Artificial Mass Simulation	131
4.2	Prototype Section Properties	132
4.3	Prototype Estimated Weights	132
4.4	AMS Model Scaling Requirements	133
4.5	Tolerances for Trial Model Elements, $\lambda_r = 1:6$	133
4.6	Machined Sections for AMS Model, $\lambda_r = 1:6$	134
4.7	Material Properties -- Prototype and Model Coupons	135
4.8	Nominal Material Properties	136
4.9	Model Elements as Force Transducers	137
4.10	AMS Model Instrumentation	138
4.11	Prototype - Model Comparative Data Channels	139
4.12	AMS Model Test Files	140
4.13	AMS Model -- Base Welding and Dead Load Application	142
4.14	Dynamic Properties -- Free and Forced Vibration Tests	142
4.15	Prototype and Model Peak Values	143
A.1	Interpolation Example	260

LIST OF ILLUSTRATIONS

1.1	Application of Various Methods of Structural Analysis ...	3
3.1	Block Diagram of Dynamic Testing System at Stanford	13
3.2	Classification of Shake Tables	15
3.3	Shake Table Performance Spectrum--Stanford Shake Table ..	20
3.4	Maximum Base Shear	22
3.5	Shake Table Sensitivity	29
3.6	Shake Table Amplitude Envelope	30
3.7	Shake Table Rotational Modes	30
3.8	Sine Wave Performance	31
3.9	Displacement Response Performance--Stanford Shake Table .	34
3.10	Acceleration Response Performance--Stanford Shake Table .	35
3.11	Displacement Response Spectra from Displacement Records-- Stanford Shake Table	38
3.12	Tripartite Response Spectra--Stanford Shake Table	39
3.13	Response Spectra from Acceleration Records--Stanford Shake Table (1:5 Scale True Replica Model)	40
3.14	Response Spectra from Acceleration Records--Stanford Shake Table (1:10 Scale True Replica Model)	41
3.15	Silastic Mercury Gage	53
3.16	Dump Time vs. Block Size	58
3.17	Minimum Block Size for Uninterrupted Data Transfer	59
3.18	Basic Data Reduction Package	66
4.1	Prototype Structure at U. C., Berkeley	144
4.2	Plans and Elevations of the Prototype Structure	145
4.3	Prototype Girder-to-Column Connection	146
4.4	Prototype Primary Beam-to-Column Connection	147

LIST OF ILLUSTRATIONS (Continued)

4.5	Prototype Secondary Beam-to-Girder Connection	147
4.6	Prototype Column Base Plate	148
4.7	Prototype Floor Weight Support Mechanism	148
4.8	Plans and Elevations of the Model Structure	149
4.9	Model Girder-to-Column Connection	150
4.10	Model Primary Beam-to-Column Connection	151
4.11	Model Secondary Beam-to-Girder Connection	151
4.12	Model Column Base Plate	152
4.13	Heliarc Welding Process	153
4.14	Model Element Specifications	154
4.15	Machined Model Elements	154
4.16	Model Frame Welding Procedure	155
4.17	Girder-to-Column Connection Before Heat Treatment	156
4.18	Model Frame Instability	156
4.19	AMS Model Structure	157
4.20	Visual Comparison--Prototype and Model	159
4.21	Model Material Tests--Column Base Material vs. Flange Coupon	161
4.22	Model Material Tests--Column Flange vs. Girder Flange Coupons	161
4.23	Model Material Tests--Column Base Material vs. Strain Rate	162
4.24	AMS Model Subassembly Tests	162
4.25	AMS Model Subassembly--Instrumentation (Typ.)	163
4.26	Model Subassembly--Girder Tip Load vs. Deflection	164
4.27	Model Subassembly--Girder End Moment vs. Panel Strain ...	165

LIST OF ILLUSTRATIONS (Continued)

4.28	Subassembly Tests--Girder Tip Load vs. Deflection	166
4.29	Subassembly Tests--Girder End Moment vs. Panel Strain ...	166
4.30	Subassembly Tests--Girder End Moment vs. Panel Shear Distortion	167
4.31	AMS Model Instrumentation--Plan	168
4.32	AMS Model Instrumentation	169
4.33	Panel Zone Distortion Measurement	171
4.34	Prototype and Model Mode Shapes	172
4.35	Model Inelastic El Centro Tests--45 ⁰ Panel Strain vs. Table Input Intensity	173
4.36	EC25 - Relative Displacement Response Spectra from Table and Input Record Accelerations	174
4.37	Relative Velocity Response Spectra from Table and Input Record Accelerations	175
4.38	Absolute Acceleration Response Spectra from Table and Input Record Accelerations	176
4.39	Expanded Response Spectra from Shake Table Accelerations	177
4.40	Test Structure Floor Response Spectra	178
4.41	Input and Dissipated Energy	179
4.42	Shake Table Motion	180
4.43	Floor Displacements	181
4.44	Floor Accelerations	182
4.45	Story Drift	183
4.46	Base Shear from Strain Gages vs. Accelerometers ..	184
4.47	Story Shear	185
4.48	Joint Panel Deformations	186

LIST OF ILLUSTRATIONS (Continued)

4.49	EC25 - RMS of Shake Table Motion	187
4.50	RMS of 3rd Floor Motions	188
4.51	RMS of Joint SA Panel Deformation	189
4.52	Analytic Elastic Response	190
4.53	EC100 - Relative Displacement Response Spectra from Table and Input Record Accelerations	191
4.54	Relative Velocity Response Spectra from Table and Input Record Accelerations	192
4.55	Absolute Acceleration Response Spectra from Table and Input Record Accelerations	193
4.56	Test Structure Floor Response Spectra	194
4.57	Input and Dissipated Energy	195
4.58	Shake Table Motion	196
4.59	Floor Displacements	197
4.60	Floor Accelerations	198
4.61	Story Drift	199
4.62	Base Shear from Strain Gages vs. Accelerometers .	200
4.63	Story Shear	201
4.64	Joint Panel Deformations	202
4.65	RMS of Table Motion	203
4.66	RMS of 3rd Floor Motions	204
4.67	RMS of Joint SA Panel Deformation	205
4.68	Analytic Elastic Response	206
4.69	Girder Gage Moment vs. Panel 45° Strain-- Joint SA	207
4.70	Girder Gage Moment vs. Panel Shear Distortion-- Joint SA	208

LIST OF ILLUSTRATIONS (Continued)

4.71	ECL30 - Relative Displacement Response Spectra from Table and Input Record Accelerations	209
4.72	Relative Velocity Response Spectra from Table and Input Record Accelerations	210
4.73	Absolute Acceleration Response Spectra from Table and Input Record Accelerations	211
4.74	Test Structure Floor Response Spectra	212
4.75	Input and Dissipated Energy	213
4.76	Shake Table Motion	214
4.77	Floor Displacements	215
4.78	Floor Accelerations	216
4.79	Story Drift	217
4.80	Base Shear from Strain Gages vs. Accelerometers .	218
4.81	Story Shear	219
4.82	Joint Panel Deformations	220
4.83	RMS of Shake Table Motion	221
4.84	RMS of 3rd Floor Motions	222
4.85	RMS of Joint SA Panel Deformation	223
4.86	Analytic Elastic Response	224
4.87	Girder Gage Moment vs. Panel 45° Strain-- Joint SA	225
4.88	Girder Gage Moment vs. Panel Shear Distortion-- Joint SA	226
4.89	AE100 - Relative Displacement Response Spectra from Table Accelerations	227
4.90	Relative Velocity Response Spectra from Table Accelerations	228

LIST OF ILLUSTRATIONS (Continued)

4.91	AE100 - Absolute Acceleration Response Spectra from Table Accelerations	229
4.92	Test Structure Floor Response Spectra	230
4.93	Input and Dissipated Energy	231
4.94	Shake Table Motion	232
4.95	Floor Displacements	233
4.96	Floor Accelerations	234
4.97	Story Drift	235
4.98	Base Shear from Strain Gages vs. Accelerometers .	236
4.99	Story Shear	237
4.100	Joint Panel Deformations	238
4.101	RMS of Shake Table Motion	239
4.102	RMS of 3rd Floor Motions	240
4.103	RMS of Joint SA Panel Deformation	241
4.104	Analytic Elastic Response	242
4.105	Girder Gage Moment vs. Panel 45° Strain-- Joint SA	243
4.106	Girder Gage Moment vs. Panel Shear Distortion-- Joint SA	244
A.1	Interpolation Formulation	263
A.2	Integration Formulation	263
A.3	Differentiation Formulation	263
A.4	Interpolation Example 1	264
A.5	Interpolation Example 2	264
A.6	Interpolation Example 3	265
A.7	Interpolation Example 4	265

LIST OF ILLUSTRATIONS (Continued)

A.8	Derivative Example	266
A.9	Derivative and Integral Example	267
A.10	Smoothing Examples - Time Histories	268
A.11	Smoothing Examples - Frequency Attenuation	269

Chapter 1

Introduction

Analytical methods utilizing continuum mechanics and discretization techniques are applicable to most structural engineering problems, provided the boundaries of theoretical knowledge and of practical analysis capabilities are not exceeded. For problems which involve complex structures and possible material and/or geometric non-linear behavior, such as are encountered in earthquake engineering, the capabilities of mathematical modeling may be surpassed. In such cases, experimental studies serve as an alternate means of analysis and as a means of extending the limits of theoretical knowledge.

Early experimental work was often hampered by high expenses, low accuracy and excessive time consumption due to the lack of adequate instrumentation and control devices. Recent developments in the computer and electronics industries have made experimentation a competitive proposition, especially for the study of complex behavior. The advent of the minicomputer and electronic transducers has released the experimental researcher from the limitations previously imposed on the quality and quantity of data measurements allowed, permitting detailed measurement of structural behavior. It is currently possible to utilize the minicomputer to monitor and control experimental tests, perform data acquisition and evaluate the test data.

Experimental analysis can be performed on either unscaled prototypes or scale models of elements, subassemblies and complete structures. For greatest test versatility and control, laboratory testing is most applicable to experimental analysis. However, due to size constraints,

testing of complete structures in the laboratory will generally be limited to small-scale models. Provided the effects of the modeling scale are considered such small-scale model testing can provide reliable simulation of the prototype.

Considering the relatively high costs and specialized knowledge required for model analysis such studies are only justifiable when an advantage over analytical methods can be clearly demonstrated. A qualitative illustration of the relative effort and expense as a function of the problem difficulty for the cases of conventional structural analysis, computer analysis and model analysis is presented in Figure 1.1. The figure indicates that model analysis serves as an optimal solution technique within two ranges: one where both analytical and model solutions are feasible but model solutions are more cost efficient, and a large region where analytical capabilities are currently inadequate to solve the problem. Since in the field of earthquake engineering the line designating the limit of analytical capability is still fairly far to the left, the latter range of model testing is quite extensive.

Currently, earthquake simulators provide the most versatile resource for exciting the dynamic response of a test structure. Though it is physically impossible to completely duplicate the ground motion produced by an earthquake, shake tables possess the capability to generate earthquake-like motion and enable the measurement of input and response correlations for a test structure.

The primary task in the development of a small-scale replica model is to simulate all aspects of the prototype structural system which may contribute to the earthquake response characteristics of interest. Modeling theory, as derived from dimensional analysis, establishes the correlation functions (scaling laws) by which the geometry, material

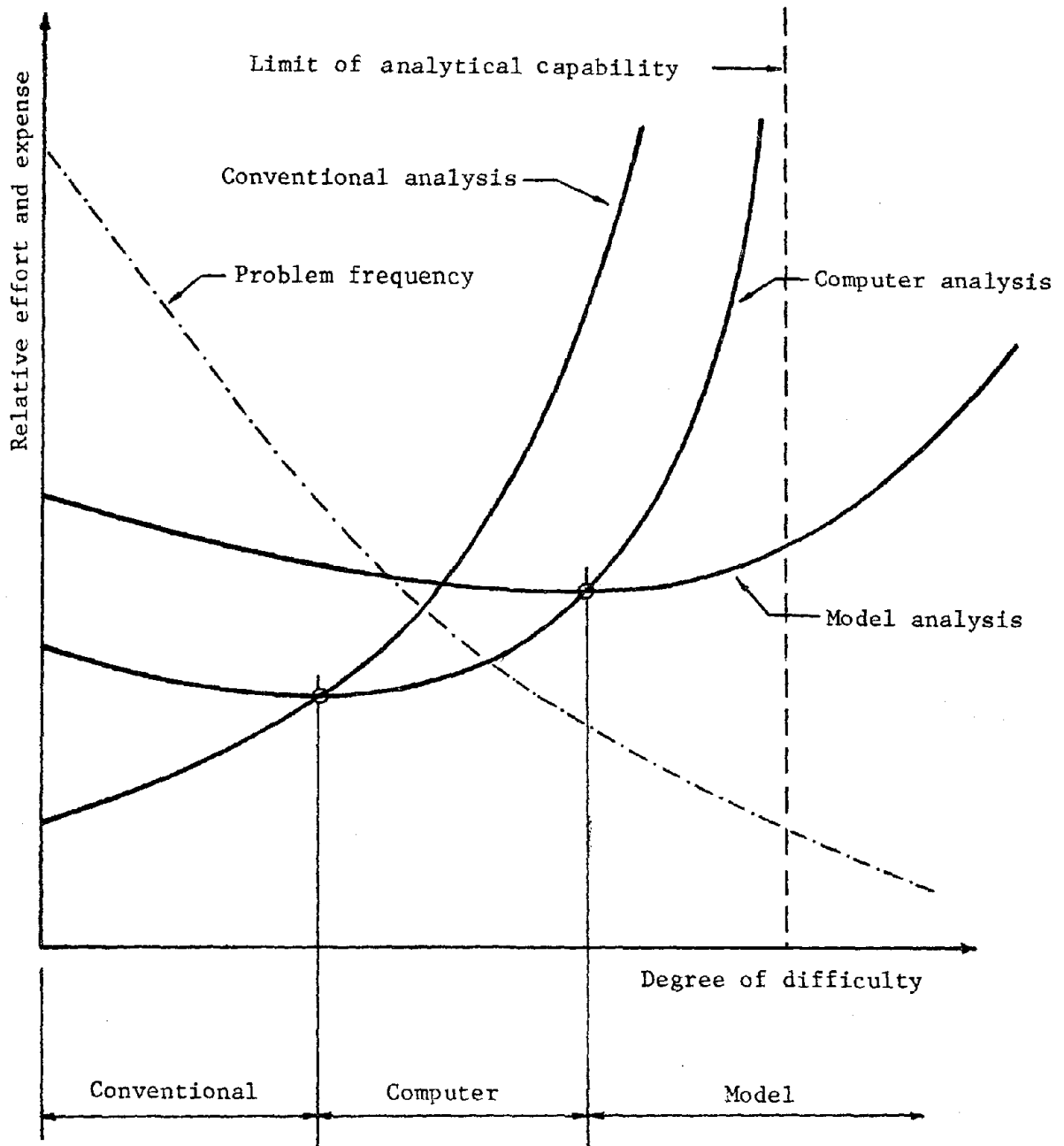


Figure 1.1 Application of Various Methods of Structural Analysis (17)

properties, boundary conditions and loading of the model and prototype can be related. Provided these relationships are satisfied and that no important effects were neglected in the scaling formulation the model will serve to duplicate the desired prototype characteristics.

For a comprehensive review of existing literature related to model analysis of structural response to earthquakes the interested reader is directed to Reference 21. However, to provide some introduction to past work in the area of model analysis, a condensed discussion of representative published works is presented with emphasis on modeling of steel-frame structures.

The book by Hosdorf (17) provides an excellent general introduction to model studies. It does not go deeply into any one aspect of model analysis but covers many topics and gives a healthy perspective of the place of model analysis in structural engineering. Many interesting case studies are also discussed. A research study progress report (21) concerning a general investigation of model analysis presents a more comprehensive discussion of dynamic modeling in earthquake engineering.

Material scale-effects which must be considered when performing model tests of steel structures are discussed in References 26, 34 and 35. Fabrication techniques which may be applied to small-scale models are presented in References 2 and 25.

The test facilities at the University of California at Berkeley have been used extensively for experimental studies. The 20 ft x 20 ft shake table is used primarily for testing of structures which may be considered to be large-scale pseudo models (7, 8, 9, 10, 16, 41). The structural elements are usually made of actual structural material, such as small hot-rolled steel sections or concrete reinforced with small

reinforcing bars. In size, the structures may be roughly one-half that of actual structures. The seismic input motion is usually not scaled according to model similitude laws as the test results are used primarily to provide an input and response correlation for purposes of computer program development and verification.

Actual replica models are also tested at the Berkeley facility. One example is the 1:30 scale model of a reinforced concrete high curved overcrossing (46). This model was built of microconcrete and closely follows dynamic similitude laws. The modeling method used in this study, artificial mass simulation, is of particular interest as it is a major topic of this dissertation.

A thorough study on static and dynamic modeling of steel and reinforced concrete structures was carried out in the sixties at MIT (2, 15, 25). Reference 25 provides considerable information on the problems of element fabrication and member joining encountered when steel is used as the model material.

Physical models in earthquake engineering have been used more extensively in Europe than in the United States. References 5, 6, 22 and 30 describe some of these model studies and contain information on modeling of buildings, bridges, dams and nuclear reactor components and containment vessels. Several model studies on the seismic behavior of structures were also carried out in Japan (31, 43).

It is evident that the dynamic test facilities required for model analysis are of extreme importance. A general discussion of the facilities required for experimental studies in earthquake engineering is presented in References 17, 21, and 39. These reports describe the application of earthquake simulators and minicomputers to model studies and also consider necessary instrumentation. Specific information

concerning the use of shake tables for providing test structure excitation is available in References 23, 33 and 40, while the use of mini-computers for control and data handling in dynamic tests is discussed in References 28 and 38. Requirements on the instrumentation system and feasible measuring devices are summarized in References 19 and 36.

Chapter 2

Objectives and Scope

The primary objectives of this research effort are to develop methodologies for dynamic model testing and to illustrate the applicability of small-scale model analysis to earthquake engineering. This task is accomplished through the development of an adequate dynamic test facility and of techniques for model fabrication, testing and analysis and through evaluation of test results of an actual small-scale model study.

1. Dynamic Test Facility: An integrated testing system has been developed at Stanford University to permit suitable model excitation as well as measurement, recording and manipulation of pertinent response parameters. This system serves as an illustrative example for a general discussion of the test system requirements in the area of dynamic model analysis. For instance, when a shake table is used as a source of model excitation, it must be considered that similitude laws will present specific demands on the table performance. Similarly, scaling of length and time will also significantly affect the design of a suitable instrumentation and data acquisition system. The application of minicomputers to dynamic model testing is considered for generating and controlling the input signals to the excitation sources, recording a large number of response measurements at high sampling rates, reducing the data to a form useful to the experimental researcher, and displaying reduced data.

2. Model Fabrication, Testing and Analysis: This phase of the

research is concerned primarily with steel-frame building structures. Suitable techniques are needed for fabrication of model elements and model construction when mild steel is used as the model material. Items which must be considered are joints and connections, support conditions, construction and testing sequence, and suitable tolerances. Procedures for testing and analysis are developed in conjunction with a small-scale model study. Many categories of experiments, including material and component testing, free vibration tests and forced vibration earthquake simulator tests are required to adequately define the behavior of the model structure. Analysis quantities, consisting of directly measured quantities and derived correlations, must be displayed in the time and frequency domains to enable an evaluation of test results.

3. Model Experimentation: A small-scale model study serves as an aid in the development of the test system and as a verification of the methodologies derived on the previous topics. To provide a measure of the accuracy of response prediction by the model, a prototype whose structural characteristics and response history are accurately known is required to permit a direct correlation between model and prototype. The applicability of one type of model analysis, artificial mass simulation, to building structures is demonstrated and the particular characteristics of this modeling procedure are considered.

EXPERIMENTAL FACILITIES FOR DYNAMIC MODEL STUDIES

3.1 General Discussion

In order to perform extensive dynamic studies of small-scale replica models of civil engineering structures it is necessary to have available a fully developed earthquake simulation, instrumentation, and data handling system. The design goals for this system can be summarized as follows:

- (1) Allow the reproduction of any type of input motion within the capacities of the shake table. Periodic motions such as sine waves and square waves as well as random motions can be easily produced by electronic signal generators and used to drive the shake table. The primary task at hand is to utilize the digital to analog (D-A) conversion capability of an in-house computer system, permitting the reproduction of any digitized wave form, such as past earthquake time history recordings. It must also be possible to scale these time histories to meet the requirements of modeling theory, i.e., scaling of time and displacement.
- (2) Devise an instrumentation system, consisting of sufficient electronic sensors and signal conditioners, capable of measuring all parameters pertinent to the response of models. The quantities to be measured are accelerations, frequency and damping characteristics, displacements, deformations, strains and internal forces. The sensitivity of the electronic sensors must be sufficiently high to permit accurate measurement of response parameters at model scales.

- (3) Develop an analog to digital (A-D) conversion system with the capacity to scan multiple data channels at minimum time intervals on the order of one millisecond or less and to store this data in readily accessible form. The data channels would correspond to output signals from transducers such as accelerometers, linear variable differential transformers (LVDT), potentiometers and strain gage circuits.
- (4) Create a network of computer programs to allow visual display of the measured time history response as well as to determine derived response characteristics such as force and energy terms.

Since it is difficult to anticipate the needs of future researchers it is also necessary to incorporate the capacity for modification and expansion. This is best accomplished through logical construction of computer program segments and extensive documentation.

The primary task of an earthquake simulation and data acquisition system as related to model studies is to permit the accurate measurement and analysis of those parameters whose influence is of importance to the earthquake response behavior of the prototype structure. Available means must exist to measure the pertinent response quantities of the model while it is subjected to some relevant input motion and to perform a transformation to the prototype reference frame for analysis of expected prototype integrity. Not only will the system be required to provide measurement of model response but also of material and structural component tests necessary to fully define the structural model.

The design requirements of this system must take into consideration the specific nature of modeling theory as dictated by dimensional analysis. Various physical quantities will generally be scaled in some proportion to their values in the prototype reference frame. An obvious consideration

is scaling of length parameters as defined by the model scale, l_r . Other scaling requirements exist which can often be expressed in terms of l_r . Time must be scaled, usually in the ratio of either $\sqrt{l_r}$ or l_r , illustrating that input motion and model response will occur at a much faster rate than for the prototype structure. This will mandate the necessity for high-speed data acquisition and the ability to control the rate of input motion to the model structure. Yet some physical quantities may not be scaled from the prototype to model reference frame, such as accelerations and strains for true replica models. These variable similitude requirements create a need for a highly versatile experimental system to provide optimum test reliability.

An experimental system has many integral components necessary to accomplish the task of model analysis. Each component has specific design requirements yet must work in conjunction with other components of the system. There also exist alternatives for some components of the system, yet certain choices are clearly superior to others.

For instance, several methods can be used to provide input energy to the structural model. In the laboratory, practicable choices for inducing controlled motions are vibration generators mounted on the model and earthquake simulators (shake tables). A vibration generator mounted on the model could provide information concerning non-linear behavior, but is severely limited in the character of input motion possible. Problems may also be encountered in physically mounting a shaker on a small-scale model, simply due to size reduction of the structure. A shake table would provide the greatest versatility for replica-model studies since virtually any character of input motion, such as sinusoidal wave forms, random motion, and actual past or anticipated future earthquakes, could be duplicated within the capacity of the shake table. A well designed shake table would then be a most powerful tool for dynamic model studies.

The pertinent model response quantities must also be defined to provide requirements on necessary instrumentation and data reduction. Certain desired quantities may be different for specific model studies, requiring "custom" instrumentation design, yet certain common instrumentation requirements will exist for nearly all models. These requirements can be defined generally as direct measurement of displacement, accelerations and strains. From these quantities can be deduced response spectra, Fourier spectra, energy distribution, ductility demands, internal and external forces, and other information for use in analysis of expected prototype performance.

The dynamic test facilities at the John A. Blume Earthquake Engineering Center, Stanford University, were developed and coordinated to form an integrated testing system for dynamic model studies and as such will serve as an example for discussions throughout this report. A block diagram of the system is presented in Figure 3.1 and shows the basic components necessary for scale model investigations, such as:

1. Digital computer system with digital to analog (D-A) and analog to digital (A-D) conversion capabilities for generation of input motion and for high-speed data acquisition.
2. Shake table capable of supplying desired input motion to the model structure.
3. Cyclic testing apparatus for material studies and tests of structural components such as beam-column subassemblies.
4. Network of computer programs and output display units for analysis of experimental results through extraction of desired response quantities.
5. Experimental measuring devices (transducers) and necessary signal conditioners required to measure desired response quantities.

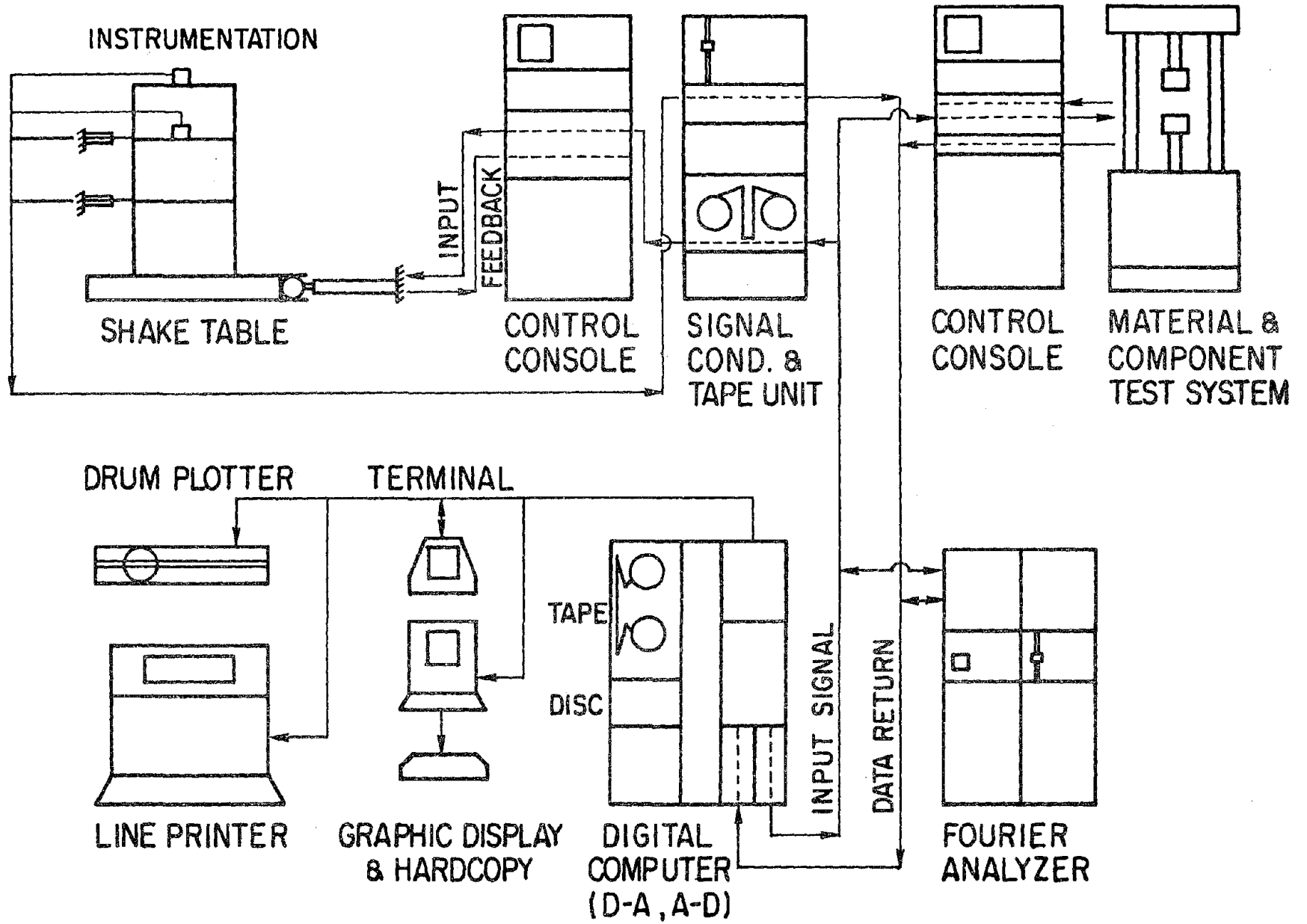


Figure 3.1 Block Diagram of Dynamic Testing System at Stanford

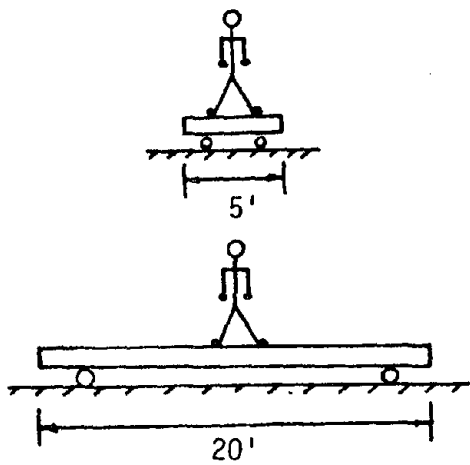
3.2 Earthquake Simulation by Means of Shake Tables

3.2.1 Design and Performance Requirements for Shake Tables

A suitable earthquake simulation system is of principal concern for use in experimental studies of small-scale dynamic models. The task at hand is to provide desired structural excitation necessary for studies of model response. Though different alternatives exist for methods of inducing vibratory motion in the structural model, as mentioned previously, the shake table is the most versatile and accurate means of duplicating the conditions experienced by an actual prototype structure during an earthquake.

Various shake tables are in existence and may be conveniently classified by size as small for dimensions less than 10 ft X 10 ft, medium for tables between 10 ft and 30 ft square, and large for tables exceeding dimensions of 30 ft. Examples of existing or proposed shake table facilities are illustrated in Figure 3.2. The larger tables are valuable tools in gaining understanding of structural behavior and in development of design requirements for engineering structures through testing of full-scale prototypes or large-scale models. Yet, high development and operating expenses as well as problems meeting similitude requirements somewhat limit their application for model research. Smaller-sized tables are better suited for small-scale model analysis, not only on the basis of size requirements, but also on the basis of their ability to satisfy similitude laws for scaling of input displacement, acceleration, and frequency.

One question that always arises, no matter what the size of the table, is how many directions of table motion are required to provide truly representative test results. Real earthquakes obviously have no restrictions on direction of motion. Thus, to completely reproduce the



Location	Dimensions ft	Payload Limit lb	a_{max},g		$d_{max},\pm in.$		f_{max},Hz
			Hor	Vert	Hor	Vert	
<u>SMALL (<10 ft.)</u>							
Stanford Univ.	5 X 5	5000	5	--	2.5	--	50
Univ. of Calgary	4.5 X 4.5	2000	20	--	3	--	...
ISMES	10 X 6.5	300	100	--	...	--	800
<u>MEDIUM (10-30 ft.)</u>							
U.C., Berkeley	20 X 20	100,000	1.5	1.0	5	2	15
Univ. of Illinois	12 X 12	10,000	7	--	4	--	100
Corps of Engr.	12 X 12	12,000	34	60	2.2	1.8	200
Wyle Lab	20 X 18	60,000	6	6	6	6	100
<u>LARGE (>30 ft.)</u>							
National Research Center, Japan	50 X 50	1,000,000	0.6	1.0	1.2	...	16
Berkeley--Proposed	100 X 100	4,000,000	0.6	0.2	6	3	...

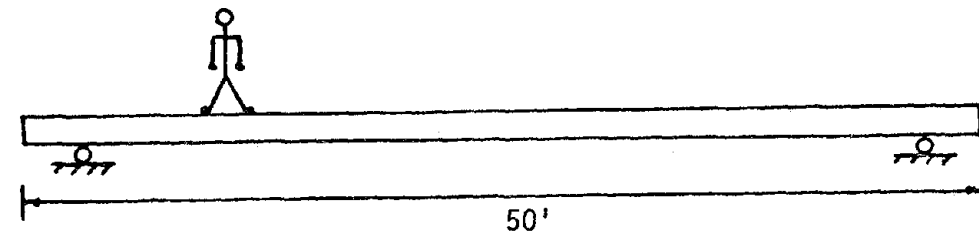


Figure 3.2 Classification of Shake Tables

ground motion at a structural site an earthquake simulator would have to be capable of movement in three reference directions, two horizontal and one vertical, assuming that ground motion is homogeneous over the base of the structure and that rotational modes of ground motion can be neglected.

It is not within the scope of this report to enter the discussion on multi-component simulation of seismic ground motions. This section is only concerned with the reproduction of a specified table motion in one characteristic direction. The uni-directional shake table at Stanford will be used as an illustrative example.

Most simulator systems share common principles of operation. A force actuator, generally electro-dynamic or hydraulic, is used to drive a platform according to some programmed time history of motion. A closed-loop servo system may be utilized to monitor table response relative to input command generating continuous correction signals for control of table response. Shake table displacement is the most common control parameter, thus a displacement transducer would be used as a feedback measuring device. As displacement signals are necessary for input command to the table, electronic integrating circuits are necessary if velocity or acceleration input is desired.

Considerable attention should be given to the design of the support method for the simulator platform. A well designed table should have a support system characterized by low friction to minimize distortion of the desired table response and by rigidity to prevent adverse table motions such as pitch and yaw. The capacity to support large loads will also be necessary, even for small-scale replica model studies. Additional weight requirements would be imposed for studies involving large soil masses for soil-structure interaction research. Examples of various

methods which have been utilized to provide support for the simulator platform are given in Table 3.1.

Table 3.1
METHODS FOR SUPPORTING SHAKE TABLES

Simulator Location	Support Method	Payload Capacity	Size
U.C. Berkeley	Air pressure and vertical actuators*	100,000 lb	20' X 20'
ISMES	Oil film	300 lb	10' X 6½'
University of Illinois	Flexural supports	10,000 lb	12' x 12'
Stanford University	Roller bearings	5,000 lb	5' x 5'

*Enables vertical motion.

Further engineering design considerations for the earthquake simulator involve the simulator platform and the force actuator-reaction mass. The shake table requires considerable rigidity, both in-plane and out of plane, and should possess adequate mass to help minimize feedback interference effects from a vibrating model on the table. A large reaction mass is also essential to provide a firm base for the force actuator.

Several general design goals for shake table performance capabilities can be derived from the requirements of similitude laws for scaling of length, acceleration and time for small-scale dynamic models. Since displacements in models will be considerably decreased by scaling of prototype lengths, large shake table displacements will usually not be required. On the contrary, the simulator system will have to accurately reproduce displacements of a very small order of magnitude, requiring considerable shake table sensitivity. As an example, consider a model with a length scale of 1:5, subjected to the properly scaled El Centro, 1940 earthquake. The N-S displacement component, derived by numerical

integration of the acceleration time history, shows a maximum prototype displacement of approximately 4.3 in. When reduced to satisfy similitude laws the maximum shake table displacement is 0.86 in. A model with $\ell_r = 1:10$ would require peak displacements of only 0.43 in.

Acceleration capability requirements may be very high as necessary accelerations on the table will generally be equal to or greater than the accelerations of the prototype time history. Most true replica models require an acceleration ratio, a_r , of one while a gravity neglected model composed of prototype material needs an acceleration scale of $a_r = 1/\ell_r$ for proper simulation of inertial effects. Again considering the El Centro component with a peak ground acceleration of 0.35g, a model with $\ell_r = 1:10$ would require table accelerations of 0.35g and 3.5g for true replica and gravity neglected models, respectively. It can then be seen that high shake table acceleration capacity is required for small-scale model testing, producing the need for a relatively powerful force actuator.

These displacement and acceleration requirements also lead to compaction of the time scale, generally by a ratio of $t_r = \sqrt{\ell_r}$ for true replica models and by $t_r = \ell_r$ for gravity neglected models. Thus the shake table motion will occur at a much faster rate than for the prototype reference, establishing the necessity for high frequency capabilities for the earthquake simulator as specified by the inverse of the time scale. The El Centro prototype earthquake has an acceleration frequency range of approximately 0-8 Hz, which when scaled for a true replica or a gravity neglected model with $\ell_r = 1:10$ produces shake table frequency needs of 0-25 Hz and 0-80 Hz, respectively.

The performance capacities for an actual earthquake simulator can be summarized in a performance spectrum derived from steady-state sinusoidal input motion. The spectrum obtained for the hydraulically driven table

at Stanford University is shown in Figure 3.3. From 0 Hz to approximately 1.5 Hz displacement is the controlling factor, as limited by the maximum table travel of ± 2.5 in. For the unloaded table, over the frequency range from 1.5 Hz to 13 Hz the shake table velocity limitation of 24 in/sec becomes decisive, while the acceleration limit of approximately 5g will control for frequencies in excess of 13 Hz. However, oil column resonance will reduce the acceleration capacity considerably for frequencies in excess of 50 Hz.

Loaded shake table performance capabilities are more difficult to define than those for the unloaded case. For a rigid mass on the table the acceleration capacity would be reduced roughly in proportion to the added mass, as governed by the maximum actuator dynamic force capacity (see Figure 3.3). However, a test structure will have a far different effect on shake table response than would a rigid mass. Model contribution to shake table performance will be apparent in both the frequency characteristics of the table and the maximum required actuator force to produce a necessary acceleration amplitude level.

Test results have shown that a structure with a specific natural frequency of vibration will distort shake table response for input motion at that given frequency (40). This feedback effect is caused by the large amplification of input motion by a test structure with low damping, producing high base shears which are then transferred to the table. However, tests with earthquake-type motions have shown little distortion due to model feedback effects.

Structure response feedback will determine the actuator force capacity required to produce a given acceleration amplitude on the shake table. For model studies, a conservative estimate of the demand on the actuator force can be obtained from the expression

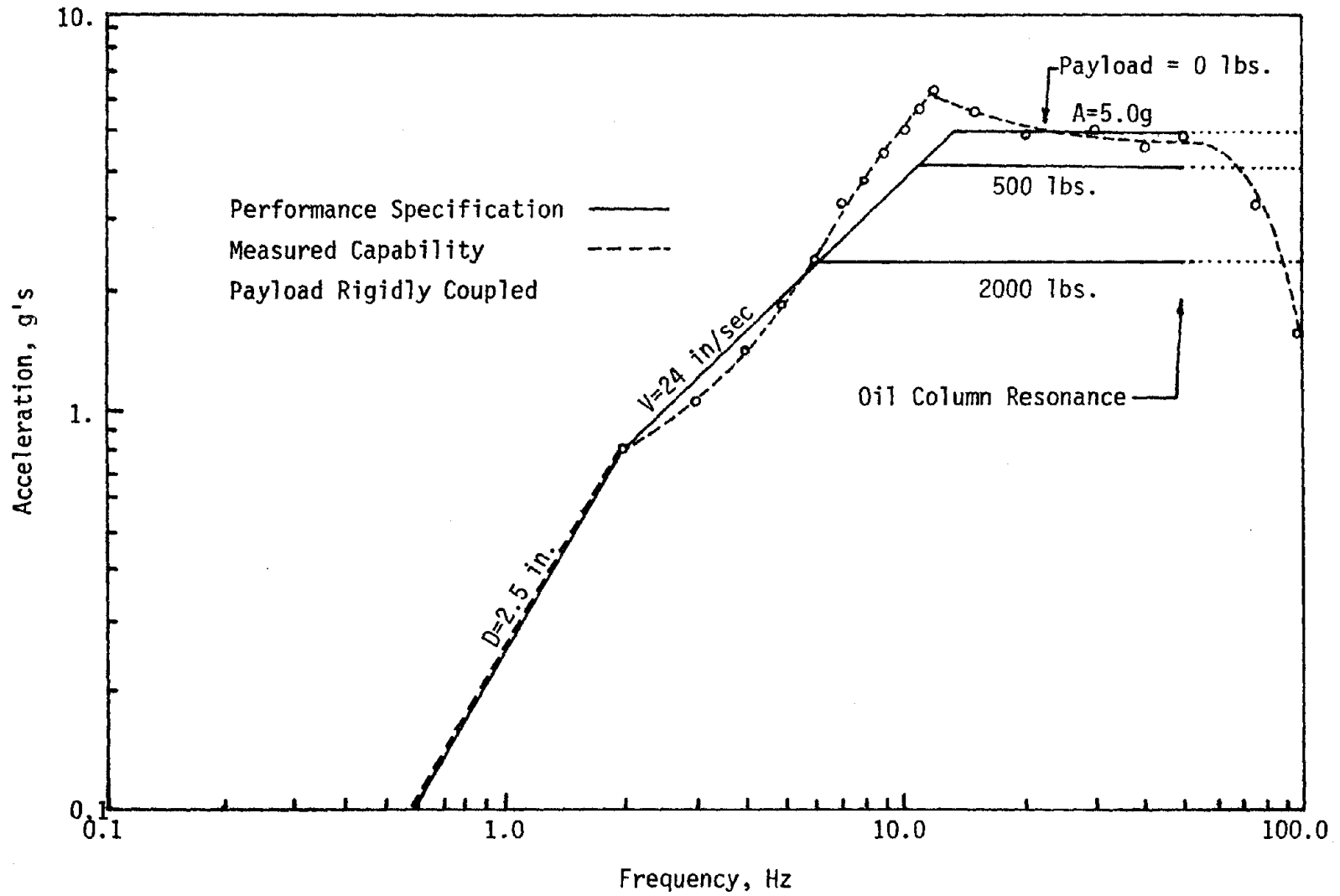


Figure 3.3 Shake Table Performance Spectrum--Stanford Shake Table

$$F_{\text{dyn}} = W_t a_r a_{\text{max}}/g + V_p F_r \quad (3-1)$$

where: F_{dyn} = actuator dynamic force
 W_t = shake table weight
 a_r = model acceleration scale
 a_{max} = maximum prototype acceleration
 g = gravitational acceleration
 V_p = maximum prototype base shear
 F_r = model force scale

This estimate is rather conservative, as peak input acceleration and peak model base shear are assumed to occur at the same instant and with the same direction of application. Also, peak acceleration values may not have a considerable influence on model response, thus shake table reproduction of the general intensity level of the input motion may only be required.

Within limitations of a shake table in the frequency domain (see Figure 3.3 and the discussion to follow) and assuming negligible model feedback effects, an actuator that can produce the force given by Eq. 3-1 will assure reproduction of an input signal whose acceleration does not exceed a_{max} . Thus, Eq. 3-1 can be used as a basic (although conservative) criterion for the dynamic force requirement on shake tables.

To utilize this equation it will be necessary to estimate the maximum base shear the prototype structure will experience under the specified seismic motion. For experimentation on structures subjected to severe earthquakes the base shear is limited to the base shear capacity (see Figure 3.4) which usually can be estimated.

Many of the performance demands which are placed on an earthquake simulator for different types of model tests can be illustrated by the following simple example.

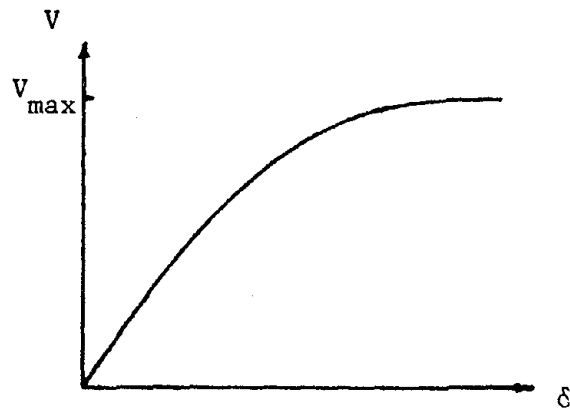


Figure 3.4 Maximum Base Shear

Let us assume that the Stanford shake table is to be used to test a model of a six story braced steel frame prototype building with base dimensions of 48 ft X 48 ft. The weight of the building is 900K and it is estimated that the base shear capacity is approximately equal to 40 percent of the weight, i.e., 360K. The structure is to be subjected to 1.5 times the El Centro N-S component producing the following prototype earthquake parameters.

maximum displacement: $1.5 (4.38 \text{ in.}) \cong 6.4 \text{ in.}$

maximum velocity: $1.5 (13.2 \text{ in./sec}) \cong 20 \text{ in./sec}$

maximum acceleration: $1.5 (0.35g) \cong 0.5g$

frequency range of interest: 0 - 8 Hz

The weight of Stanford's shake table is 2000 lbs, the payload capacity is 5000 lbs, and the actuator is rated for 11,000 lbs. The table size is 5 ft X 5 ft, which permits a 1:10 scale model test of the prototype structure.

Three types of models are investigated, utilizing steel or a suitable copper alloy ($E_r = 0.53$) as possible model materials. The mass

distribution in the structure is such that artificial mass simulation at story levels is feasible. It is also presumed that the gravity induced stresses in the critical elements are sufficiently small to investigate as a possible alternative a model in which a simulation of gravity forces is not necessary. The basic scaling laws for three types of 1:10 scale models and the corresponding simulator performance requirements are shown in Table 3.2.

Table 3.2 shows that a steel model with artificial mass simulation (Column 1) could not be tested on the Stanford shake table because of the excessive model weight. However, if the model is made of a suitable copper alloy (Column 2) the table could reproduce the required input motion. A steel model without simulation of gravity forces (Column 3) is also inappropriate since the high acceleration (5g) cannot be reproduced with the 11,000 lb actuator. Also, significant distortion would have to be expected in this case in the reproduction of high frequency components of table motion (see Figure 3.3).

3.2.2 Generation of Input Motion

Various types of shake table input motion are necessary to conduct a thorough investigation of all pertinent model response characteristics. These motion types fall into two basic categories--signals produced by electronic signal generators and complex waveforms requiring computer analysis and control.

Signal generators can be incorporated into a simulation system network with relative ease, requiring only electronic compatibility between the signal device and the shake table input control module. Signal generators are available to produce artificial signals such as sinusoidal waveforms and white noise. Sinusoidal wave forms are used to explore the

Table 3.2
EARTHQUAKE SIMULATOR--PERFORMANCE REQUIREMENTS

			Steel Model with Artificial Mass Simulation		Copper Alloy Model with Artificial Mass Simulation		Steel Model without Simulation of Gravity Forces	
			(1)		(2)		(3)	
			scaling	value	scaling	value	scaling	value
Scaling Laws	Length	$l_r =$		0.1		0.1		0.1
	Time	$t_r =$	$l_r^{1/2}$	0.32	$l_r^{1/2}$	0.32	l_r	0.1
	Velocity	$v_r =$	$l_r^{1/2}$	0.32	$l_r^{1/2}$	0.32		1.0
	Acceleration	$a_r =$		1.0		1.0	l_r^{-1}	10.0
	Forces	$F_r =$	l_r^2	0.01	$E_r l_r^2$	0.0053	l_r^2	0.01
	Model Weight	$W_r =$	l_r^2	0.01	$E_r l_r^2$	0.0053	l_r^3	0.001
Performance Reqts.	Max. Table Disp. (in.)			0.64		0.64		0.64
	Max. Table Vel. (in./sec)			6.4		6.4		20.0
	Max. Table Acc. (g)			0.5		0.5		5.0
	Frequency Range (Hz)			0-25		0-25		0-80
	Model Weight (lbs)			9,000		4,770		900
	Max. Dyn. Force (Eq. 3-1)			5,600		3,820		13,600

response of a test structure to a given frequency and amplitude of input motion under steady state conditions. Such tests are useful in determining a spectral envelope of structural response amplification for a given model, yielding information on natural frequencies, mode shapes and damping. Single frequency component input may also be used to isolate a given mode of structural response by providing input energy only at that corresponding natural frequency, enabling further determination of mode shapes and modal damping.

Various spectral methods are available for gaining response information for an elastic structure from tests using white noise input (3 , 12, 29). These methods permit further definition of modal response characteristics through Fourier spectrum analysis. White noise tests consist of subjecting a test structure to table input motion with uniform spectral energy, enabling the determination of energy distribution during stationary dynamic response of the structural model.

Of primary importance to the earthquake simulation system is the ability to reproduce desired time histories which simulate earthquake motion. These time histories may be actual recordings of past earthquakes or generated representations of hypothesized earthquakes. The capacity must also exist to scale this earthquake motion, both in displacement amplitude and time rate, to satisfy similitude laws for the particular model under study.

Digitized time history recordings of past earthquakes are commonly available from a number of sources, the California Institute of Technology and the United States Geodetic Survey for example. These records are generally in the form of instrument corrected acceleration time histories and corresponding integrated velocity and displacement records, conveniently stored on magnetic tape. The displacement time history will be of principal

concern for input control of the shake table, yet may possess certain distortions due to numerical inaccuracies of digital integrations. These errors will generally be characterized by distortion of the extremely low-frequency end of the displacement time history, on the order of 0.0-0.1 Hz. Significant distortion of table acceleration can also be caused by too large time intervals of digitized displacement records which often necessitates the in-house integration and base-line correction of acceleration records to arrive at more refined displacement records for shake table control.

Information is available in the literature on the generation of artificial earthquake time histories (18, 37 , 42). These methods generally utilize some random signal, such as white-noise, modified to fit spectral and real-time characteristics of earthquakes to produce the desired time history. Though actual earthquake motion is not truly random in nature, the effect of a random-process artificial earthquake on a structural system is similar to that for an actual earthquake. Since the character of future seismic events is difficult to predict, due to a lack of knowledge concerning strong earthquake motion, such artificial earthquake experimentation may be useful, especially for a statistical approach to prototype response integrity.

The problem now remains to convert these digitized representations of earthquake motion to an analog voltage signal compatible with shake table requirements. This signal would correspond to an acceleration, velocity or displacement command for shake table control. Hardware and software computer facilities are required to perform the digital to analog conversion necessary to produce the required command signal. Various minicomputers have this capacity and can generally provide data acquisition as well as earthquake generation. Computer programs must also be

developed to perform the task of analog conversion, and may be called upon to perform additional conditioning required by the specific simulation system at hand. Model scaling of the earthquake time history can be attained through variation of the amplitude and rate of output of the voltage signal.

Once the analog time history signal has been produced it can be input directly to the shake table. However, since most laboratory computer systems do the double duty of signal generation and data acquisition, interim storage of the voltage time history on an analog tape recorder for subsequent input to the table is often preferred. This will free the computer to be utilized more efficiently for data acquisition purposes, enabling the rapid sampling rates required by small-scale dynamic model tests.

3.2.3 Measures of Shake Table Performance

Certain performance criteria must be established to assure adequate duplication of the input motion by the earthquake simulator. As certain imperfections are bound to be inherent in the shake table system, some distortion of the table motion will be observed. These distortions of table response must not be of such a severity as to alter the structural behavior of a small-scale model from that expected for the prototype structure. In addition, adequate table reproduction performance is essential to provide accurate comparison with results from analytic studies and experimental investigations performed on other simulator systems.

As shake table motion and corresponding distortions of that motion are of an extremely complex nature a single measure of the adequacy of signal reproduction is difficult to define. Various subjective comparisons of input signal versus shake table response, both in the time and

frequency domain, can be utilized to provide some measure of simulator capabilities.

It should also be mentioned that shake table control settings, such as for sensitivity and gain, may vary with such parameters as frequency, amplitude and table payload to provide optimum performance. These influences must be investigated and proper procedures established for making these adjustments for a given model test. Increases in table payload will generally have a significant, though not necessarily detrimental, effect on the quality of table reproduction, requiring shake table performance tests with various model weights.

The adequacy of alternative modes of shake table control, if available, should also be investigated to determine whether displacement, velocity or acceleration control gives optimum performance for a given simulator system.

A thorough investigation of table performance would utilize several types of input motion, as listed below.

1. Square wave
2. Sinusoidal wave
3. Narrow band signal with several distinct frequency components
4. White noise, modified by high and low-pass filtering
5. Actual earthquake time histories, with various model scaling factors.

Each form of motion would provide specific insight to the shake table response characteristics. Following is an explanation of methods of performance analysis which make use of these input signals. Sample case studies from performance investigations conducted on the earthquake simulation facility at Stanford University are also presented with suggested causes of observed behavior.

Shake table rate of response and stability can be investigated using square wave input. These tests will provide information on shake table sensitivity, and necessary settings to provide optimum table response. A shake table with extreme sensitivity will tend to exhibit lack of stability characterized by convergent oscillations as shown in Figure 3.5a, while too low sensitivity will hinder shake table ability to track a command signal, illustrated in Figure 3.5b. This characteristic should be investigated for various amplitudes and frequencies. However, appropriate sensitivity settings for a given model payload would be difficult to define using this method, as shock loading of this nature may damage a small-scale structural model.

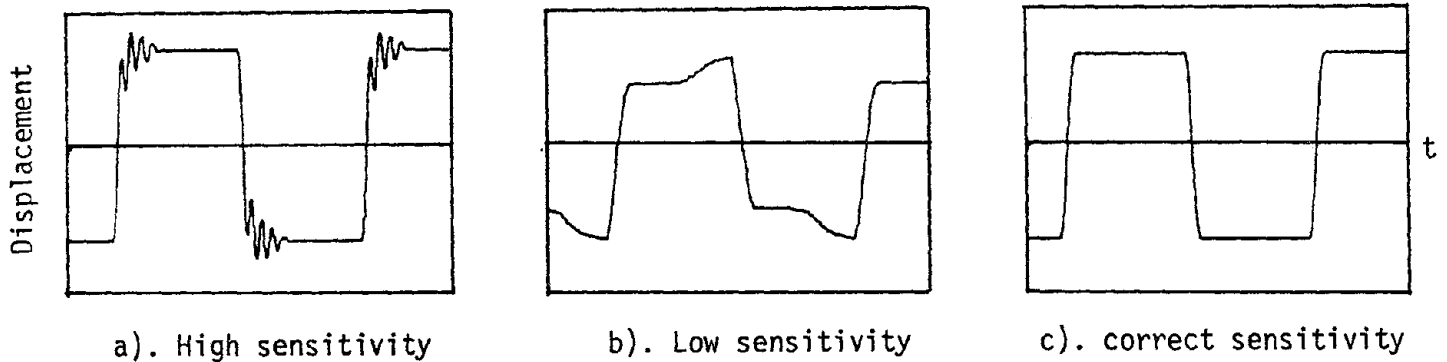


Figure 3.5 Shake Table Sensitivity

Single frequency sine wave motion will provide considerable performance information. An initial test would involve comparison of input amplitude to response amplitude at various frequencies of motion, yielding an amplitude spectra envelope of shake table response (Figure 3.6). This test

would also serve to define the accuracy of shake table control settings and shake table frequency performance limitations. Additional information could be obtained from this test series by scanning for shake table resonances, such as for a rocking or rotational mode of vibration, by suitable locations and orientations of measuring devices (Figure 3.7). These modes should be located and identified for future consideration of possible contribution to the response of specific models.

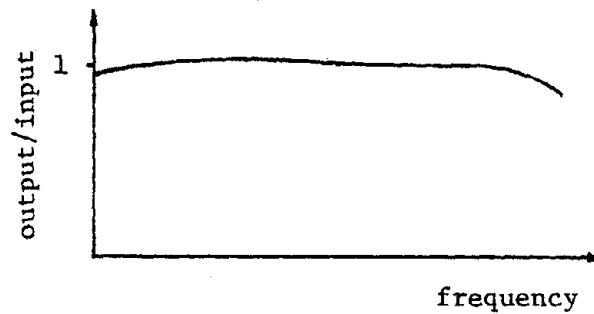


Figure 3.6 Shake Table Amplitude Envelope

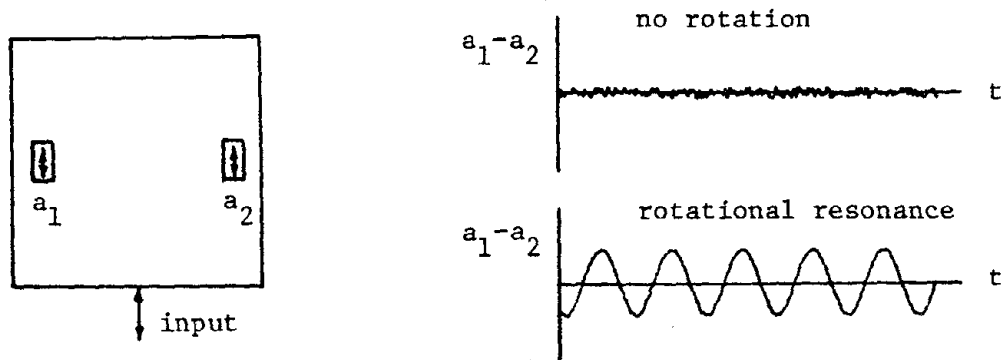


Figure 3.7 Shake Table Rotational Modes

Further analysis with sine wave input would involve visual observation of the recorded time history, to provide a qualitative comparison to desired response, and comparison in the frequency domain using Fourier analysis. For a single component sine wave the Fourier spectrum consists of a single frequency impulse, thus any additional frequency components observed in the response signal of the shake table would signify distortion of the input signal. This distortion would be characterized by various frequency components with different amplitude, phase and frequency values and would permit measurement of the distortion energy relative to the input energy corresponding to the given sinusoidal wave (Figure 3.8).

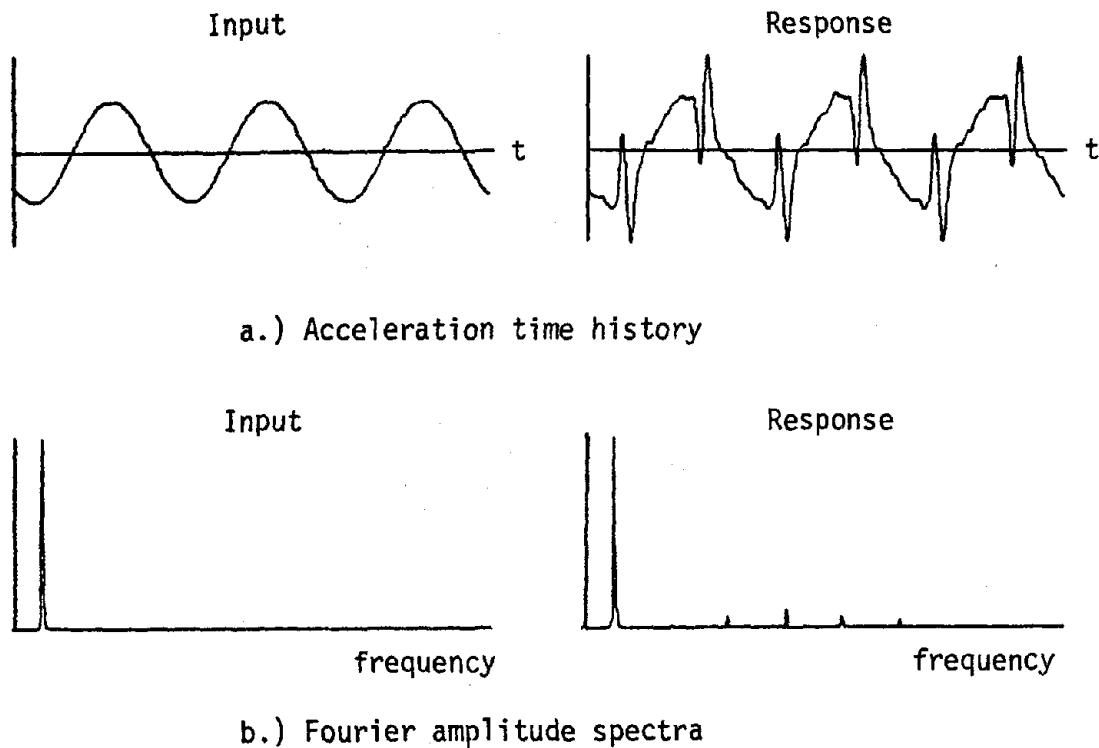


Figure 3.8 Sine Wave Performance

The use of a time history signal composed of several distinct frequency components could be used to find similar information as for single sine waves, but would also show any interaction effects between frequency components. This type of test would also better simulate earthquake input characteristics while still possessing distinct properties which allow less complex definition of shake table behavior.

Various Fourier spectrum analysis approaches utilize random input signals to define the response characteristics of a linear system. White noise, modified by filtering to a given frequency range, can be used as input to the shake table, enabling calculation of the table transfer function and coherence function through spectrum averaging techniques. For perfect duplication of input motion the transfer function would show uniform amplitude versus frequency with zero shift in phase. Any variation in amplitude or phase would illustrate performance inadequacies of the earthquake simulator. Such distortions could then be considered as deterministic, provided the coherence function is approximately equal to unity for the frequency range of interest. Variation of the coherence function from a value of one would indicate that shake table distortions and the corresponding measured transfer function are not a stationary or statistically definable process.

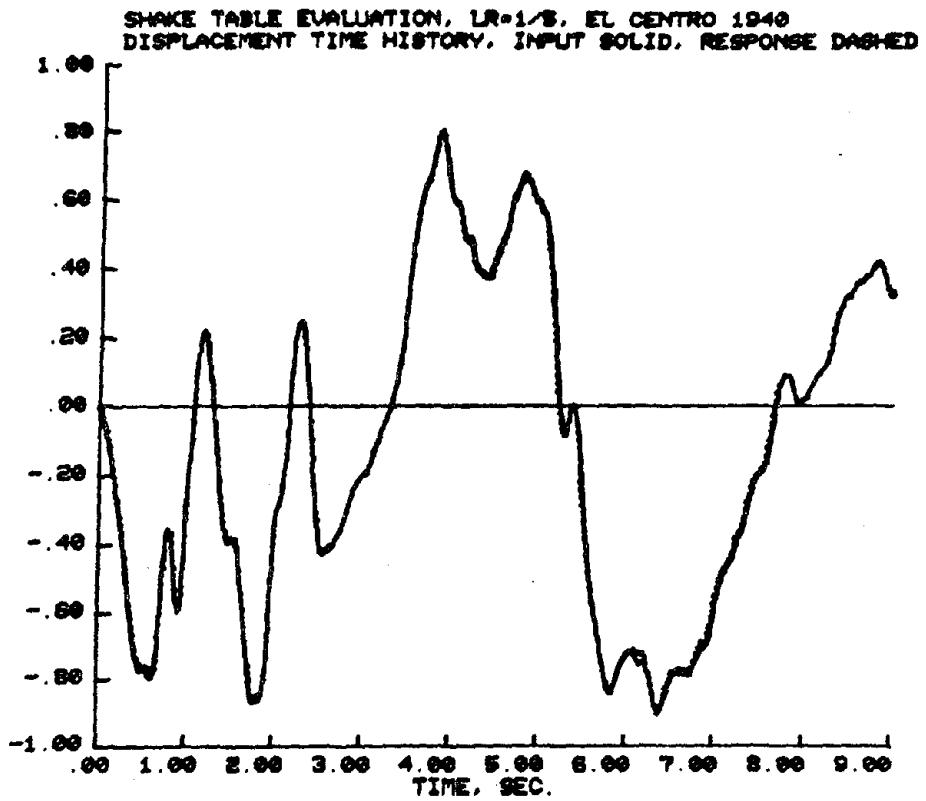
Problems may be encountered with such Fourier spectral methods concerning the requirements on input and response signal characteristics. Generally, shake table response accelerations are best suited for such analysis, yet a displacement input may be desirable for optimum shake table control. For accurate analysis, then, the acceleration time history corresponding to the input displacement record must have fairly uniform spectral energy, such as for a white noise process. Analog integrating devices could be utilized to provide the required displacement control

signal, but may also distort the input signal during the double integrating process. Imperfections due to the electronic integrating circuits would be difficult to isolate from actual shake table distortions.

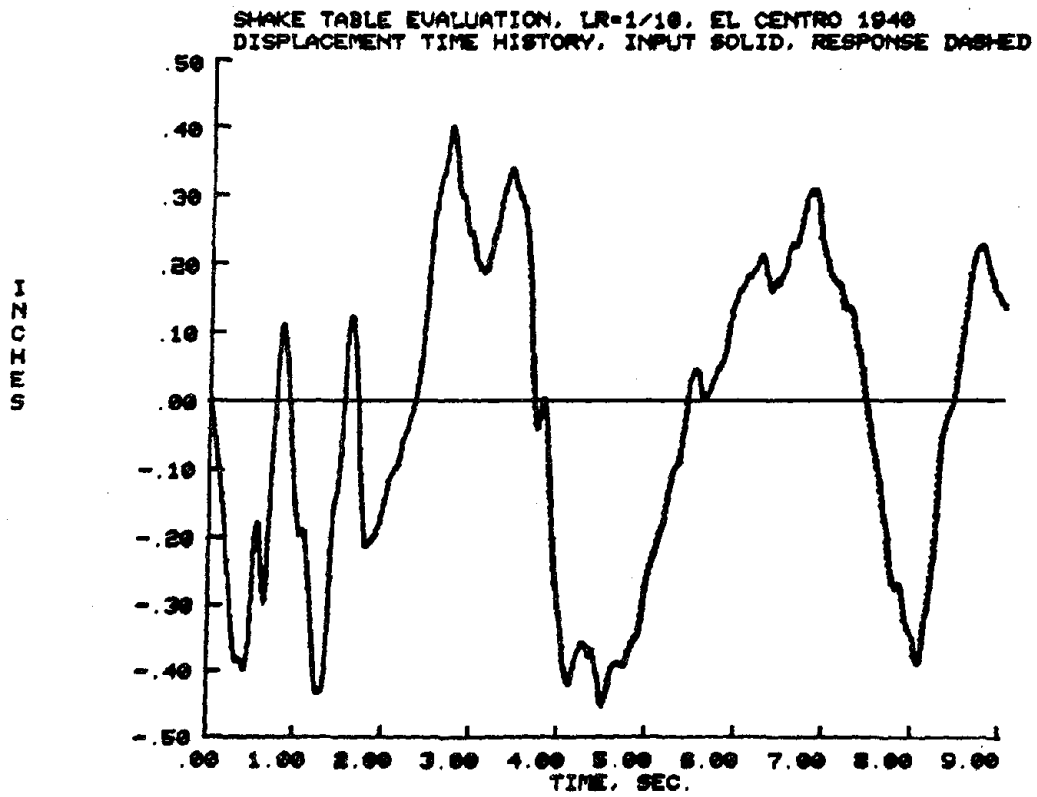
Of primary interest in dynamic model studies is the response behavior of a structural system to input motions characteristic of an actual earthquake. It is then necessary to establish some general guidelines for shake table performance to ensure adequate representation of such input motion.

An initial, subjective determination of the quality of shake table reproduction can be made by visual comparison of the time history response of the table with the input record. These comparisons, generally of the displacement and acceleration time histories, would be necessary for various model scaling factors and different values of shake table payload. Such observations can be quite informative in the identification of shake table performance irregularities. Displacement time history comparisons will usually not provide as much insight as acceleration comparisons. As displacements are commonly used by the system as a control parameter, reproduction of displacements is generally quite good. Also, certain table inadequacies are characterized by high-frequency distortions which would not be readily apparent in a displacement record.

As an example of time history duplication, let us consider the time history plots for displacement and acceleration response of the unloaded Stanford University shake table, with the N-S component of the El Centro 1940 earthquake as input (Figures 3.9, 3.10). These tests were performed using the earthquake displacement record as an input command, modified for a 1:5 and 1:10 scale true replica model test. The displacement response is almost identical to the original earthquake record. A comparison of accelerations shows that high-frequency distortions, characterized by "spikes" in the table acceleration response, are apparent and are of

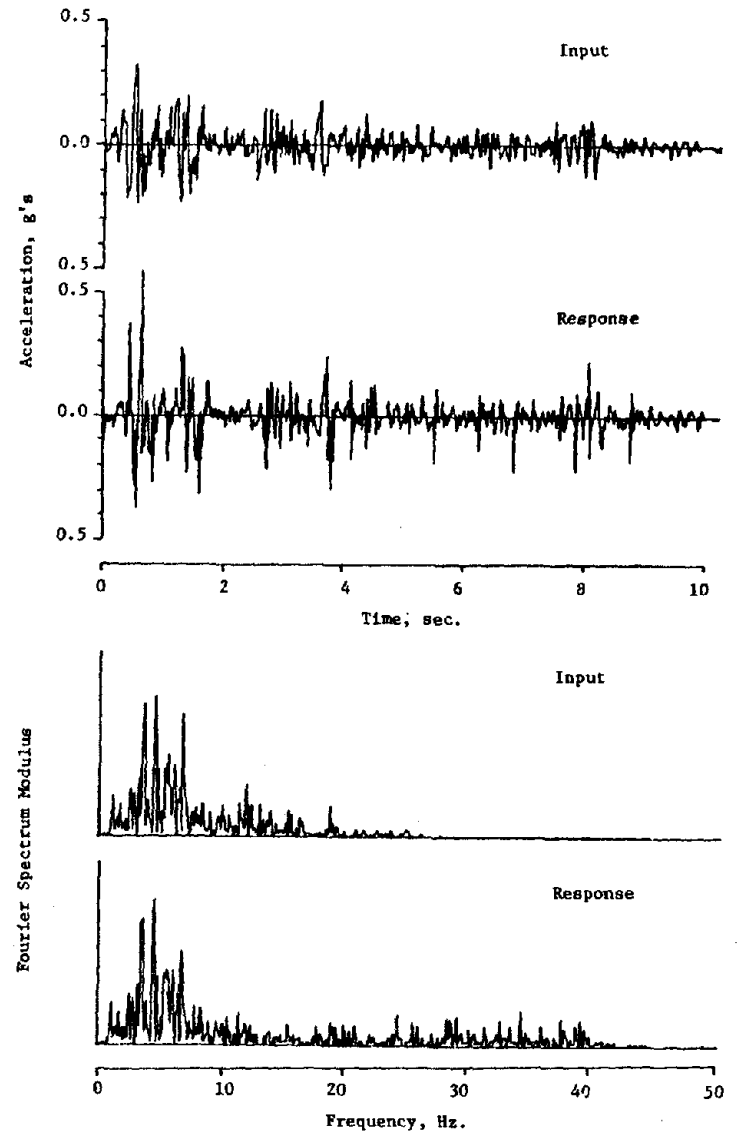
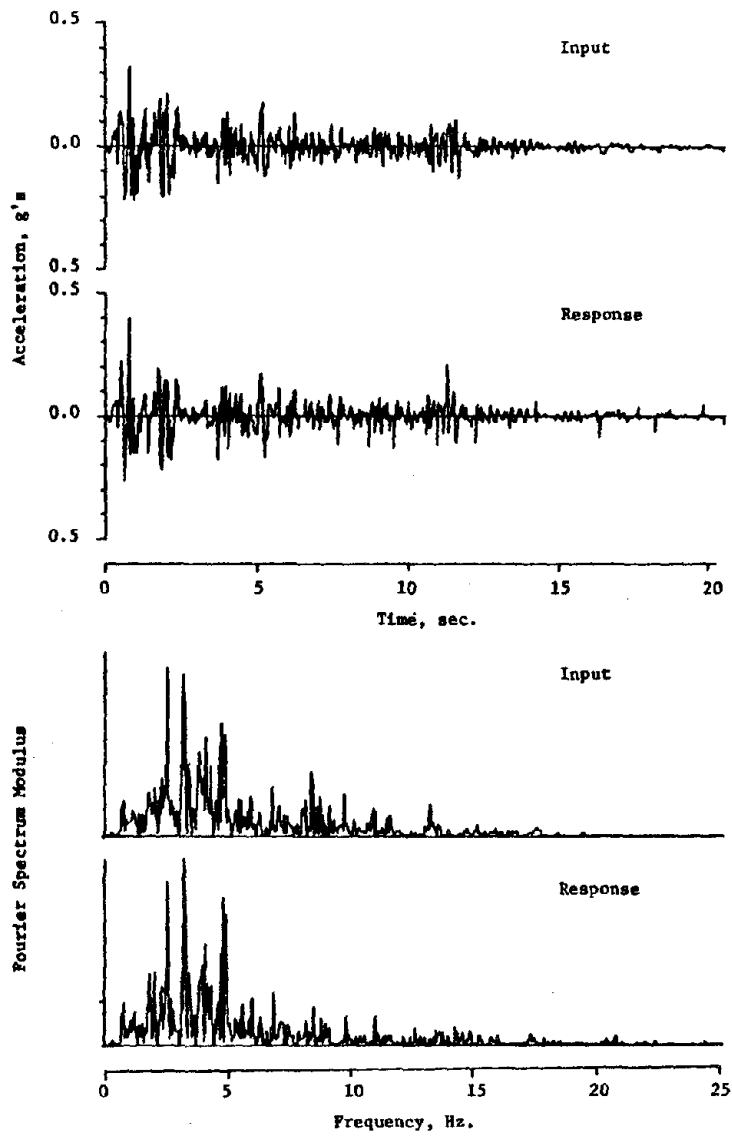


(a) For 1:5 Scale True Replica Model



(b) For 1:10 Scale True Replica Model

Figure 3.9 Displacement Response Performance--Stanford Shake Table



(a) For 1:5 Scale True Replica Model

(b) For 1:10 Scale True Replica Model

Figure 3.10 Acceleration Response Performance--Stanford Shake Table

increasing severity with smaller modeling scales. Further investigations showed that this phenomenon was caused by static friction, "stiction," in the shake table support and drive mechanisms. This stiction occurs at each point where shake table velocity has reached a zero value.

A Fourier analysis of the acceleration signal (Figure 3.10) shows that the energy of the shake table response is in close agreement with that for the original earthquake record for lower frequency ranges. However, high-frequency distortion is apparent due to shake table stiction. Other irregularities can be attributed to numerical inaccuracies inherent in the methods used to create a shake table compatible displacement record from the measured El Centro accelerations as well as to additional shake table inadequacies.

Similar comparisons of input and response can be made for an acceleration input mode of operation. In this case the actual earthquake acceleration record was input to the shake table and processed by analog integrators to provide the necessary displacement control signal. This method of operation did not provide optimum results on the Stanford shake table due to a lack of required sensitivity to produce the necessarily small input displacements which are derived from model similitude. This inadequacy became more apparent for smaller modeling scales and correspondingly smaller displacement requirements, and is distinguished by regions of zero table response where input commands are below table sensitivity capacities.

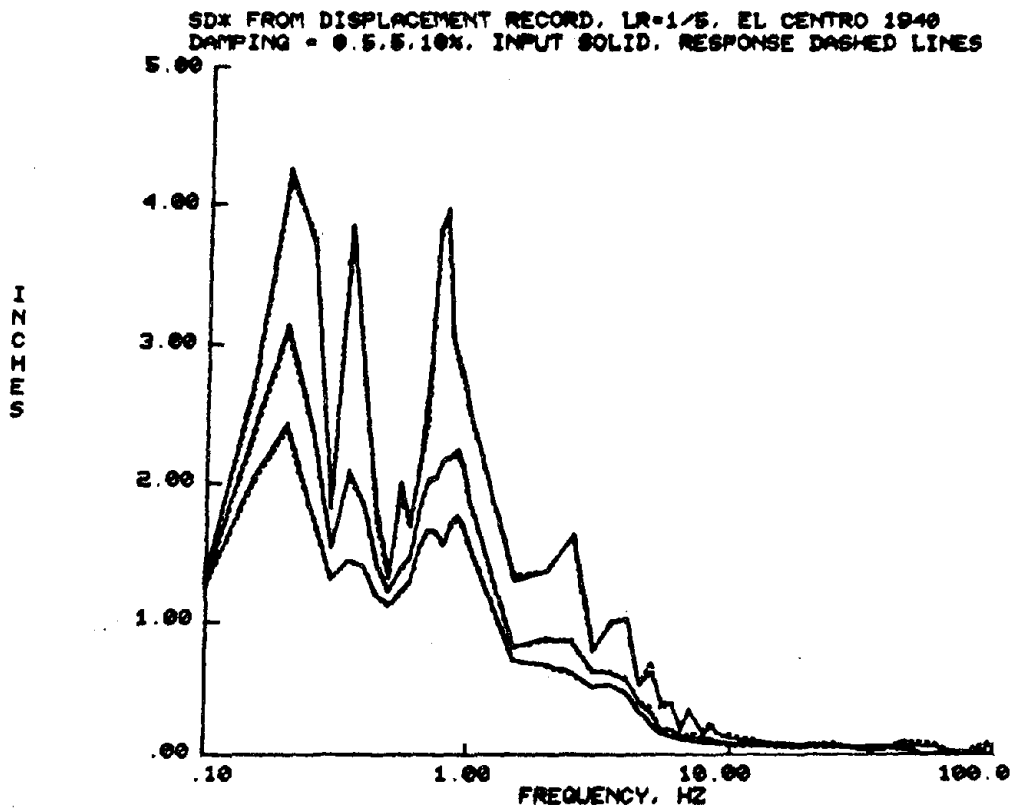
Response spectra analysis possibly provides the single most comprehensive method of earthquake simulator performance evaluation applicable to small-scale model studies. As structural response can be idealized as a composite of individual modal contributions, response spectra are an accurate means of illustrating the maximum response demand on a model structure. Thus, to generate the same character of earthquake response

behavior in the small-scale model as anticipated for the prototype structure, the shake table motion response spectra should show favorable comparison with that for the prototype earthquake. Response spectra for both linear-elastic and non-linear oscillators could serve as criteria to define the suitability of simulator motion.

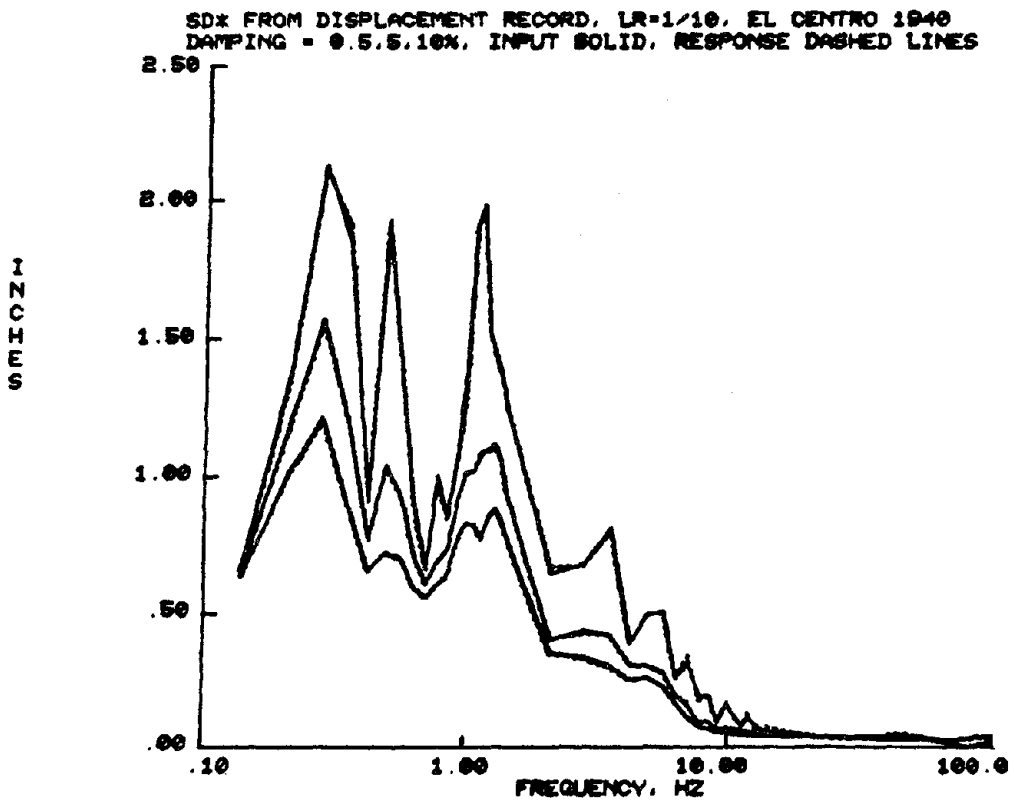
Response spectra calculated from either displacement or acceleration time histories are possible alternatives to be used to illustrate shake table abilities. As mentioned previously, comparisons of displacement response will not provide particular insight into table inadequacies. The test results shown in Figure 3.11 were obtained from displacement time histories for an unloaded table condition, and show virtually no apparent differences for the displacement response spectra.

Comparisons of response spectra calculated from the actual earthquake and shake table response acceleration time histories provide considerably more information concerning table behavior. Tripartite plots derived for such a comparison on the Stanford shake table are shown in Figure 3.12.

A more detailed study would involve calculation of individual displacement, velocity and acceleration response spectra, as each spectra will serve to illustrate table behavior for a particular frequency range. The displacement response spectra would tend to show any table distortion at low frequencies, while median and high frequency range behavior inadequacies would be amplified by velocity and acceleration response spectra, respectively. Such test results are shown in Figures 3.13 and 3.14 for the unloaded Stanford facility and for different values of oscillator damping. While the displacement and velocity response spectra show adequate performance for this simulator, the high-frequency "stiction" problem becomes apparent by the amplification of oscillator response at higher frequencies. Though most small-scale models will tend to have fundamental natural



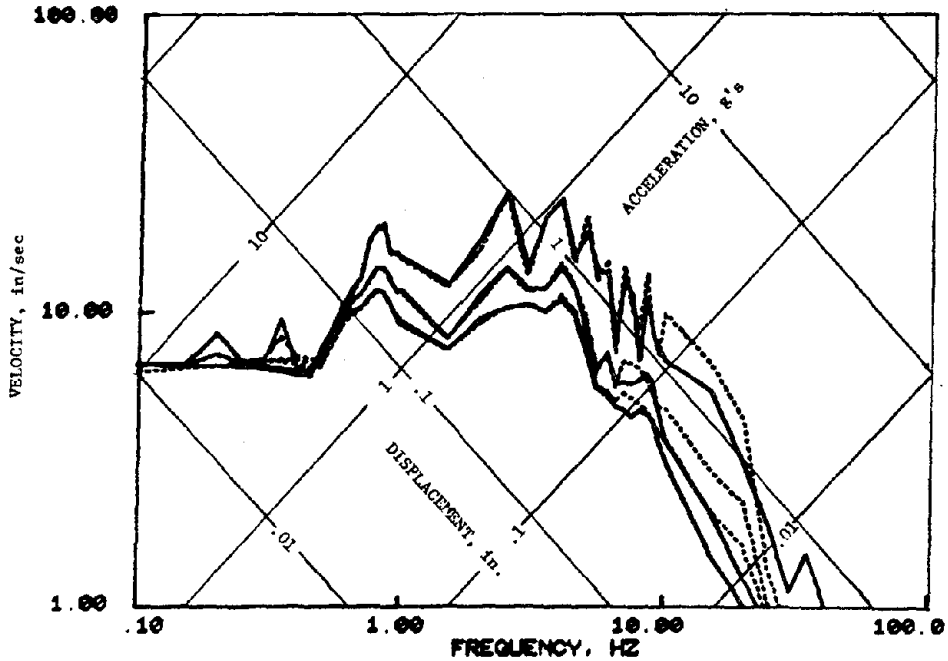
(a) For 1:5 Scale True Replica Model



(b) For 1:10 Scale True Replica Model

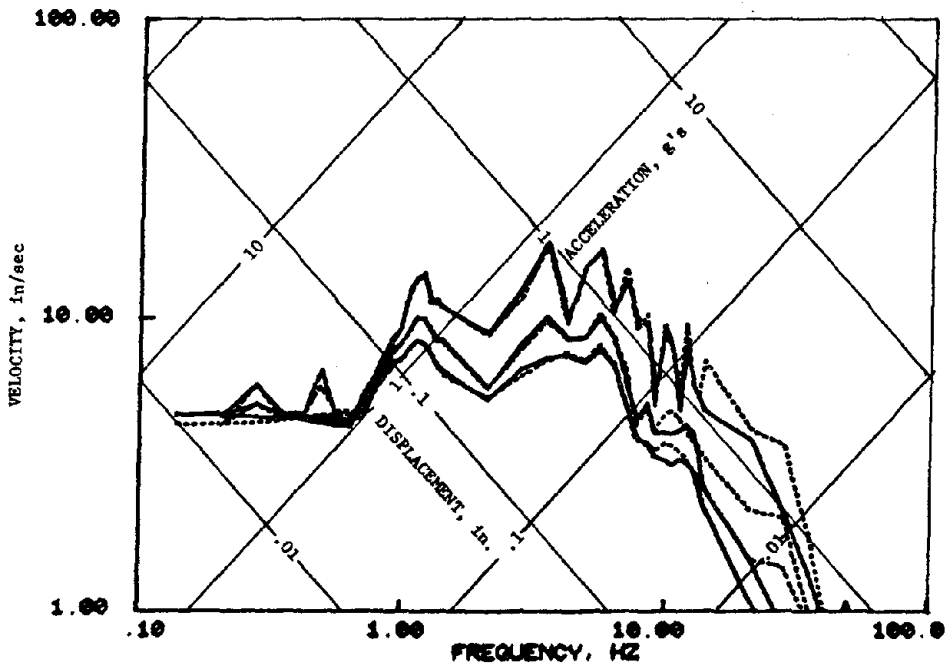
Figure 3.11 Displacement Response Spectra from Displacement Records--
Stanford Shake Table

SHAKE TABLE EVALUATION, LR=1/5, EL CENTRO 1940
DAMPING = 0.5, 5.0, 10.0 %
INPUT = SOLID LINE
RESPONSE = DASHED LINE



(a) For 1:5 Scale True Replica Model

SHAKE TABLE EVALUATION, LR=1/10, EL CENTRO 1940
DAMPING = 0.5, 5.0, 10.0 %
INPUT = SOLID LINE
RESPONSE = DASHED LINE



(b) For 1:10 Scale True Replica Model

Figure 3.12 Tripartite Response Spectra--Stanford Shake Table

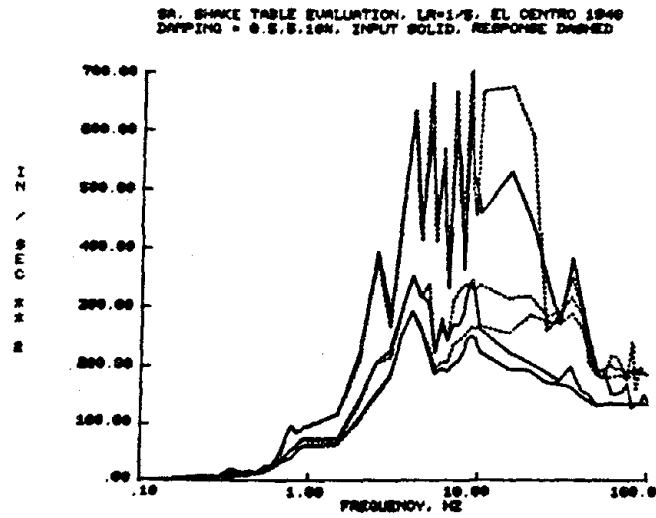
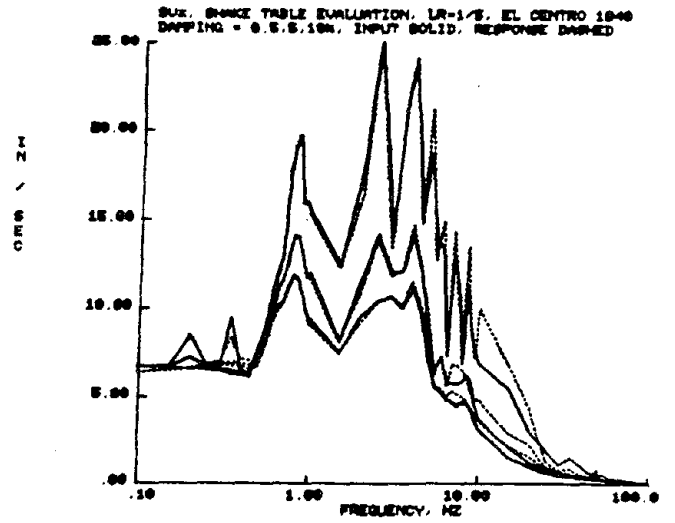
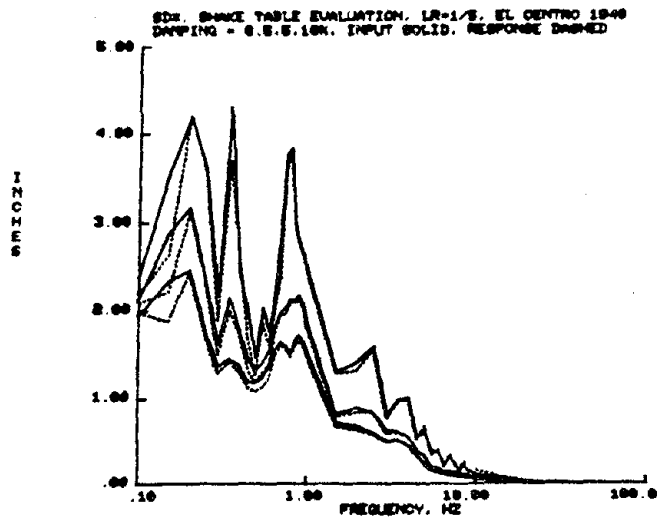


Figure 3.13 Response Spectra from Acceleration Records--Stanford Shake Table (1:5 Scale True Replica Model)

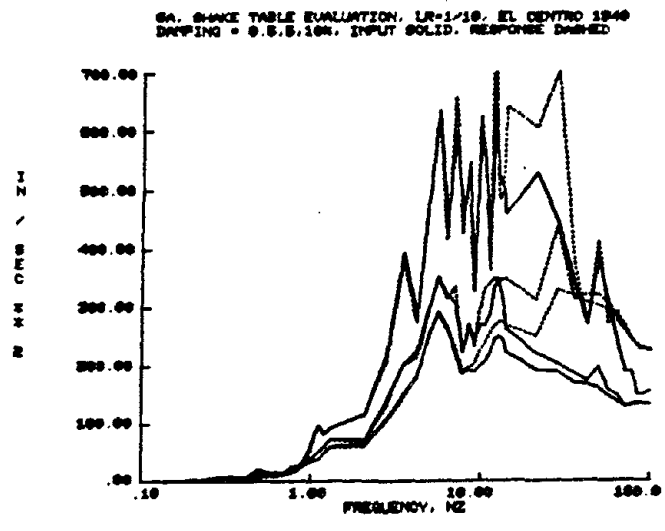
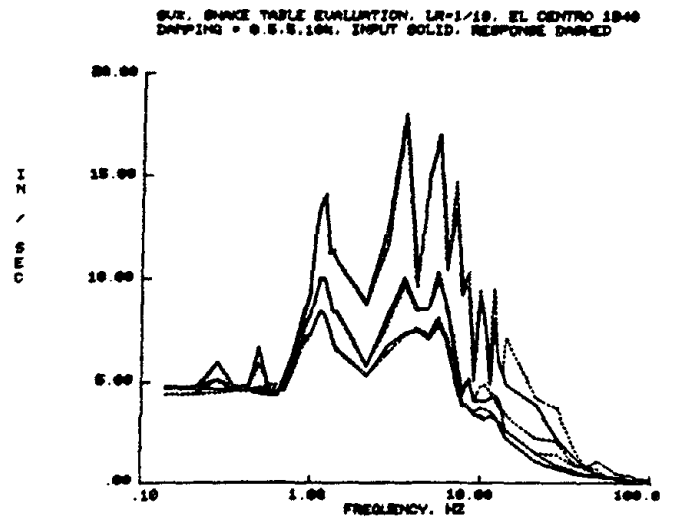
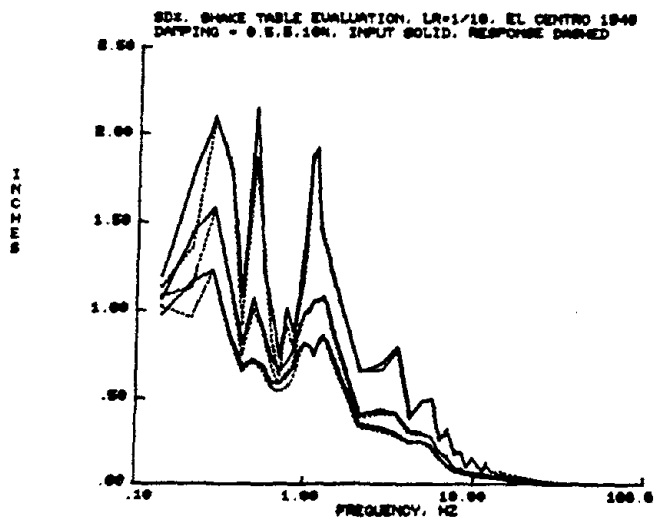


Figure 3.14 Response Spectra from Acceleration Records--Stanford Shake Table (1:10 Scale True Replica Model)

frequencies below this region of response distortion, the stiction phenomenon may contribute to higher modes of vibration.

As model behavior past the linearly-elastic range is of considerable importance to earthquake engineering research, the response of a non-linear oscillator to shake table motion is also desirable as a measure of simulator adequacy. Response behavior from such a study should produce results similar to those obtained for a linear oscillator with high viscous damping, which will lessen the effects of shake table distortions by smoothing of the response spectra envelope.

Iterative methods for improving spectral performance of earthquake simulators have been developed (23). These methods involve calculation of a transfer function corresponding to the shake table response characteristics under actual conditions for a given model test. The input time history is then modified by this transfer function to form an input command signal to the shake table, which when distorted by the particular shake table response behavior produces the desired spectrum. Such methods do require the capability for simultaneous computer output of the shake table input command and sampling of the table response to be effective, which may be beyond the capacity of some experimental systems.

Single degree of freedom time history response can also be used for comparison of shake table response characteristics. In such studies the response of an oscillator with given values of natural frequency and damping is calculated under loading conditions of the actual earthquake motion and of the measured table motion. A point by point comparison of the two time history responses can then be made as a measure of simulator reproduction capabilities. However, this type of analysis requires so many control parameter variations that its usefulness is somewhat limited. Many different comparisons would have to be made for different fundamental

frequencies and values of viscous damping to provide a complete overview of table response. Various yield-criteria would also have to be defined if non-linear oscillator response was to be used to provide additional comparisons.

Finally, the requirement of precise duplication of time history oscillator response is usually not a necessary requirement for model analysis studies. The goal of a small-scale model study is not necessarily a complete duplication of prototype time history response but a simulation of the same general behavior concerning intensity levels and ductility demands as for the prototype structure. Since model behavior will be dependent on many other factors besides shake table performance abilities, such as material properties, construction techniques, modeling approximations, etc., which will further serve to alter model response, such stringent requirements on simulator capabilities are usually not necessary.

3.3 Material and Component Test System

3.3.1 Performance Requirements

Detailed information concerning material properties and structural component behavior is required to enable proper simulation of prototype response by a small-scale replica model subjected to dynamic loading. Thus, a material and component test system must be an integral component of the dynamic test facility. The material and component test objectives can be stated in general terms:

- 1.) Define mechanical properties, either material or structural, to enable prototype-model response correlation.
- 2.) Verify the adequacy of fabrication techniques.
- 3.) Evaluate and calibrate instrumentation.

The performance requirements of this test system will be affected by the scaling laws derived from dimensional analysis as were those of

the earthquake simulation system, i.e., scaling of time and length parameters, leading to the necessity of well-controlled tests at various loading rates. For this type of testing, a servo-feedback controlled loading system driven by hydraulic pressure is most applicable. Such a device operates in a fashion similar to hydraulically driven shake tables as described in Section 3.2 except that displacement may not be the only parameter applicable to system control. In fact, system control may be provided by displacement, strain or load feedback, providing a wide range of testing applications. For instance, by utilizing specimen strain for system control the effects of strain rate on material properties can be studied in great detail.

Length scaling may produce very small specimens for testing on the material and component test system. Thus, adverse loading effects must be minimized to produce reliable test results. As an example, uniaxial tests of coupons taken from scaled rolled sections must be properly aligned to eliminate loading eccentricity, which would lead to non-uniform yielding of the specimen. Small specimens will also demand extreme system sensitivity to provide adequate control of the test and good resolution of test results.

3.3.2 Input Command Signal

Various types of input command signal may be desirable for a particular test. The chosen signal would be used for control of the test system, either by displacement, strain or load feedback. Several types of signal forms which may be useful are:

1. Ramp loading
2. Triangular wave
3. Sinusoidal wave
4. Complex waveforms

Obviously, rate effects are of considerable importance in dynamic model studies and must be evaluated to provide meaningful correlation between model and prototype structures. Static and dynamic material tests will often utilize specimen strain for control of the test system. In this way, strain rate can be used for classification of material properties which vary as a function of loading rate. Displacement or load control may be utilized where strain does not provide adequate control over the testing system or where strains are no longer applicable for system control. Thus, displacement control is most desirable for structural component tests.

In the following discussion of input signal forms, the term "loading rate" may apply to either strain, displacement, or load rate control, whichever is most applicable to a given test situation.

A ramp signal may be used to provide a constant loading rate and is most useful for unidirectional material tests. Either tension or compression material tests can be performed at various values of strain rate to provide a standard of comparison for test results.

Cyclic tests of either materials or components may utilize triangular or sinusoidal wave forms for system control. Triangular waves provide essentially a constant rate of loading, however a discontinuity occurs at each peak. This abrupt change in loading rate polarity may cause significant problems with test system control and may produce considerable distortion of the desired loading signal by the inability of the test system to follow such a discontinuity.

Sinusoidal waves may then provide optimum control over system loading for a cyclic test. Not only does a sinusoidal signal provide a continuous loading rate, but also replicates more realistically the loading character experienced by a structural member or, at an even finer level, by the

structural material at a point. The sine wave would then be defined by a specific frequency or, if desired, by the maximum loading rate, which is equivalent to the peak value of the first derivative.

Under the general heading of complex wave forms are many possible types of input signals which may be desired for a given test. Random signals, such as white noise, might prove useful for model related material and component tests. However, a more useful type of loading function would be an input signal corresponding to an actual time history of response, either determined experimentally or analytically, for a critical location in the structural model. Thus, a material or component specimen could be subjected to loading conditions identical to those experienced by a counterpart in the dynamic model. This would enable experimental testing to resolve some critical aspect of model response, such as the behavior of a structural joint, by permitting full attentiveness on this one specific part.

Analog signal generators are commonly available to produce ramp, triangular and sinusoidal waveforms as well as white noise. More complex time histories will require utilization of a digital computer with digital to analog conversion capabilities for experimental loading control. Such a system would be used for material and component tests in a similar fashion as for the earthquake simulation system (Section 3.2).

3.4 Instrumentation

Successful small-scale model experimentation is dependent on an extensive network of instrumentation to provide an adequate assessment of model response behavior. This instrumentation system should consist of sufficient transducers to permit a comprehensive investigation of model and prototype integrity through direct evaluation of pertinent measured

quantities and of derived quantities, such as spectra, energy terms, story forces and member forces. Also, since an evaluation of inelastic behavior is essential to studies of structural response to earthquakes, the instrumentation system must be capable of sensing yield levels in critical components and of providing information on ductility and energy dissipation characteristics.

Scaling of physical parameters required by modeling theory will have a distinct effect on the desired character of the instrumentation system. As structural models will be considerably scaled in size, transducers will also generally have to be relatively small to enable physical connection at desired measuring nodes. Physical parameters (e.g., displacements, accelerations, loads, etc.) may vary in magnitude as some function of the length scale for the particular model under study, requiring experimental transducers with wide ranges of sensitivity to produce the accuracy levels essential for model investigations. Scaling of time will place requirements on instrument response times and good high-frequency characteristics.

A primary concern in the development of the instrumentation system is the minimization of sensor interference with model response. Adverse transducer contributions to model behavior could be caused by such sources as excessive mass, friction between instrument connections and relatively high force levels applied by sensors to the model.

If a particular transducer is mounted directly on the vibrating model, inertial effects may be critical. In the case of a high ratio of transducer to model mass it may become necessary to design the model such that the mass of the instrument is included as some portion of the model mass. The possibility of using miniature transducers, if available, could also be investigated to aid in reduction of sensor contribution to small-scale model response.

Friction effects must be minimized by careful design and alignment of experimental instruments or eliminated entirely by the use of remote measuring devices which require no actual physical connection between the model and the physical datum point. The problem of instrument misalignment has actually been observed to produce an apparent damping increase from a true value of 0.2 percent to 2 percent when a displacement transducer connection was improperly adjusted for a particular small-scale model study.

Automatic data acquisition techniques are essential to the accurate evaluation of model response. High-speed computers with analog to digital conversion capabilities are utilized to provide the sampling rates and numbers of physical measurements necessary for small-scale model studies. Any sensor devices to be used for such an experimental investigation must be compatible with the data acquisition system. Electronic transducers and corresponding signal conditioning devices will then be necessary to provide a voltage signal in proportion to some measured physical quantity for evaluation by the data acquisition system. These electronic transducers must also be capable of supplying the necessary ranges of sensitivity and performance abilities to provide the accuracy essential to model studies.

The first step in the development of an experimental system is to identify the important response quantities for successful evaluation of experimental tests. As mentioned previously, not only response quantities for direct measurement but also parameters to be used in the analytical derivation of additional representations of model characteristics must be considered. The instrumentation system must also be capable of monitoring all types of experimentation: material, structural component, and shake table tests, necessary for the successful evaluation of model response.

Following is a list of basic response quantities whose direct measurement is felt to be of primary importance to the evaluation of structural response to earthquake loadings.

1. Force--direct force measurement in certain structural elements will often be necessary to establish dynamic equilibrium of forces or energy terms and to extract basic quantities such as story shears.
2. Strain, deformation.
3. Displacement--either relative or absolute displacement measurements may be required. In the case of relative floor displacements the option exists for measuring relative displacement directly, in which case a rigid reference must be provided on the shake table, or indirectly as the difference between absolute displacement, measured relative to some datum frame outside the shake table reference, and the shake table displacement.
4. Velocity--though velocity transducers are available, velocity will commonly be obtained by differentiation of the displacement record or by integration of the acceleration time history. Again, either absolute or relative quantities may be necessary.
5. Acceleration--both linear and rotational accelerations may be of interest.
6. Angular rotation.
7. Time, frequency.

Various electronic transducers are commercially available to provide measurement of these important response parameters. However, certain custom instrumentation designs may be required for a particular model study, requiring adaption of available sensors to perform a specific

measurement. A brief list of feasible instrumentation for use in small-scale model experiments is given below.

Commercially available instrumentation:

1. Force transducers--standard axial force transducers are of limited use in dynamic model studies except perhaps for the measurement of overturning forces in columns. Most commonly used for material and component tests.
2. Strain gage--available in a wide variety of sizes and types. Post-yield gages can be used to monitor inelastic deformations.
3. Extensometer--conveniently used in material studies for strain measurement and control.
4. LVDT--linear variable differential transformer. A displacement transducer, generally requiring a.c. excitation and appropriate signal conditioning devices to provide a signal compatible with the data acquisition system. When properly aligned, they produce virtually no frictional force contributions to model response, provided lateral displacements and rotations are small at the measurement nodes. Flexible connections may be required if lateral motions and rotations exist to prevent binding of the core.
5. RVDT--for the measurement of relative rotations.
6. Potentiometer--simple to use for displacement measurements because of d.c. voltage requirements; however, they may apply relatively large force levels to the model.
7. Accelerometer--linear and rotational. Both piezoelectric and servo-balance type accelerometers are available. Piezoelectric accelerometers have advantages of small size and low mass (0.20" x 0.25" x 0.30" and 0.05 ounces for the Endevco Model 23 tri-axial accelerometer) but have disadvantages of low acceleration

sensitivity, poor low frequency response and unusual signal conditioning requirements and are best suited to shock and impact studies. Servo-balance accelerometers are characterized by a wide range of measurement application (approximately 0.001g-100g) and possess good frequency characteristics for model research, but may have some size limitations for very small models.

8. Laser interferometer--a remote device, permitting measurement of displacement with no physical connection between the model and the datum point. Laser interferometers are extremely accurate, but require constant alignment of a reflective crystal mounted on the model to provide a target for the laser beam. Thus, large rotations or displacements lateral to the beam axis would not be permitted.
9. High-speed camera--may be used not only for visual observation of model response but for determination of relative motion between structural components as a function of time.
10. Oscilloscope--for time base display of transducer response measurements.
11. Computer based timer--the data acquisition system is programmed to take physical measurements at instants very accurately spaced in time (1 μ sec resolution).

Examples of custom instrumentation:

1. Member force transducer--specially designed dynamometers capable of measuring all six force components can easily be built into individual members of structural models. Alternatively, strain gage arrangements attached directly to the structural element and calibrated through known static loads have been shown to give accurate force measurements.

2. Relative displacement transducer--model studies may require relative displacement measurements over a gage length too small for LVDT installation. Commercially available displacement transducers composed of silastic tubing filled with mercury are suitable for small-scale model applications. One such gage is illustrated in Figure 3.15. A properly pretensioned mercury gage provides a linear variation of resistance to strain provided the strain level is small compared to the unstretched length. These gages are relatively inexpensive; however, lifetimes are limited to 6-12 months. Low resistance levels of approximately 0.3 ohms/inch will require the use of unbalanced bridge configurations for most signal conditioning units, producing relatively low sensitivity and the need for shielded cable to reduce interference from external sources. In one application at Stanford University, a relative displacement transducer using an unbalanced 4-arm bridge with two 120 ohm dummy resistors and two 0.75 inch mercury gages exhibited a calibration constant of approximately 0.003 in./volt per active arm at a conditioner sensitivity of 0.01 mv/v. Individual calibration of each gage is also required to enable desired measurement accuracies.

3.5 Data Acquisition

The purpose of the data acquisition system is to permanently record the voltage signal from a block of experimental transducers which respond to some physical quantity, such as strain, load, displacement, acceleration, etc. The performance characteristics of the system must be such that the signal recording is sufficient to permit desired analysis of the experimental results and should be adaptable to model and component (e.g.,

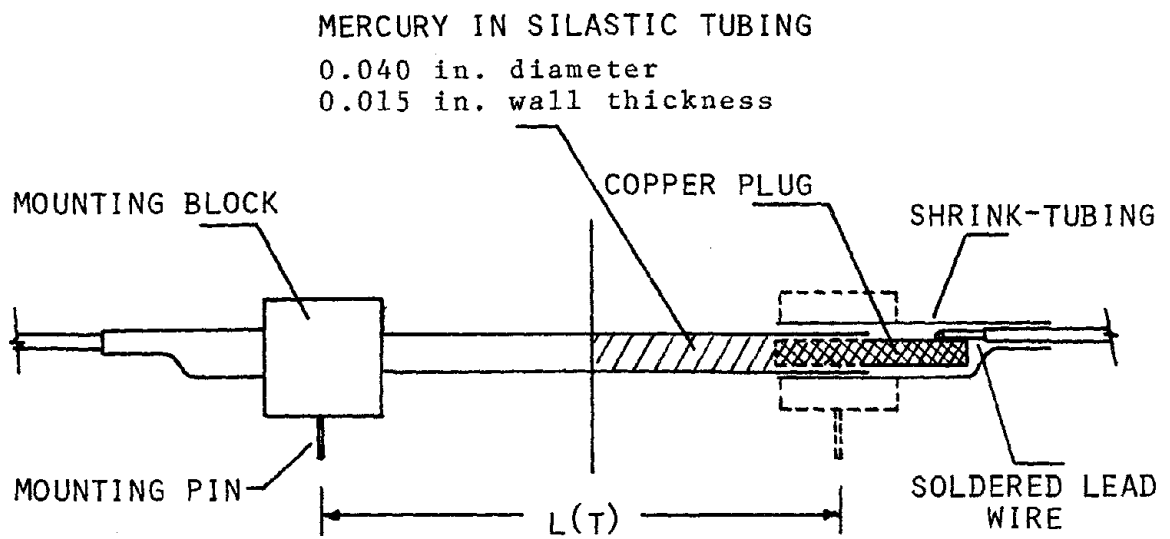


Figure 3.15 Silastic Mercury Gage

material, subassembly) tests. In addition, the data acquisition system must be compatible with the instrumentation system in regard to voltage signal requirements.

Various types of experimental recording devices are available, ranging from mechanical plotters, oscilloscopes and photo-recorders to high-speed computer systems with analog to digital (A-D) conversion capabilities. For the purpose of experiments related to small-scale replica models subjected to dynamic excitation, it will become apparent that a modern, digital computer system is essential to model experimentation. Such a system should be capable of performing essentially instantaneous scans of a block of data channels at fixed intervals of time for the duration of a dynamic test. For example, the Stanford University system performs sampling and digital conversion at the rate of 45,000 samples/second in a single block scan of up to 32 data channels. Even at such rapid rates, however, a finite length of time will be required to perform the complete data scan, approximately one milli-second for all 32 channels of the Stanford system. Thus, related channels to be compared in later data analysis must be sequentially grouped to minimize errors due to phase differences between recordings.

A digital recording system must be capable of high signal resolution to permit accurate experimental measurement and analysis of data. The resolution capabilities of the data acquisition system should be greater than or equal to the measurement accuracy supplied by the instrumentation system. For the Stanford system, the capacity is a total range of ± 10.235 volts at 0.005 volts resolution, permitting signal definition at 0.05 percent of full range, a capacity greater than that of most transducers and corresponding signal conditioners.

The requirements of dimensional analysis for replica modeling will have a direct effect on the necessary performance abilities of the data acquisition system, primarily in regard to the sampling rate capacity of the system. As time will generally be scaled in some proportion to the length scale, the data collection system will have to sample instrument output at a similarly increased rate. As an example, consider the simplified derivation of control parameters for a 1:10 scale true replica model given below.

Example 1: Model Test Sampling Rate

Given: prototype structure with fundamental period $T_p = 1.0$ sec

$$l_r = 1:10$$

$$t_r = \sqrt{l_r} = \sqrt{1/10}$$

$$\text{Model fundamental period: } T_m = T_p / \sqrt{10} = 0.32 \text{ sec}$$

For adequate response resolution of the fundamental mode and of possible higher modes and transient vibrations, choose sampling rate producing 40 scans/fundamental cycle.

$$\text{Required sampling period: } \Delta t = T_m / 40 = 0.008 \text{ sec}$$

Thus the system would be required to perform a data block scan every 8 milliseconds for this particular example. Models with greater time scaling requirements, either due to a higher model scale or a different type of model (e.g., gravity-neglected models with prototype material; $t_r = l_r$) would produce even more rapid sampling necessities.

Material tests conducted as part of a model study may produce even more severe requirements on high-rate data sampling capacity. As the rate of loading in a structural model is increased over that for the prototype, the required loading rate for a material test will be similarly increased, creating the necessity for high strain-rate testing. For adequate resolution of experimental data the sampling rate will be increased, as illustrated in the following example.

Example 2: High Strain Rate Material Test

Strain Rate $\dot{\epsilon} = 0.02$ in./in./sec.

Yield Strain of Material $\epsilon_y = 0.0012$ in./in.

If 20 data points are desired to define the stress-strain diagram to yielding, the required sampling period is $t = 0.0012 / (0.02 \times 20)$
 $= 0.003$ sec.

The number of data channels required to record all important aspects of model response should also be considered. Generally, the more complex the phenomenon under study, the more measurement nodes necessary for response evaluation, producing a similar requirement for the data acquisition system. Material and component experiments, however, will usually require fewer channels for proper behavior measurement than would an actual model experiment.

These high resolution, high-rate, multi-channel requirements for the data acquisition system can be satisfied by a digital computer with A-D capacities. A further advantage to such a system is that the experimental data is immediately converted to digital form, permitting the utilization of digital methods of response analysis.

Another consideration is the need for adequate storage space, readily accessible to the computer system, for the large number of data points generated by a single experiment. With the high sampling rates and multi-channel requirements of small-scale model research it is not uncommon for one test to produce more than one million data points. In addition, computer access to this storage area must be possible with minimal interference with the data acquisition process, which would reduce data sampling efficiency. Two methods of auxiliary storage are commonly available, and utilize either magnetic disc or tape units.

On some computer systems the primary advantage of using magnetic disc storage is that the data may be continuously stored as the test progresses. This method of transfer produces no interruptions in the data string, and will be limited in sampling rate essentially by the maximum disc transfer time. An example of such a system is the facility at the University of California, Berkeley, which has the capacity for 128 data channels with a maximum sampling rate of 20,000 samples/second at scan intervals of 0.01 seconds.

A magnetic tape unit is utilized for auxiliary data storage at Stanford University. Initially, the data resides as a block in computer core and is transferred to tape at discrete intervals of time with a corresponding interruption in data sampling at each data dump. The length of an interruption is the time required to transfer the block of data from one section of core to another. The actual transfer of data from core to tape is performed simultaneously with data acquisition. The observed dump time is then kept to a minimum value, and is a function of the block size utilized in core, as shown in Figure 3.16.

Since the transfer of data from core to tape will take a finite length of time, as determined by the tape storage rate, the transfer from a preceding data dump must be completed before the occurrence of the next dump. As the time between data transfers is a function of the sampling rate, block size, and number of data channels, and since the tape transfer time is solely dependent on the block size, the requirements to satisfy this condition can be summarized in a diagram such as that shown in Figure 3.17. As can be seen, tape transfer time may be of concern primarily for tests with high sampling rates (less than 2 milliseconds) and a large number of data channels.

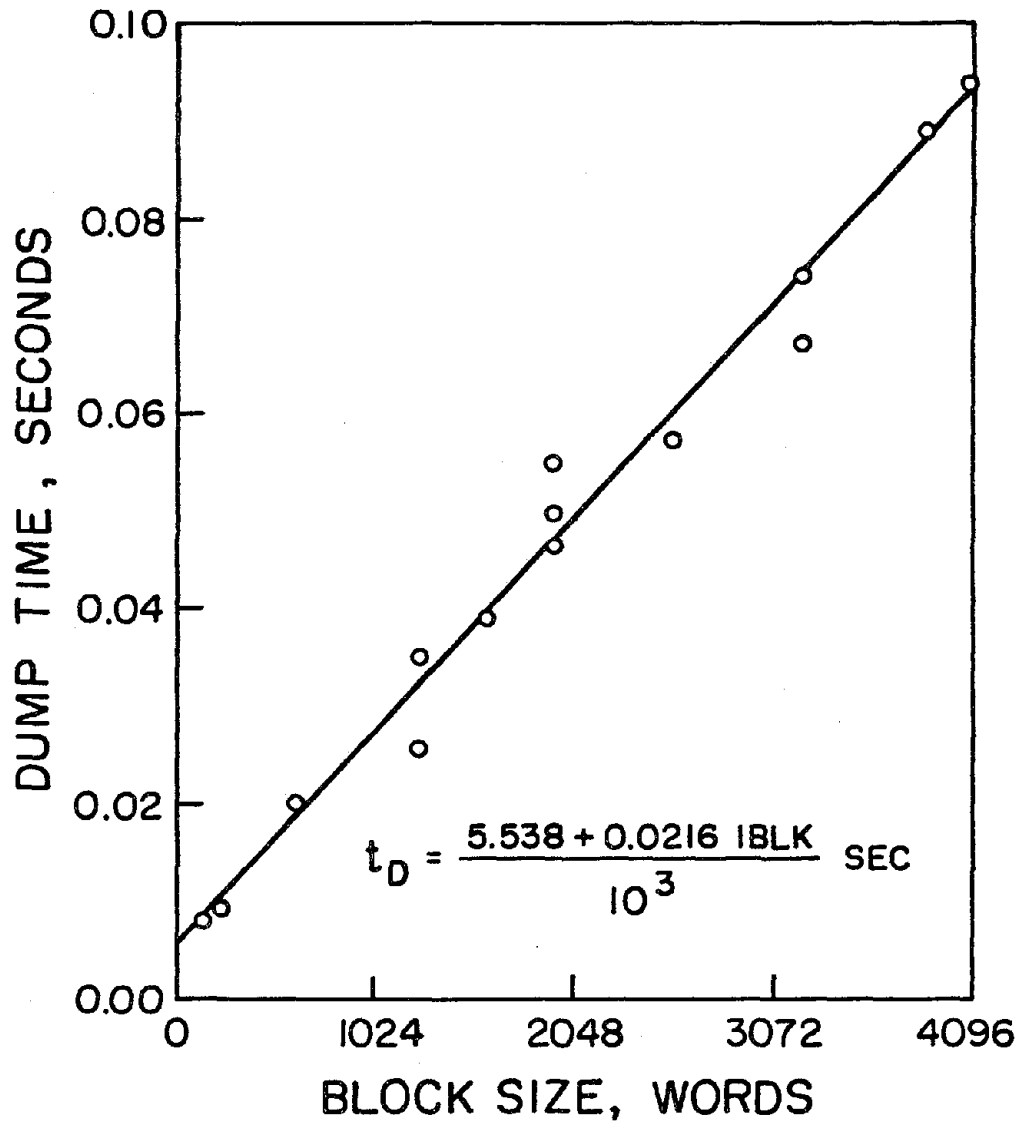


Figure 3.16 Dump Time vs. Block Size

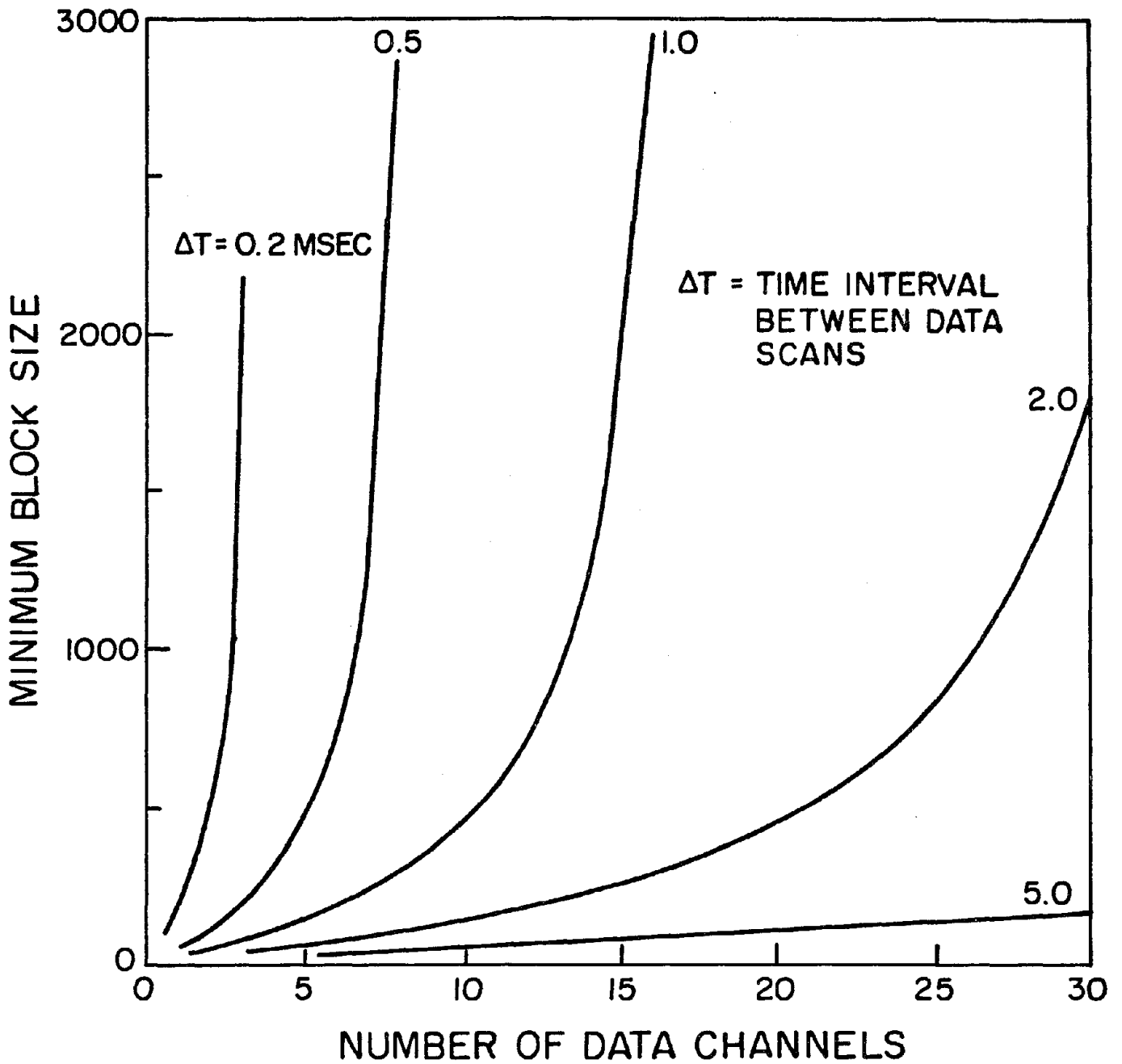


Figure 3.17 Minimum Block Size for Uninterrupted Data Transfer

For most tests a compromise will have to be reached between the number of data channels, the sampling rate and the block size in order to minimize the dump interruption and to allow complete transfer of data between dump intervals. The data channels should be chosen such that sufficient measurement nodes are available to permit accurate analysis of important response behavior, but should be kept to a minimal number to prevent extraneous data measurements, which would hinder sampling efficiency. The sampling rate will generally be dictated by the conditions of a particular test, permitting little flexibility with this parameter. However, the more rapid the sampling rate, the shorter the interval between data dumps and the greater the number of points lost at each interruption. The final parameter to be considered is the block size. A large block size will permit a greater time interval between data dumps, producing a maximum span of uninterrupted data acquisition, but will also produce a greater dump time and corresponding loss of data. An intermediate value of block size will then generally be desired to produce the greatest sampling efficiency.

Though the measurements lost at a data dump cannot be completely recovered, it is generally desirable to provide some sort of interpolation procedure, such as a third-order algebraic equation, to fill in the lost time interval. The resulting time history will be a continuous record as a function of true time. This type of procedure will usually provide acceptable results provided the dump time is small compared to the periodicity of the model response. Still, there may be a loss of transient vibrations and some distortion of model response, especially for tests where a large number of data points is lost at each dump occurrence.

Following is an example summarizing many of the aspects encountered in tape storage methods.

Example 3: Tape Storage Example--Stanford University

Consider $T_m = 0.32$ sec as for Example 1.

Assume number of channels = 15

Test criteria: Sample rate - 40 scans per fundamental cycle

Dump time - less than $T_m/4 = 0.08$ sec.

Choose: Sampling period $\Delta t = 0.32/40 = 0.008$ sec.

Block size NBLK = 3840 (3840/15 = 256 data scans/dump)

Check: Dump time (Figure 7.15) = 0.09 sec

Number of scans lost = $0.09/0.008 = 11$

Time between dumps = $(0.008)(256) = 2.048$ sec.

For this particular example, every 2.048 sec there will be a data dump with a corresponding measurement loss of 0.09 sec.

For high-rate material tests the loss of data at a dump is not permissible as the material test duration and the dump time will be of similar duration. Thus a data dump may cause the loss of a significant portion of the test results. However, since the test is short and the number of data channels is generally small, it is usually possible to store the entire test in computer core for subsequent transfer to magnetic tape after the test is completed. The high sampling rates required by such material tests can then be obtained with no loss of data due to the transfer to tape.

For any data acquisition system it is important that all pertinent test information be permanently stored with the test data file, and be accessible for later use by data reduction procedures. A list of desired information is given below.

1. Test identification, stating type of test, date, etc.
2. Number of data channels (if variable).
3. Individual channel identification, with a complete description of the parameter measured, including the physical units (e.g., inches, strain, etc.) and the calibration constant (unit/volt).
4. Sampling period.
5. Test duration.
6. Block size (if tape storage).

Most laboratory computer systems perform both data acquisition and signal generation duties. Though "simultaneous" performance of these tasks is generally possible, system efficiency will often be considerably reduced by such a procedure. Thus, the input signal for shake table or material test apparatus is generally stored on an analog tape recorder for subsequent use in the test procedure. The computer programs for data acquisition and signal generation can then be designed to provide interaction between tape recorded input command and data acquisition, permitting an "automatic" mode of experimental testing. As an example, consider the duty schedule for the system at Stanford University, as shown in Table 3.3. This table shows the interaction between the data acquisition program and the analog record stored on magnetic tape by the signal generation program, to enable a well-controlled test of model or material response.

Whether tape or disc storage is used, the experimental data will generally be stored in a similar manner. Data is recorded as a continuous, intermixed string of numbers in binary machine code. Subsequent computer analysis is necessary to sort individual channel measurements and convert the results to the actual physical measurement, which is then accessed by data reduction programs for plotting and analysis procedures.

Table 3.3

COMPUTER SYSTEM TEST SCHEDULE

Time (min.)	Tape Record Signal Generation Program		Minicomputer Data Acquisition Program
	Channel 1	Channel 2	
-6:00	0.00 volts	0.0 volts	scanning channel 2
-4:00	5.00 volts for system calibra- tion		
-3:00	0.00 volts	5.0 volts	begin timing
-2:00			scan data channels for initial datum, 1000 pts./channel
-1:00	set initial table dis- placement	0.0 volts	
-0:01			begin test sampling
0:00	output command signal end of output command signal		continue sampling to record free vibration

3.6 Data Reduction

Subsequent to data acquisition, various analysis procedures are required to enable evaluation of model and expected prototype response behavior. As a large number of data points is possible, high-speed digital computer application is essential to analysis of test results at a reasonable expenditure of time and efforts. Since the raw data recorded by the data acquisition system is commonly stored in digital form, these results are readily accessible by computer programs for digital analysis.

Initial data reduction would involve the conversion of the raw data from computer binary code to the actual physical measurement, sorting of individual data channel time histories and subtraction of the initial datum base. In addition, checks can be made for overload voltages and data read errors at this time. A permanent record of minimum and maximum voltage levels measured during data acquisition is generably useful to determine peak response levels and the adequacy of the sensitivity level of the test record--for optimum results the peak voltage demands should be close to the maximum voltage capacity of the data acquisition system. Other raw data reduction procedures would involve interpolation performed at acquisition interruptions, if required, and shifting of an individual time history if a particular experimental transducer or signal conditioner produced a significant phase shift in the test record.

Appraisal of experimental results is best accomplished through visual presentation of test data and derived quantities. Thus, plotting abilities must be developed for display of time history records, force-deformation records (e.g., moment-curvature), and frequency domain spectra. In addition, plotting programs can be designed to provide a variety of plotting-related functions, such as logarithmic axes, plot overlays, titles, scaling, etc.

Evaluation of model response can be made through both directly measured and analytically derived quantities in either the time or frequency domain. The most basic evaluation would involve direct time history comparisons of measured physical quantities, such as acceleration and strain. Other time histories, such as internal forces and velocity, could also be derived from basic time histories to allow additional evaluation.

Certain response records may be paired in an X-Y form to provide analysis of related quantities. For instance, moment-curvature comparisons would be useful to calculate ductility demands and energy dissipation characteristics.

Various energy calculations can be utilized to provide a comprehensive evaluation of model response and a means of comparing test results from multiple experimental tests on different scale models of the same prototype structure. Calculation of all pertinent energy terms, i.e., recoverable strain energy, kinetic energy, damping energy, inelastic dissipated (hysteritic) energy, and input energy, would be required for complete evaluation. Refer to Section 4.5.3 for a definition of these terms.

Frequency domain analysis, through either Fourier spectra or response spectra, provide a means of frequency content evaluation of measured time histories. Such methods are applicable to dynamic test results for evaluation of shake table performance, model fundamental modes, etc. Fourier spectrum methods also enable comparison of time history records in the frequency domain through determination of transfer relationships.

Various basic analytic procedures are required to perform the above mentioned data analysis. These procedures can be performed by a network of special purpose programs through access of data time history files.

This system, showing the more common analytic methods required for data reduction, is shown in Figure 3.18.

Finally, numerical filtering techniques may be required to enable minimization of adverse noise due either to electronic or analytic sources. Care should be taken to ensure that such methods do not provide so much filtering as to distort or eliminate important aspects of the physical response measurement.

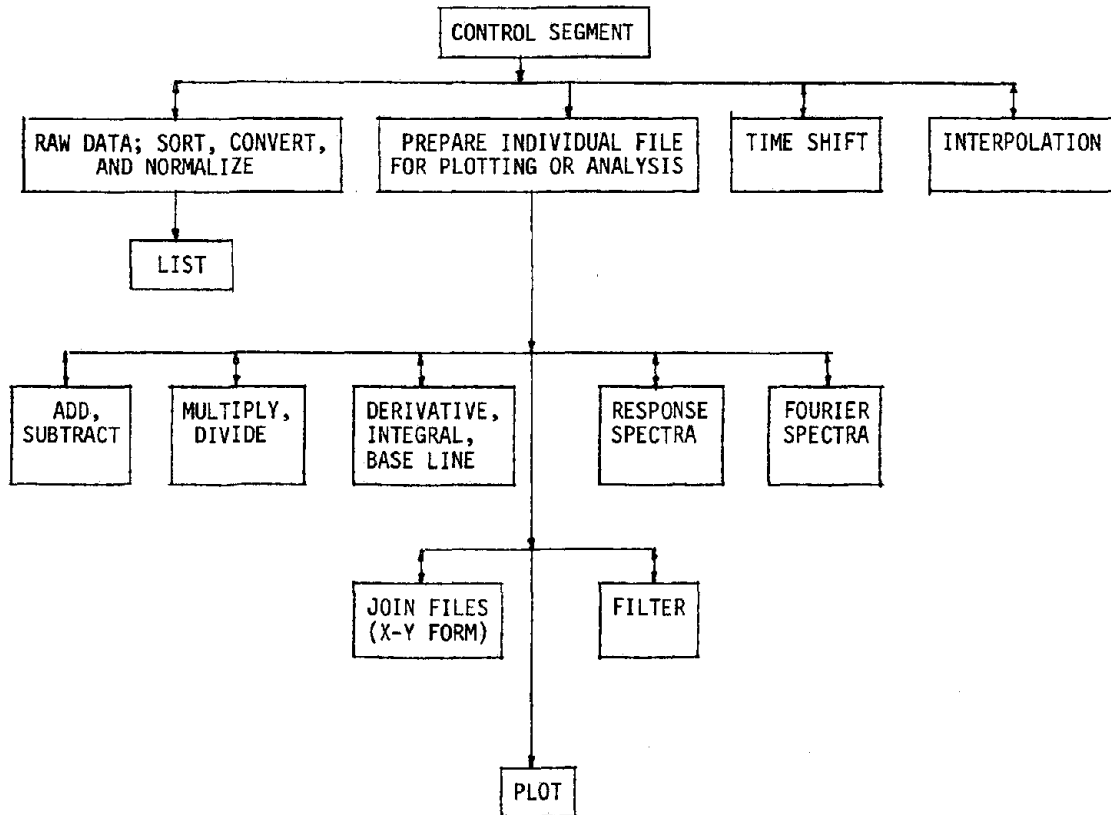


Figure 3.18 Basic Data Reduction Package

Chapter 4

MODELS OF STEEL-FRAME STRUCTURES UTILIZING ARTIFICIAL MASS SIMULATION

4.1 General Discussion

To aid in the development of methodologies for dynamic model fabrication, testing and analysis, a case study involving a small-scale replica model test is necessary. An actual model test will also serve to evaluate the experimental facilities required for such testing. Additionally, the case study should serve as an example to illustrate the feasibility of model testing as an alternative or complement to analytical procedures.

The chosen prototype structure should be sufficiently complex to enable a valid test evaluation and should ideally possess the capability for additional specific studies of such topics as the effects of bracing, floor diaphragms, infill walls, etc. To provide a basis for evaluation of modeling capabilities the prototype dynamic properties must be well-defined, so that a reliable correlation study of prototype and model response can be performed.

A form of dynamic modeling applicable to many types of building structures should be explored. However, the basic similitude requirements can take many forms, depending on the character of the prototype structure and the physical parameters considered to be directly contributory to the dynamic response of the structure. Thus, several types of models are feasible in dynamic studies.

The most general form of small-scale modeling involves true replication of gravitational and inertial effects by satisfying all pertinent similitude requirements. However, the greatest difficulty will be experienced in finding model materials with properties that satisfy these

requirements, yet still possess desirable characteristics for ease of model fabrication. For true replication of the prototype structure the model material must have a small ratio of modulus to mass density, specified as a function of the model length scale, yet still meet basic material property requirements (e.g., stress-strain curve, damping, etc.). The possibility of relaxing these material requirements through distortion of some similitude laws to enable greater flexibility of model material choice leads to what may be defined as an adequate model.

An adequate model type which is applicable to a great number of building structures where gravity effects must be included involves the addition of structurally uncoupled material to augment the density of the model structure. Thus, the structural material can be chosen to satisfy similitude requirements without regard for mass density, permitting the use of prototype materials as model materials. Yet, such modeling through "artificial mass simulation" is an ever more powerful tool, as other than prototype material may be utilized to avoid exceedence of earthquake simulator capabilities (see Section 3.2.1).

It is not within the context of this dissertation to delve into the development of similitude theory for small-scale dynamic models with inelastic capabilities. Instead, the similitude laws which must be satisfied for models utilizing artificial mass simulation are presented in Table 4.1^{*} without preamble. These requirements can be achieved for prototypes characterized as lumped mass systems but may also be feasible for some cases of distributed mass systems.

* In Chapter 4 figures and tables are presented at the end of the chapter text.

1. Lumped Mass Systems

For many types of typical building structures it is acceptable to represent the seismically effective mass by a series of masses concentrated at the floor levels (lumped masses). In this case the seismically effective mass can be decoupled from the density of the structurally effective material.

A word of caution has to be added to the seemingly trivial term "lumped mass." Such masses are those which are seismically but not structurally effective. In reality, any mass which is attached to structural components will affect the structural response. Masses at floor levels, such as a concrete slab system, will certainly affect the stress distribution in the structural elements and in many cases will be part of the structural system. Great care must be taken in positioning such "lumped masses" in models to simulate realistically the effects of gravitational and inertia forces. In many cases the distributed mass simulation discussed in 2 is preferable.

Nevertheless, when the structurally effective mass is small and a representation of the seismically effective mass by lumped masses is feasible, the structural model may be made of prototype material ($E_r = 1$) and lumped masses are then scaled in the ratio $M_r = \rho_r \ell_r^2$. For small scale model tests this often requires excessive weights which may render such tests impractical. The weight requirements may be reduced when model materials with small stiffness properties (E) are used, leading to the ratio $M_r = E_r \rho_r \ell_r^2$.

2. Distributed Mass Systems

For many types of structures a correct simulation of the mass distribution in space is essential and a simplified lumped mass system cannot be accepted. A way of constructing adequate models of such structures

would be to decouple the mass density ρ_o of the structurally effective material from an additive ρ_1 , which is to be added to the model but has no counterpart in the prototype. Thus the prototype density and stiffness would be represented by $(\rho_o)_p$ and E_p , whereas those for the model would be $(\rho_o)_m + \rho_1$ and E_m , respectively.

This modification would alter the similitude law for structural mass scaling, as follows:

$$M_r = E_r \ell_r^2$$

$$\rho_r = \frac{M_r}{\ell_r^3} = \frac{E_r}{\ell_r}$$

but

$$\rho_r = \frac{\rho_m}{\rho_p} = \frac{(\rho_o)_m + \rho_1}{(\rho_o)_p} = (\rho_o)_r + \frac{\rho_1}{(\rho_o)_p} = \frac{E_r}{\ell_r}$$

or

$$\rho_1 = \left[\frac{E_r}{\ell_r} - (\rho_o)_r \right] (\rho_o)_p$$

For instance, for a 1/20 scale model using prototype material,

$[E_r = (\rho_o)_r = 1]$, the density will have to be increased by a factor of 19. Again, weight requirements may be reduced when model materials producing $E_r < 1$ are used.

Much work needs to be done on this subject, since it is very difficult to effectively separate the seismically effective mass from the structurally effective material. For instance the scheme for adding mass could be to attach to model members amounts of lead or other soft, high-density material, arranged in such a way that it contributes negligibly to the strength and stiffness but augments the weight and inertia. The spacing of these added masses should be maximized, so as to facilitate the manufacture while still adequately approximating a

distributed inertia.

The modeling law for such distributed masses can be obtained by replacing the mass per unit volume ρ_o with some representative mass per unit length μ_o . When lead or other material with running mass μ_1 is attached to the model members, the similitude requirement becomes:

$$\mu_1 = \left[\frac{E_r}{\rho_o} \lambda_r - (\mu_o)_r \right] (\mu_o)_p$$

It appears that the practical realization of this scheme for small scale models in many cases will call for using reduced E/ρ_o model materials, thus reducing the additional mass required to provide seismic similitude.

A problem which may be encountered when using artificial mass simulation with prototype materials as model materials is the effect of strain rate. Higher strain rates, as dictated by $t_r = \sqrt{\lambda_r}$, will generally produce too high a yield strength in the model, but only by a small amount for moderately high strain rates (approximately 10% for structural steel and $\lambda_r = 1:20$).

Model tests with artificial mass simulation have been used extensively in the past for static and dynamic model studies. References 7 - 10,46 are examples of the application of such models in the field of earthquake engineering.

4.2 Case Study--Prototype and Model

4.2.1. Prototype Structure

In order to evaluate the applicability and effectiveness of small-scale model studies and to develop methods and procedures for model fabrication, testing and analysis, it is necessary to have a well-defined prototype structure with documented dynamic response behavior.

It will then be possible to establish the correlation between prototype and model input and response measurements. For that reason, a search was instigated to find a suitable structure to be considered as a prototype for model research.

In 1974, tests of a three-story, single bay steel frame structure were completed at the Earthquake Engineering Research Center, University of California, Berkeley (9 , 41). The test series was conducted primarily to experimentally verify newly developed methods of non-linear structural analysis and produced considerable test data concerning the response of the structure to dynamic motions produced by the earthquake simulator facility at Berkeley. Both elastic and inelastic response behavior to dynamic motions, including actual earthquake time history recordings, was investigated in the prototype study. This test structure was deemed to possess adequate complexity to provide a meaningful test of modeling applicability and was adopted as a prototype for a small-scale model study.

The prototype (Figure 4.1) consists of two parallel steel frames with moment-resistant, welded connections. These main frames are then joined at floor levels by bolted connections to cross beams and diagonal bracing, thus affecting floor diaphragms rigid in their own plane. End bay bracing in the column weak direction, pretensioned by turnbuckles, resists structural motion transverse to the excitation axis. The diagrams presented in Figure 4.2 show floor plans, as well as front and side elevations of the structure. Typical structural details are shown in Figures 4.3 through 4.7.

In order to provide a period of vibration in the range appropriate to actual steel buildings, and also to apply gravity loads, blocks of

concrete weighing approximately 8000 lb per floor were added to the structure. Care was taken in the design of the concrete block support mechanism to minimize the effect of the blocks on the stiffness characteristics of the girders. Adjustable vertical supports were used to enable uniform distribution of the load to the four columns. It is apparent, however, that the centers of gravity of the floor weights are above the girder axes, which produces some effect on the dynamic response of the structure.

The frames are fabricated from standard rolled shapes of ASTM A-36 grade steel. Sections W5x16 are used for the columns and W6x12 for girder and beam members. Table 4.2 lists the nominal dimensions for the sections as given in the AISC manual (27) versus the actual measured values. In Table 4.3 are presented weight estimates of the concrete blocks and various building components.

The prototype study was instigated to initially study the contribution of flexible joint panel zones to the earthquake response of the structure and to permit evaluation of mathematical models for predicting joint performance. As such, the structure is designed so that joint panel yielding occurs prior to yielding in the girders and columns. The structural detail of the column to girder connection (Figure 4.3) is of a common type and also permits strengthening of the joint panel by the addition of doubler plates to enable later studies forcing inelastic action into the girders and columns.

It is important to note that even though this test structure is obviously reduced in size from a true building structure it is not itself a scale model, but has been designed as an actual system for the Berkeley earthquake simulator study. The relatively small girder spans

and column heights were dictated by space limitations and member sections were adopted to produce a reasonable proportion of member length to cross-section. In the Berkeley study, a comparison of the test structure to the 1970 Uniform Building Code (44) requirements indicated that the seismic resistance of the structure is considerably greater than is typical of standard structures. This comparison was based on the assumption that the Berkeley structure was actually an artificial mass simulated model, $\ell_r = 1:2.5$, of an hypothesized prototype. The UBC specifications for seismic and gravity loads were then applied to this imaginary structure.

Further items concerning the characteristics of the prototype structure will be discussed in the following section and Section 4.3.3 (Model Fabrication), especially when there is some variation in model design from prototype design.

4.2.2 Model Structure

The primary task in the design of a replica model is to simulate all aspects of the prototype design which may contribute to the earthquake response characteristics. To satisfy this criterion, all of the model structural details, have to be similar to those for the prototype, except in situations where variations from prototype schemes have a negligible effect on structural behavior. Permissible distortions of the prototype may then be utilized to simplify model fabrication in some instances.

The configuration of the prototype structure is particularly suited to modeling by artificial mass simulation. Masses are already lumped at the floor levels and are essentially uncoupled from the structural framing, permitting the application of lumped mass modeling with

minimum difficulties. Such an ideal situation would generally not be possible if the prototype was an actual building structure, due to the contribution of floor diaphragms and other structural and nonstructural components. The practical resolution of such problems will require future study.

At the onset of this model study it was not yet known what method would be best suited to fabrication of the model wide flange elements. As welding or soldering of plate elements into structural shapes was one possibility (Section 4.3), a modeling length scale was chosen both to permit application of standard sheet metal gages to element fabrication and to be sufficiently small to enable a valid evaluation of small-scale analysis. Thus, a model length scale, λ_r , of 1:6 was chosen for the model structure utilizing artificial mass simulation (AMS). Also, it was decided to use prototype material as the model material, in this case structural steel, to minimize simulation problems which may be produced by the use of other materials. Since the model scale is not extremely small, only minor problems due to size and strain rate effects were anticipated and since the prototype is relatively low in weight the payload and dynamic force requirements were easily within the capacity of the existing earthquake simulator. The resulting scaling requirements for the AMS model are summarized in Table 4.4.

As the region near the joint panel zone is critical to the inelastic behavior of this structure, the detailing of the prototype girder-to-column and primary beam-to-column connections is faithfully reproduced in the model, including coping of the girder web to avoid local tearing and the use of bevel welds to ensure full penetration. The only model variation in this region is that though the bolts for the connection of

the primary beam are scaled in size they are not of friction type. Since the primary beams are hardly stressed at all, no problems due to bolt slip or failure were anticipated. The end bay bracing scheme with rod and turnbuckles is also duplicated in the model. However, some variations from the prototype design were adopted to reduce the costs and difficulties experienced in the construction of the model. Drawings showing many aspects of the model design, which may be compared to prototype configurations, are presented in Figures 4.8 through 4.12.

Though actual wide-flange sections are used for the model primary beams, such accurate duplication is not necessary for the secondary beams. The secondary beams have simple, bolted end connections in the prototype, and as such are essentially axial load carrying members (Figure 4.5). Thus, a simpler cross-section could be utilized. For the AMS model rectangular steel members are used which approximately provide the properly scaled axial and strong-axis bending stiffnesses of the wide-flange sections used in the prototype (Figure 4.11). The weak-axis stiffness is not simulated, but the rectangular section has adequate rigidity to preclude weak-axis buckling. Also, torsional stiffness is adequate to prevent any variation in model from prototype response. The use of rectangular sections for these members greatly simplified construction of the model and considerably reduced the expense incurred in element fabrication.

A rather complicated method of column base connection to the earthquake simulator platform was required for the prototype study (Figure 4.6). This connection consists of a base plate welded to the base of the column and strengthened by two parallel vertical stiffeners welded to the base plate and the column flanges. Each base plate was then fastened to a

steel footing, producing a column essentially fixed at its base with variable stiffness to the top of the stiffeners. For the model a simplified version is used, consisting of welding the column base to a small base plate, which in turn is welded to a large plate and bolted to the simulator platform (Figure 4.12). However, an analysis of the variable flexibility of the prototype connection showed that an increase of 1.3% in the model first floor height was necessary to produce the properly scaled column flexural stiffness. Thus, the model first floor column length is 0.16 inches longer than the scaled prototype free length (above column base stiffeners) of 12.50 inches.

When the angles used for floor bracing in the prototype, steel angles $2\ 1/2 \times 1\ 1/2 \times 3/16''$, are scaled by $\ell_r = 1:6$ a relatively small section is produced. For satisfaction of similitude, the model would have required a non-standard cross-section. But since a small variation in the properties of the floor bracing has a negligible effect on the total response of the structure some distortion of the section is permissible. Thus, aluminum angles, of dimensions $1/2 \times 1/2 \times 1/16''$, are used for the model. Though this section is considerably larger than the scaled prototype angle, the material stiffness of aluminum is less than that for steel, producing approximate satisfaction of the similitude requirements.

The final problem to be considered is the analysis of the floor weights required to meet similitude requirements and the design of the weight support mechanisms. The scaling law for structural mass states that the model mass must be reduced in a proportion of ℓ_r^2 or 1:36 from that of the prototype. The greatest contribution to the mass of the prototype comes from the concrete blocks positioned at floor levels, however, the weight of the structural components is not a negligible

factor. The weight of the model structural components is scaled in proportion to $\rho_r \ell_r^3$, or ℓ_r^3 in this case as prototype materials are used, instead of in proportion to ℓ_r^2 as required. Thus, the total required lumped model mass is equal to $\ell_r^2 = 0.0278$ times the lumped mass of the prototype plus $(\ell_r^2 - \ell_r^3) = 0.0231$ times the weight of the prototype structural components at the floor levels. An additional refinement can be obtained by including some portion of the column weight in the weight of the floor level structural components. The proportion used for the AMS model was 3/8 of the column weight as determined by Rayleigh's method with the assumption of a trigonometric deflected shape. The resulting lumped mass requirements are shown in Figure 4.8.

As the mass must be scaled in proportion to ℓ_r^2 rather than ℓ_r^3 the density of the material used for the lumped masses must be approximately ℓ_r^{-1} or six times the prototype density if the floor weights are to be of the scaled physical dimensions of the prototype. This is an important consideration, as the eccentricity of the floor mass center of gravity and the girder center-line should be replicated in the model to produce the same structural response. The effect of this eccentricity and of the support mechanisms was analyzed and found to contribute to the response by increasing the girder end moment and shear by approximately 2% and 10%, respectively. Any variation of the model scheme from that of the prototype should thus be minimized.

A problem arises in finding a readily accessible and relatively inexpensive material to be used for lumped masses with sufficient density to approximate this condition. Assuming a density of 145 lb/ft^3 for the plain-concrete lumped masses of the prototype, a material weighing 870 lb/ft^3 would be required for the model, versus available densities of 490 lb/ft^3 for steel and 710 lb/ft^3 for lead.

A compromise was finally reached between the required density of the floor masses and the scaled dimensions. By increasing the plan dimension of the masses perpendicular to the excitation axis, steel could be used for the model weights with only small increases in the other dimensions. Thus, the model floor center of gravity is approximately 2.70" above the girder center line versus the desired 2.04". This discrepancy is felt to have little effect on the overall response of the dynamic model.

The horizontal and vertical support mechanisms for the model are essentially the same as for the prototype.

4.3 Model Fabrication Techniques

Proper model fabrication is concerned with the simulation of prototype geometry and initial state of stress and with the ability to faithfully reproduce all details that may significantly influence the response characteristics.

It must be recognized that certain characteristics are easier to simulate than others, and some will be almost impossible to replicate at small model scales. In carefully designed models such phenomena as initiation and propagation of yielding, buckling of members and frames, and local and lateral torsional buckling can be properly simulated, whereas localized problems at connections can hardly ever be studied on small scale models. For instance, at welded beam-column joints where in small scale models the welds usually will be oversized, it would be inappropriate to study such localized characteristics as weld fracture or column flange distortion; these effects are better investigated with full size subassembly tests. Thus, model fabrication should not be confined and overly complicated by design objectives which are impossible

to achieve.

Standard tolerance limits for steel structures should be scaled geometrically to provide acceptable tolerances for model construction and element fabrication. The ability to produce a small-scale model within these acceptable tolerances will often place an upper limit on the usable model scale. Also, the major contribution to the success of model fabrication will be the skill of the technician who must apply special methods to satisfy the close tolerances required by model research.

Since the use of prototype material for a dynamic model is often desirable because it enables simplification of model material scaling requirements, careful consideration of the feasibility of using prototype material for the modeling of steel-frame structures is required. The use of prototype material also facilitates the simulation of special characteristics, such as structural joint behavior, by using a similar fabrication method for the model as for the prototype.

4.3.1 Element Fabrication

For models of steel structures utilizing prototype material, structural shapes may be fabricated from bar stock through machining (milling), rolling or die extruding, or by joining of individual plate elements through welding, soldering or gluing. Any one of these methods is feasible, provided the maximum expected stresses can be transferred through the connecting media, and subsequent heat treatment will relieve fabrication stresses and produce the desired strength properties. However, with the exception of hot-rolling, it will hardly be possible to reproduce the residual state of stress present in structural shapes. This shortcoming must be considered when buckling problems play an important role

in the model test.

1. Fabrication from Bar Stock. Although time-consuming, machining of structural shapes is an attractive method of element fabrication. In this procedure, a length of bar stock is formed into a structural shape by removal of unwanted material. For example, a wide-flange section could be fabricated by cutting of two U-shaped channels along each side of a rectangular bar. As bar stock is commonly available in a wide range of grades, including ASTM grade A36, it should be possible to sufficiently match prototype material properties.

Possible problems with this method include warpage of thin-walled sections due to the initial stress state present in the bar stock. Initial heat treatment of the base material before machining is recommended to reduce this state of stress. Also, the machining process may alter material properties close to the surface but generally not to a large degree, especially if heat treatment of the machined member is utilized.

The primary attraction to machining is that cross-sections can be produced to very close tolerances, in the order of ± 0.005 in., with thicknesses down to approximately 0.025 in. This would enable fabrication of scale model sections to approximately 1:20 scales.

Hot rolling and die extrusion of small-scale structural shapes are feasible alternatives in cases where many identical members are required. However, rolling may be the only possible way to simulate the initial stress state in prototype structural shapes, if this criterion is critical to a particular model study.

2. Joining of Plate Elements. Helium arc welding (TIG) and silver-soldering are possible alternatives for element fabrication. Thin strips of sheet metal with the required dimensions and material properties

are joined by the appropriate process. To prevent warpage of the specimens, particularly with silver-soldering, the process should be conducted in an elevated temperature environment. Also, a step-wise procedure of alternating sides and backstepping will prove useful in minimizing heat distortions.

Undesirable features of welding of such thin specimens are the oxidation of the material adjacent to and opposite the welding surface and the possibility of burn-through. Back-up gas (purging) may be used to reduce this oxidation while the use of argon as the inert gas will permit the use of lower arc voltages and minimize the chance of burn-through. Also, both resistance and electron beam welding may suffer from weld gaps and slight deviations of the web from the flange center-line for wide-flange sections leading to separation of the flange and web under load, as was reported in a MIT research study (25).

The high stress demands in model elements may restrict the use of silver-soldering to only low-stressed secondary members. For wide-flange sections, these stress demands may be most critical at structural connections, where high tensile stresses are induced at the flange-web interface. Excessive longitudinal shear may also limit the use of this method. Gluing, due to very low strength, is definitely applicable only to secondary members.

4.3.2 Element Connection

The simulation of structural connections such that the geometry and the effects on the adjacent material are properly represented is an important aspect of model fabrication. Such connections can be considered to be of two types--primary and secondary connections. Primary connections are important structural links with high stress demands while

secondary connections are expected to carry relatively low stress levels.

The two common methods of joining prototype steel-frame elements are bolting and welding. For primary connections, the same type of connection will generally be required for the model to enable attainment of required strength and ductility characteristics.

Bolting provides connection of structural elements in a similar fashion as for the prototype, provided bolt sizes and holes are of the properly reduced size and bolt strength and ductility capacities satisfy similitude requirements. Friction type connections will require that additional considerations be given to scaling of frictional forces and prestressing requirements. High-strength bolts may be difficult to obtain in small sizes required for small-scale models, thus they may have to be fabricated by in-shop machining.

Model welding will be required to simulate prototype welded connections where high strength capacity is required. Generally, model weld sizes will be larger than required by geometric scaling due to difficulties producing a full-penetration weld at such reduced scales. Also, considerable care should be taken to prevent loss of base material due to excessive burning and contamination of the weld due to oxidation.

Welding utilizing the heliarc, TIG (tungsten-inert gas) process is most applicable to small scale models. In the TIG process (Figure 4.13), the tungsten electrode is not consumed. Rather, a filler rod is fed into the arc, melted, and propelled toward the joint being formed. Shielding of the arc is obtained with inert gas which prevents oxidation of the weld. The gas atoms are ionized and carry the arc from the electrode to the item being welded. The inert gas best suited to this work is argon, which minimizes the required arc voltage and is also suitable

as a back-up gas to prevent oxidation on the back sides of the material being welded. Two types of filler rod which were found to produce good results are Industrial Stainless 410 and Stainless 308, with diameters of 0.030 in.

Even with the use of argon gas to minimize arc voltage, localized distortions due to heat effects are difficult to control. Thus, clamping and stress relieving of completed model frames may be required to satisfy scaled tolerances. The clamping mechanism should be designed to provide only the minimum confinement required to eliminate distortions. The stress relieving is performed at a temperature below any phase change or annealing temperature of the material.

Secondary elements will enable utilization of additional model construction techniques due to low stress demands. These methods may use silver-solder or epoxy as the connecting medium, or low-strength bolted connections with relaxed tolerances.

4.3.3 AMS Model Fabrication

The previous two sub-sections were concerned with methods of model fabrication, while in Section 4.2 the design goals of a specific small-scale model were developed. The task now remains to apply these methods to attain the desired end product, a replica model utilizing artificial mass simulation and prototype material.

In Figure 4.14 are shown the geometrically scaled prototype cross-sections required for the AMS model. The dimensions shown were obtained from the actual measured dimensions of the prototype members. As the first major effort in the construction of the model, these structural elements must be produced with great accuracy from a material which simulates the prototype material, ASTM A36.

The alternatives which were felt to be applicable to this model study are silver-soldering, heliarc welding and machining. However, analysis of the strength of the silver-soldered connection indicated that this method would not be sufficient for primary members, yet silver-soldering might prove useful for fabrication of lower stressed secondary elements.

To determine the effectiveness of these methods in producing a reliable model element, trial girder specimens of 24 in. length were produced. Sheet metal of appropriate dimensions was used for fabrication of the silver-soldered and welded specimens while ASTM A36 grade bar stock was used for the machined member. Neither the welded or silver-soldered specimens were fabricated at an elevated temperature. The heliarc TIG process with argon gas and Stainless 308, 0.03 in. diameter rod was used for the welded beam.

The specimen resulting from silver-soldering exhibited extreme heat distortions, making this method infeasible unless a furnace is used to uniformly heat the sheet metal strips to the solder flow temperature. As the applicability of this procedure to the AMS model was limited, no further development of silver-solder techniques were explored.

A summary of the accuracy of the trial sections produced by welding and machining are presented in Table 4.5. While the machined specimen satisfied all the presented tolerances the welded girder exceeded the AISC standard mill practice tolerance for camber by 300%. However, with practice and subsequent heat treatment it is felt that accurate elements could be obtained by this method, but the problem of flange-web separation discussed in Section 3.4.1 still remains.

From the results of this test, it was decided to utilize machining to produce the required model elements. Bar stock of A36 designation and dimensions $3/4 \times 1 \ 1/4$ in. and 1×1 in. were used for the girder and column members respectively. As the bars were hot-rolled and as the model sections were to be cut from the center of the stock, no heat treatment of the base material was deemed necessary. Photographs of a typical column and girder member are shown in Figure 4.15, while the geometric properties of the model elements are given in Table 4.6.

The girder and column members were not the only elements which required fabrication. Additional elements, such as secondary beams, stiffener plates, beam mounts, back-up bars, erection plates, etc., had to be produced and properly dimensioned. Machining of base material was again utilized for the fabrication of the multitude of elements required for one replica model. Essentially, the effect of every important detail of the prototype had to be duplicated in the model.

Once these elements had been constructed, the remaining job was to connect these members into a model framework. Most critical were the fully-welded girder-to-column connections required for the two moment-resisting plane frames, and as such these connections required extensive consideration. A detailed, step-by-step practice was developed for the construction of the AMS model.

1. Stiffeners and Secondary Beam Mounts. The secondary beam mounts and the column and girder stiffeners, which had been fabricated slightly oversize to compensate for shrinkage during the welding process and to facilitate placement by lightly tapping into place, were accurately positioned and tack welded into place. They were then fully welded by the heliarc process previously described, while care was taken

to provide back-up gas and to alternate weld locations to minimize scaling and heat distortions. The resulting girder elements were satisfactory, but the columns exceeded the AISC tolerance for camber by approximately 300%. As one side of the column flange was always connected to the stiffener by one weld, a bevel weld, while the other side required two fillet welds (as provided in the prototype) the heat effects were not symmetrically distributed, producing this high camber. Subsequent heat treatment, at 1100°F for one hour followed by in-furnace cooling, of the columns while clamped in a straight position reduced this camber to acceptable levels. Girders and columns were subjected to light sand-blasting after welding to remove any scaling on the columns and girders.

2. Layout of Primary Frame. An erection plate, which would also serve as a back-up for the girder web weld, and one back-up bar were positioned and tack-welded to the column flange at each joint location. The second back-up bar was clamped to the girder end by surgical clamps, then the two primary frames were layed out by bolting the girders to the erection plates, permitting close alignment to specified clearances and dimensions. The frames were then clamped to an essentially rigid base frame in a manner which permitted longitudinal model member expansion due to welding heat but confined flexural and torsional movements (Figure 4.16). Teflon sheets were used to help minimize friction at the clamped locations.

3. Welding of Primary Frames. Due to the initial problems with heat effects, which are obviously more intense in models than is characteristic of prototype fabrication, it was apparent that erection stresses would be impossible to simulate in this model. Thus, the

final welding procedure was designed to minimize heat distortions, not to replicate the effects of the prototype fabrication. This discrepancy in prototype and model stress history was deemed to be of minor consequence for this model study, however special methods may be required to simulate this aspect in frames with a high degree of redundancy. The welding procedure was to initially tack-weld all of the column-girder connections followed by full welding of the girder web to the column face for all joints, then welding of the flange connections. Back-up gas was not necessary for these connections, as no further welding of back surfaces was required. Care was taken during the flange welding to carry the bead across the full width of the girder flange and to prevent scalloping of the flange by burning. Finally, the column base plates were positioned and welded. A completed girder-column joint, illustrating the discoloration in the region of heating, is shown in Figure 4.17.

4. Heat Treatment of Primary Frames. The resulting plane frames showed little distortion due to the final welding. However, the frames did exhibit a tendency to buckle elastically out of place, possibly due to compressive forces developed in one or more of the girders (Figure 4.18). Heat treatment was utilized to relieve the stresses developed by the welding process, thus producing an essentially zero initial stress state and eliminating this buckling phenomenon. Since little confinement of the frames was required, only small weights were used to position them on a precisely flat plate. The assembly was then subjected to an 1100°F temperature for one hour, followed by in-furnace cooling to room temperature. This procedure removed all out of plane tendencies.

5. Fabrication of Completed Model. After light sand-blasting to

remove scaling, the strain gage instrumentation was applied to the primary frames along with the connections for the displacement transducers (Section 4.5.2). The primary frames were then connected by means of the cross-framing elements, i.e., primary beams, secondary beams and diaphragm bracing. The completed assembly was initially only loosely bolted, followed by careful alignment and final tightening of the connections. Lock washers were used at many of these connections to help prevent loosening during the extensive test procedure to follow. At this point, the model was positioned on the shake table and welded to the table support plates, the structure was vertically loaded by means of the steel plates and the end bay bracing was attached and pretensioned.

An overview of the completed AMS model is presented in Figure 4.19. The final small-scale model is, visually, a remarkable replica of the prototype structure. The photographs in Figure 4.20 show a comparison of general views and details of the prototype and model. In many instances, it is difficult to distinguish model from prototype. However, the real proof of replication is forthcoming: the ability of the small-scale model to duplicate the critical aspects of the prototype dynamic behavior.

4.4 Material and Component Tests

4.4.1 Objectives

Material and component tests play a vital role in successful small-scale replica modeling. The objectives of such preliminary testing, as repeated from Section 3.3, can be grouped into three general categories.

1. Define mechanical properties, either material or structural, to enable model-prototype response correlation.
2. Verify the adequacy of fabrication techniques.
3. Evaluate and calibrate instrumentation.

For the subject model case study more specific requirements can be identified for these initial tests. Also, since some information is available from the prototype study, in the form of coupon and subassembly tests, the results of the corresponding model tests will form a limited basis for comparison.

4.4.2 Material Tests

The primary goal of the material tests related to the AMS model study was to evaluate the pertinent mechanical properties of the actual material utilized in the model to determine the adequacy of prototype simulation. For this purpose, tests of coupon specimens cut from actual structural members were performed. Also, some measure of the accumulative effects of model element fabrication techniques was obtained by comparing the results of the model coupon tests to those performed on the AMS model bar stock base material.

As the AMS model utilized the same material as the prototype structure, low-carbon steel of ASTM A36 designation, and as the selected model length scale, 1:6, was not extremely small, extensive tests of material behavior were not deemed necessary. Adequate evaluation of material simulation was possible from the results of uniaxial tension tests under

conditions of monotonic loading. Since the model coupons were cut from girder and column elements processed in an identical fashion as those used in the model structure, the effects of machining and stress relieving are inherently included in the results. Also, strain rate effects deserve some attention, and were evaluated through several tests performed at increased loading rates. This abbreviated test of material mechanics was sufficient for this study as the main requirement was that adequate information be available to enable identification of possible sources of model-prototype response variation.

Section 3.3 discussed the usefulness of strain rate as a basis for comparison of model and prototype material test results. Thus, specimen strain rate is usually desirable for control of the material test systems though this is not always possible due to various difficulties. The prototype study (9) lists load rate as a material test parameter, which would indicate that specimen axial load was used for test system control. For a uniaxial tension test under load control the strain rate is constant until the yield point is reached, after which an instability is produced at the yield plateau, creating a very high strain rate.

Attempts at using strain control for the model coupon tests indicated that strain did not provide adequate test system control for the small, narrow specimens. As the Stanford material test system is a feedback controlled hydraulic system, at the initiation of the test the load undergoes small amplitude cycles about zero value. For the model coupon the compressive forces produced by the cyclic phenomenon often produced buckling of the specimens. As an alternative, actuator stroke control was used which, for these small specimens, produces essentially a bi-linear strain rate with only a slight discontinuity

occurring at the specimen yield point provided the gage length is not much less than the specimen free length and the strain-hardening region is not reached. For the model base material tests, strain control was used with no difficulties. As a basis for comparison of the model and prototype results the strain rate during the elastic portion of the stress-strain curve will be presented.

Coupon specimens for both the prototype and model tests were cut from flanges and webs of both girder and column members. However, in-house tests on the model base material were performed only on the column material, while mill-test reports are utilized for the girder base material.

The measured quantities to be utilized for prototype and model material evaluation were axial load, from which stress can be deduced, and strain measured over a finite gage length. In the model study, the analog-to-digital conversion capability of the laboratory computer facility was utilized for data acquisition. Thus, strain and stress time histories were recorded, enabling determination of actual strain rates as well as stress-strain relationships. The high-speed capability of the test facility also enabled accurate testing at elevated loading rates. For all of the test results presented, strain rates of 2×10^{-4} in./in./sec and smaller are considered to be "static" tests.

For illustrative purposes, typical test records from the model material test series are presented in Figures 4.21 through 4.34. In Figure 4.21, the stress-strain curve for the column base material is compared to the result of a column flange coupon test. The behavior of column and girder flange material is shown in Figure 4.22, while the effect of strain rate in a test of the column base material is illustrated in Figure 4.23.

Properties which can be derived from the results of the model and prototype coupon tests are presented in Table 4.7, while a summary of nominal values for the most pertinent quantities from prototype coupon and model coupon and base material tests is given in Table 4.8.

The yield strength of the model column material can be seen to be consistently greater than that for the prototype. From the results of the static tests the model column coupons exhibit a yield stress approximately 10 to 20% greater than the prototype column material, while model and prototype girder coupons indicate similar yield levels. Since for the model study initial yielding will occur in the joint panel zone, the column web yield level will determine the overall yield intensity of the structure. However, the effect of strain rate on material properties must be considered before making any final conclusions concerning model versus prototype anticipated yield level.

As a basis for comparison, a strain rate corresponding to cyclic response at the test structure's fundamental frequency (approximately 2.5 Hz for the prototype) with amplitude of $2\epsilon_y$ can be arbitrarily chosen. If harmonic strain response is assumed, the strain rate at ϵ_y is then 0.04 in./in./sec for the prototype and 0.1 in./in./sec for the model material.

Based on available information on strain rate effects in mild steel (26) the prototype material yield strength would increase from 42.7 ksi to 52.4 ksi when the strain rate is increased from 0.00003 in./in./sec to 0.04 in./in./sec. Similarly, σ_y of the model material would increase from 45.6 ksi to 57.0 ksi when changing the strain rate from 0.0002 in./in./sec to 0.1 in./in./sec. Thus, it is expected that the yield strength of the column web in the model test will be approximately 10% higher than that in the prototype test. This relative

increase is justifiable since the static material yield strengths differ already by 7%, however, the large increases in yield strengths, as predicted from the data in Reference 26, could not be verified in this study. Several pilot tests carried out on the model material have shown much smaller increases in yield strength at high strain rates (see Tables 4.7 and 4.8).

An interesting effect indicated by the material tests is the apparent reduction of elastic modulus for the model material after element fabrication. As the coupon and base material tests were performed on the same facility, this low modulus value cannot be explained solely on the basis of instrument error. A possible explanation can be developed from the character of the model element fabrication process, machining. As the mill generally cuts across the member longitudinal axis, sufficient grain orientation may occur to produce this phenomenon. This effect of modulus reduction appears to be somewhat countered, however, as a proportional increase in elastic modulus was observed in the high strain-rate model column coupon test.

4.4.3 Component Tests

Prior to the actual construction of a complex small-scale model it is desirable to have some means of evaluating the fabrication and testing techniques to be utilized in the test study. In the case of the AMS model, the prototype test program included the test of a girder-column subassembly under conditions of cyclic load reversals. The results of this component test can be used to provide an initial evaluation of the proposed techniques for fabrication of the AMS model. Additionally, the instrumentation scheme required to sense the inelastic response and deformation of the structure can be developed and

calibrated.

Two model subassembly specimens were scaled after the prototype subassembly and fabricated in a similar manner as the AMS model structure (see Section 4.3), with one exception. The bevels at the girder ends of the model structure are opposed, thus facilitating welding of the final frame assemblies, while the model subassemblies utilized the standard prototype procedure of upward facing bevels (Figure 4.24). This variation is felt to have little effect on the accuracy of prototype simulation.

The instrumentation network utilized in the prototype study is not entirely suitable for use with a small-scale model. The difficulties of performing, at model scales, similar measurements as in the prototype study required extensive development of an applicable instrumentation scheme. Figure 4.25 illustrates the array of experimental transducers utilized in the model subassembly test series.

Similar procedures as for the prototype experiment were used for measurement of girder tip load, tip deflection, joint panel strains and member internal forces, only on a much reduced scale. For instance, strain gages are greatly reduced in size from those used in the prototype study. Also, a miniature stacked-rosette was used for measurement of the panel 45° strains, versus a 90° L-rosette utilized in the prototype study.

The difficult task was to enable determination of the joint panel shear distortion through measurement of the relative displacement between the panel diagonal corners. The prototype scheme of utilizing LVDT transducers for the measurement was not practical over the model gage length of approximately 1.23 in. In the first model subassembly test, pre-tensioned strain gages were stretched over the gage length. Though

this system proved to be deficient in several aspects, the principle of using a pretensioned resistance gage was sound. Elastic mercury gages were used in the second subassembly test and proved to be a promising transducer for this measurement application. A more detailed description of the mercury gage can be found in Section 3.4, while information concerning measurement of the joint shear distortion can be found in Subsections 4.5.2 and 4.5.3.

The mounting procedure for the subassembly tests rendered the specimen statically determinate. Thus, the member internal forces can be calculated at any location from the girder tip load and geometry. This was not the case in the model structure, thus it was necessary to have some means of measuring member end forces. One procedure would have been to measure the element extreme fiber strains and utilize the elementary beam formulas of $M = \epsilon EI/y$ to calculate the bending moments and $P = \epsilon EA$ for member axial loads. However, due to the variability in actual strain from the assumed distribution it was more desirable to calibrate a specific strain gage and wide flange section against known internal forces. In fact, use of elementary formulas would have produced errors of the order of 10% from actual member forces.

The prototype subassembly loading was provided through manual control of a hydraulic jack. Specimen response was continuously monitored as a basis for control of the test. When the output from the 45° panel strain gage reached a designated value, valves were adjusted to provide a cycle of reversed loading. The test proceeded with a few cycles at each strain amplitude until a panel strain ductility factor of approximately eight was obtained.

In the model test series, stroke control of an automated hydraulic testing apparatus was utilized to provide cyclic girder tip deflection.

A sine wave was used for input control, with the wave period adjusted for each amplitude cycle as a function of the desired 45° panel strain intensity as given by $T = 4(\epsilon/\epsilon_y)(5 \text{ sec.})$. Thus, an average strain rate of 3×10^{-4} in./in./sec was maintained.

For the first subassembly test, two cycles were applied at each displacement setting, with a rather large displacement amplitude interval between subsequent cycle pairs. The first specimen was then tested to a panel strain ductility of about twenty. At this point girder flange buckling was observed as well as considerable scaling of the girder flange, extending approximately one inch from the column face. Apparently, yielding had spread from the panel zone into the girder. However, this high intensity level would not be reached in the AMS model earthquake simulator tests.

In the second model subassembly test, only one cycle was performed at each setting, but with a much finer amplitude increment between cycles, to a ductility factor of approximately eight. The output from an extensometer mounted at the girder end indicated that no yielding had occurred in the girder at this amplitude.

The laboratory minicomputer system was used for data acquisition and analysis for the model component study. All model results were converted to prototype units by appropriate scale factors derived for an AMS model with $\lambda_r = 1:6$ (Table 4.4). Thus, a direct comparison of model and prototype results can be made, but the inverse of the scale factors given in Table 4.4 must be applied to the presented model results to determine actual model subassembly force levels and response parameters.

Figures 4.26 through 4.30 present the response curves derived from the subassembly tests. In Figures 4.26 and 4.27 are given the model

subassembly load-deflection and moment-panel 45° strain curves. Skeleton curves of the prototype test results are compared to the peak cyclic amplitudes derived from the model tests for load-deflection, moment-panel 45° strain and moment-panel shear distortion in Figures 4.28, 4.29 and 4.30 respectively. Also shown in Figures 4.29 and 4.30 is the analytic prediction based on a method presented by Krawinkler, et al. (20).

As mentioned previously, the scheme for measuring model panel zone distortion in the first subassembly test did not provide adequate response measurements. Also, an unexplained 90% loss in mercury gage sensitivity between gage calibration and subassembly test number two reduced the effectiveness of these distortion measurements. For this reason, the model moment-panel distortion curves are not presented. However, after recalibration of the mercury gages, it was possible to read peak amplitudes for both of the model subassembly tests to produce the comparison presented in Figure 4.30, though the accuracy of the model measurements is somewhat questionable. In the earthquake simulator test series, care was taken to prevent this mercury gage sensitivity degradation from reoccurring.

As would be expected from the results of the material tests, the model subassembly specimens exhibit a somewhat higher strength than the prototype subassembly. Another obvious difference is the higher post-elastic stiffness of the model. Due to the difficulty of adequately scaling weld sizes, the effective joint panel area was smaller for the model than for the prototype (see Section 4.3) and the elements surrounding the panel zone were relatively stiffer. Consequently, the model panel zone yielded and strain hardened more uniformly and at a somewhat higher force level. In the earthquake simulator test, this

combination of higher joint strength and greater inelastic stiffness can be expected to provide greater energy dissipation in the AMS model than in the prototype for a given amplitude of deformation.

It should be mentioned that some irregularity exists in the prototype skeleton curves presented in Figures 4.28 through 4.30, which were taken from the prototype test report (9). The moment-deformation response curves show equal moment amplitude for positive and negative moments. Since the girder tip load and end moment are simply related by a constant, the load-deflection response curve should also exhibit equal load amplitude excursions about the plot abscissa. However, the presented negative load levels appear to be of too small amplitude as compared to the other prototype response curves.

In the elastic region, the model and prototype results compare favorably. However, at the yield point, the model subassemblies exhibit a yield plateau with a significant deformation offset (see Figure 4.27). To enable the peak amplitude comparison to the prototype skeleton curve it was necessary to subtract this initial offset from the model deformation measurements. This plateau phenomenon can be explained by the increased weld size in the model, producing the effect of a shear panel with almost rigid boundary conditions. An essentially uniform stress state is then developed in the model joint, leading to the sudden yielding observed. In the prototype specimen, the stress level would be maximum at the center and decrease towards the panel extremities, producing the more commonly observed gradual stiffness degradation. In the first inelastic earthquake simulator model test this effect did produce some disagreement between the model and prototype results. However, since this effect was not apparent in cycles subsequent to the initial inelastic excursion, no problems due to this phenomenon were

evident in earthquake tests after the initial yield excursion.

The results obtained from calibration of the elastic strain gage bridges as internal force transducers for model element forces are presented in Table 4.9. As can be seen, the actual results vary considerably from those predicted by elementary beam formulas. From the two model subassembly tests, this method of internal force measurement produces accurate estimates of member moment, however the axial force estimates are somewhat variable, primarily due to the smaller strain levels characteristic of the axial force component.

4.5 Earthquake Simulator Tests

4.5.1 Objectives

The earthquake simulator tests of the AMS model served as a comprehensive evaluation of the applicability of one form of small-scale model analysis to an important aspect of earthquake engineering. Additionally, an actual model test was necessary to determine the effectiveness of the dynamic testing facility discussed in Chapter 3 and to develop methods for correlation of small-scale model and prototype response.

The primary task of the AMS model study was to replicate pertinent prototype behavior as measured in the Berkeley test study. Since the basis for model response evaluation was limited to the results of the prototype study, the model instrumentation, dynamic loading procedures and parameters for evaluation of test results were governed by those of the prototype experiment. For instance, model earthquake simulator motion was matched to prototype input, the El Centro, 1940, North-South record and an artificial earthquake composed of discrete spectral components. Also, instrumentation suitable for a small-scale model was

required to duplicate measurements of prototype response behavior and to enable the determination of the effectiveness of prototype replication through comparison of basic dynamic characteristics, i.e., amplitude and frequency constant of inelastic response to earthquake excitation.

In the model test series no attempt was made to compensate for anticipated contributions to deviations in model from prototype response, e.g., size and rate effects. Instead, possible sources of discrepancies were evaluated as suggested from the results of the AMS model material and component tests (Section 4.4). Future model tests could account for these discrepancies by slight alterations of model test parameters.

4.5.2 Instrumentation and Data Acquisition

The objective of the model instrumentation system was essentially to duplicate measurements of the prototype test study, only at model scales. However, in many cases prototype-scale instrumentation methods were not entirely suitable for use in a small-scale model study, requiring the development of new techniques to enable measurement of similar response parameters. The prototype earthquake simulator study utilized 67 and 28 data channels to monitor structure and shake table response, respectively. As the Stanford testing facility is limited to 32 channels, it was necessary to eliminate redundant and non-essential measurements to stay within testing capacities and to enable greater test efficiency. Since the test structure was braced in the transverse direction to prevent response in directions other than that of the unidirectional input motion, instrumentation of one AMS model frame was sufficient to monitor structural response, as could be concluded from the Berkeley experiments. Further reduction in the number of data channels was possible by concentrating on the first floor level of the

model structure. The prototype study indicated that this is the most critically stressed region, though inelastic action also occurred at other floor levels. However, thorough instrumentation of the lowest level was sufficient to serve as a measure of prototype replication.

The instrumentation network utilized for the AMS model study is illustrated in Figure 4.31 while channel assignments and calibration constants are presented in Table 4.10. A total of 30 data channels were utilized and each model measurement had a counterpart in the prototype test results. Sequential channel assignment was used in the model study to minimize possible problems due to phase shifts of related channels. This was not done for the prototype study, thus several derived prototype results did exhibit phase shift effects, as will be discussed in Subsection 4.5.6.

A detailed description of the characteristics of the Stanford data acquisition system can be found in Section 3.5. At this point, specific data acquisition parameters must be defined for the AMS model study.

As the anticipated model fundamental frequency was about 5 Hz, it was decided to perform data block scans at 0.01 sec intervals to produce 20 points per fundamental cycle and approximately 5 points per second mode cycle. This sampling rate is in approximate agreement with the time-scaled prototype rate and produced adequate resolution of the model response. In all cases sampling was initiated approximately 1 sec before the input motion started and continued after the end of the seismic record to measure final free vibrations.

With 30 data channels, a data block size of 1920 necessitated a data transfer to magnetic tape every 0.64 sec with a 0.047 sec dump time. Thus, four data scans were missed at each dump, or approximately 20% of a fundamental cycle. Third-order interpolation performed during data

reduction did enable significant restoration of this discontinuity.

Experimental measurements consisted of global and local response quantities. Photographs of the AMS model instrumentation set-up are shown in Figure 4.32.

Global Response Measurement. The global response parameters consisted of floor displacements and accelerations. The prototype displacement transducers, wire potentiometers, were not suitable for use with a small-scale model as the force produced by the connecting cable is relatively large compared to the model weight and would contribute to model response. Thus, linear variable differential transformers (LVDT), which have little influence on specimen response due to their low friction characteristics, were used in the model study.

The displacements at the first and second floor were measured by a single LVDT at each level while two LVDT's were used at the third floor, the same arrangement as for the prototype. The use of two displacement transducers at the third floor permitted detection of any torsional response. As the model instrumentation was confined essentially to one frame only, this information was necessary to ensure that test measurements are representative of the entire structure.

The LVDT's at the first and second floor were mounted on a stiff instrumentation frame which was attached directly to the shake table platform. Thus, measurements were of model relative floor displacements. The LVDT rods were connected to the mid-span of the cross-frame primary beams.

The LVDT's at the top floor were mounted on a frame isolated from the shake table and measured the absolute third floor displacement. Relative displacement was calculated by subtraction of the table displacement.

The LVDT rods were connected to the column flanges at the level of the third floor framing.

Servo-accelerometers provided accurate measurement of the floor accelerations. One instrument was mounted at each floor level to record longitudinal accelerations. Also, the model instrumentation included one transverse accelerometer at the third floor to measure possible transverse response.

The prototype accelerometers were mounted at the mid-span of the cross-frame primary beams. If the model accelerometers had been attached by this arrangement the instrument mass would have contributed to the local response of the primary beam which may have produced questionable response measurements. This problem was avoided by mounting the model accelerometers at the mid-height of the steel floor-weights.

Measurement of the Stanford earthquake simulator response was provided by an accelerometer and LVDT attached to the simulator platform. The LVDT output was also used for servo-feedback displacement control of the shake table, as discussed in Section 3.2.

Local Response Measurement. The local response measurements were of two types--elastic and inelastic. Local strain measurements at locations where sections remained elastic were used for the deduction of member internal forces. Other transducers were used to sense the inelastic response of the structure.

Foil resistance strain gages were mounted on model girder and column element flanges for the determination of member forces. The gages were calibrated against known forces during the model subassembly tests for girder and column flexural moments and column axial load (see Subsection 4.4.3). The gage locations were scaled from those used for the prototype study and are sufficiently removed from member ends to maintain

elastic behavior at the gage (see Figure 4.31).

Wheatstone bridges with two active arms were utilized at locations where only member flexural moment was to be recorded. Single-arm bridges were used at the base of the first floor columns to enable measurement of axial force as well as flexural moment. The two-arm bridges were temperature compensating while the single-arm bridges were not. However, since the tests were of short duration no temperature fluctuations during this period were likely.

The joint panel 45° strain and overall shear distortion were used as a basis for comparison of the inelastic response of the model and prototype structures. The model study utilized a foil stacked-rosette, rather than two single gages used in the prototype study, mounted at the center of the panel zone to measure the 45° strain. A two-arm bridge was used to provide an average measure of the strain magnitude in the two orthogonal directions.

The overall shear distortion of the joint panel, γ , was determined from the relative diagonal displacement of the corners of the panel zone. The prototype instrumentation scheme of using LVDT's for this measurement was not applicable at small model scales. Thus, mercury resistance gages, mounted on pins at the column stiffener-flange junctions, were suspended diagonally across the model joint. A detailed description of the mercury gage can be found in Section 3.4 while the formulation for γ is presented in Subsection 4.5.3.

4.5.3 Parameters for Correlation of Model and Prototype Response

Various parameters can be used to enable a comprehensive evaluation of the earthquake simulator test results. The quantities to be used for response correlation between model and prototype are composed

of directly measured response parameters, such as floor displacements and accelerations, and derived quantities which are determined from mathematical manipulation of one or more measured quantities, e.g., response spectra and energy terms. These quantities can be further classified as global and local response parameters, as discussed in the previous subsection.

All quantities to be used for model-prototype correlation will be presented in the prototype reference frame. Thus, actual measured model quantities are multiplied by the appropriate modeling scale factors derived from dimensional analysis to convert to prototype units. The scaling laws for the 1:6 scale AMS model were presented in Section 4.2, Table 4.4. Each measured model parameter has a counterpart in the prototype study. These directly comparative data channels are presented in Table 4.11.

In most cases, presented time histories are truncated to 9 seconds (prototype time) to aid in the visual observation of the dynamic response. This time span includes the region of peak model and prototype response for all of the tests presented, though in the high intensity tests some inelastic action did occur after this cut-off period. Thus, input and dissipated energy plots are also presented for the full duration of the tests.

Time shifting of the prototype and model response histories is used to provide a common starting time just prior to earthquake simulator motion. Also, since the measured model natural frequency during the dynamic tests did not precisely match the desired value of $\sqrt{6} f_{\text{proto}}$, a time correction factor is applied to the model response quantities, as defined by

$$\beta_t = \frac{1}{\sqrt{6}} \left(\frac{f_{\text{model}}}{f_{\text{proto}}} \right)_{\text{measured}}$$

to aid in the comparison of model and prototype response time histories. The value of β_t for various tests is shown in Table 4.12. For perfect agreement with similitude requirements, β_t should be equal to one. This factor was not applied to shake table response functions.

Following is a brief description of the parameters used in the evaluation of the AMS model earthquake simulator test and in the prototype response correlation study.

Response Spectra. Relative displacement, velocity and absolute acceleration response spectra were calculated from the measured Stanford and Berkeley shake table motion and from the El Centro input command record for damping values of 0.5, 2 and 5% of critical damping. For the elastic tests an expanded set of spectra is presented to illustrate the table response in the spectral region of the structure natural frequency and for observed damping values. Also, floor response spectra, which illustrate the loading demands that would be placed on floor mounted components of an engineering structure, are presented for zero damping in the region of the test structure's first and second modal frequencies. These figures are also useful for determining the predominant frequencies of structural response.

Energy. Input and dissipated energy curves are presented for both the 9 second time period and for the entire test duration. These curves illustrate the intensity of inelastic response versus the actual energy transferred from the earthquake simulator to the test structure.

The input energy is determined from the expression

$$IE = \int V_o \dot{X}_o dt$$

where

$$V_o = \text{structure base shear}$$

$$\dot{X}_o = \text{shake table velocity}$$

The dissipated energy is calculated from the imbalance of the input energy and the stored energy, where the latter is composed of the test structure's kinetic energy and recoverable strain energy

$$SE = KE + RSE$$

where

$$KE = \sum_{i=1}^n \frac{1}{2} m_i \dot{x}_i^2$$

$$RSE = \sum_{i=1}^n \frac{V_i^2}{2K_i}$$

and

$$m_i = \text{story mass}$$

$$\dot{x}_i = \text{absolute velocity at level } i$$

$$V_i = \text{story shear at level } i$$

$$K_i = \text{story stiffness at level } i \text{ relative to level } i-1$$

$$n = \text{number of floors.}$$

Dissipated energy is then derived from the expression

$$DE = IE - SE$$

The values of IE and DE derived from these equations are very sensitive to small measurement inaccuracies and may not be extremely accurate. For instance, the DE in the model response did exhibit

occasionally a slight decrease with increasing time which is physically impossible.

An alternative expression for direct calculation of the dissipated energy, based on the approximation that the base shear can be calculated from the floor accelerations, is

$$DE = - \sum_{i=1}^n \int \left[\sum_{j=1}^n m_j \ddot{x}_j \right] \left[d(x_i - x_{i-1}) \right]$$

where

x_i = absolute displacement at level i

\ddot{x}_j = absolute acceleration at level j

The second formulation for DE is difficult to apply due to phase shifts between acceleration and displacement data measurements produced by the data acquisition system. Even very small phase shifts did lead to appreciable errors in the integration for the dissipated energy.

Table Motion: Measured shake table displacement and acceleration, as well as velocity derived from differentiation of displacement, are presented for comparison of the Stanford and Berkeley table response.

Floor Displacement: The test structure's floor displacements relative to the shake table displacement are one measure of the global response.

Floor Acceleration: Another global response parameter is the absolute acceleration of each floor level measured in the direction of input motion.

Story Drift: Story drift is determined from the displacement of each floor level relative to the displacement of the floor immediately below. In the case of the first floor the story drift is simply equal to the relative floor displacement.

Base Shear: The most accurate way of calculating the test structure's base shear is from the first-floor column moments measured by the strain gages mounted at the top and bottom of the column. This method of calculating this response quantity is compared to the estimate of base shear determined from the floor masses and absolute accelerations. This estimate neglects dissipated energy. A value of 9300 lb and 258 lb per floor is estimated for the prototype and model structure, respectively.

Story Shear: The model and prototype story shears are estimated from the floor masses and accelerations.

Panel 45° Strain, ϵ_{45} : Local inelastic response correlation is provided by the girder-column joint panel strain measured at a 45° angle to the member axes. This strain measure is approximately equal to the peak strain in the joint panel.

Joint Distortion, γ : The cumulative effect of the inelastic deformation in the girder-column joint is illustrated by this parameter. The relationship of γ to the measured relative displacement between the diagonally opposite panel corners is illustrated in Figure 4.33.

R.M.S.: The root-mean-square values for shake table displacement, velocity and acceleration, 3rd floor displacement and acceleration, and joint panel 45° strain and distortion are presented in time-history form.

Elastic Single Degree-of-Freedom System: The analytical time-history response of an oscillator to measured shake table motion gives considerable insight into the characteristics of the earthquake simulator reproduction capabilities for the model and prototype tests. The measured model and prototype natural frequency and damping are used to define the oscillator. The viscous damping is determined from the logarithmic decrement, evaluated through least-squares analysis, of the

structure's free-vibrations measured immediately following shake table motion.

For the inelastic dynamic tests additional response parameters are presented in the form of hysteresis curves.

Girder Moment vs. ϵ_{45} and γ : The girder moment measured at the strain gage location, 12 in. from the column flange (prototype dimension), is plotted against these deformation quantities. These hysteresis curves illustrate the strength and stiffness properties of the highest stressed elements as well as the localized ductility demands placed on these elements.

4.5.4 Testing History

An attempt was made during the AMS model test series to record all aspects of the model fabrication, loading and testing to permit complete evaluation of the state of stress in the model. Thus, every step which contributed to the initial conditions of the model at the time of dynamic testing must be considered as part of the test history.

As the completed model frames were stress-relieved after fabrication and the stresses induced by bolting of the cross-framing elements are small, the first significant contribution to stress histories came from welding of the column base plates to the shake table mounting fixture. Due to heat effects and possible but non-measurable misalignment of the base plates the welding procedure was anticipated to produce a measurable state of stress in the model. Thus, data were recorded from the three girder strain gage bridges to measure this effect.

After welding of the base plates, several free-vibration tests were performed prior to the application of the gravity load to enable a check of the instrumentation system. During the application of the

gravity weights data was recorded continuously from strain and displacement transducers. From the cumulative effects of the base welding and the dead-load application the stress-state of the model was well defined prior to any dynamic tests.

Various elastic tests were performed to define the model's dynamic properties, i.e., natural frequencies, mode shapes and damping. The methods felt to be applicable to the small-scale model study were forced and free vibration tests. In the forced vibration tests the frequency of the sinusoidal input motion was varied continuously until the peak response of the desired mode was observed. Mode shapes and natural frequencies could then be recorded.

Free vibration response studies utilized either sinusoidal input motion, tuned to the desired mode, or narrow-band white noise centered at the anticipated natural frequency to initially excite the model. The shake table motion was then quickly but smoothly stopped, enabling the determination of natural frequency, mode shape and modal damping from the resulting free vibrations. This method is felt to be the most effective for defining the dynamic properties of a test structure mounted on an earthquake simulator.

The prototype dynamic properties were determined from free and forced vibration tests where excitation was supplied by a 680 lb shaker mounted at the first floor level. The contribution of this added dynamic mass is difficult to define, thus some inaccuracy in the prototype property measurements can be expected. Also, since the test structure was not mounted on the shake table but on the laboratory floor for these tests, the flexibility of the Berkeley shake table support mechanism did not contribute to the model response as it would for the earthquake tests.

In the earthquake simulation test series the model and prototype test structures were subjected to two types of table motions, namely the North-South component of the 1940 El Centro earthquake and an artificial earthquake. The artificial earthquake was constructed for the prototype test series from 360 harmonics ranging from 0.05 to 18 Hz. A filter was then used to provide peak spectral amplitude in the region 0.4-2.0 Hz. The prototype El Centro command displacement signal was generated from double integration of the acceleration record.

For the model test series double integration was also used to provide the necessary El Centro shake table command signal. However, due to differences in numerical processing the resulting table displacement for the model study was somewhat different from that of the prototype study. Since this difference in prototype and model command signal was in the very low frequency range, no appreciable discrepancies in the structural response were produced by this phenomenon.

For the artificial earthquake the measured Berkeley shake table response to the full intensity motion (AE100) was used to generate the command signal for the Stanford table. Thus, compensation for Berkeley's table distortions was provided and the only source of disagreement between the model and prototype table motion was produced by response distortion of Stanford's earthquake simulator.

A complete record of the AMS model earthquake simulator test history is presented in Table 4.12. The notation EC and AE signify El Centro and artificial earthquake tests, respectively. The shake table intensity is also given as a percentage of the maximum prototype tests for El Centro and artificial earthquake input. Thus, "EC30-II" is the second El Centro test at an intensity setting of 30% of the prototype full-intensity earthquake.

Initially, several elastic tests were performed to determine that all testing systems were functioning as planned and also to provide a comparison to the prototype elastic tests. During the inelastic test series an attempt was made to duplicate the prototype test history to provide similar degrees of inelastic behavior. Each model test is then directly comparable to the respective prototype test.

4.5.5 Evaluation of Preliminary Tests

The initial stress state of the AMS model is defined by the data collected during welding of the column base plates and during application of the floor weights. The girder moments measured at the locations of the flexural strain gage bridges are presented in Table 4.13. In this table the moments measured at each of the three instrumented locations after base welding and after placement of the steel weights, in sequence from floors one through three, are given. From these data it can be seen that the moment induced at the SB location by the column base welding contributed to a high initial stress. In fact, the total initial moment at SB was nearly 25% of that required to produce yielding in the joint panel zone.

Since the prototype structure utilized bolting instead of welding of the column base plates it is likely that the stresses induced by attachment of the prototype base plates to the shake table produced lower stresses than for the model. Yet, the stress effects from placement of the floor weights is similar for the prototype and model test structures. Thus, the high initial stress in the model can be expected to contribute to initial yielding at a lower input intensity than for the prototype. This illustrates how seemingly minor factors may considerably influence the results of a small-scale model test.

A comparison of the model and prototype natural frequencies, modal

damping and mode shapes is given in Table 4.14. Also, the normalized mode shapes are presented graphically in Figure 4.34.

When viewing these results it must be remembered that the prototype tests were conducted with a 680 lb shaker mounted at the 1st floor level. To minimize the distortion of the observed properties the prototype forced vibration test results are used to define mode shapes and natural frequencies for the first two fundamental modes. During forced vibration the shaker mass does not contribute to the structure mass since it is moving independently of the test frame. Since in the prototype study the third mode was not excited under forced vibration, free vibration results are used for the prototype third mode definition as well as for all modal damping values. All of the presented dynamic properties of the model are derived from the results of free vibration tests.

As can be seen, the natural frequencies of the model are within 5% of the prototype values for the three fundamental modes. The mode shapes are also in close agreement except for the somewhat higher amplitude of the prototype response at the first floor. It is felt that the shaker mounted at this level accounts for the discrepancy.

The results for the modal damping values show somewhat greater variance. One contribution to this lack of agreement is that the damping values are quite small and were observed to vary somewhat from test to test. Also, the third floor displacement transducers were found to contribute considerably to the low amplitude energy dissipation characteristics of the model. The first mode damping value with the third floor LVDT's disconnected was 0.17%, indicating that the feedback from these instruments nearly doubled the apparent damping value for the first mode. This effect was not observed on higher mode damping values or on natural

frequencies or mode shapes. The first and second floor LVDT's were of a different type with smoother bores than the third floor LVDT's and did not contribute to the model response to such a significant degree.

Since the preliminary prototype tests were conducted with the test structure mounted on the laboratory floor and with no displacement transducers connected to the structure the damping values can be anticipated to be higher for the structure mounted on the table with instrumentation attached.

4.5.6 Evaluation of Earthquake Simulator Tests

Many earthquake simulator tests of ranging intensity were performed on the prototype and model test structures to enable a complete evaluation of the elastic and inelastic response characteristics. The total amount of data generated by the two test series is too vast to present in compact form, so only a general discussion of the results is presented in this section. Also, the results of several representative tests are shown in Figures 4.36 to 4.106, with relevant annotations in the text, to illustrate in detail the adequacy of prototype simulation by the small-scale model.

The results of initial, low-intensity elastic model tests indicated that the model response was considerably less than prototype response for the same intensity of input motion. Table response spectra, derived for the actual observed prototype and model damping values, illustrate the reason for this discrepancy. (See the following discussion of test EC25). As the observed viscous damping of the test structures was quite small, the amplitude of response was dependent only on a narrow range of input frequency components and was very sensitive

to local variations in the input response spectra. Since the model natural frequency was slightly greater than the desired value of $\sqrt{6}$ times the prototype frequency the model responded to a different local value of input spectra than did the prototype. Table reproduction irregularities produce an additional source of error. From these initial elastic tests it was then estimated that an intensity multiplier of approximately 2.0 would be required for both the model El Centro and artificial earthquake tests to develop the same amplitude of model response as that observed for the prototype. For instance, to match the prototype EC25 test the El Centro earthquake at a 50% intensity setting would be necessary for input to the model structure.

An intensity multiplier value of 2.0 was then used for many of the model elastic tests. Though this procedure did produce reliable elastic test results, as input amplitude was increased to levels sufficient to produce inelastic response it was found to be no longer valid. When the test structure yields the frequency of response shifts downwards, encompassing a wider range of the input spectrum. Thus, the sensitivity to local values of input frequency content is greatly reduced. Also, it was observed in both the prototype and model tests that the structure contributed to the input motion at higher amplitudes of input motion through feedback. The observed table response spectra then tended to indicate local maxima at the predominant frequencies of structural response. For all of the presented inelastic tests no intensity multiplier was applied to the model shake table input command. Thus, the model response parameters are derived directly from the actual observed behavior of the AMS model.

A critical state exists for low-intensity inelastic tests. During the initial stages of a dynamic test the structure responds elastically

until sufficient energy is transferred to the structure to initiate yielding. Until this threshold level is reached the response of the structure will still be dependent only on a narrow spectral input window. For high-intensity inelastic tests this threshold level is reached early in the test, reducing the importance of this phenomenon, though some contribution to prototype-model discrepancies is still apparent.

As was discussed previously, the high initial moment at location SB did contribute to early initial yielding of the AMS model at that joint. Yielding quite possibly occurred at joint NA also, though this is difficult to determine as no instrumentation was installed at this location. The AMS model underwent initial yielding during the first EC25 test with an intensity multiplier of 2.0, while this was only a high-intensity elastic test for the prototype structure. The total peak girder moment at girder-column connection SB, determined from the summation of the moment due to column base welding, dead load application and dynamic motion, was approximately 280 kip-in. while the measured yield moment in subassembly tests 1 and 2 was 210 and 240 kip-in., respectively.

The girder moment-joint deformation yield plateau observed during the model subassembly tests was also apparent during the first inelastic cycle at each joint of the AMS model. This phenomenon did not occur during subsequent inelastic cycles and so was not a major problem for successful modeling of the prototype.

After initial yielding of the model test structure a redistribution of stresses negated the effect of the high initial stresses. Thus, the EC25 model test was repeated, again with an intensity multiplier of 2.0, to enable comparison with the prototype results for a high

intensity elastic test.

Results from inelastic tests subsequent to the first fully inelastic test, EC30, showed essentially no permanent offset of deformation, as would be produced if yielding was not primarily confined to the joint panel zones but extended into the structural members. Response histories then appeared as a wave form oscillating about a zero mean value.

The response of the prototype and model structures during the dynamic tests was predominantly in the first mode. The higher frequency content of the Artificial Earthquake did excite some second mode response in both structures, though the first mode still dominated.

From the results of the model inelastic test series an interesting observation can be made. The structure inelastic ductility demand is essentially a linear function of the intensity of the shake table input motion. Figure 4.35 illustrates this behavior pattern for the El Centro test series. Extrapolation of this response function enables the prediction of input motion intensities required to produce desired levels of model response.

The earthquake simulator tests chosen for detailed presentation consist of three El Centro tests, EC25, EC100 and EC130, and one test with the Artificial Earthquake as input, AE100. The elastic EC25 test is actually the second 25% El Centro test performed on the model, as was mentioned previously. The EC100 and AE100 tests duplicate the full intensity inelastic tests of the prototype series. As will be discussed later in this section, the 130% intensity El Centro test was chosen for the model study from linear extrapolation of the ductility demand versus input intensity response function to produce response levels in the model similar to those of the prototype EC100 test.

A summary of peak input and response measurements for these tests is given in Table 4.15 for the prototype and model structures. Several pertinent observations can be made from these results. The model EC25 test actually utilized the El Centro input at 50% intensity as an intensity multiplier of 2.0 was used in an attempt to match prototype and model spectral input components at the structure natural frequency. Thus, the measured Stanford shake table acceleration is roughly twice that for the prototype. From the results of this test an actual spectral ratio of approximately 1.6 was observed, as can be seen in Figure 4.39. This indicates that the model structural response will be about $2.0/1.6 = 1.25$ times prototype response, as is the case.

The time correction factor, β_t , varies from a value of 1.06 for the EC25 test to 1.02 for the AE100 test. This indicates that the model natural frequency was roughly two to six percent higher than the desired value of $\sqrt{6} f_{\text{proto}}$. As a test progressed, this produced a phase shift between the model response relative to the prototype response and, more importantly, to the Stanford shake table motion which was scaled precisely to $t_r = 1:\sqrt{6}$. For $\beta_t = 1.02$ the model response led the prototype response relative to the input motion by nearly 0.2 sec., 40 percent of the fundamental period of the structure after 9 seconds of test.

Fundamental frequencies and viscous damping values were obtained from free vibrations measured immediately after the EC25 input motion had ceased for both the model and prototype structures. Since these values were determined for the fully instrumented structures mounted on the shake table they indicate the actual dynamic properties of the structures as tested, and show some variation from the values obtained during preliminary free and forced vibration tests, particularly in the case of the prototype study. The prototype natural frequency and damping

was found to be 2.18 Hz and 0.47%, respectively, while the model responded at 2.33 Hz (5.71 Hz real time) with a measured damping value of 0.28% of critical.

The test results presented in Figures 4.36 to 4.106 for the example earthquake simulator tests illustrate in detail the correlation of the model and prototype response through the character of the input motion and through global and local response parameters. Unless otherwise noted, the prototype response is depicted by a solid line while a dashed line is used for model results in these figures. As for the most part the presented test results are self-explanatory, every aspect of the tests will not be discussed. Instead, comments will be limited to notable points.

1. El Centro, 25% Intensity Test--Elastic

The use of an intensity multiplier for the model EC25 test input motion somewhat complicates the presentation of the results. Since the input motion was increased by a factor of two in an attempt to obtain the same level of response amplitude in the model as was observed for the prototype, the measured Stanford table displacement, velocity and acceleration time histories are scaled by a factor of 0.5 to enable direct comparison to the prototype input motion. This was also done for the model table response spectra (Figures 4.36-4.38). All other response curves, including the narrow-band response spectra, are presented as they were actually measured.

The prototype table response spectra indicate considerable amplification of the input signal in the frequency range of 5-10 Hz which is most noticeable in the velocity and acceleration spectra (Figures 4.37a and 4.38a). One suspected source of this distortion is a spurious signal, possibly caused by a tape drive malfunction, at the beginning

of the table input motion. Though the frequency content of this signal is well-removed from the prototype fundamental natural frequency a contribution to second mode response is likely. More importantly, this initial input may have produced some forced vibration response of the prototype structure prior to instigation of the earthquake motion. Thus, the prototype had conditions of initial velocity and displacement at the beginning of the test while the model structure response began from an initial static state, contributing to the tendency for higher prototype than model response during the dynamic tests.

The narrow-band response (Figure 4.39), calculated for frequencies neighboring the structure fundamental mode illustrate the influence of local spectral variations on the structural response in the elastic region. The model and prototype predominant frequencies of response are derived from the floor spectra (Figure 4.40) and free vibrations.

As this is a high-intensity elastic test, the primary source of dissipated energy is from elastic damping. Under this heading of elastic damping many mechanisms contribute to energy dissipation, including material damping and instrumentation friction effects. As can be seen in Figure 4.41, model input energy is considerably higher than for the prototype for the initial 9 seconds, but it must be remembered that an actual input intensity of 50% of El Centro was used for the model input rather than 25%. Since the base shears do not differ significantly between model and prototype (see Figures 4.46 and 4.47), most of the difference in input energy must be attributed to discrepancies in velocities of prototype and model shake table motions. The regions of negative slope on the dissipated energy curves for the model are produced at data dump locations because of a low signal to noise ratio

for this low-intensity test, reducing the accuracy of the interpolation procedure (see Sections 3.5 and 3.6).

The table displacement and velocity time histories shown in Figure 4.42 are not directly comparable due to differences in command signal generation. This difference is exhibited primarily in the very low frequency range, i.e., less than 0.5 Hz, and does not adversely affect the accuracy of prototype simulation by the AMS model.

Other global and local response parameters continue to show good correlation between the model and prototype results, with somewhat higher model response than for the prototype. As was discussed earlier, a direct comparison would require that all model response measurements be multiplied by approximately 0.8. Similar results are also obtained from a response analysis of a single degree of freedom system subjected to the actual measured table motions (see Figure 4.52). The dynamic properties of the mathematical model were defined by the natural frequency and fundamental damping observed during free vibration of the model and prototype after the EC25 input.

2. El Centro, 100% Intensity Test

The cyclic signal observed prior to the prototype EC25 test is also apparent in the EC100 test and can be seen at the beginning of the table acceleration time history (Figure 4.58). Also, Berkeley table response spectra again indicate large amplification in the 5-10 Hz frequency range (Figures 4.54a and 4.55a). This spurious signal is felt to be a contributing factor for prototype response histories showing initially higher amplitude than for the model.

The variation in model and prototype amplitude of response is more apparent at a local level than from the global response histories.

Though inelastic action is primarily confined to the joint panel zones the global response of the structure is developed from many contributions, including elastic flexural, shear and axial deformations, as well as the joint panel inelastic deformation.

The model rms of table displacement presented in Figure 4.65 shows much higher amplitude than for the prototype test. This is due to low frequency filtering of the prototype shake table signal. The high rms values for prototype table acceleration are produced by the inadvertent cyclic input prior to the earthquake test.

The elastic analytical one degree of freedom response to the measured Stanford and Berkeley table motion shown in Figure 4.68 also illustrates that the prime source of model and prototype discrepancies is the character of the earthquake simulator response.

The prototype hysteresis plots presented in Figures 4.69 and 4.70 must be interpreted with considerable caution. A substantial time difference between sampling of the girder moment and the joint deformation channels tended to increase or decrease the apparent hysteresis loops depending on which parameter was leading in phase. For joint SA, the tendency was to produce an overly large estimate of the area of the hysteresis loops and a greater number of inelastic cycles than actually occurred. Even with this effect, it is evident that the prototype structure was subjected to a higher deformation demand and a greater number of inelastic excursions than was the AMS model.

3. El Centro, 130% Intensity Test

As the table motions were somewhat different and the strength of the model beam-column joints was a little higher, the model response fell short of the prototype response to the EC100 input. Thus, an

additional model test at elevated intensity was performed to produce desired levels of response. Linear extrapolation of the model table input intensity versus panel 45° strain indicated that an El Centro intensity of approximately 130% would be required to produce strain demands matching those observed during the prototype 100% El Centro test.

Considerably better correlation between the model and prototype test results was obtained for this test. However, the AMS model continued to exhibit high amplitude response during the second half of the 9 second time history segment while the prototype reached peak amplitudes at an early stage of the test.

Table motion response curves (Figure 4.76) show considerable variation for model and prototype since the model input is 130% of El Centro while the prototype input is El Centro at 100% intensity.

The analytical elastic predictions of structural response (Figure 4.86) continue to indicate that the model test structure is less sensitive to the Stanford table motion than is the prototype to the Berkeley motion. However, since the inelastic threshold level was reached quite early in the test, similar model and prototype response was produced.

4. Artificial Earthquake, 100% Intensity Test

The AE100 test enables an evaluation of model simulation of the prototype response to input motion with different properties than the El Centro earthquake. For the model Artificial Earthquake test series the actual measured Berkeley table response record was used as input to the Stanford shake table. Thus, model and prototype table motions are directly comparable. Using the prototype table response as model input command eliminated the effects of Berkeley table distortions on

successful model-prototype correlation, and produced only one possible source for discrepancies in model versus prototype input motion, i.e., the reproduction capabilities of the Stanford earthquake simulator.

Good correlation of input motion is apparent from the response spectra (Figures 4.89-4.91) and table motion time histories (Figure 4.94), though the Stanford table was not able to fully reproduce the abrupt peaks in the prototype input spectra. The slight phase shift of the model table time histories relative to the prototype is caused by the finite resolution capability of the computer based timer used for generation of the model input command signal for storage on analog tape and is also possibly due to some variation in tape playback speed.

Generally very good correlation of response amplitudes is attained for this earthquake simulator test at both the global and local levels of structural response. The only significant variation is that the model exhibits a second portion of high-intensity inelastic response beginning approximately seven seconds into the test, while this is not observed for the prototype. As mentioned previously, the time correction factor, β_t , indicates that as the test progresses a constantly increasing phase difference between the model and prototype response is produced. Thus, while for the prototype structure at $t = 6.5$ sec. input motion opposes structural motion and decreases the amplitude of response, the same input motion produces increased dynamic amplitudes for the model. This phenomenon can also be observed from the energy curves given in Figure 4.93, where the prototype input energy and dissipated energy curves reach a common value at $t = 6.5$ sec. indicating that prototype motion has momentarily ceased, while an abrupt increase in model input energy produced a large increase in inelastic response.

Significantly more second mode response is apparent from the model

and prototype test results than for the El Centro tests. Still, the structure response is predominantly of the fundamental mode.

4.5.7 Summary--Model vs. Prototype Response

Several specific conclusions can be drawn from the results of the AMS model study in relation to the accuracy of prototype simulation and possible sources of discrepancies. In general, the nature of inelastic response is duplicated by the small-scale dynamic model by yielding of the joint panel zones in shear. Thus, the critical elements for model and prototype are identical, with the yielding of these zones producing similar response characteristics for the two test structures.

The adequacy of prototype simulation is illustrated by the similar dynamic properties and energy dissipation characteristics of the model through correlation of global and local response parameters. The basis for comparison is the amplitude and frequency content of structural response and the ductibility demand and number of inelastic excursions.

Three primary sources of error serve to prevent exact duplication of prototype behavior. These discrepancies are produced by the differences in prototype and model initial stress state, weld sizes and earthquake simulator motion. The first two factors are concerned with the accuracy of the small-scale model as a representation of the prototype while the latter is a problem that exists with the experimental test facilities.

The high initial internal forces in the model, produced by welding of the column base plates to the simulator platform, contributed to yielding at a lower input intensity level than was required for the first prototype inelastic response. However, after first yielding

of the model had occurred a redistribution of internal forces eliminated the effect of the initial stress so that no problems were produced by this source in subsequent inelastic tests.

The overly large welds of the model structure produce a stiffer system as the resulting model joint panel zones are smaller than the scaled prototype panels. This effect is apparent in the somewhat higher yield strength and greater inelastic stiffness of the AMS model in relation to the prototype. However, the influence of the distorted weld size is not so severe as to cause considerable variation in prototype and model response.

A secondary effect, also believed to be produced by the oversized model welds, is the yield plateau exhibited by the model at the first inelastic excursion. The stiffening contribution of the large boundary welds of the joint panel tends to produce a uniform shear stress over the panel zone which may contribute to this virgin yield phenomenon. Since this effect was not observed in subsequent inelastic test it was not a source of difficulty.

Dynamic tests illustrate that the reproduction capability of an earthquake simulator has a great influence on the ability of a small-scale model to accurately duplicate the response of the prototype to a given input motion. This dependence is apparent in both elastic and inelastic test results, though a structure responding elastically is considerably more sensitive to local fluctuations of the table motion spectrum than is a structure behaving inelastically. Still, sufficient energy must be transferred to the structure at the elastic level before the threshold required to produce inelastic action can be reached. Once inelastic action does occur, this dependence on a narrow range of input frequency is reduced.

Even for a perfect model some apparent discrepancies will exist in prototype-model correlation due to these table distortions and will appear in the form of amplitude and phase differences between the two structures. However, for most cases the response of a suitable shake table will sufficiently reproduce the general character of earthquake motions which will enable a valid test of a small-scale model, though exact duplication of test structure response between different experimental facilities is impossible. Many different input time histories may then be used to ensure that the dynamic behavior of the structure has been adequately defined.

Additional less critical but possible sources of error in the AMS model study can be identified.

1. Material size and strain rate effects could become more severe at smaller model scales, though they were not a major problem at $\lambda_r = 1:6$.
2. Slight differences in natural frequencies and damping tend to produce phase shifts between prototype and model response which may contribute to discrepancies.
3. The distortion of some prototype elements to simplify construction of the small-scale model may have produced some slight differences in behavior. For instance, the model utilized rectangular secondary beams versus the wide flange sections of the prototype. Thus, all mechanical properties of this member could not be simulated. However, the slight alteration of the structural system is justified by the reduction in fabrication efforts.
4. Different instrumentation and data acquisition procedures may influence structural response measurements. For instance,

prototype accelerometers were mounted on cross-beams, where local vibrations may be recorded, while model accelerometers were attached to the floor weights. Also, phase errors produced by the prototype data acquisition system create apparent discrepancies between model and prototype response parameters.

From the test results the AMS model has been shown to be an accurate replica of the prototype structure, with the major source of observed response discrepancies being the character of the input motion supplied by the respective earthquake simulators. Any actual differences in the model and prototype structural systems are secondary to this effect.

Table 4.1

MODELING LAWS FOR ARTIFICIAL MASS SIMULATION

Scaling Parameters*		Artificial Mass Simulation	
		any material	prototype material
length	<u>ℓ_r</u>	ℓ_r	ℓ_r
time	t_r	$\ell_r^{1/2}$	$\ell_r^{1/2}$
frequency	ω_r	$\ell_r^{-1/2}$	$\ell_r^{-1/2}$
velocity	v_r	$\ell_r^{1/2}$	$\ell_r^{1/2}$
gravitational acceleration	<u>g_r</u>	1	1
acceleration	a_r	1	1
structure mass	M_r	$E_r \ell_r^2$	ℓ_r^2
strain	ϵ_r	1	1
stress	σ_r	E_r	1
modulus of elasticity	<u>E_r</u>	E_r	1
displacement	δ_r	ℓ_r	ℓ_r
force	F_r	$E_r \ell_r^2$	ℓ_r^2
energy	$(EN)_r$	$E_r \ell_r^3$	ℓ_r^3

* 1. Subscript "r" refers to a ratio of model to prototype parameter (e.g., the model scale, $\ell_r = \ell_{\text{model}} / \ell_{\text{prototype}}$).

2. Underlined scale ratios are chosen by the investigator.

Table 4.2

PROTOTYPE SECTION PROPERTIES

	Girder - W6x12		Column - W5x16	
	Nominal	Actual	Nominal	Actual
b (in)	4.00	4.016	5.00	5.000
d (in)	6.00	6.031	5.00	4.968
t _w (in)	0.230	0.243	0.240	0.246
t _f (in)	0.279	0.284	0.360	0.367
A (in ²)	3.54	3.607	4.70	4.700
I _x (in ⁴)	21.7	22.19	21.3	21.01
S _x (in ³)	7.25	7.35	8.53	8.48
Z _x (in ³)	8.23	8.37	9.61	9.55

Table 4.3

PROTOTYPE ESTIMATED WEIGHTS

	Concrete Blocks 1b	Columns 1b	Girders 1b	Cross Beams 1b	Bracing 1b	Misc. 1b	Total 1b
3rd Floor	8240	214	274	402	50	120	9300
2nd Floor	8100	342	274	402	50	120	9288
1st Floor	8060	384	274	402	50	120	9290

Table 4.4

AMS MODEL SCALING REQUIREMENTS

Scaling Parameters*		Scale	Value
length	\underline{l}_r	1:6	0.1667
time	t_r	$\underline{l}_r^{1/2}$	0.4082
frequency	ω_r	$\underline{l}_r^{-1/2}$	2.4495
velocity	v_r	$\underline{l}_r^{1/2}$	0.4082
gravitational acceleration	\underline{g}_r	1:1	1.0000
acceleration	a_r	1	1.0000
structure mass	M_r	$E_r \underline{l}_r^2$	0.0278
strain	ϵ_r	1	1.0000
stress	σ_r	E_r	1.0000
modulus of elasticity	\underline{E}_r	1:1	1.0000
displacement	δ_r	\underline{l}_r	0.1667
force	F_r	$E_r \underline{l}_r^2$	0.0278
energy	$(EN)_r$	$E_r \underline{l}_r^3$	0.00463

*Underlined scale ratios are chosen by the investigator.

Table 4.5

TOLERANCES FOR TRIAL MODEL ELEMENTS, $\underline{l}_r = 1:6$

	Tolerances	Measured Deviations	
	Scaled Standard Mill Practice	Welded Specimen	Machined Specimen
Flange out of Square	<0.04"	0.03"	0.01"
Camber	<0.025"	0.10"	0.02"
Sweep	<0.05"	0.08"	0.01"

Table 4.6

MACHINED SECTIONS FOR AMS MODEL, $\lambda_r = 1:6$

	Model Girder (W6x12 Prototype)				Model Column (W5x16 Prototype)			
	Specified	Actual Average	Tolerance*	Actual Maximum	Specified	Actual Average	Tolerance*	Actual Maximum
b (in)	0.669	0.670	+0.04/-0.03	±0.004	0.833	0.833	+0.04/-0.03	±0.005
d (in)	1.005	1.006	±0.02	±0.007	0.828	0.829	±0.02	±0.008
t _w (in)	0.041	0.040	--	±0.004	0.041	0.041	--	±0.004
t _f (in)	0.047	0.047	--	±0.007	0.061	0.062	--	±0.006
A (in ²)	0.1002	0.1028	±0.003	±0.005	0.1306	0.1356	±0.003	±0.005
I _x (in ⁴)	0.01712	0.01768	--	--	0.01621	0.01681	--	--
Camber (in)	--	--	.025	.02	--	--	.038	.01 [†]
Sweep (in)	--	--	.05	.01	--	--	.038	.04
Flange out of Square (in)	--	--	.04	.01	--	--	.04	.01

*Tolerances are scaled values from standard mill practice, AISC Steel Construction Manual (27).

†Column camber increased to .05 in. after welding of stiffeners and heat treatment.

Table 4.7

MATERIAL PROPERTIES -- PROTOTYPE AND MODEL COUPONS

Property	Prototype Girder			Prototype Column			Model Girder			Model Column				
	w	f	f	w	f	f	w	f	f	w	w	f	f	f
$\dot{\epsilon}_{\text{elastic}}$ (in/in/sec)	$3(10^{-5})$	$2(10^{-5})$	$8(10^{-6})$	$3(10^{-5})$	$2(10^{-5})$	$4(10^{-5})$	$2(10^{-4})$	$2(10^{-4})$	$2(10^{-4})$	$2(10^{-4})$	$2(10^{-4})$	$2(10^{-4})$	$2(10^{-4})$	$2(10^{-1})$
$\dot{\epsilon}_{\text{strain hardening}}$	$2(10^{-3})$	$8(10^{-4})$	$3(10^{-4})$	$2(10^{-3})$	$8(10^{-4})$	$2(10^{-3})$	$2(10^{-4})$	$2(10^{-4})$	$2(10^{-4})$	$2(10^{-4})$	$2(10^{-4})$	$2(10^{-4})$	$2(10^{-4})$	$2(10^{-1})$
E ($\times 10^3$ ksi)	30.9	30.9	30.7	30.3	30.1	29.5	27.7	28.0	23.9 [†]	--	26.3	27.5	26.8	30.1
σ_y^{upper} (ksi)	51.8	--	40.1	45.5	39.5	42.6	--	--	--	--	48.7	49.3	47.0	58.5
σ_y (ksi)	47.4	37.9	39.5	42.7	38.0	39.0	42.6	40.5	40.3	--	45.6	46.3	46.5	51.2
σ_{ult} (ksi)	67.6	63.7	63.5	65.0	--	65.4	67.8	63.8	--	66.8	--	--	65.3	--
E_{st} (ksi)	490	880	590	480	650	650	600	610	550	--	450	380	400	400
E_{st}/E (%)	1.6	2.8	1.9	1.6	2.1	2.2	2.2	2.2	2.3	--	1.7	1.4	1.5	1.3
ϵ_{st} (milli - in/in)	24.5	14.6	15.8	27.0	18.3	21.0	15.1	12.9	14.2	--	16.4	19.9	19.4	24.3
$\epsilon_{\text{st}} - \epsilon_y$ (milli - in/in)	22.9	13.3	14.4	25.5	17.0	19.6	13.6	11.4	12.5	--	14.6	18.1	17.4	22.2
$\epsilon_y/\epsilon_{\text{st}}$ (%)	15	12	12	18	14	15	11	12	12	--	11	9	9	8

*Location is indicated as "w" for web, "f" for flange coupon.

[†]Measurement error was assumed responsible for the low E value.

Table 4.8
NOMINAL MATERIAL PROPERTIES

Property	Material	Model Base Material			Model Coupons			Prototype Coupons	
	Girder ₁	Column		Sheet Metal ₂	Girder	Column		Girder	Column
σ_y (ksi)	39	43	47	54	41	46	51	42	40
E (ksi)	-	33500	31000	31400	27900	26900	30100	30800	30000
σ_u (ksi)	63	67	-	70	66	66	-	65	65
$\dot{\epsilon}$ (in/in/sec)	-	$2(10^{-4})$	$2(10^{-2})$	-	$2(10^{-4})$	$2(10^{-4})$	$1.5(10^{-1})$ ₃	Varies	Varies

1. Mill test report.
2. Sheet metal used for model stiffeners.
3. Strain rate of $1.5(10^{-1})$ corresponds to a ductility factor of 2 at the model natural frequency (5.5 Hz).

Table 4.9

MODEL ELEMENTS AS FORCE TRANSDUCERS

	Girder	Column	
	$M_G / \frac{\text{flex}}{\epsilon_G}$ (in-lb/ $\mu\epsilon$)	$M_c / \frac{\text{flex}}{\epsilon_c}$ (in-lb/ $\mu\epsilon$)	$P_c / \frac{\text{axial}}{\epsilon_c}$ (lb/ $\mu\epsilon$)
Subassembly 1	0.942	1.063	3.205
Subassembly 2	0.930	1.063	3.906
Difference	1.3%	-	19.7%
Average	0.935	1.063	3.522
Theoretical	1.020	1.176	3.937

1. All strains are extreme fiber strains in 10^{-6} in/in.
2. Calibration values are only applicable to a particular strain gage type.
3. Theoretical values are based on nominal dimensions and an elastic modulus of $29(10^6)$ psi.

Table 4.10

AMS MODEL INSTRUMENTATION

Channel No.	Description	Units	Units/Volt (model dimensions)
1	Displacement input command	v	1.00
2	Table displacement	in	varies
3	Table acceleration	g	0.1
4	1st floor relative displ.	in	0.1
5	2nd floor relative displ.	in	0.1
6	3rd floor absolute displ., B	in	0.29802
7	3rd floor absolute displ., A	in	0.29348
8	1st floor acceleration	g	0.10 (1.0)*
9	2nd floor acceleration	g	0.10 (1.0)
10	3rd floor acceleration	g	0.10 (1.0)
11	3rd floor transverse accel.	g	0.10
12	Girder moment, 1st floor, SA	in-lb	225.229
13	Panel ϵ_{45} , 1st floor, SA	millistr	0.97561
14	Panel γ , 1st floor, SA	millirad	2.48815
15	Column moment, 1st floor, above, SB	in-lb	102.458
16	Column moment, 1st floor, below, SB	in-lb	102.458
17	Column strain, exterior face, base, SB	microstr	481.928
18	Column strain, interior face, base, SB	microstr	481.928
19	Panel ϵ_{45} , 1st floor, SB	millistr	0.97561
20	Panel γ , 1st floor, SB	millirad	2.40339
21	Girder moment, 1st floor, SB	in-lb	225.229
22	Girder moment, 1st floor, NB	in-lb	225.229
23	Column moment, 1st floor, above NB	in-lb	102.458
24	Column moment, 1st floor, below NB	in-lb	102.458
25	Column strain, interior face, base, NB	microstr	481.928
26	Column strain, exterior face, base, NB	microstr	481.928
27	Panel ϵ_{45} , 1st floor, NB	millistr	0.97561
28	Panel γ , 1st floor, NB	millirad	2.57159
29	Panel ϵ_{45} , 2nd floor, NB	millistr	0.97561
30	Panel γ , 2nd floor, NB	millirad	2.31224

*Floor accelerometer sensitivity at 1.0 g/volt for high intensity tests

Number of channels = 30

Sampling period = 0.01 sec

Table 4.11

PROTOTYPE - MODEL COMPARATIVE DATA CHANNELS

Prototype Channel	Description	Model Channel	
4	Table displacement	2	
6	Table acceleration	3	
24	Panel γ , 1st floor, NA, front	28	
25			front
26			rear
27	Panel γ , 1st floor, SA, front	14, 20	
28			front
29			front
30			rear
31	rear		
32	1st floor displacement	4	
33	2nd floor displacement	5	
34	3rd floor displacement, A	7	
35		B	
36	1st floor acceleration	8	
37	2nd floor acceleration	9	
38	3rd floor acceleration	10	
57	Girder moment, 1st floor, SA	12	
64		NB	
71		SB	
75	Panel ϵ_{45} , 1st floor, SA	13	
78		NB	
81		SB	
58	Column moment, base, NB	25 + 26	
59	Column moment, 1st floor, below, NB	24	
65	Column moment, base, SB	17 + 18	
66	Column moment, 1st floor, below, SB	16	

Table 4.12

AMS MODEL TEST FILES

Model File	Description	Imult (If #1)	Shake Table Range	Shake Table Span (%)	Test Duration (Sec)	Prototype File	Comments	Time Mult., β_t	Date
-	Dead load 1st floor					13			
-	2nd					14			
-	3rd					15			
1	Free vibr., 3rd mode						Without 3rd floor LVDTs		
2	2nd						"		
3	1st						"		
4	1st								
5	3rd								
6	2nd								
7	1st								
8	1st						Without 3rd floor LVDTs		
9	Forced vibr., 2.5 Hz		4	2.0		17			
10	EC10		4	37.6	30	19			12/13/78
11	EC20		4	75.2	30	25		1.07	
12	AE20		4	22.7	20	26			
13	EC25	2.0	2	37.6	30	49	Joint SB initial yield	1.06	12/15/78
14	EC20-II	2.0	3	75.2	30	25			12/20/78
15	EC25-II *	2.0	3	94.0	30	49		1.06	
16	AE20-II	2.0	4	45.4	30	26			
17	EC30	1.9	2	42.9	30	28	First totally inelastic test	1.04	
18	AE40		4	45.4	20	30			
19	EC30-II	1.8	2	40.6	25	28		1.04	
20	AE40-II	0.8	4	36.4	20	33	No yielding observed		
21	EC50	1.8	2	67.7	25	35			12/20/78
22	EC30-III		3	56.4	25	28	No yielding observed		12/27/78
23	EC62.5		2	47.0	25	38			
24	EC62.5-II		2	47.0	25	40			
25	AE53.3		4	60.6	20	43			

Table 4.12, continued

Model File	Description	Imult (If #1)	Shake Table Range	Shake Table Span (%)	Test Duration (Sec)	Prototype File	Comments	Time Mult., β_t	Date
25	AE66.7		4	75.8	20	45			
27	EC75		2	56.4	25	52			
28	EC75-II		2	56.4	25	55			
29	EC75-III		2	56.4	25	58			
30	EC87.5		2	65.8	25	61			
31	AE66.7		4	75.8	20	63			
32	AE100	*	3	56.8	25	66	Highest intensity AE	1.02	
33	EC100	*	2	75.2	30	69	-	1.04	
34	EC20-III		4	52.9	20	25	Repeat EC series with	1.07	1/2/79
35	EC25-III		4	66.1	20	49	proto table response	1.07	
36	EC30-IV		4	79.3	25	28	as model table input	1.07	
37	EC100-II		2	52.9	25	69	↓	1.05	
38	EC100-III		2	52.9	25	69			1/3/79
39	EC130	*	2	97.7	30		Highest intensity EC	1.04	1/8/79

Table 4.13

AMS MODEL -- BASE WELDING AND DEAD LOAD APPLICATION

Channel No.	Location	Total Girder Moment* (kip-in), After;			
		Welding	Weights on Floor		
			1	2	3
12	SA	12	-14	-17	-16
21	SB	-30	-57	-60	-60
22	NB	6	-20	-23	-23

- * 1. Girder moment at strain gage location.
 2. Positive moment corresponds to upward curvature.
 3. Model moments converted to prototype values.

Table 4.14

DYNAMIC PROPERTIES -- FREE AND FORCED VIBRATION TESTS

Mode Floor	Model			Prototype ²		
	1	2	3	1	2	3
3	1.00	1.00	0.46	1.00	1.00	0.46
2	0.75	-0.69	-1.00	0.77	-0.62	-1.00
1	0.37	-0.95	0.86	0.41	-1.23	1.03
Nat. Frequency ¹ (Hz)	2.4	8.3	15.5	2.3	7.8	15.2
Damping (%)	0.28	0.16	0.29	0.11	0.08	0.57

1. Prototype time reference.
 2. Prototype structure with 680 lb shaker at the first floor.

Table 4.15

PROTOTYPE AND MODEL PEAK VALUES

Parameter	EC25		EC100		EC130 ⁽³⁾		AE100	
	P	M ⁽²⁾	P	M	P	M	P	M
Table Acceleration, filtered (g)	0.16	0.37	0.53	0.49	0.53	0.54	0.56	0.52
3rd Floor Relative Displ. (in)	1.22	1.41	3.29	2.76	3.29	3.37	2.65	2.70
3rd Floor Acceleration (g)	0.62	0.80	1.38	1.31	1.38	1.57	1.85	1.82
Base Shear (kip)	12.8	16.3	29.5	29.8	29.5	34.5	26.8	29.0
ϵ_{45} (millistrain)	1.02	1.10	5.75	4.52	5.75	6.01	3.74	3.94
γ (milliradian)	1.92	2.48	10.01	8.04	10.01	10.28	6.35	7.11
Girder Moment, gage (kip-in)	134	141	263	236	263	269	212	239
Ductility Demand ⁽⁴⁾ ϵ_{45}	0.78	0.85	4.42	3.48	4.42	4.62	2.88	3.03
γ	0.80	1.03	4.17	3.35	4.17	4.28	2.65	2.96
β_t ⁽⁵⁾	--	1.06	--	1.04	--	1.04	--	1.02

(1) P signifies prototype structure, M is for model.

(2) Model EC25 test used an intensity multiplier of 2.0. A posterior evaluation of response spectra has shown that the best intensity multiplier would have been 1.6, i.e., for direct comparison the model response values in this column should be multiplied by $1.6/2.0 = 0.8$.

(3) Prototype results from EC100 are compared to model EC130 test.

(4) Ductility demand is based on the yield values obtained from analytical analysis ($\epsilon_{45y} = 1.3 \text{ m}\epsilon$, $\gamma_y = 2.4 \text{ mrad}$) using the procedure of Krawinkler, et al (20)

(5) Time correction factor is discussed in subsection 4.5.3.

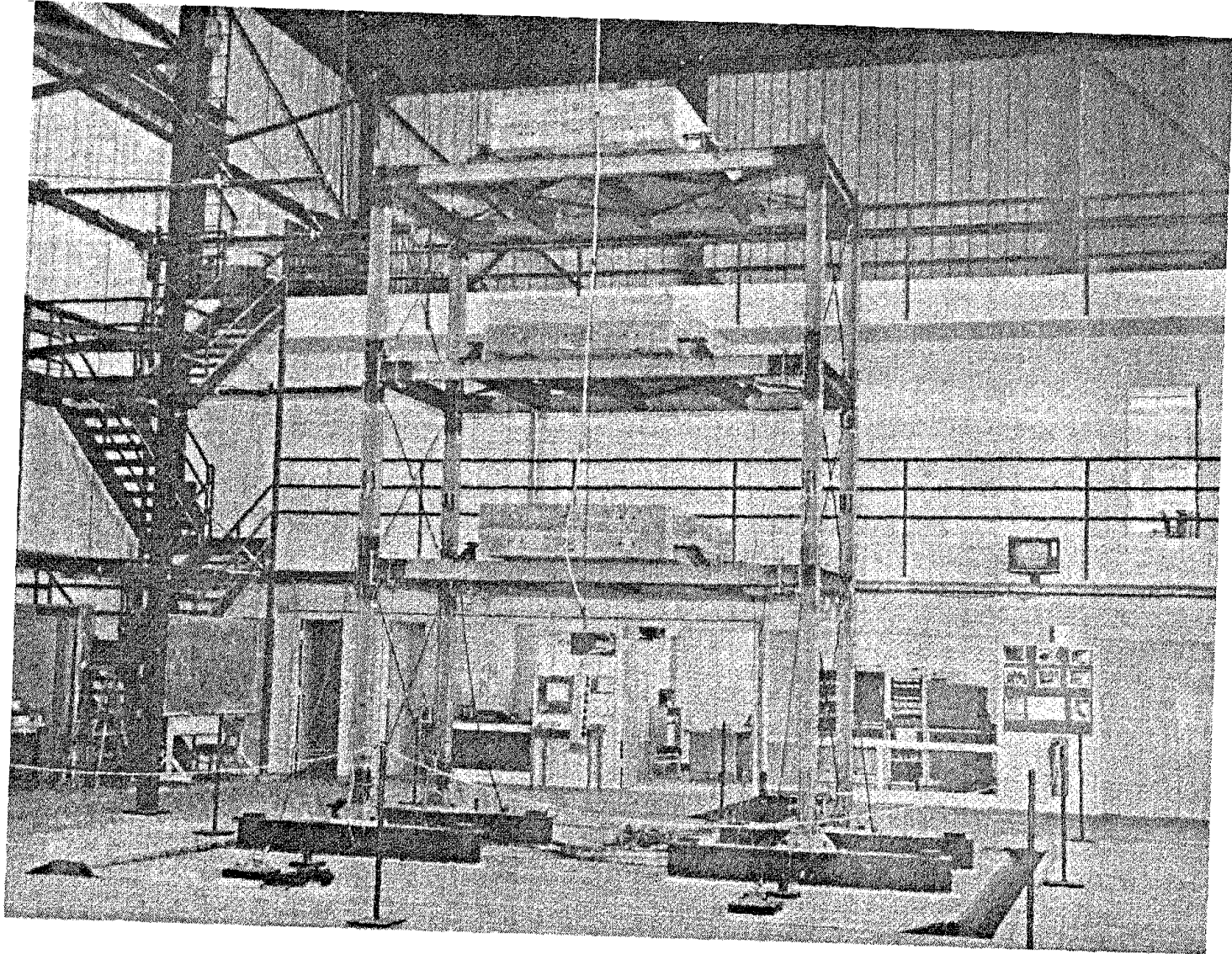


Figure 4.1 Prototype Structure at U.C., Berkeley

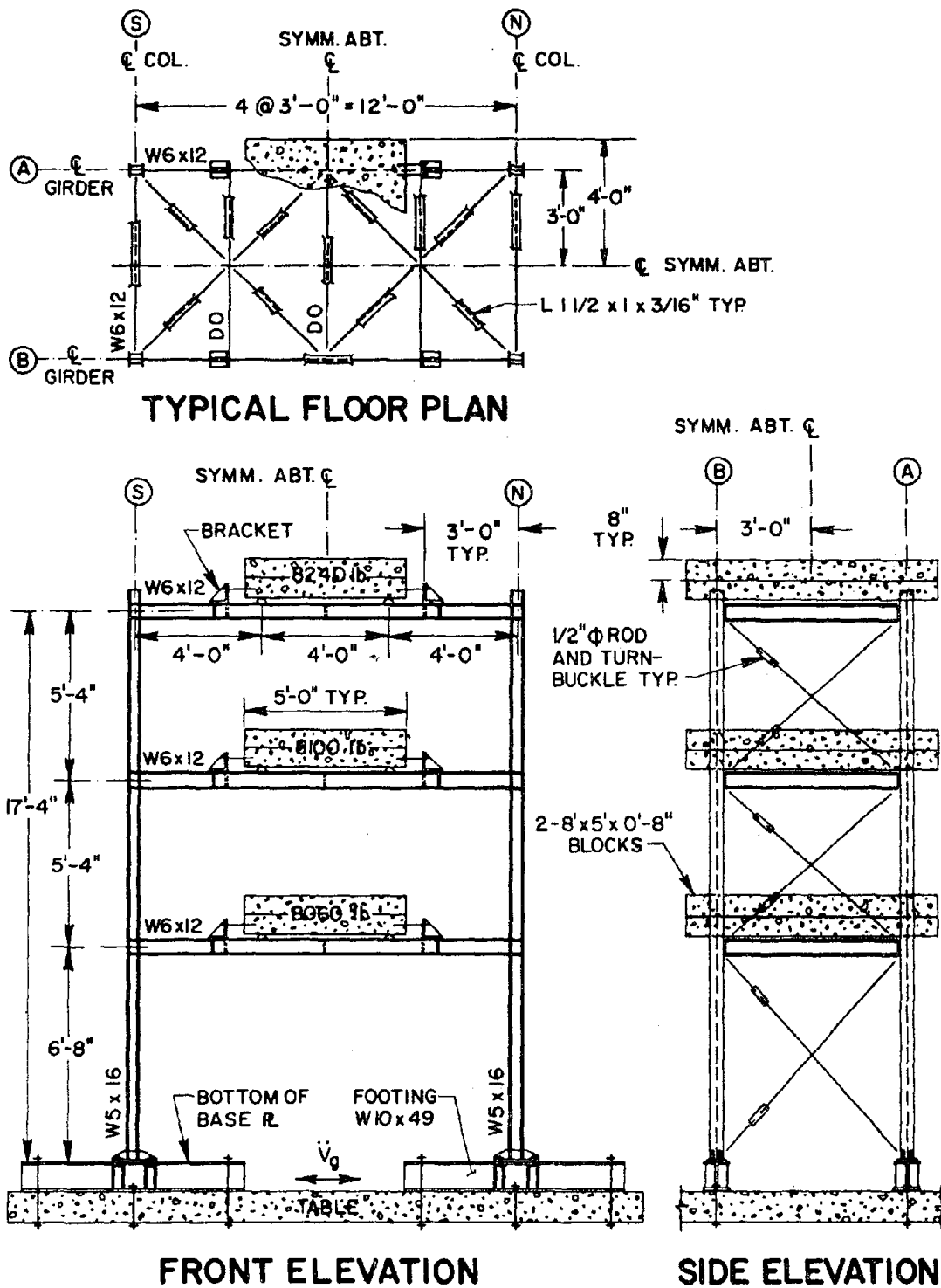
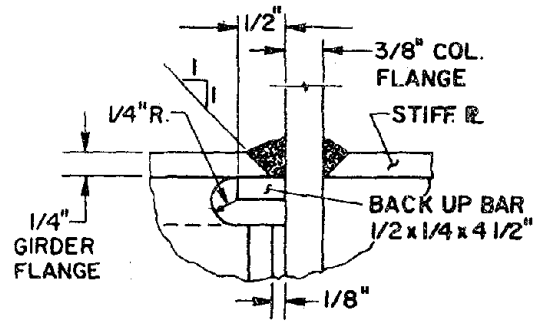
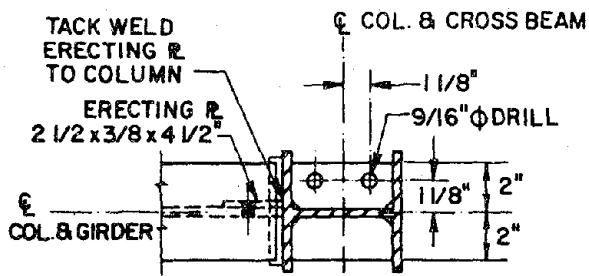
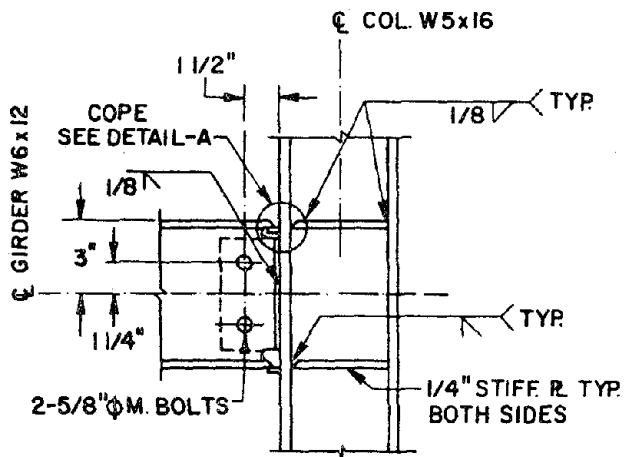


Figure 4.2 Plans and Elevations of the Prototype Structure

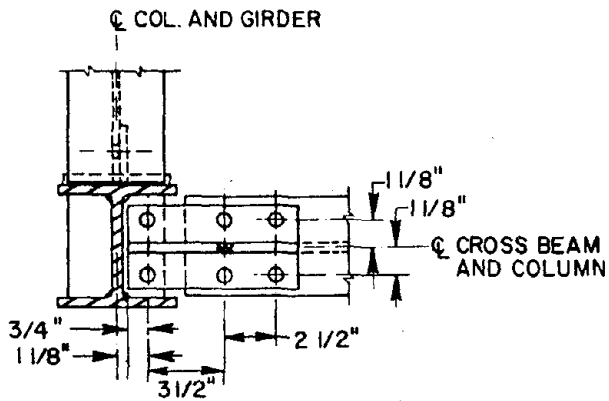


DETAIL-A

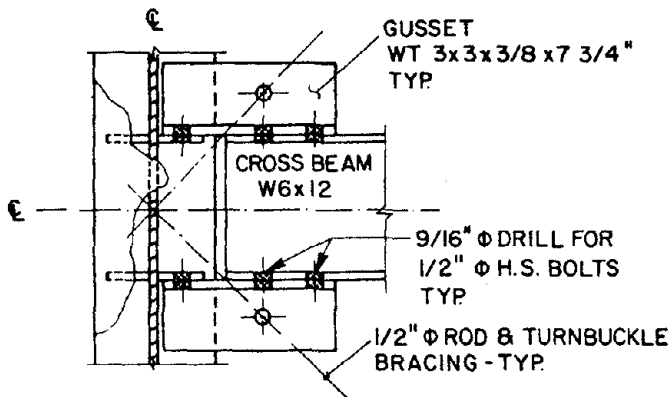


TYPICAL CONNECTION AS BUILT

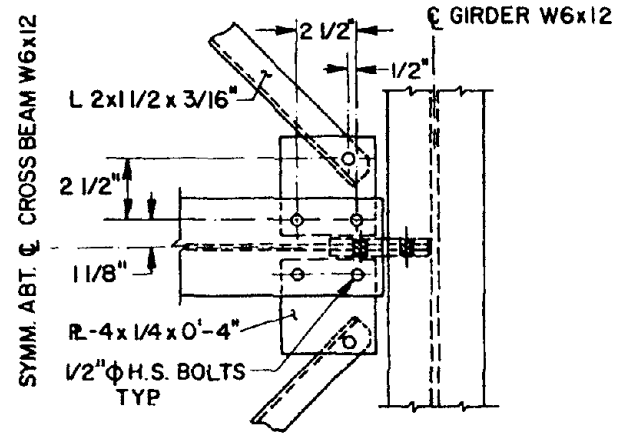
Figure 4.3 Prototype Girder-to-Column Connection



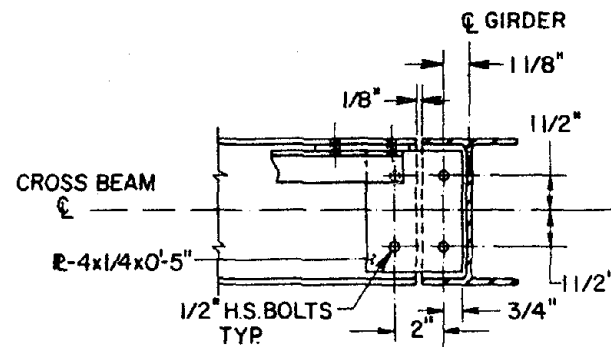
TOP VIEW



FRONT VIEW



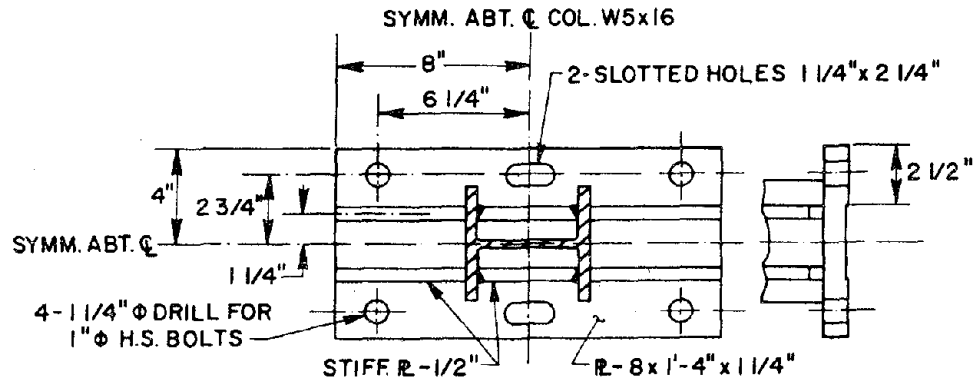
TOP VIEW



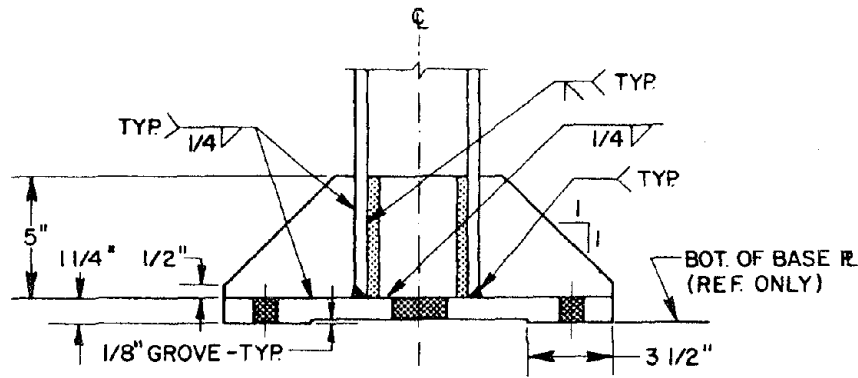
SIDE VIEW

Figure 4.4 Prototype Primary Beam-to-Column Connection

Figure 4.5 Prototype Secondary Beam-to-Girder Connection

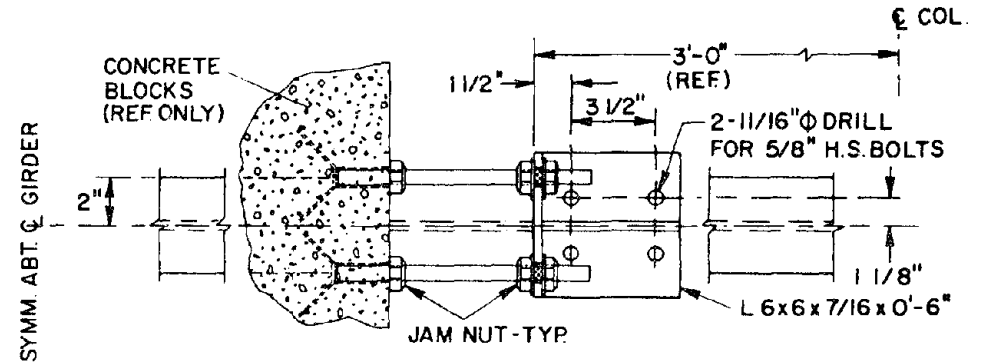


TOP VIEW

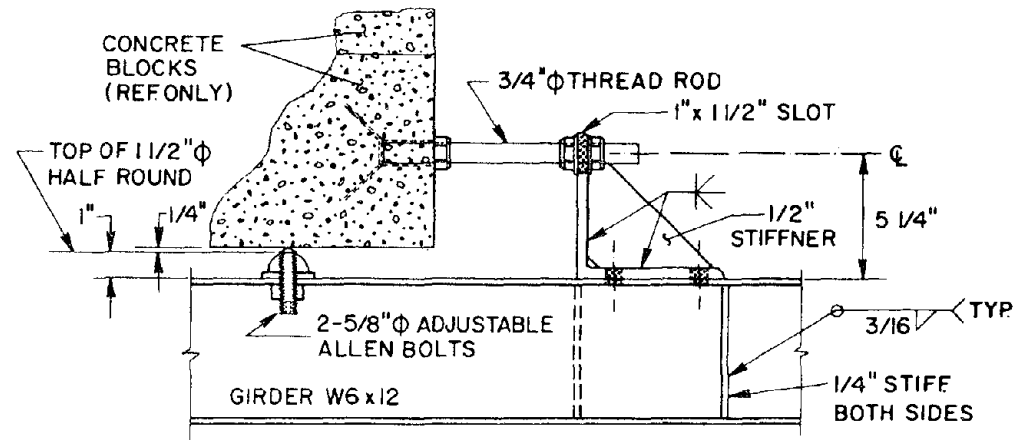


FRONT VIEW

Figure 4.6 Prototype Column Base Plate

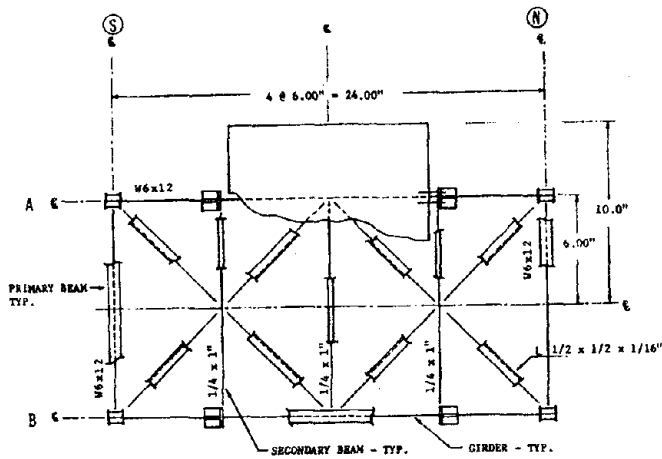


TOP VIEW

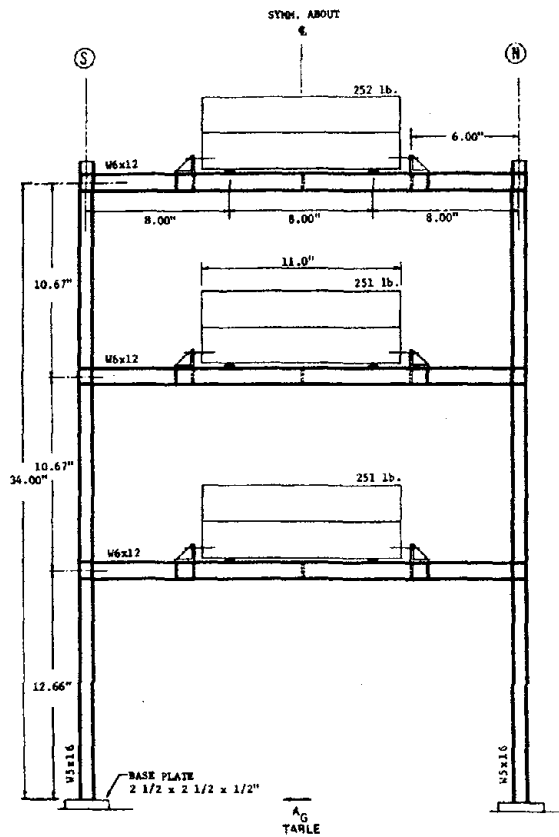


FRONT VIEW

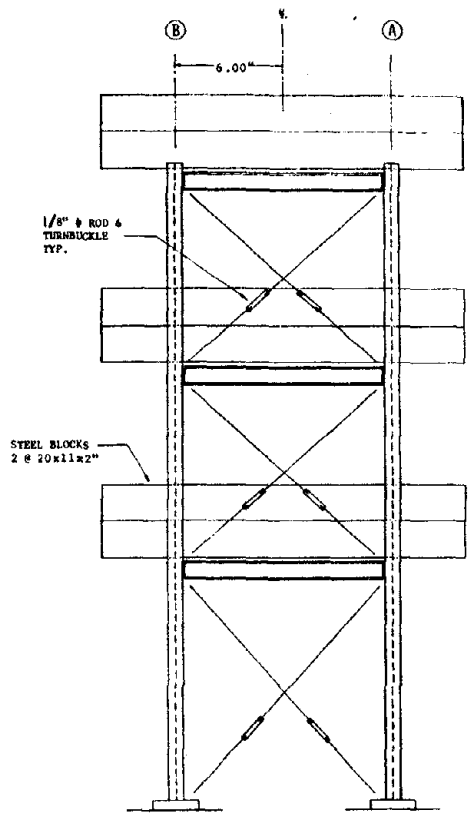
Figure 4.7 Prototype Floor Weight Support Mechanism



TYPICAL FLOOR PLAN



FRONT ELEVATION



SIDE ELEVATION

Figure 4.8 Plans and Elevations of the Model Structure

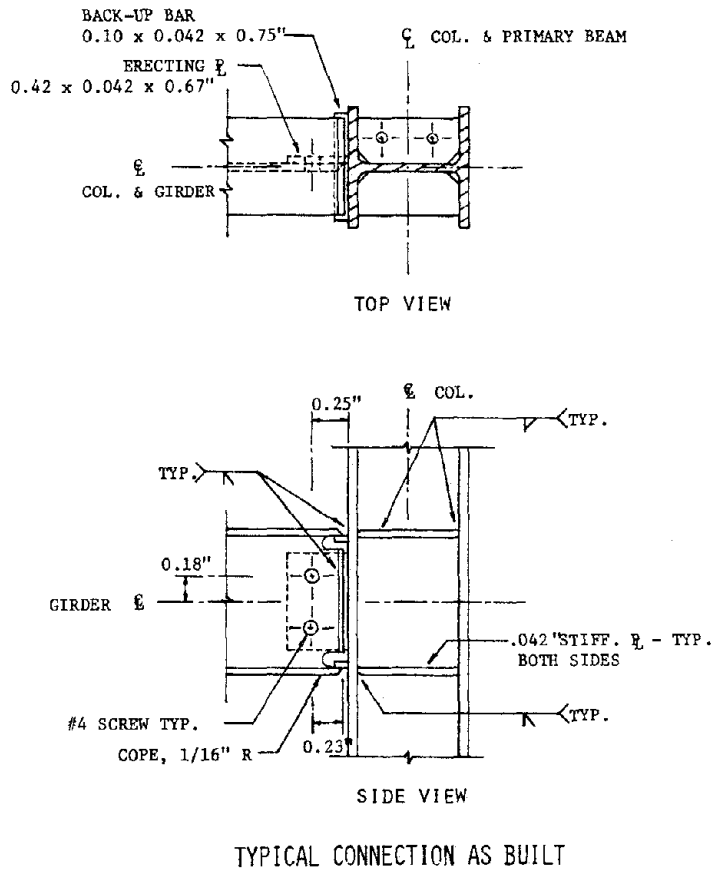


Figure 4.9 Model Girder-to-Column Connection

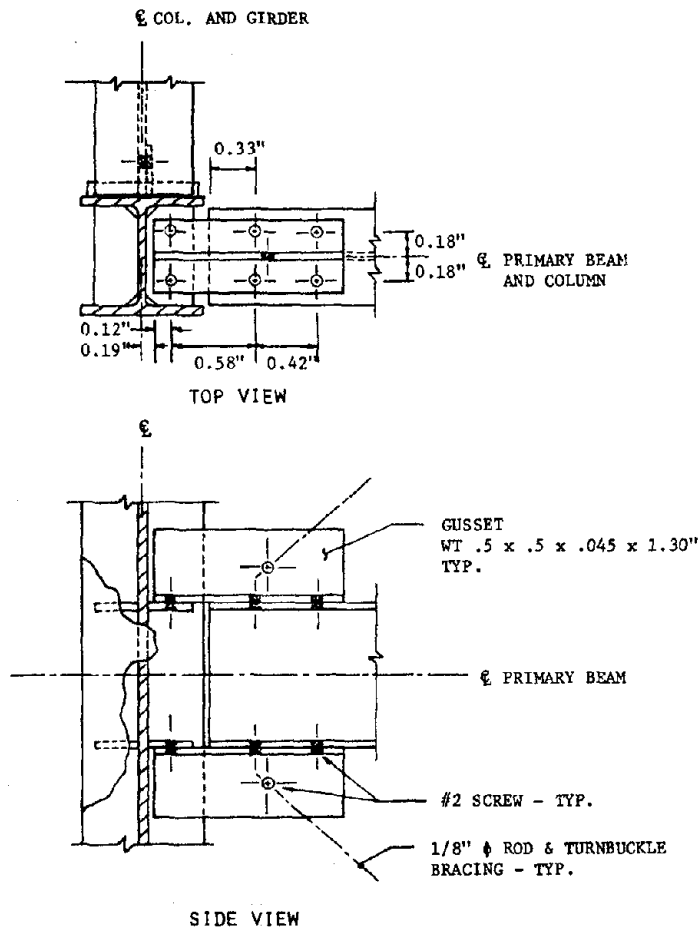


Figure 4.10 Model Primary Beam-to-Column Connection

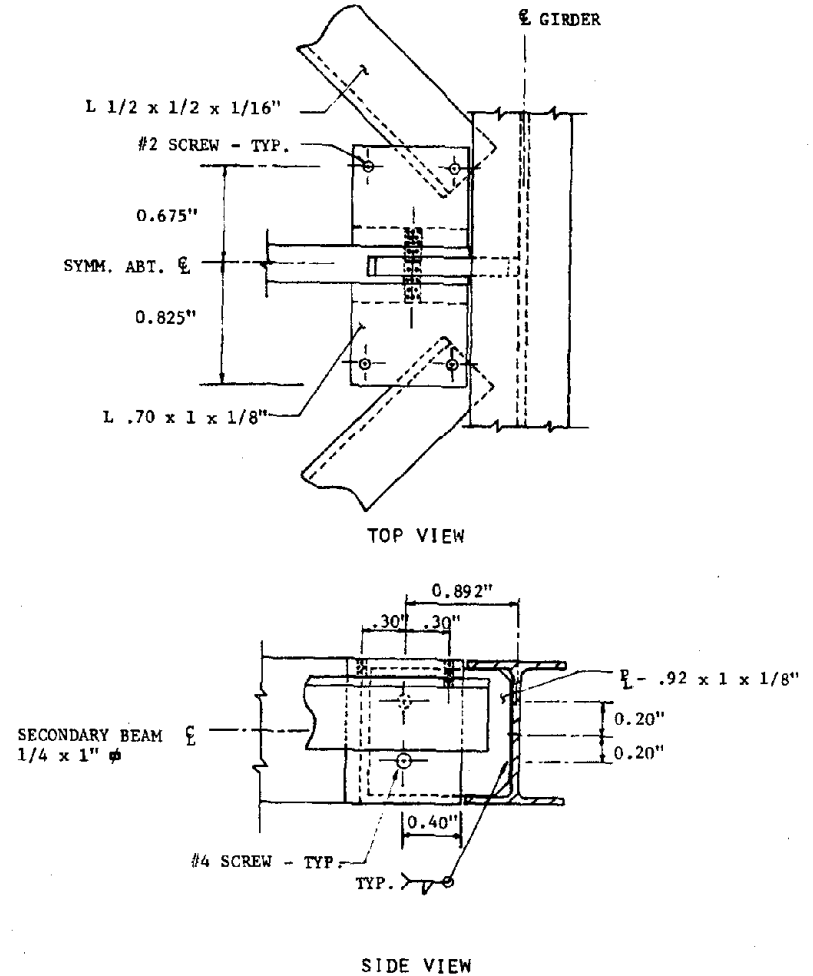


Figure 4.11 Model Secondary Beam-to-Girder Connection

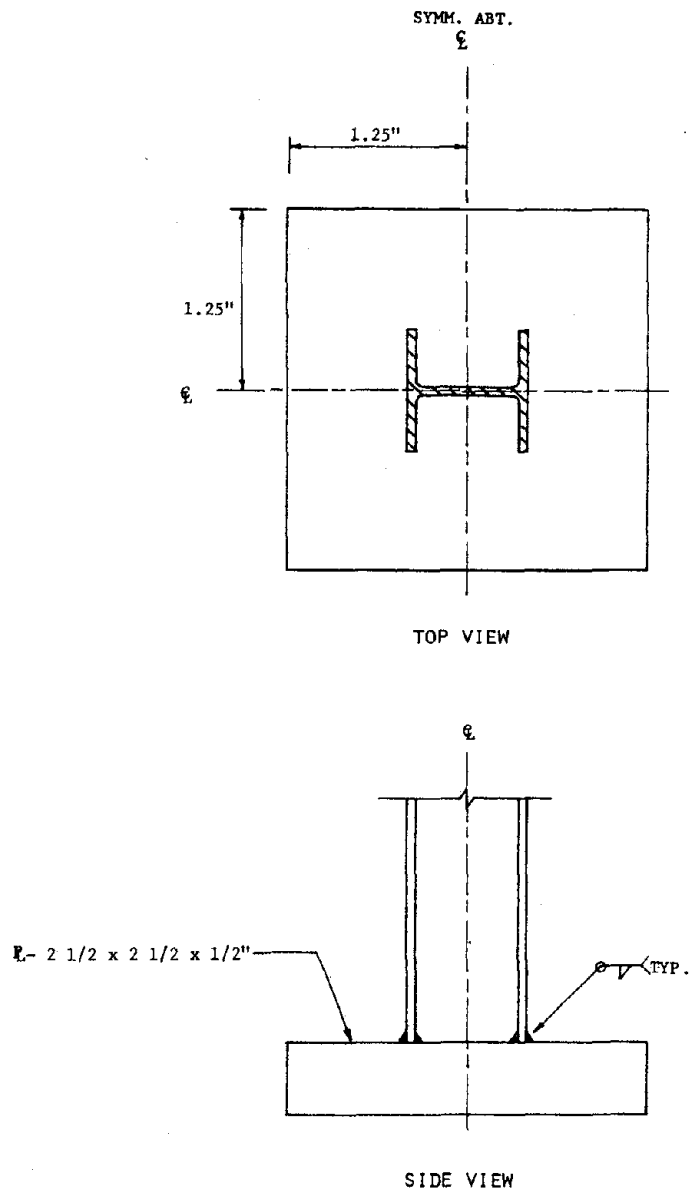


Figure 4.12 Model Column Base Plate

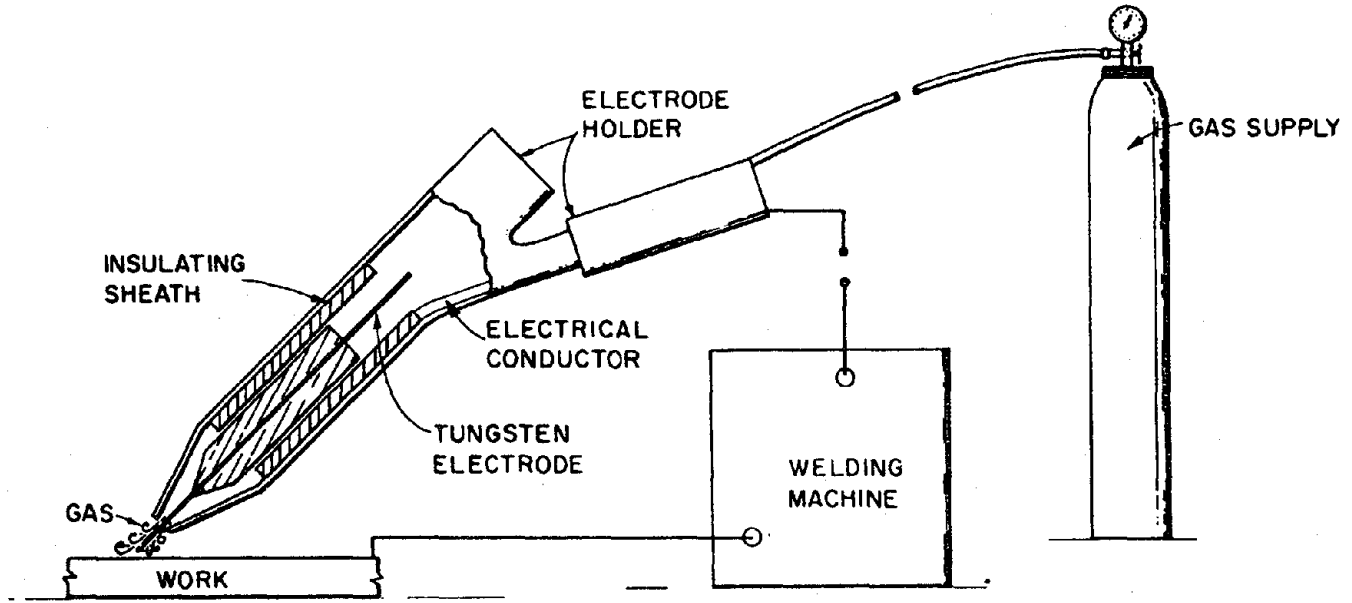


Figure 4.13 Heliarc Welding Process (Ref. 25)

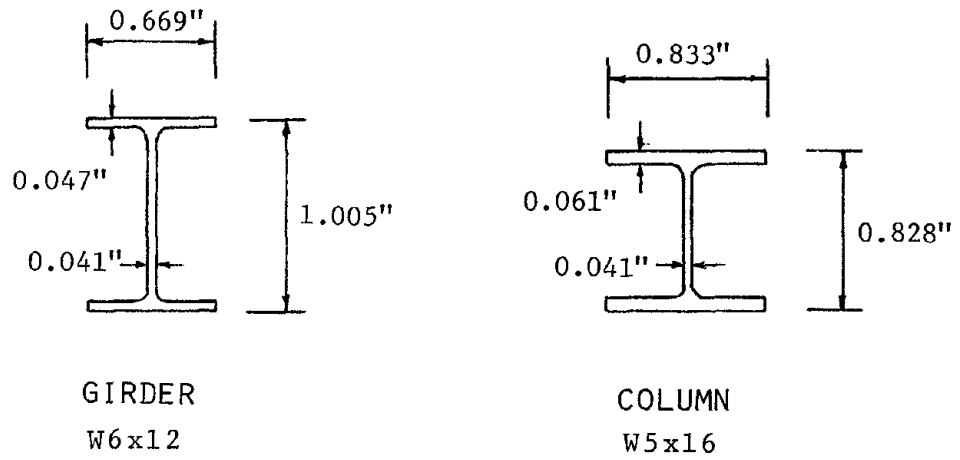


Figure 4.14 Model Element Specifications

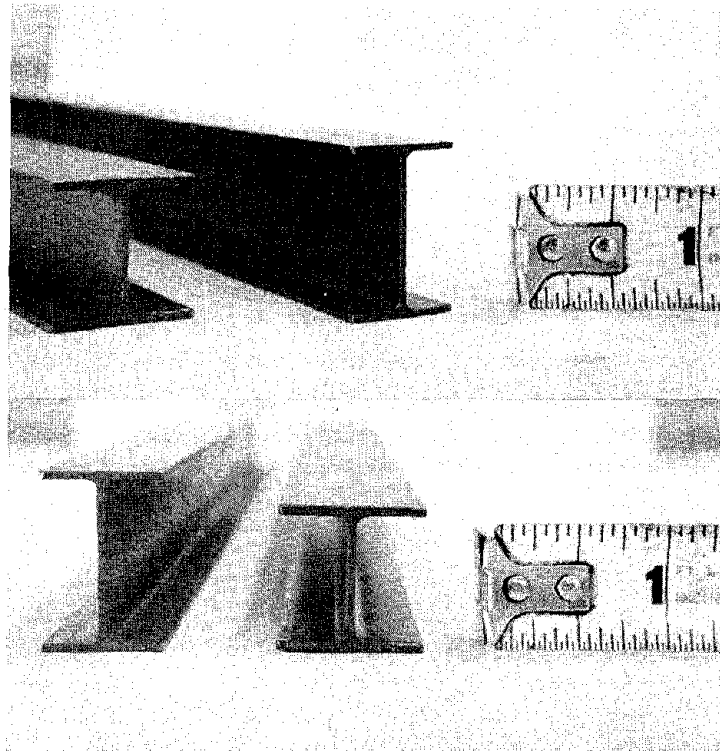
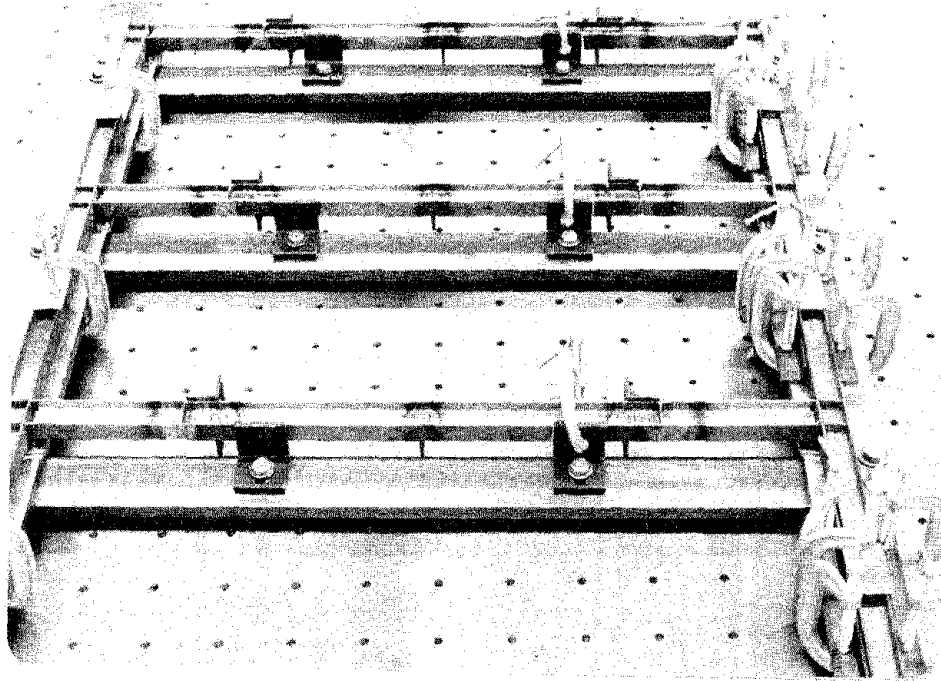
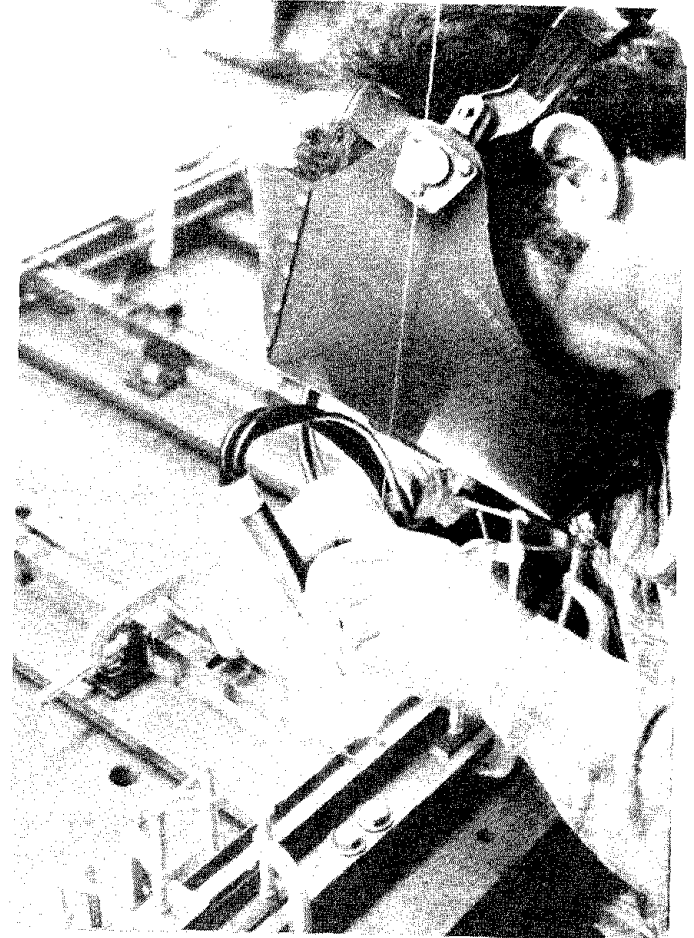


Figure 4.15 Machined Model Elements



a.) Frame positioned and clamped



b.) Welding of girder-column connection

Figure 4.16 Model Frame Welding Procedure

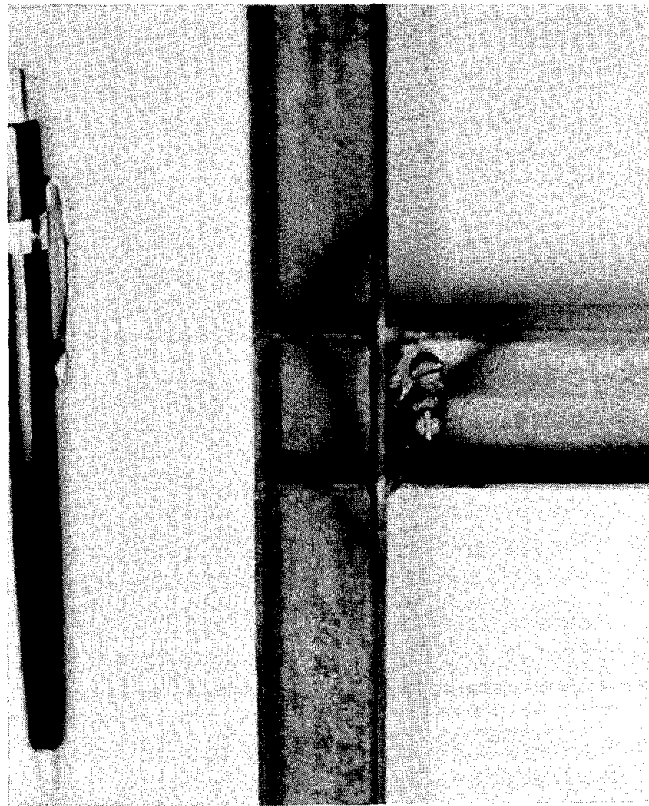
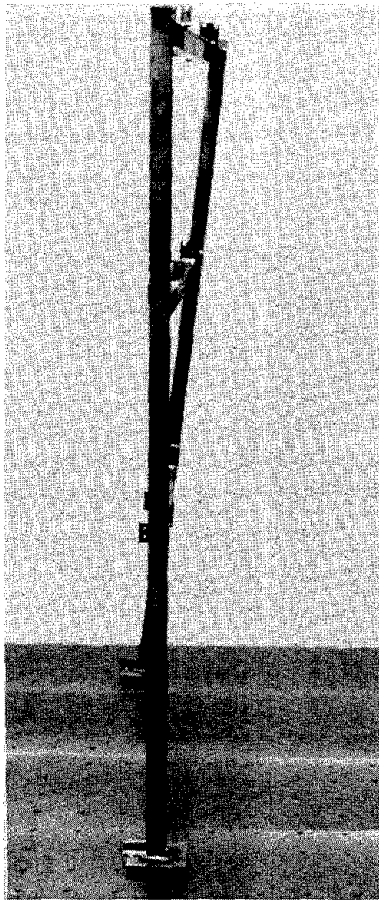
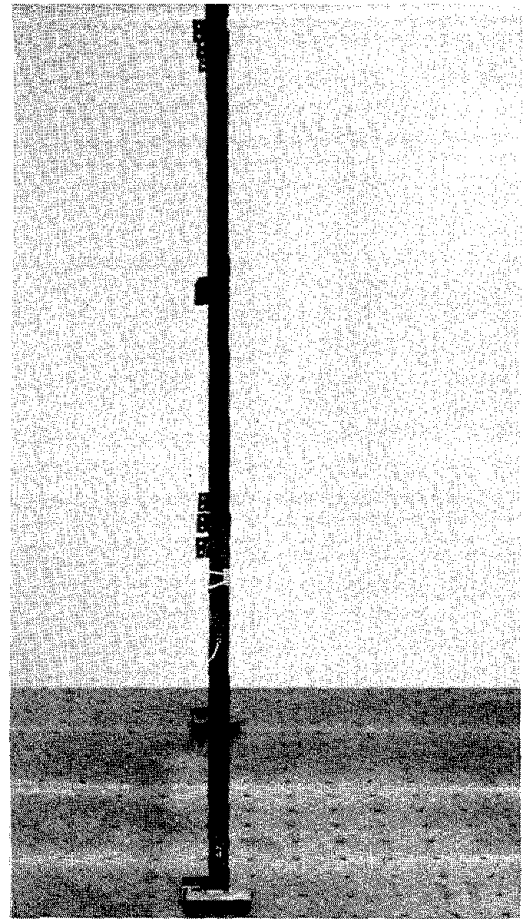


Figure 4.17 Girder-to-Column Connection Before Heat-Treatment

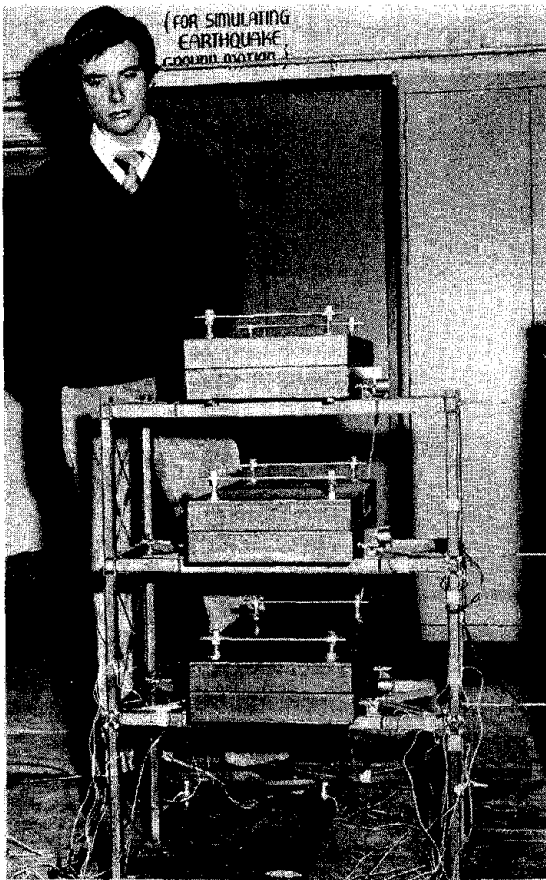


a.) Before heat-treatment

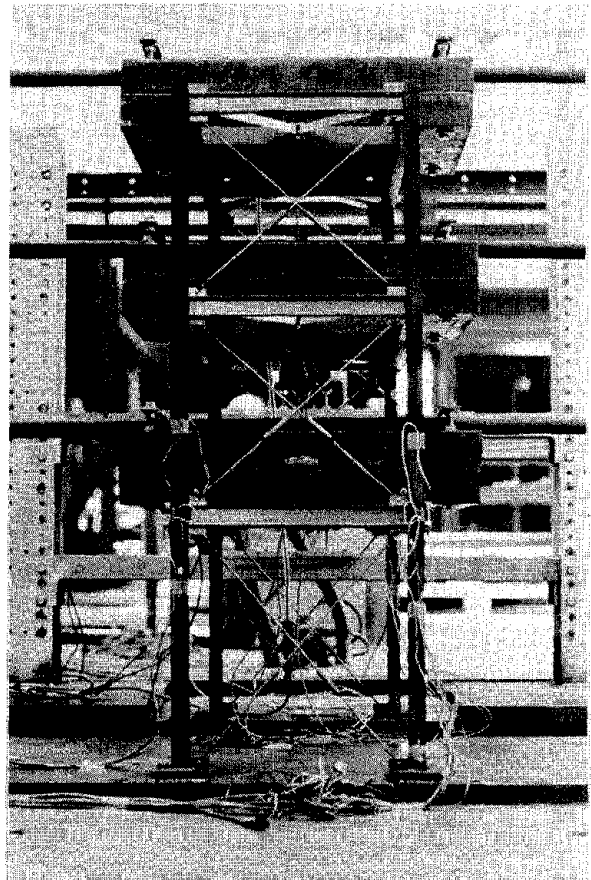


b.) After heat-treatment

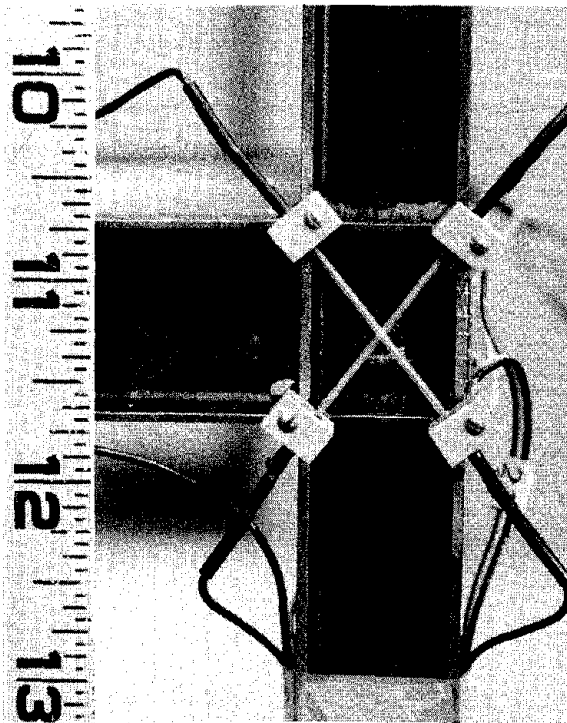
Figure 4.18 Model Frame Instability



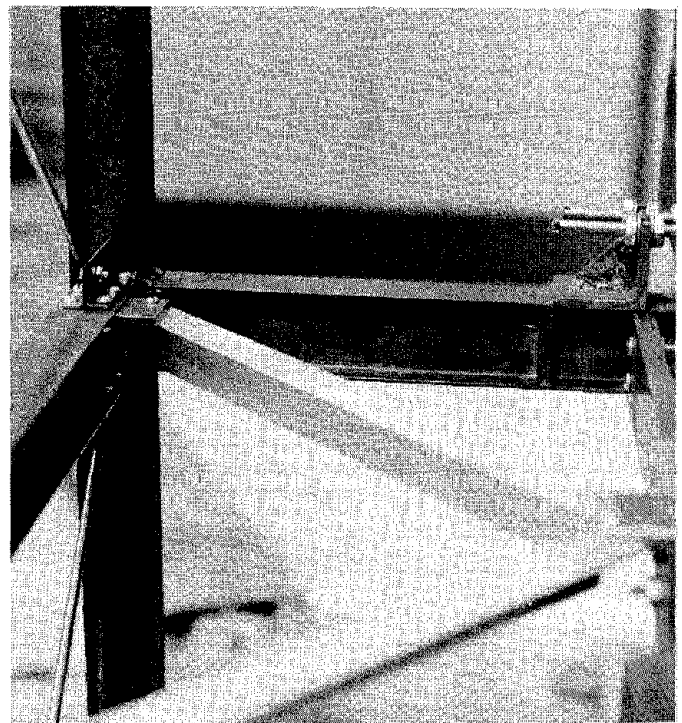
a.) Front elevation



b.) Side elevation

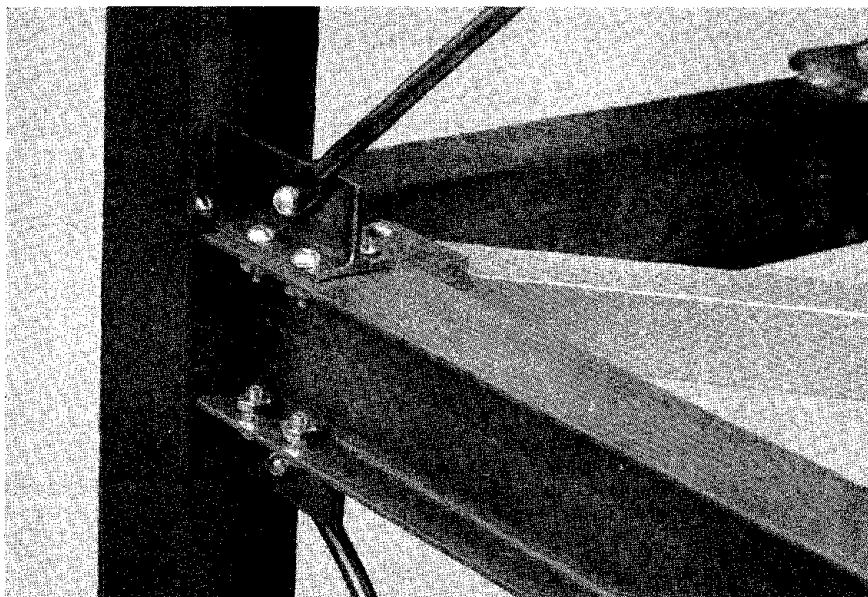


c.) Girder-Column Connection

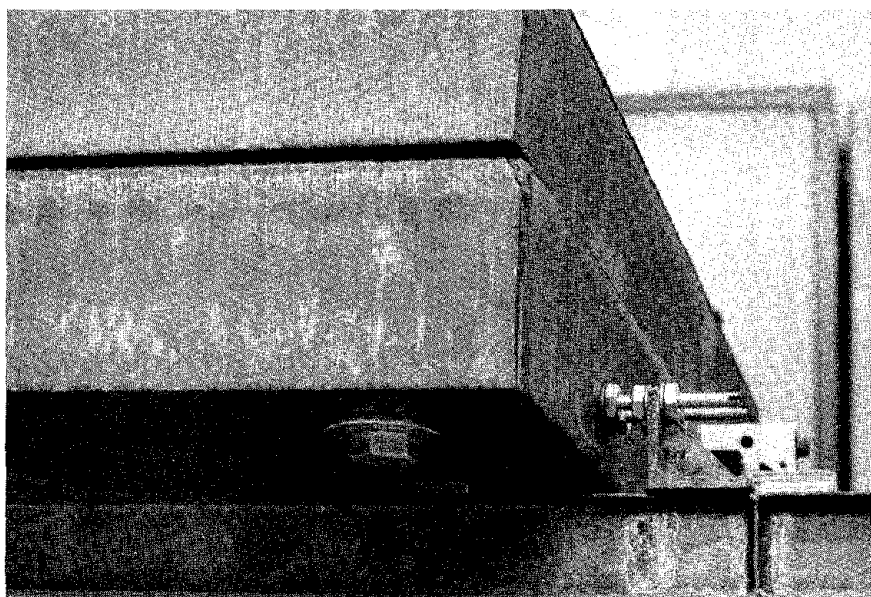


d.) Beam Connection and Floor Bracing

Figure 4.19 AMS Model Structure

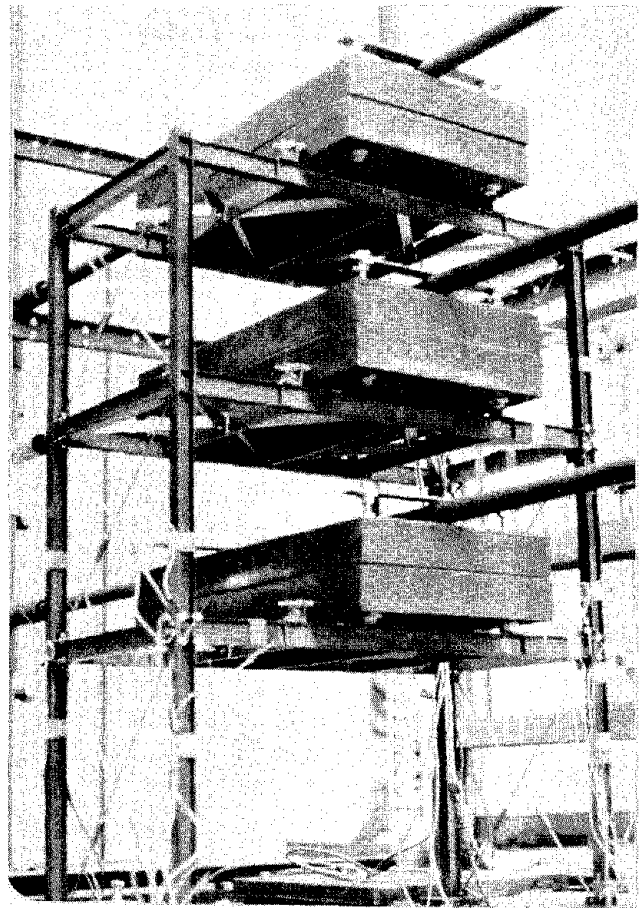
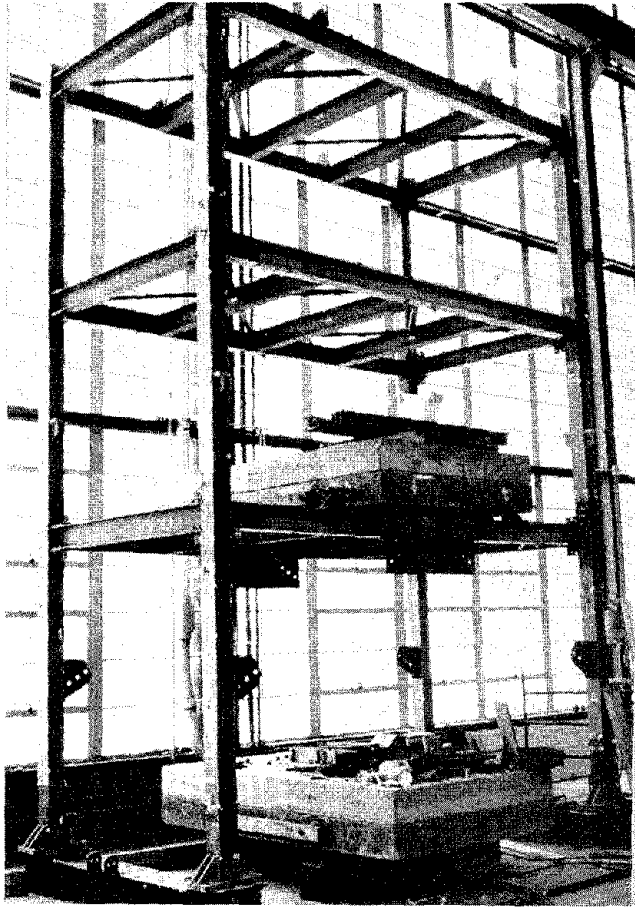


e.) Primary beam and bracing connection

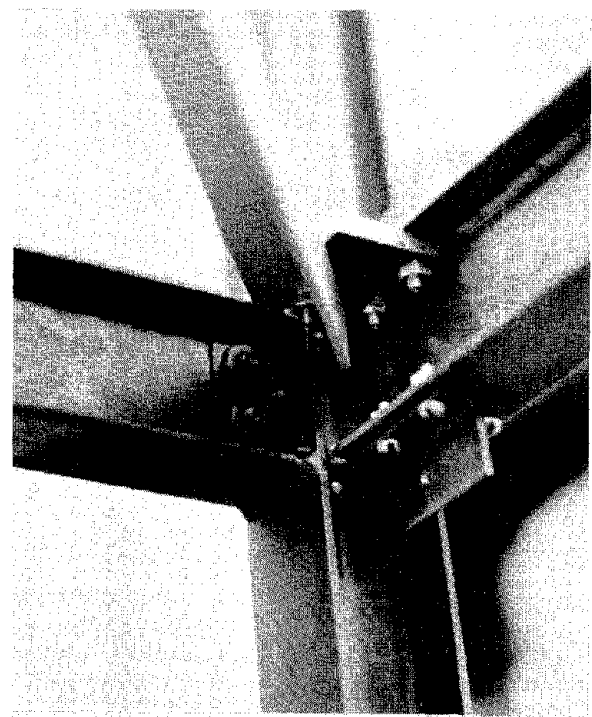
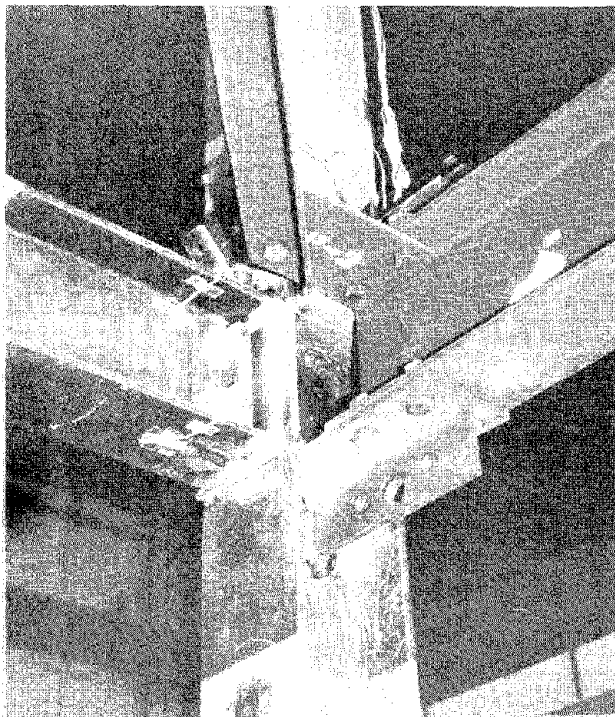


f.) Floor weight support mechanisms

Figure 4.19, cont. AMS Model Structure

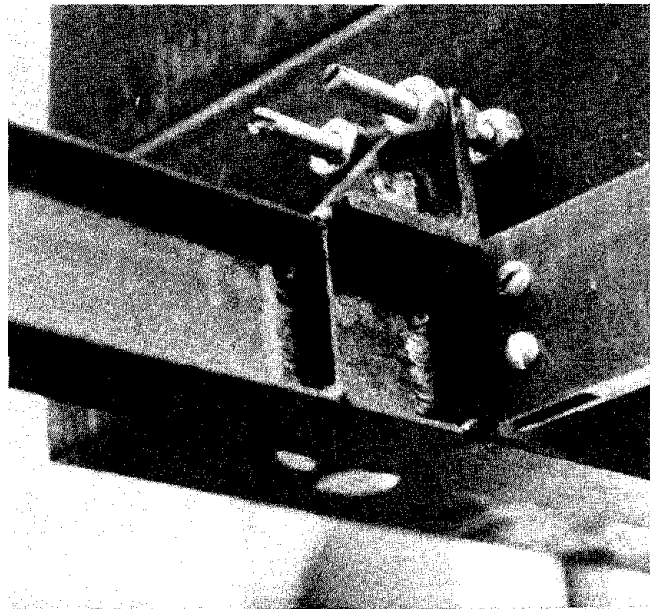
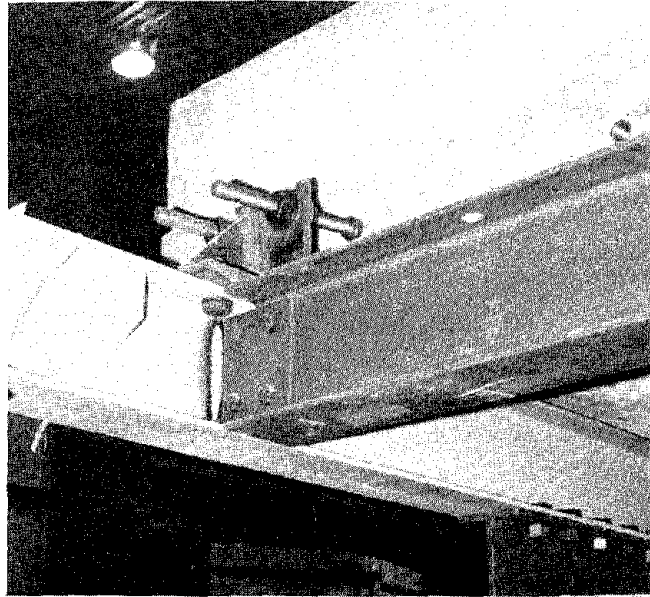


a.) General overview

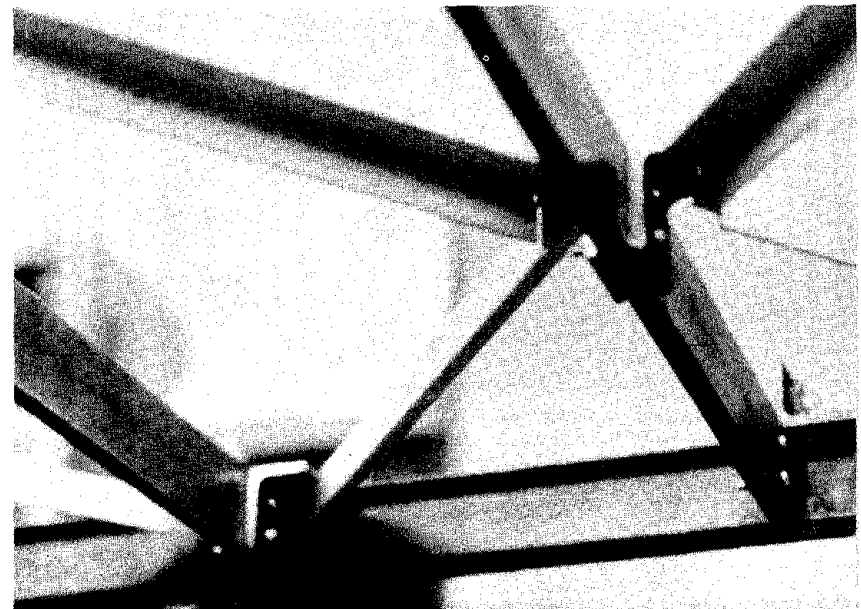
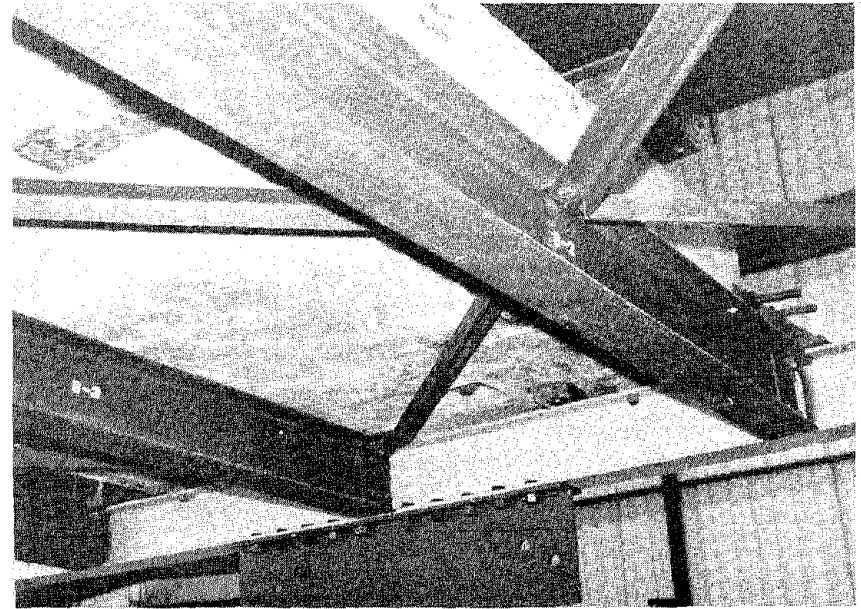


b.) Primary joint

Figure 4.20 Visual Comparison -- Prototype (left) and Model (right)



c.) Lateral weight support and secondary beam



d.) Secondary beams and floor bracing

Figure 4.20, cont. Visual Comparison -- Prototype (top) and Model (bottom)

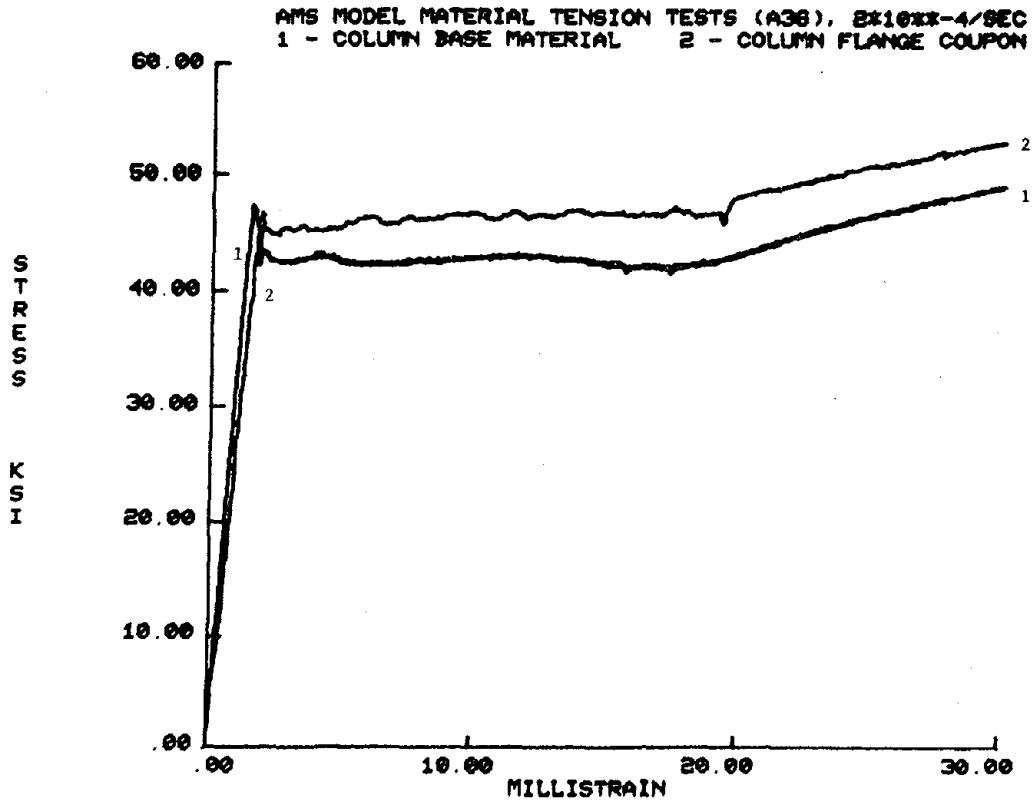


Figure 4.21 Model Material Tests -- Column Base Material vs. Flange Coupon

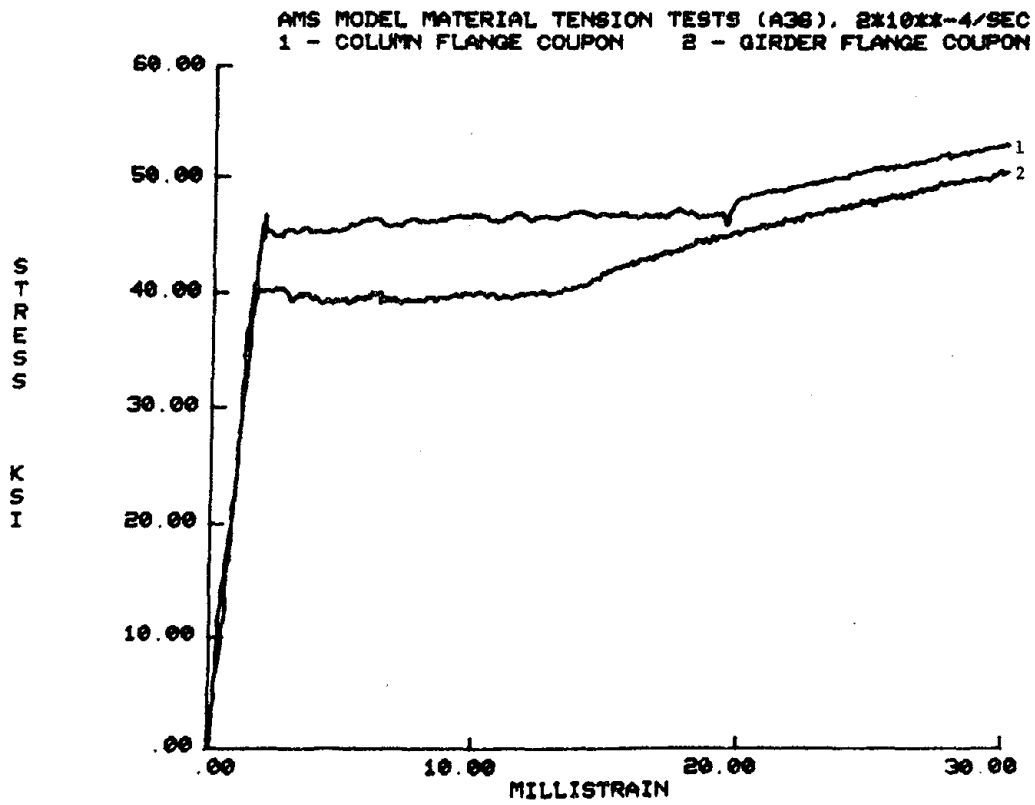


Figure 4.22 Model Material Tests -- Column Flange vs. Girder Flange Coupons

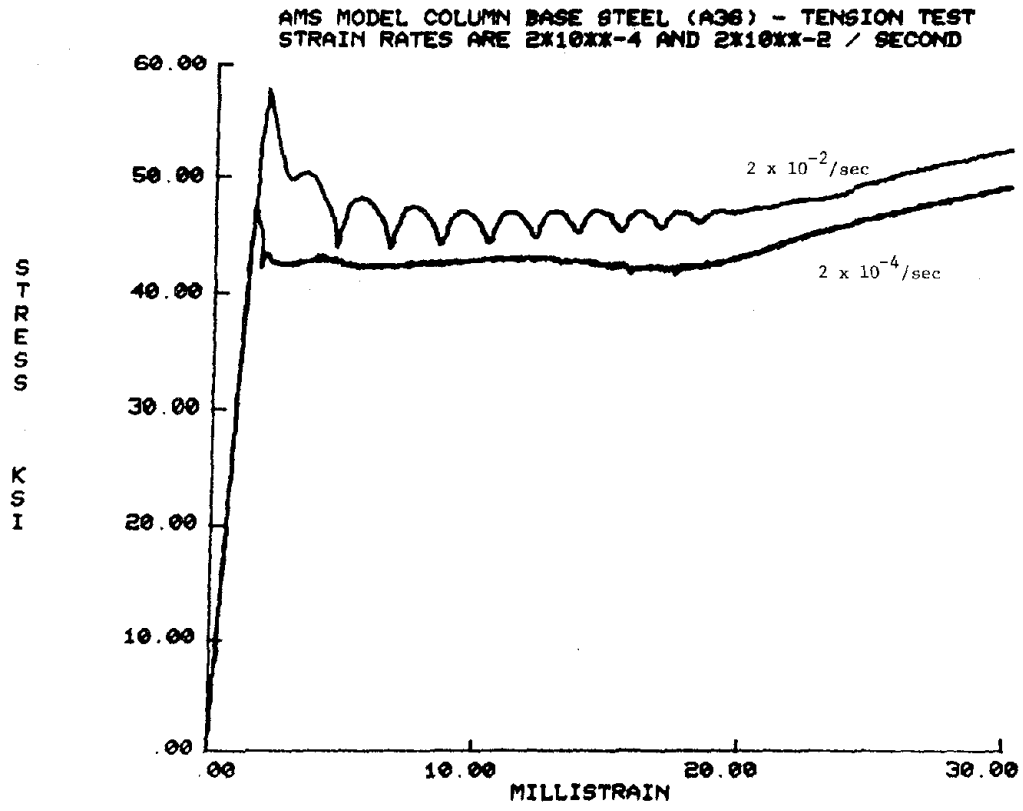


Figure 4.23 Model Material Tests -- Column Base Material vs. Strain Rate

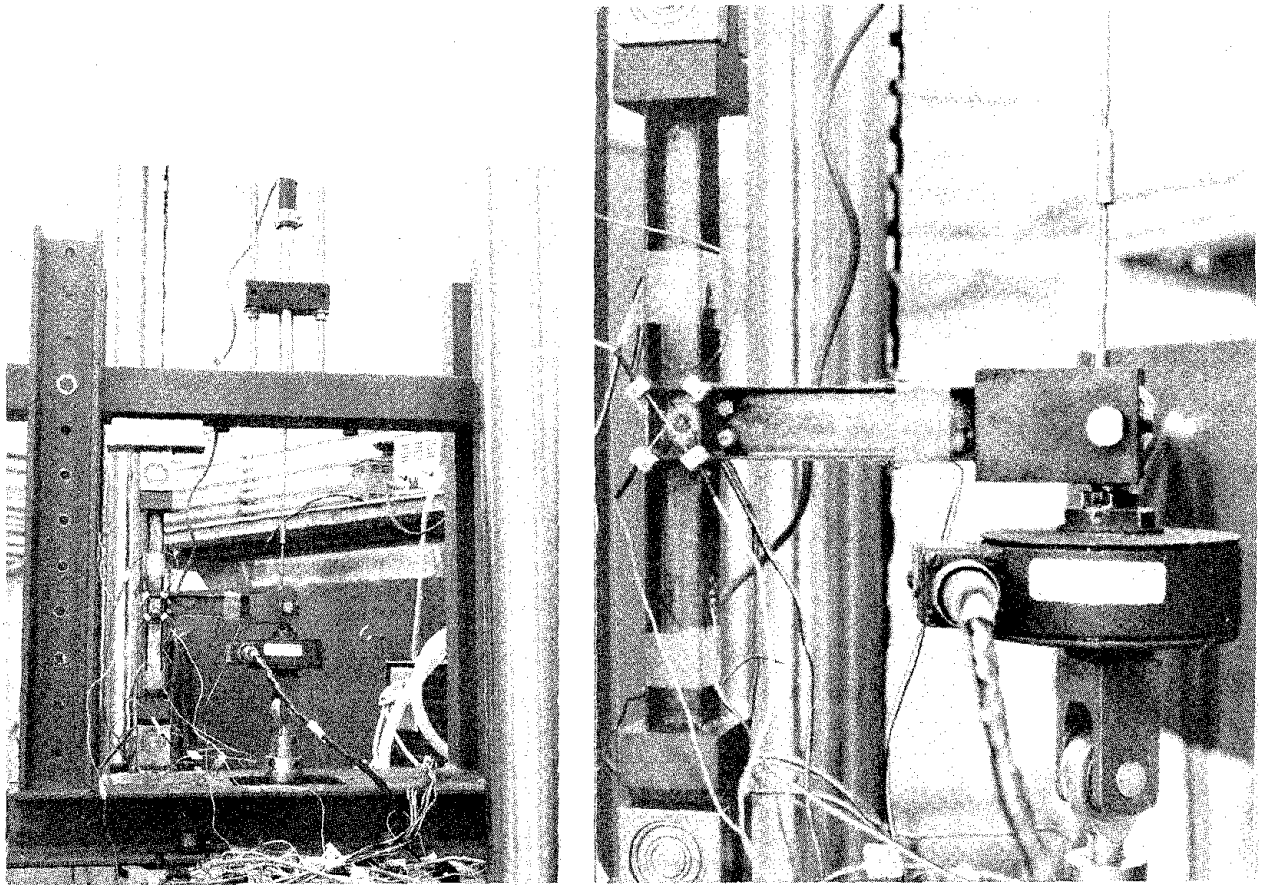


Figure 4.24 AMS Model Subassembly Tests

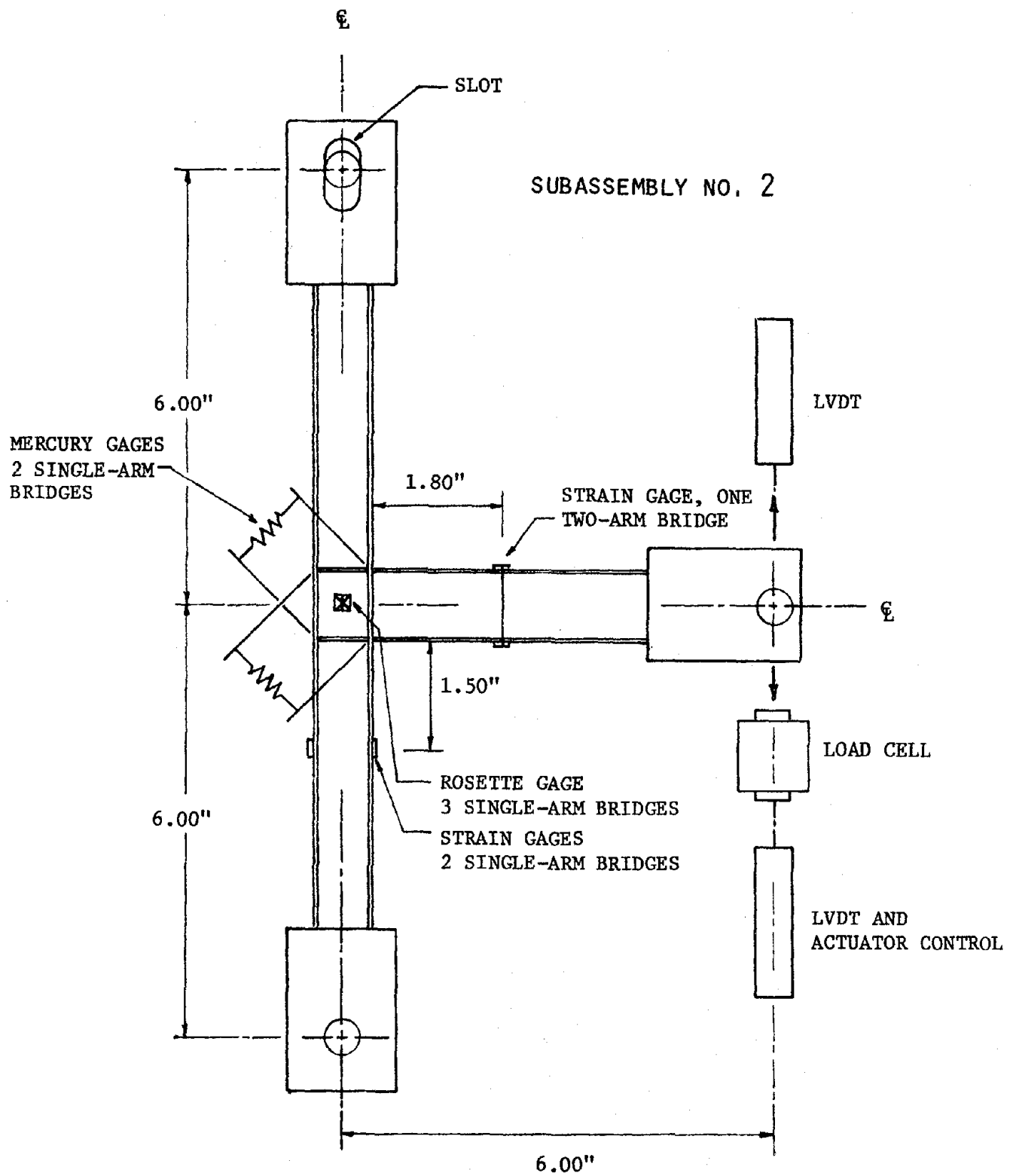


Figure 4.25 AMS Model Subassembly -- Instrumentation (Typ.)

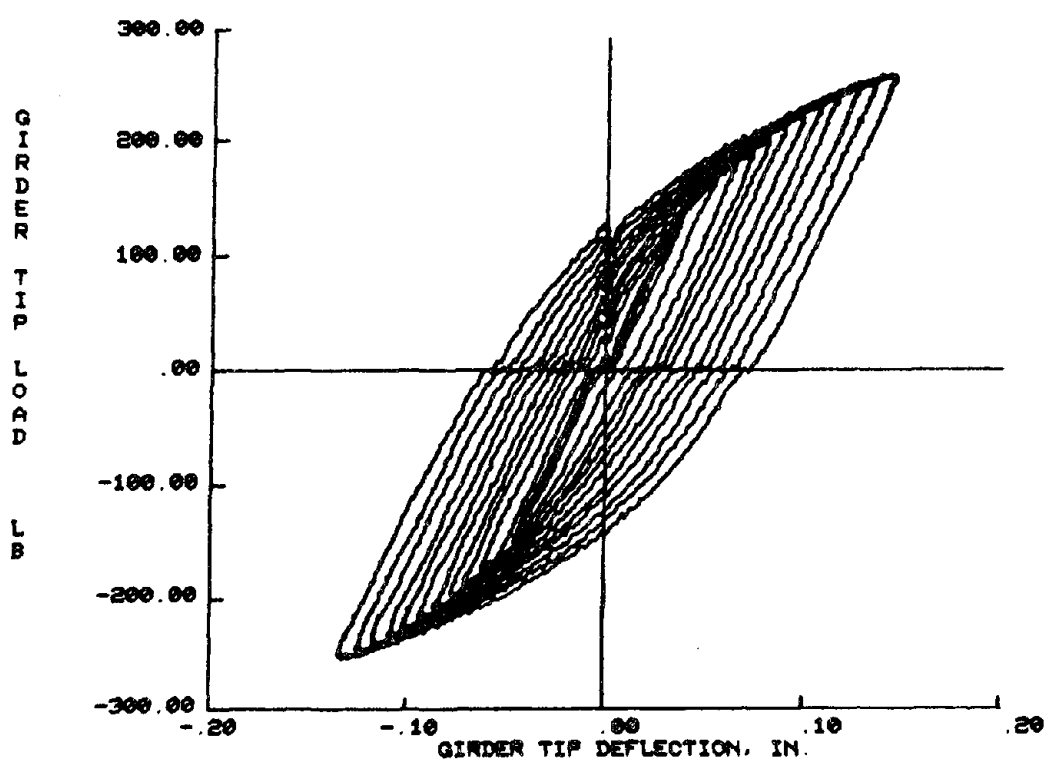
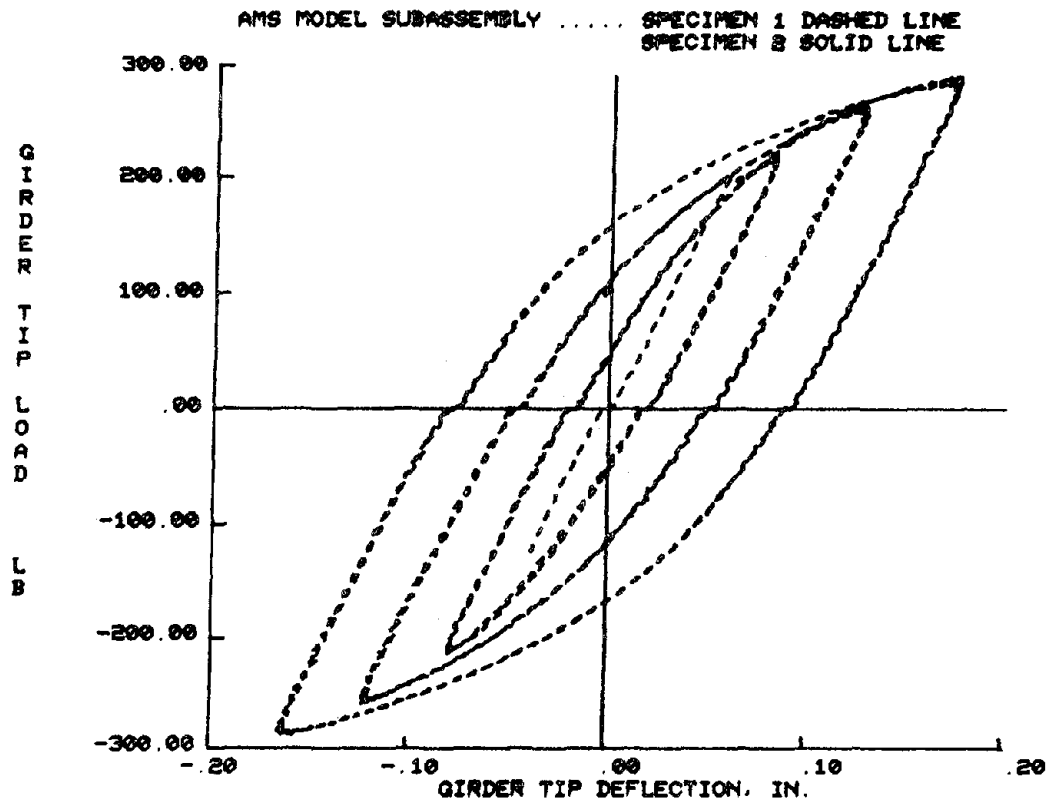


Figure 4.26 Model Subassembly -- Girder Tip Load vs. Deflection

S1C3U18
S2C3U11

AMS MODEL SUBASSEMBLY SPECIMEN 1 DASHED LINE
SPECIMEN 2 SOLID LINE

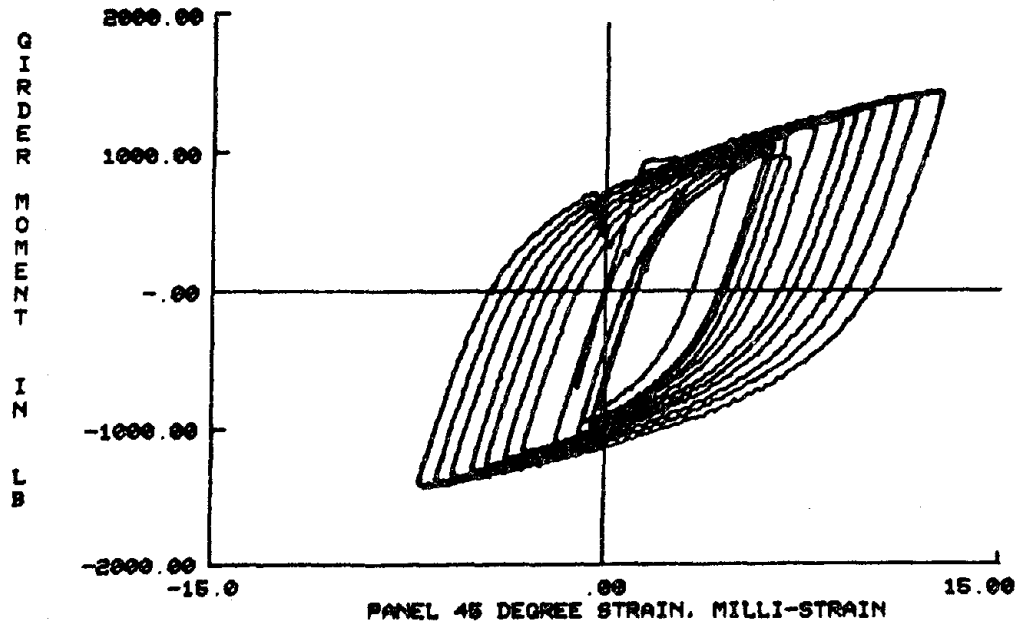
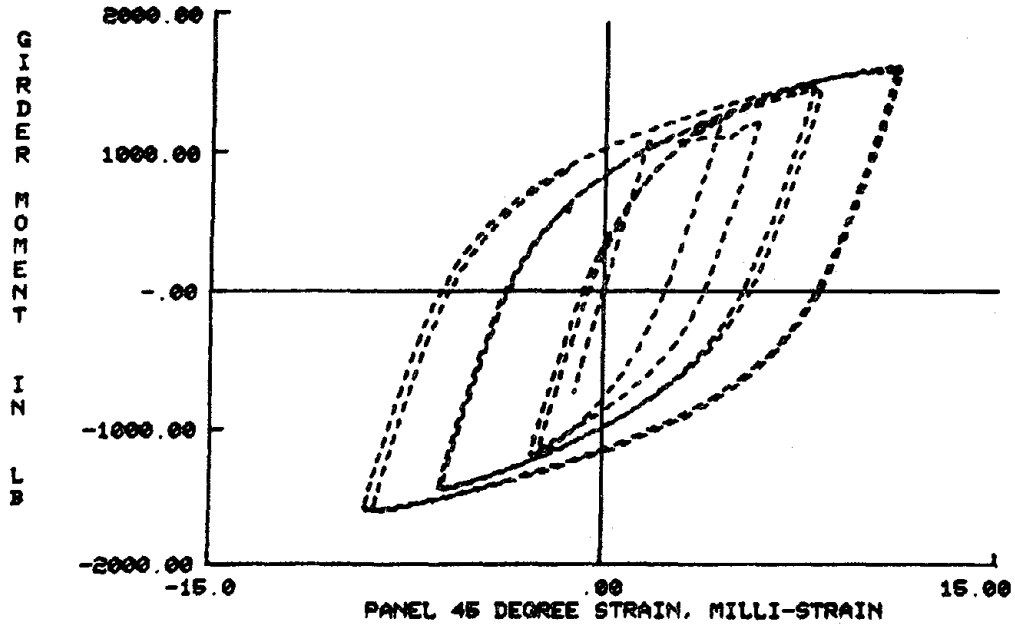


Figure 4.27 Model Subassembly -- Girder End Moment vs. Panel Strain

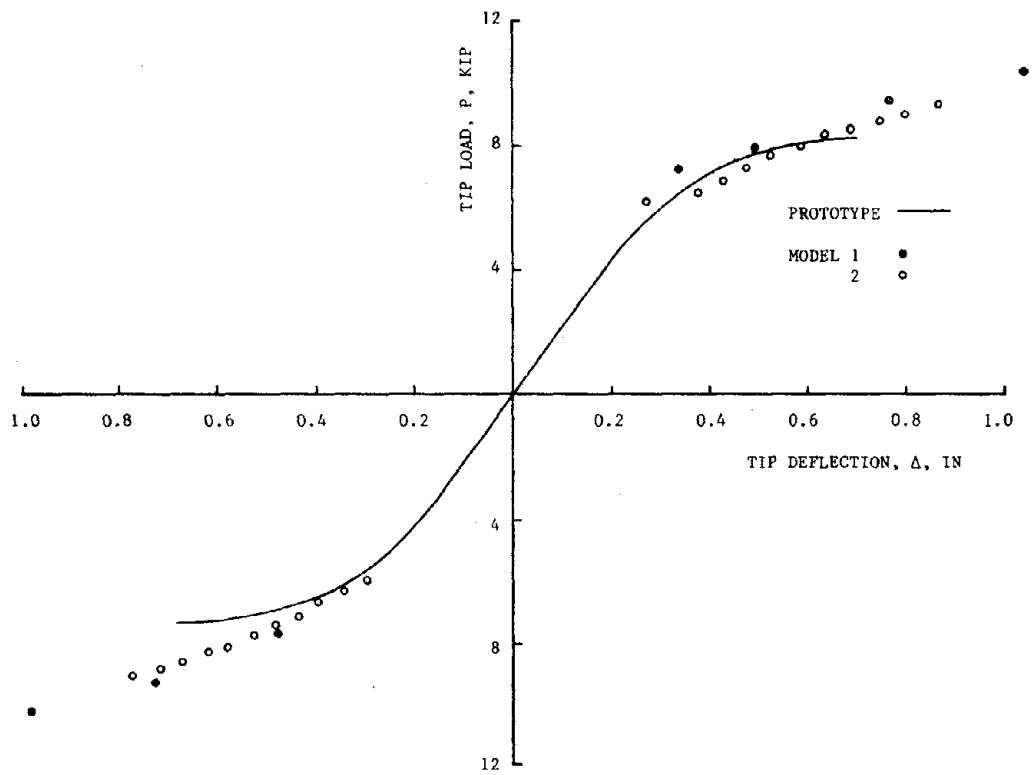


Figure 4.28 Subassembly Tests -- Girder Tip Load vs. Deflection

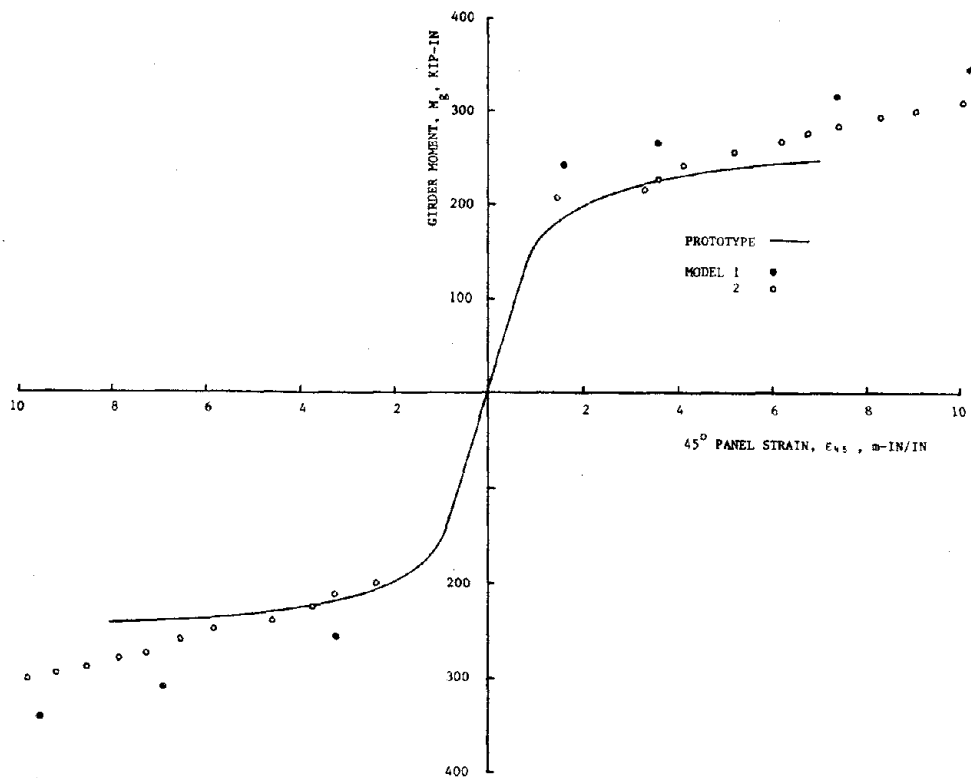


Figure 4.29 Subassembly Tests -- Girder End Moment vs. Panel Strain

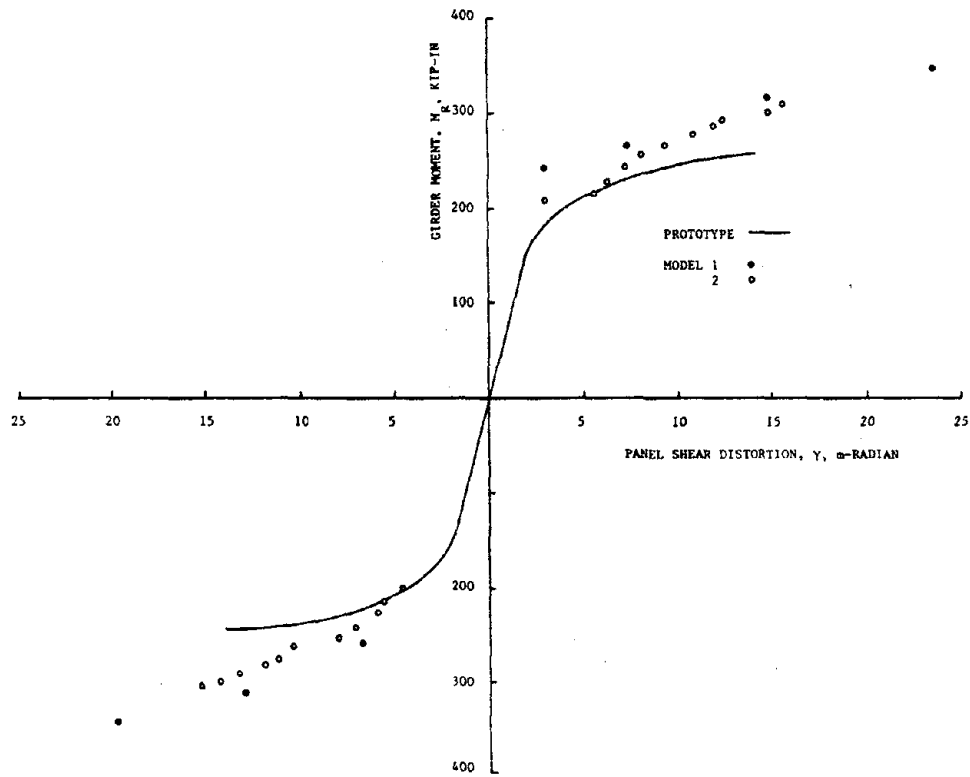
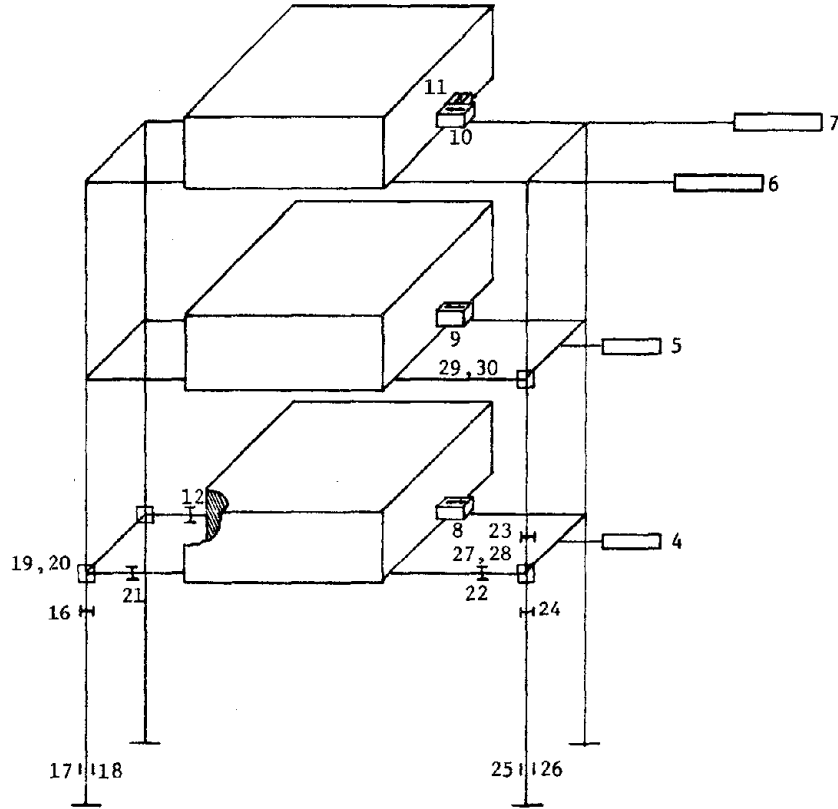
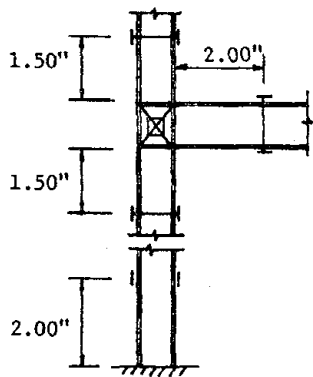


Figure 4.30 Subassembly Tests -- Girder End Moment vs. Panel Shear Distortion

INSTRUMENTATION CHANNEL ASSIGNMENTS



TYP. LOCATIONS



KEY



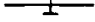


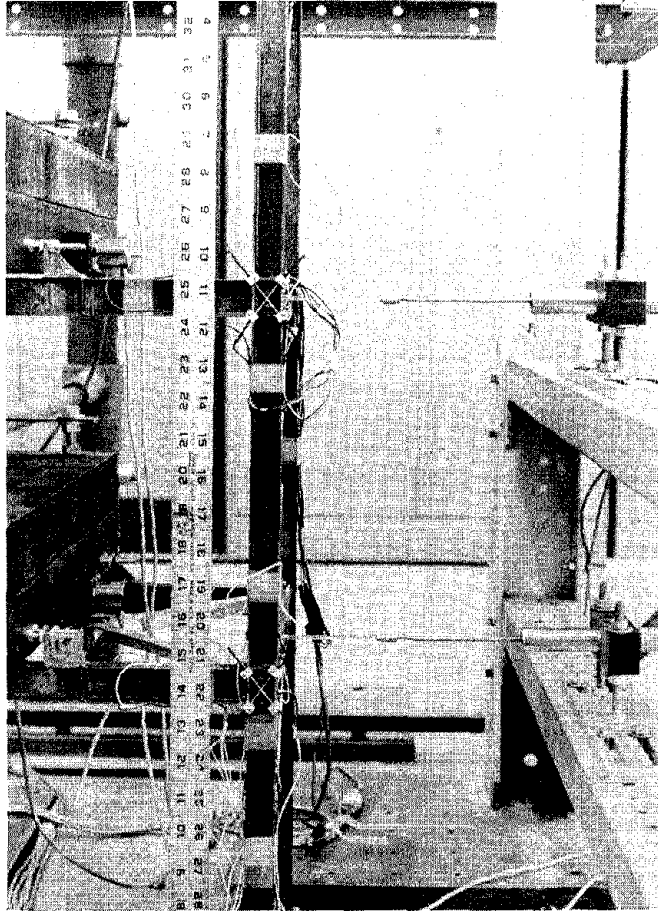
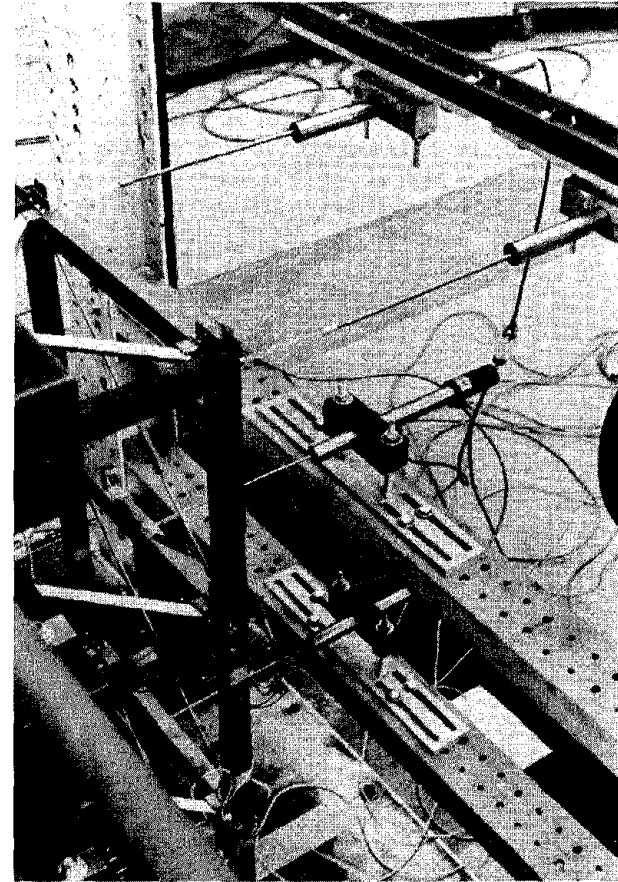
- LVDT 
- ACCELEROMETER 
- STRAIN GAGES
TWO-ARM BRIDGE
FLEXURAL 
- STRAIN GAGES
2 SINGLE-ARM BRIDGES
FLEXURAL & AXIAL 
- PANEL ROSETTE
& MERCURY GAGES 

Figure 4.31 AMS Model Instrumentation -- Plan

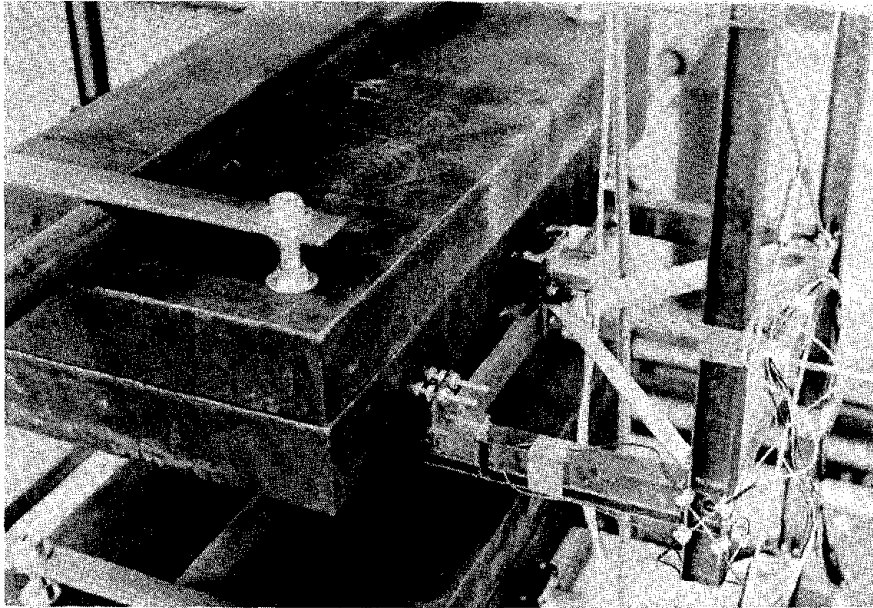


a.) General view

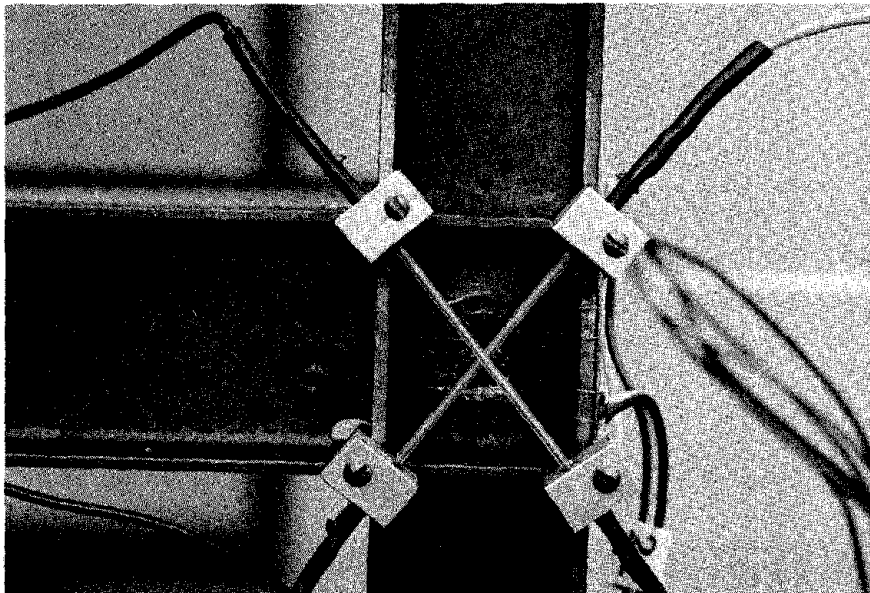


b.) LVDT installation

Figure 4.32 AMS Model Instrumentation

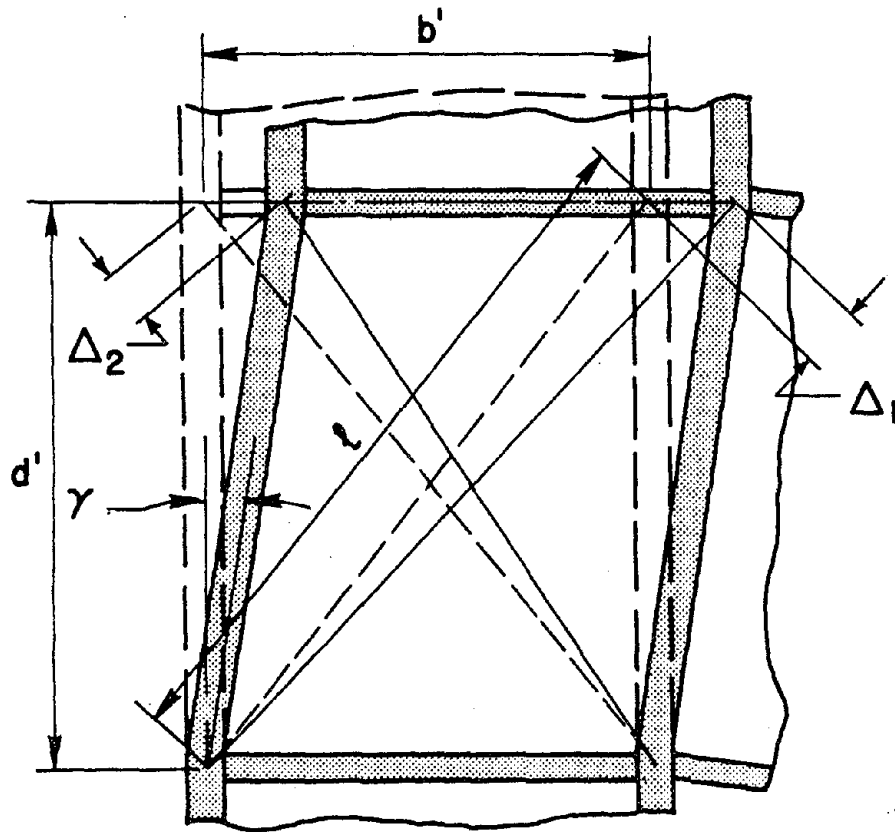


c.) Accelerometer mounted on weight



d.) Joint mercury gages and rosette

Figure 4.32, cont. AMS Model Instrumentation



$$\gamma = \frac{\Delta_1 + \Delta_2}{2} \times \frac{l}{b' \times d'}$$

Figure 4.33 Panel Zone Distortion Measurement (Ref. 9)

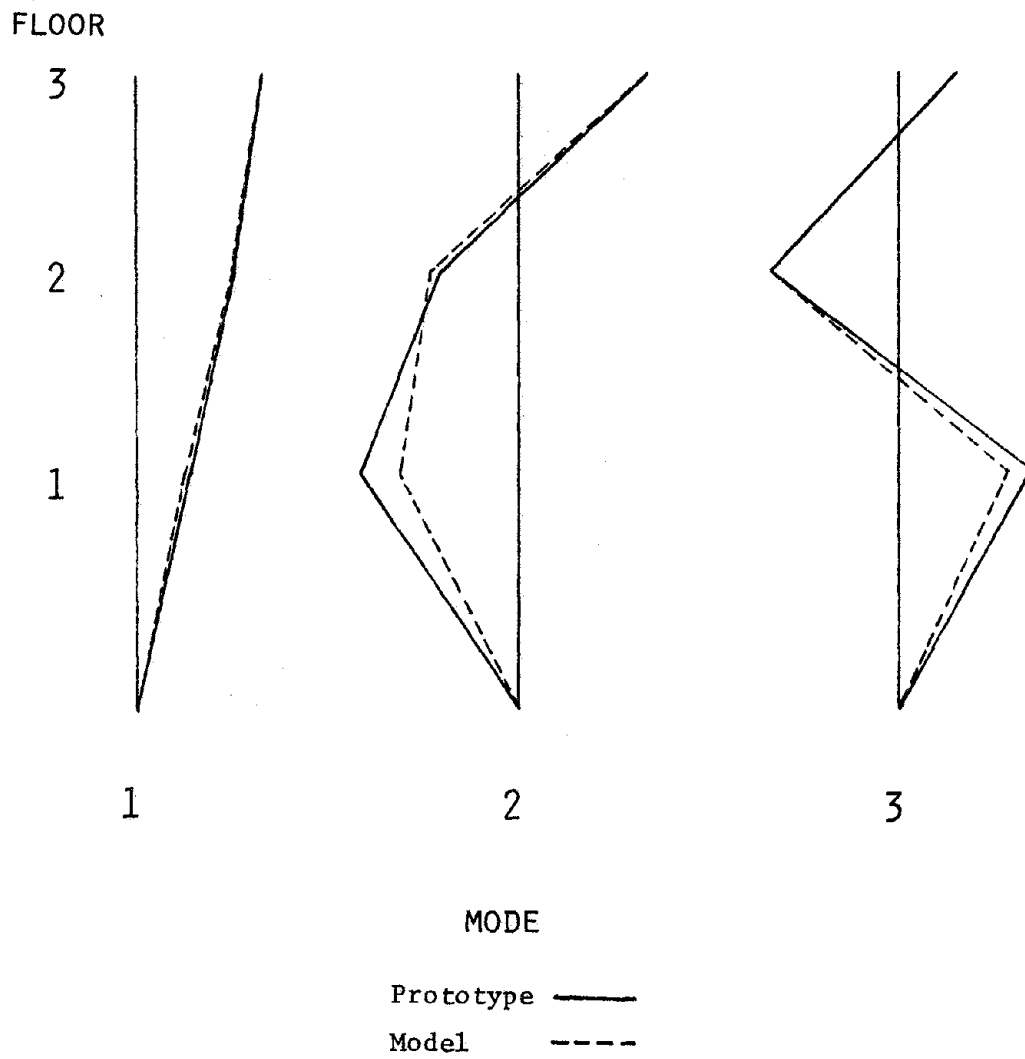


Figure 4.34 Prototype and Model Mode Shapes

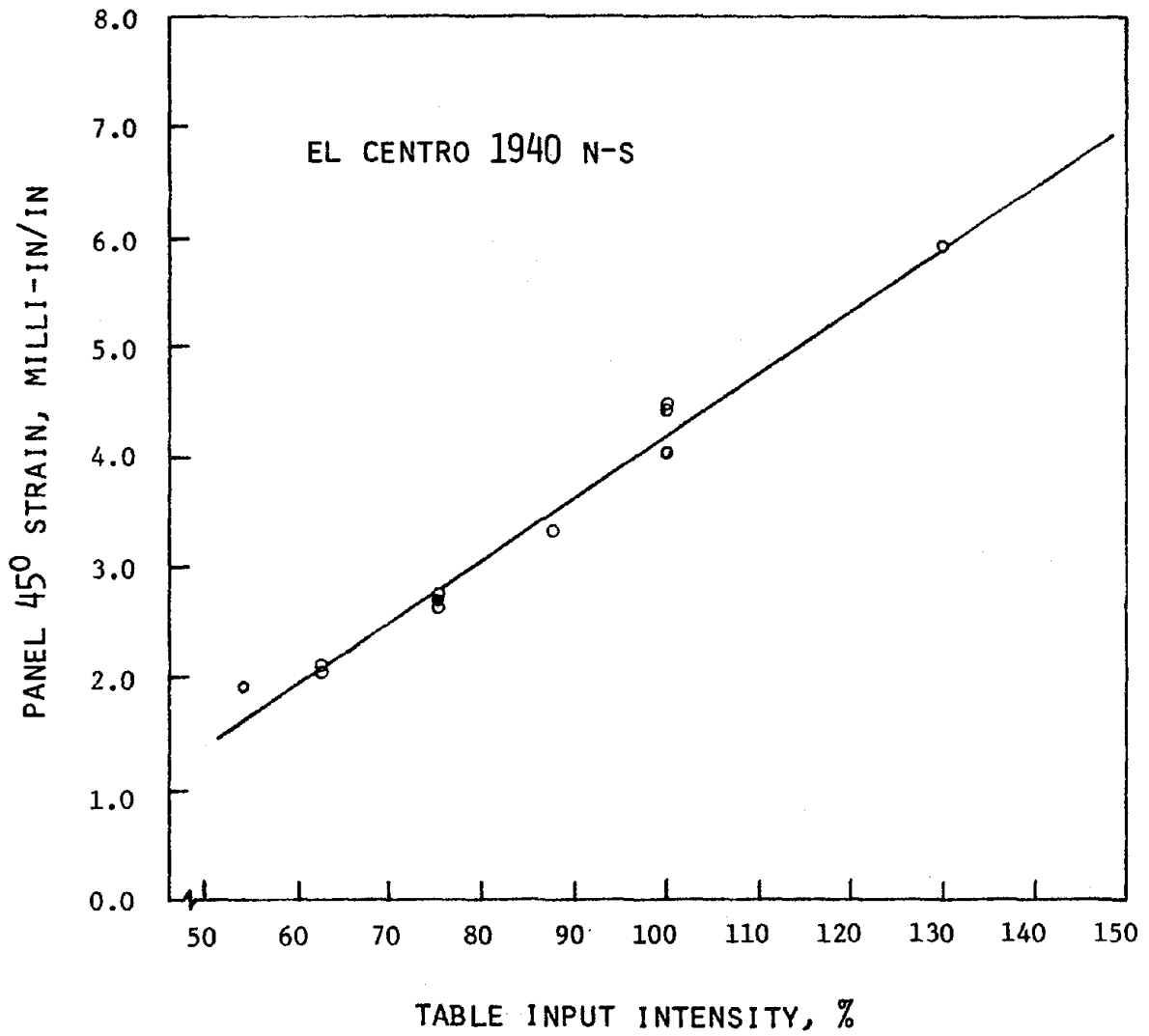


Figure 4.35 Model Inelastic El Centro Tests -- 45° Panel Strain vs. Table Input Intensity

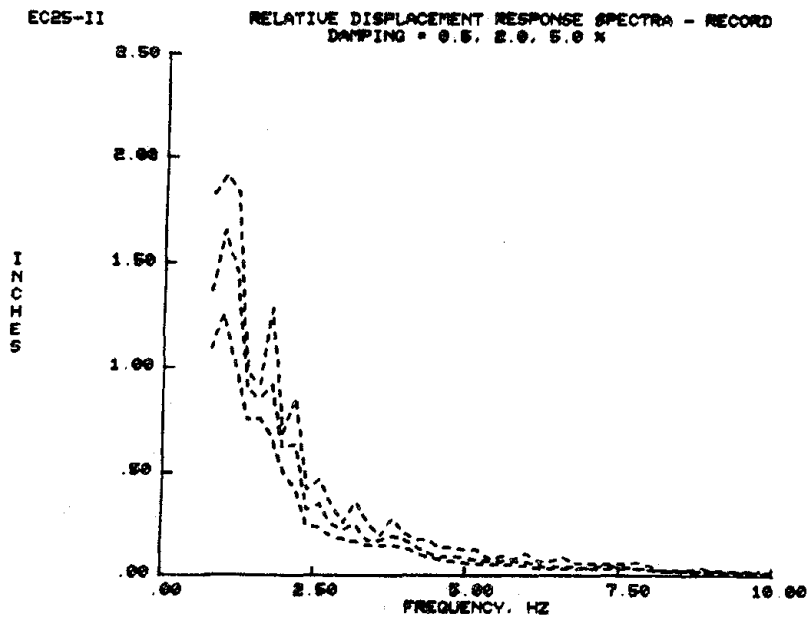
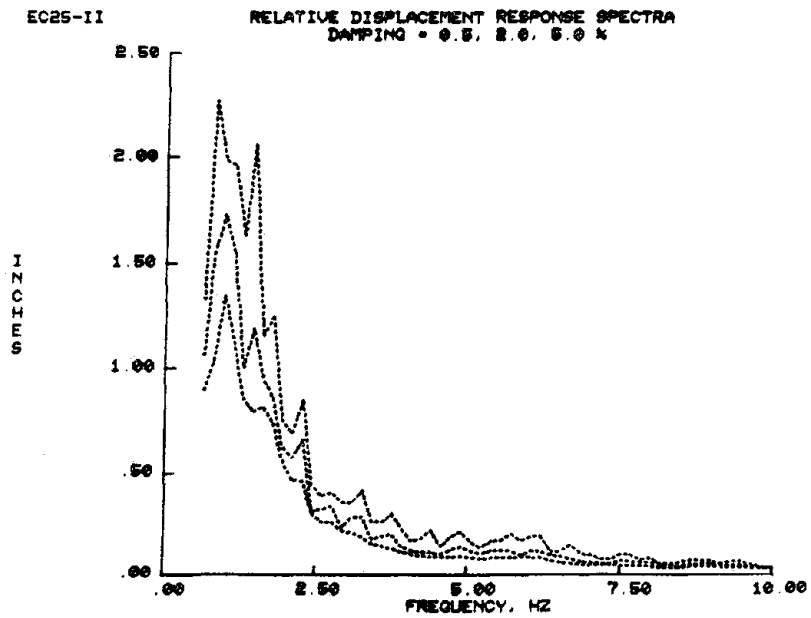
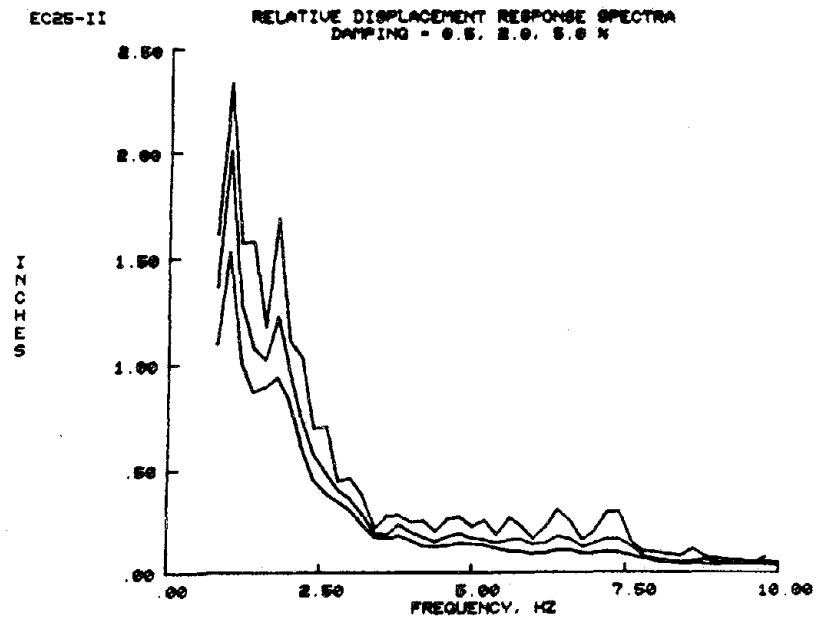


Figure 4.36 EC25 -- Relative Displacement Response Spectra from Table and Input Record Accelerations

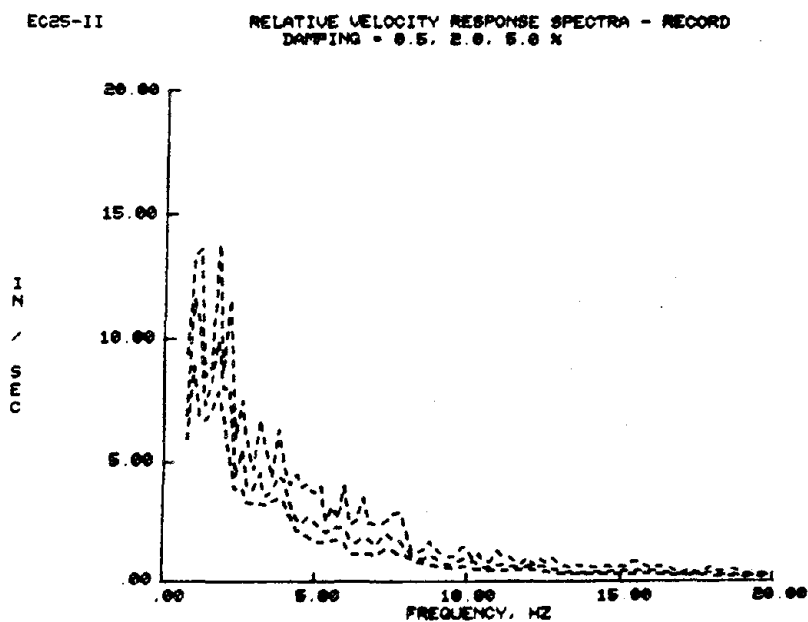
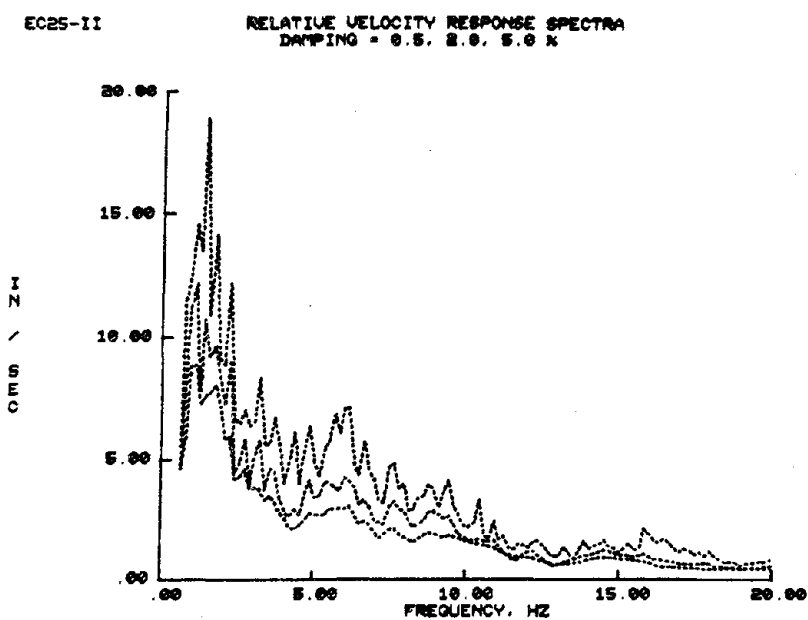
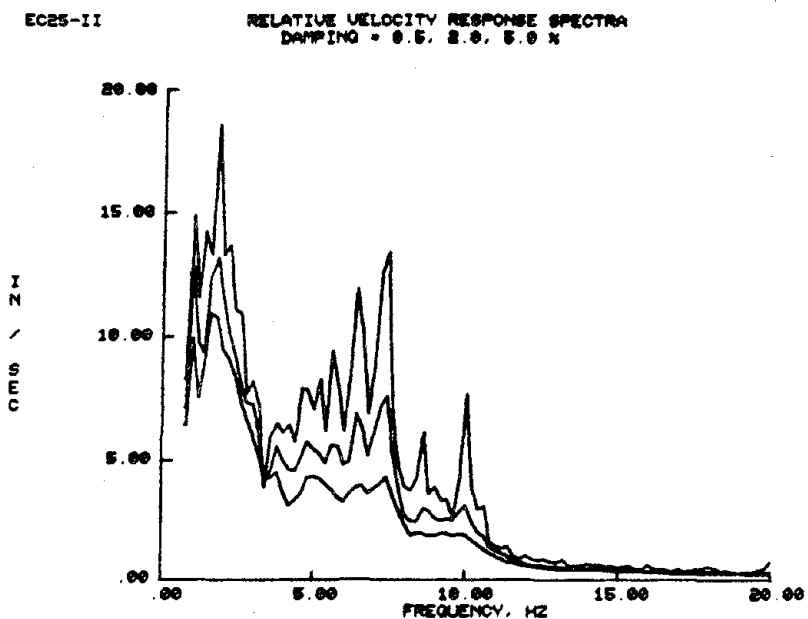
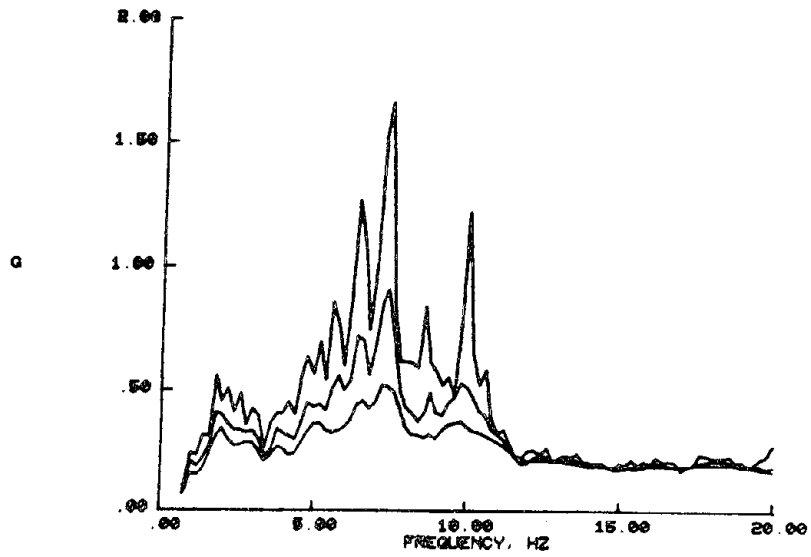


Figure 4.37 EC25 -- Relative Velocity Response Spectra from Table and Input Record Accelerations

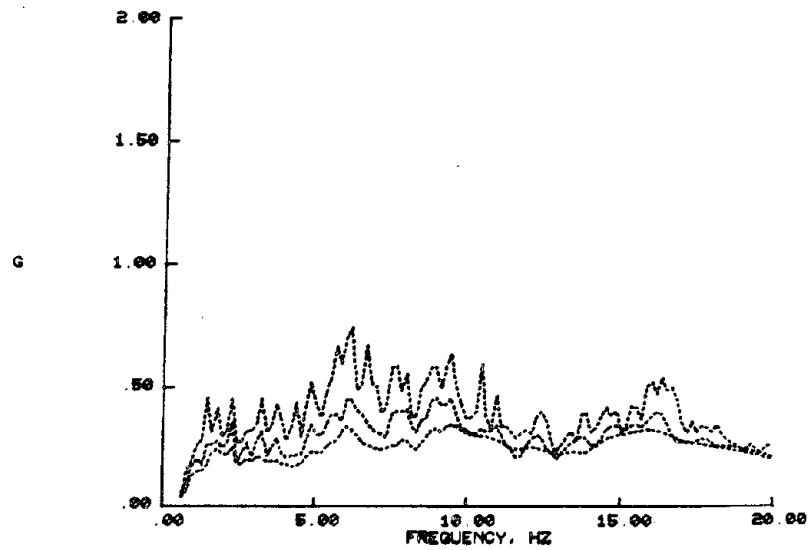
EC25-II

ACCELERATION RESPONSE SPECTRA
DAMPING = 0.5, 2.0, 5.0 %



EC25-II

ACCELERATION RESPONSE SPECTRA
DAMPING = 0.5, 2.0, 5.0 %



EC25-II

ACCELERATION RESPONSE SPECTRA - RECORD
DAMPING = 0.5, 2.0, 5.0 %

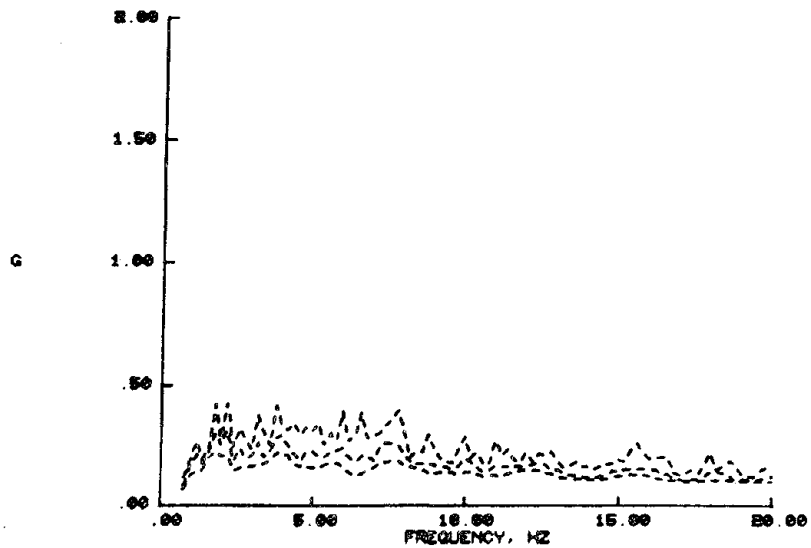


Figure 4.38 EC25 -- Absolute Acceleration Response Spectra from Table and Input Record Accelerations

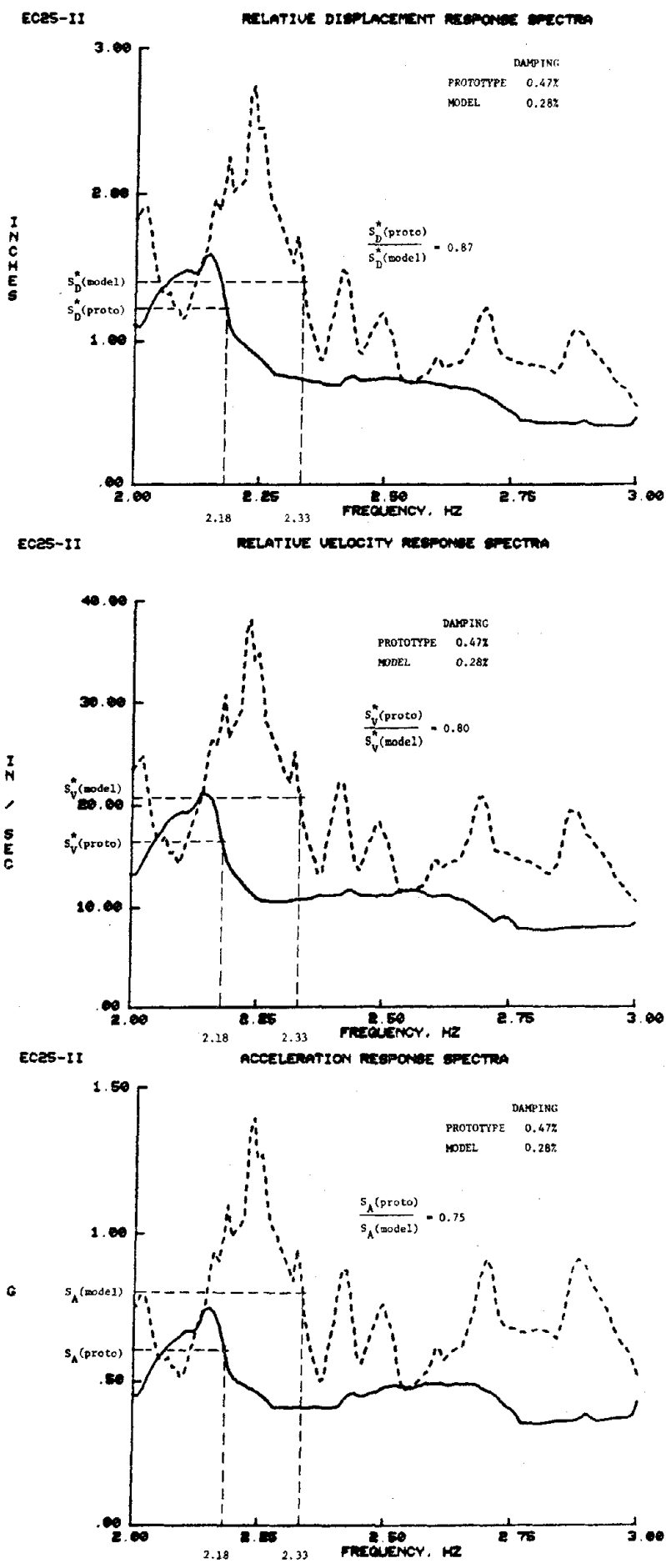
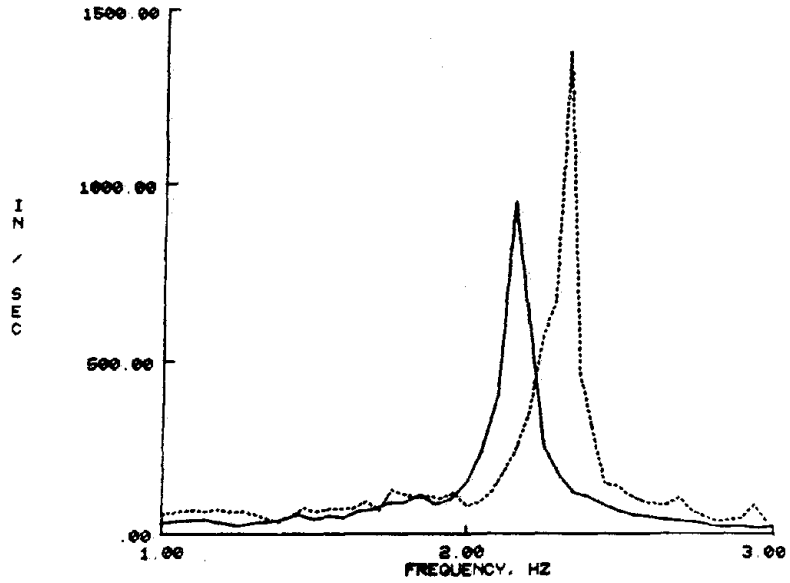


Figure 4.39 EC25 -- Expanded Response Spectra from Shake Table Accelerations

EC25-II SUM OF 2ND FLOOR ACCELERATION, 1ST MODE, DAMPING = 0.0



EC25-II SUM OF 2ND FLOOR ACCELERATION, 2ND MODE, DAMPING = 0.0

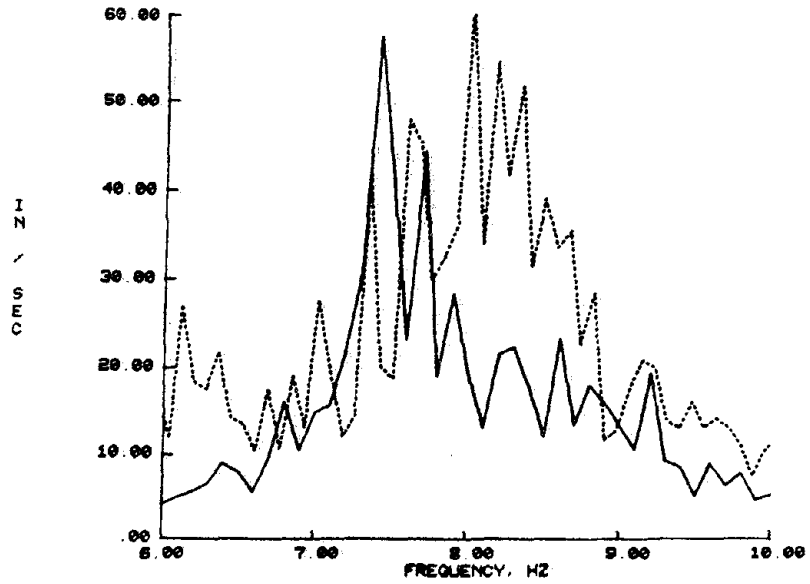
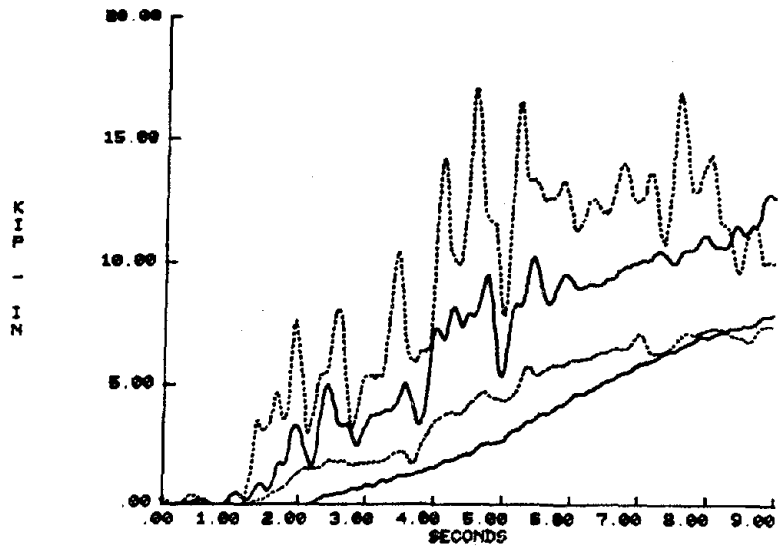


Figure 4.40 EC25 -- Test Structure Floor Response Spectra

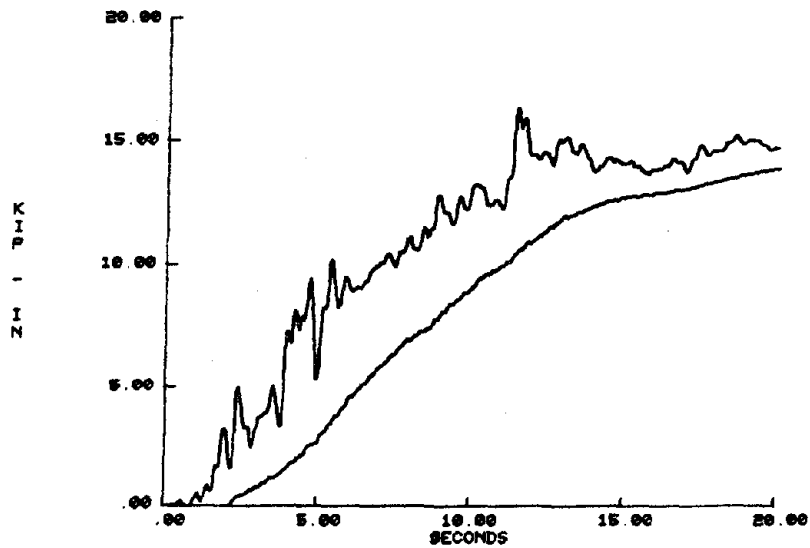
EC25-II

INPUT ENERGY VS. DISSIPATED ENERGY



EC25-II

PROTOTYPE INPUT ENERGY VS. DISSIPATED ENERGY



EC25-II

MODEL INPUT ENERGY VS. DISSIPATED ENERGY

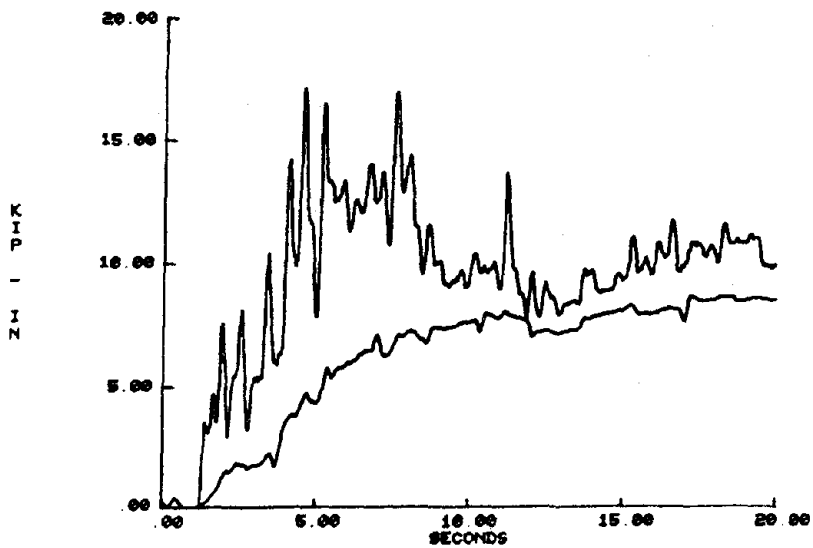
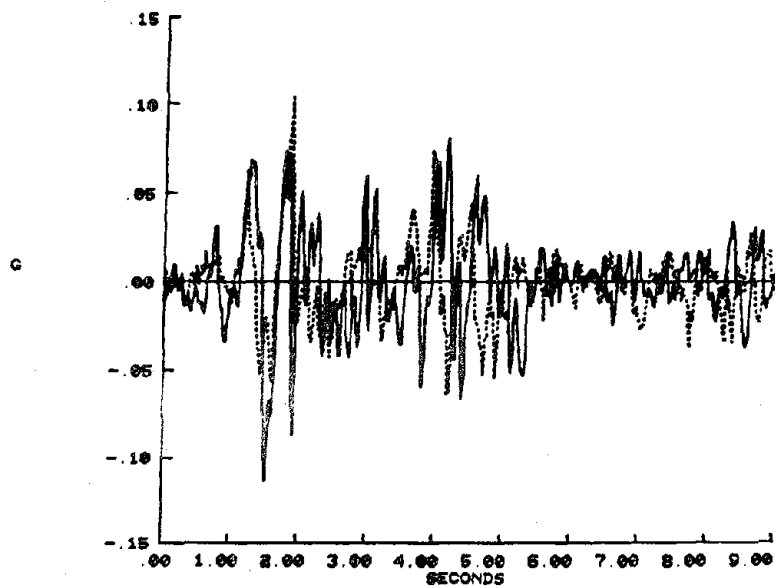


Figure 4.41 EC25 -- Input and Dissipated Energy

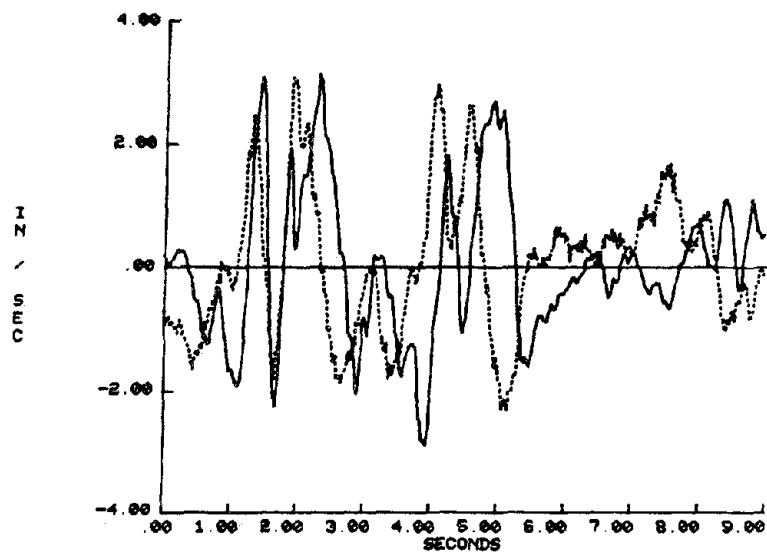
EC25-II

TABLE ACCELERATION



EC25-II

TABLE VELOCITY



EC25-II

TABLE DISPLACEMENT

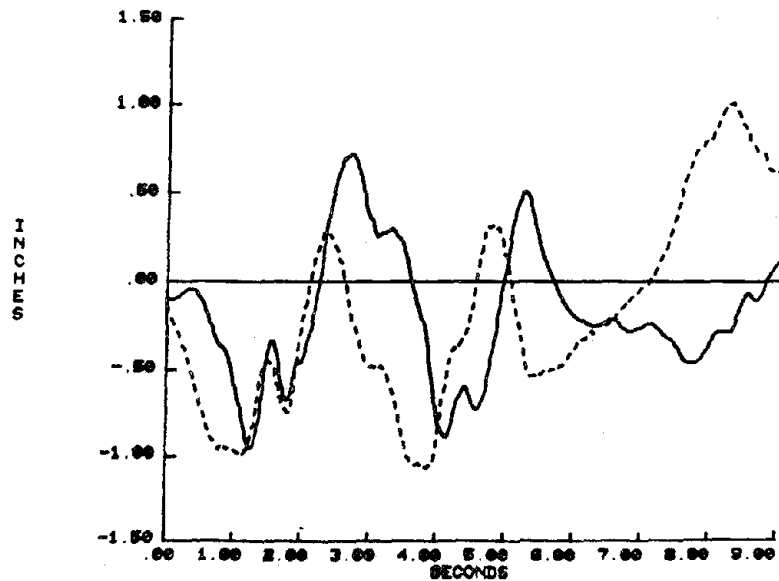


Figure 4.42 EC25 -- Shake Table Motion

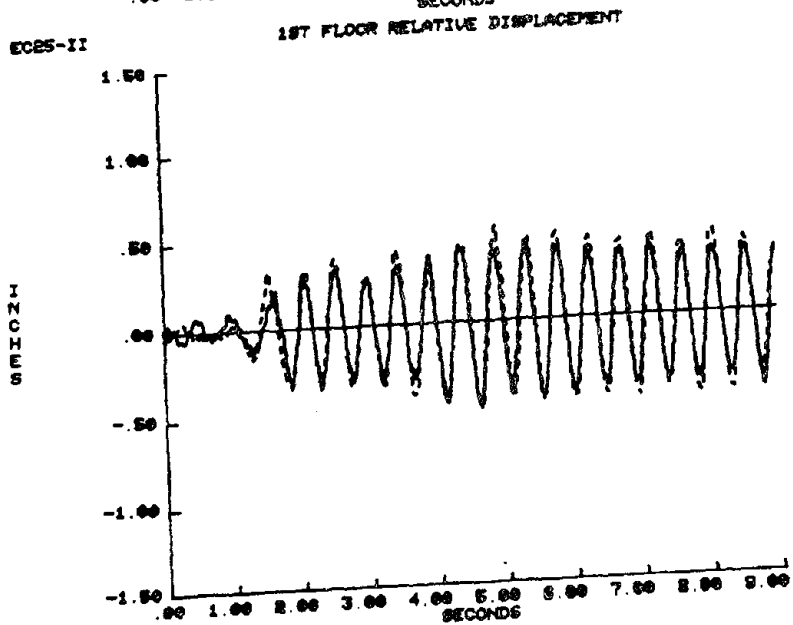
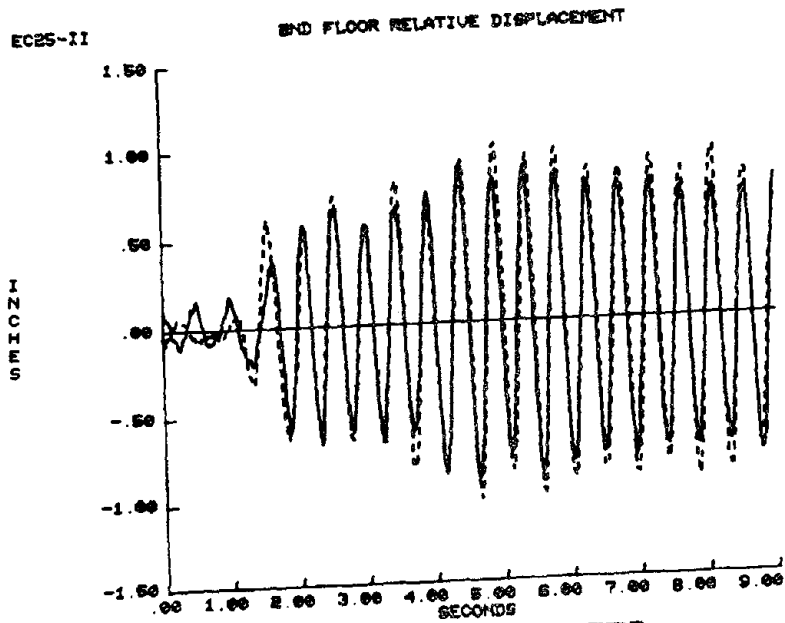
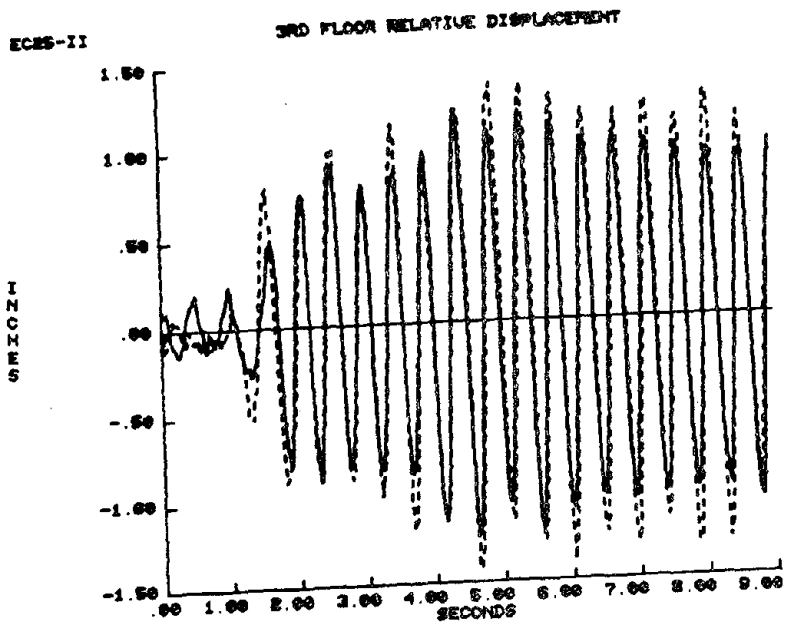
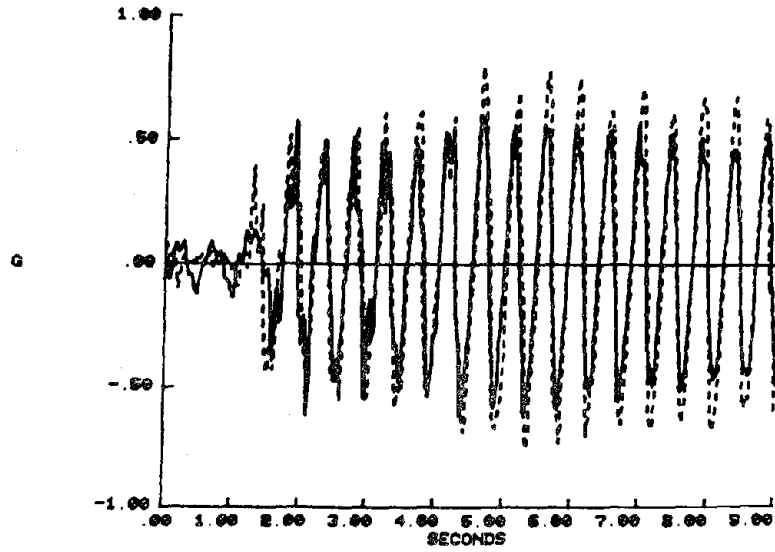


Figure 4.43 EC25 -- Floor Displacements

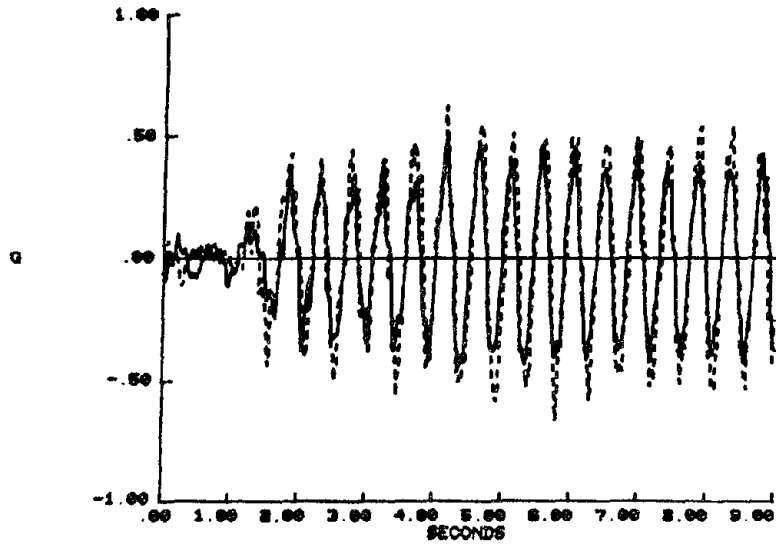
EC25-II

3RD FLOOR ACCELERATION



EC25-II

2ND FLOOR ACCELERATION



EC25-II

1ST FLOOR ACCELERATION

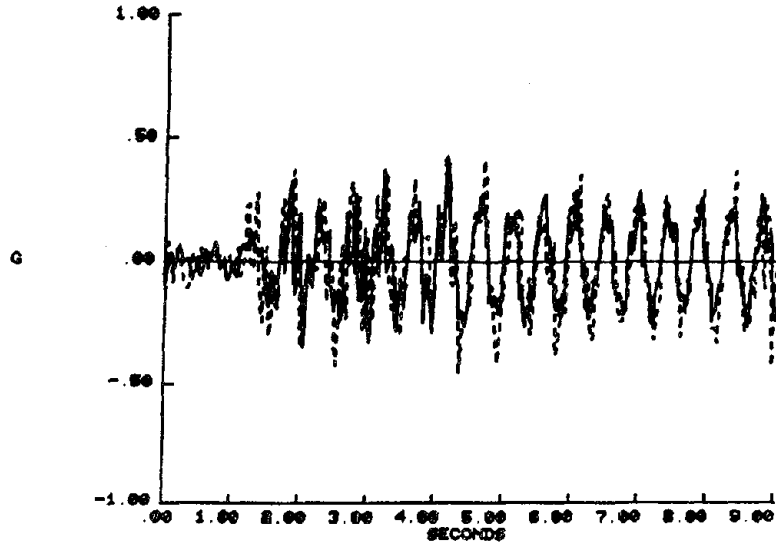


Figure 4.44 EC25 -- Floor Accelerations

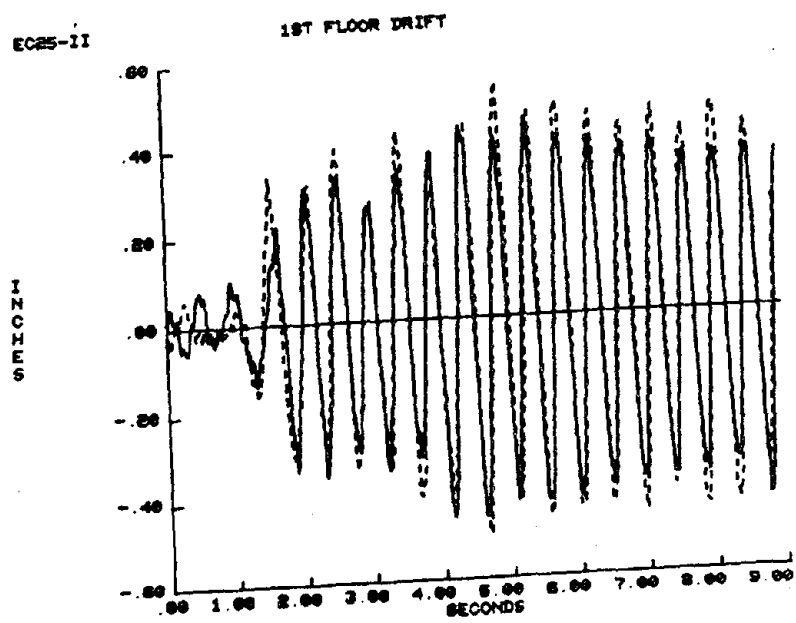
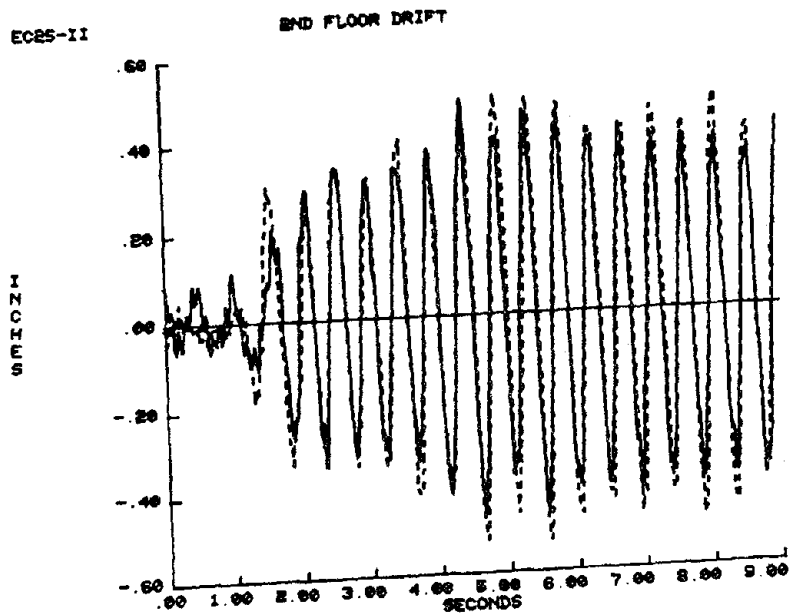
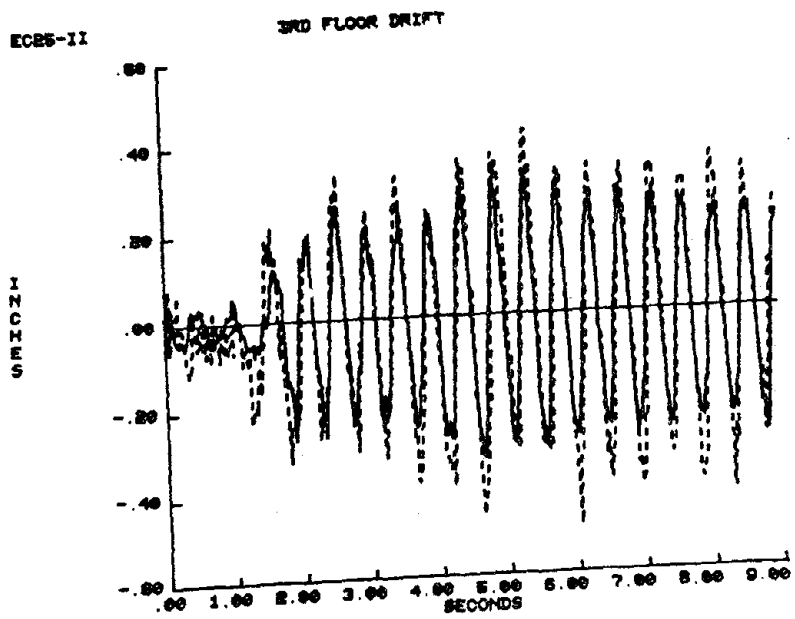


Figure 4.45 EC25 -- Story Drift

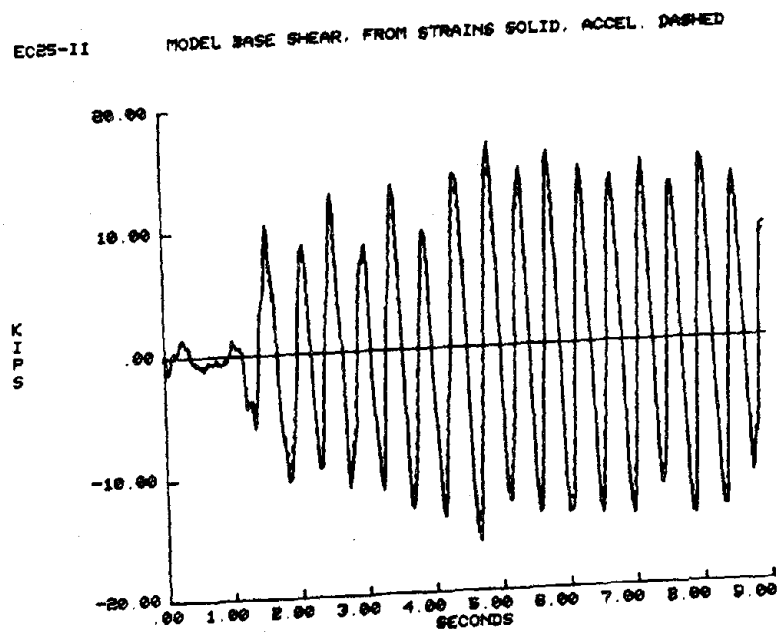
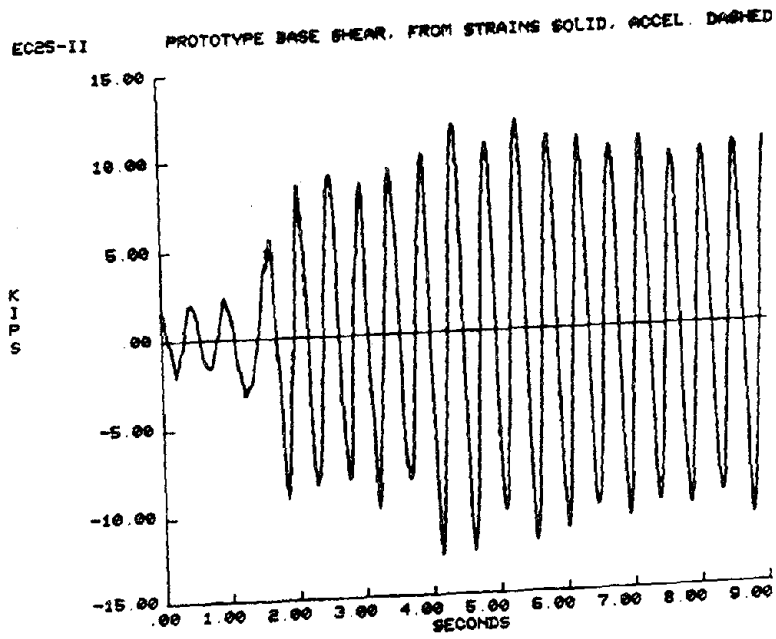


Figure 4.46 EC25 -- Base Shear from Strain Gages vs. Accelerometers

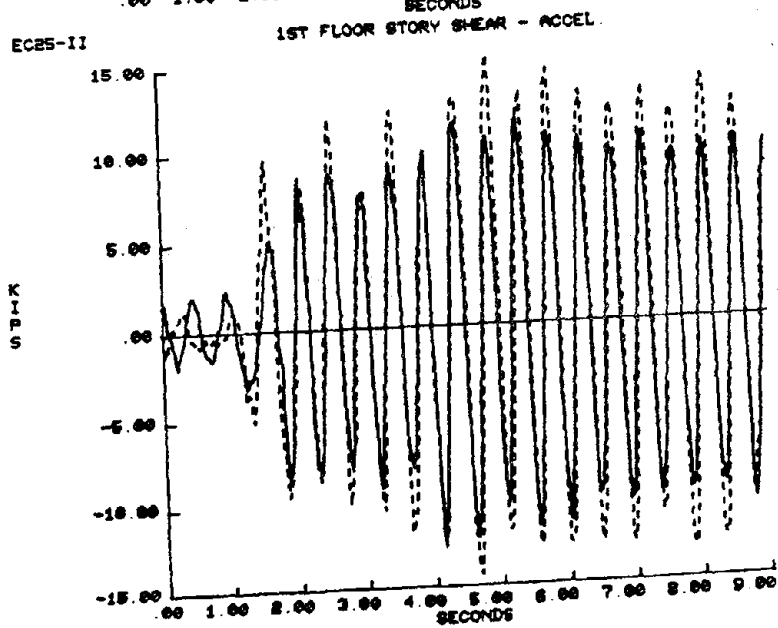
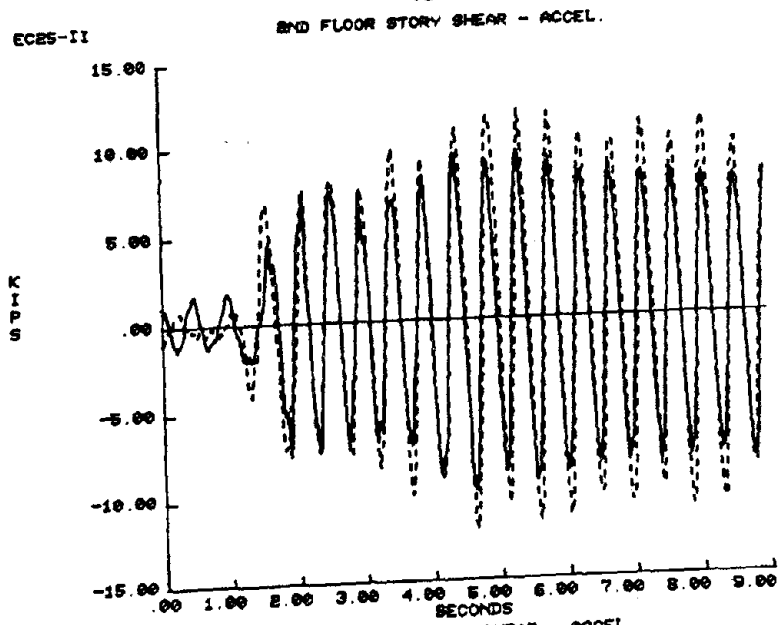
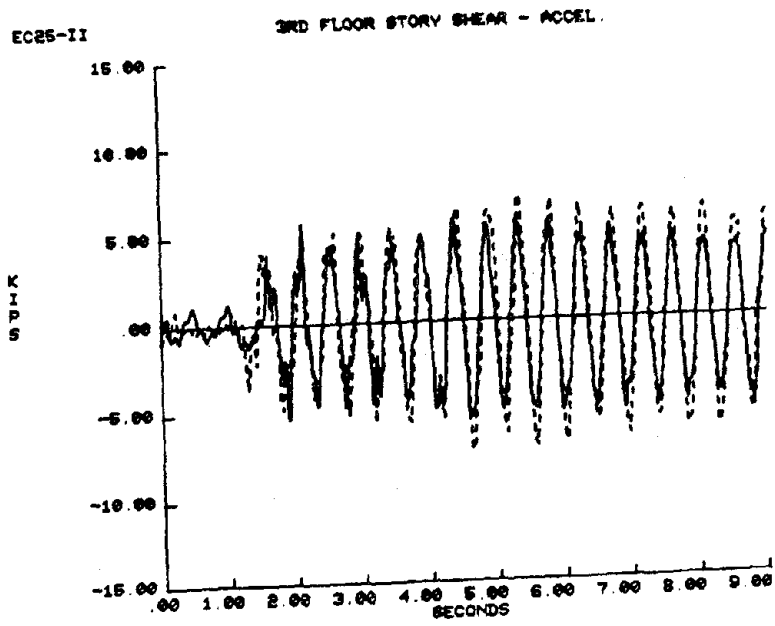
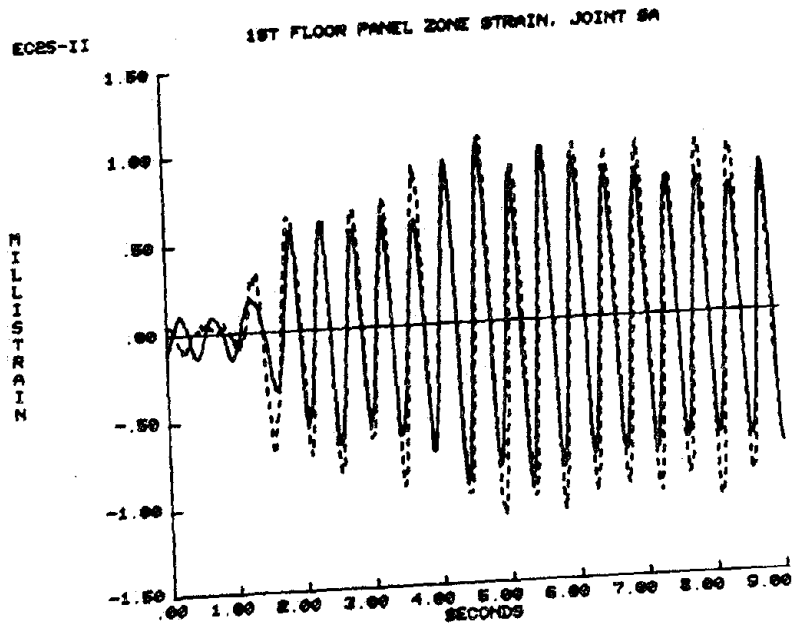
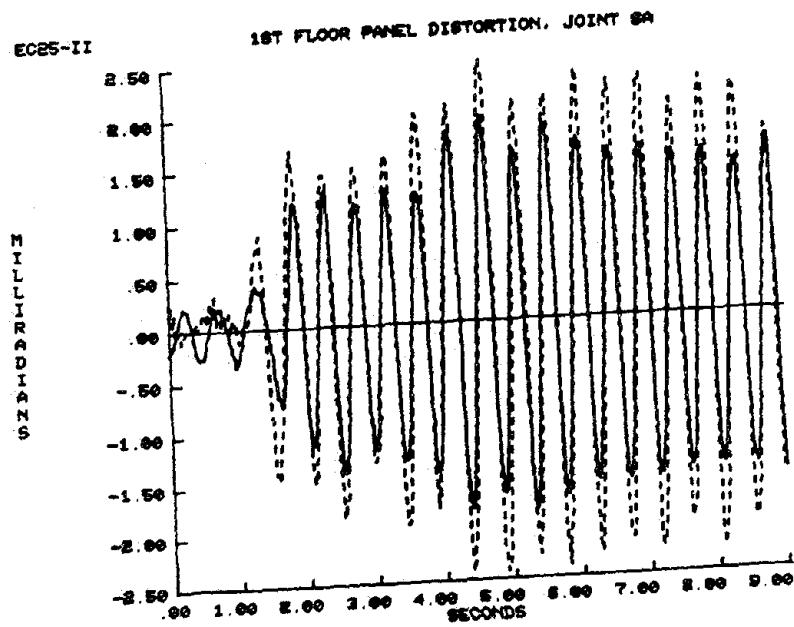


Figure 4.47 EC25 -- Story Shear



a.) Panel zone 45° strain -- joint SA



b.) Panel shear distortion -- joint SA

Figure 4.48 EC25 -- Joint Panel Deformations

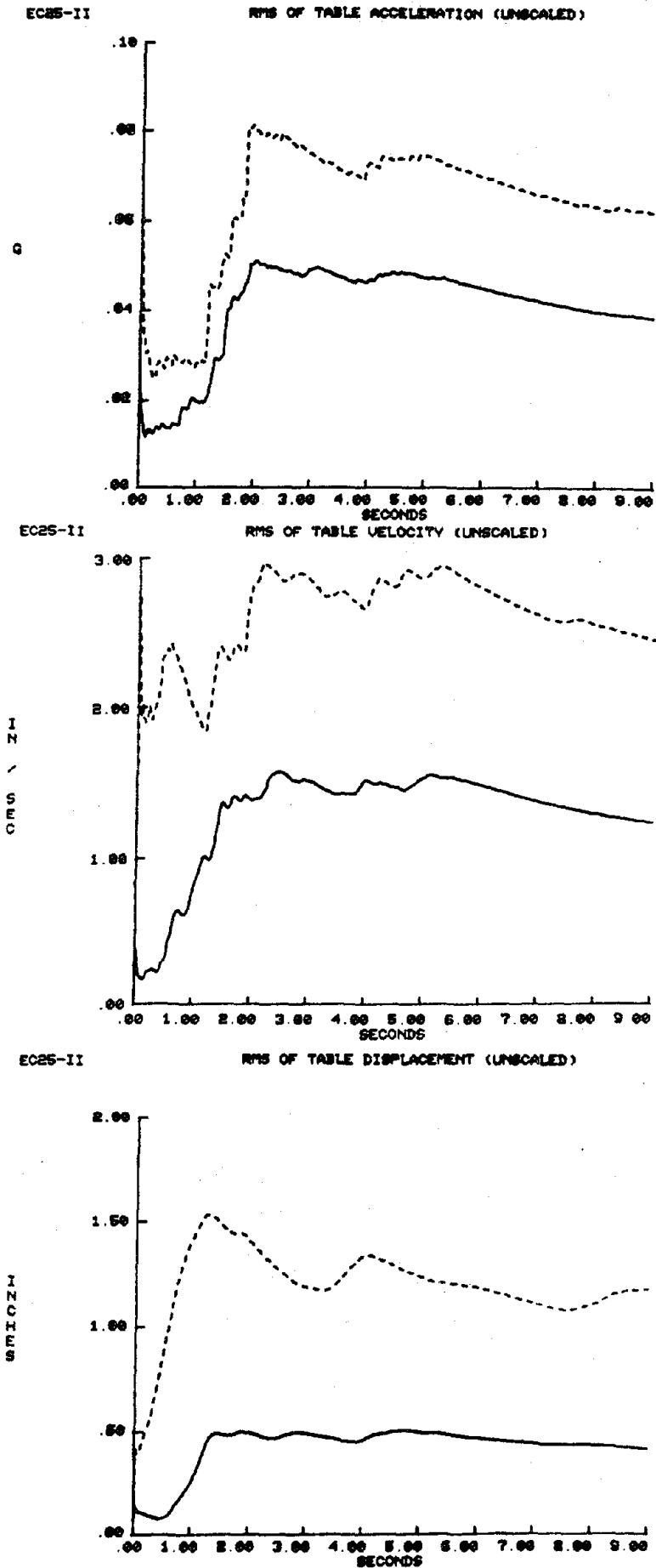


Figure 4.49 EC25 -- RMS of Shake Table Motion

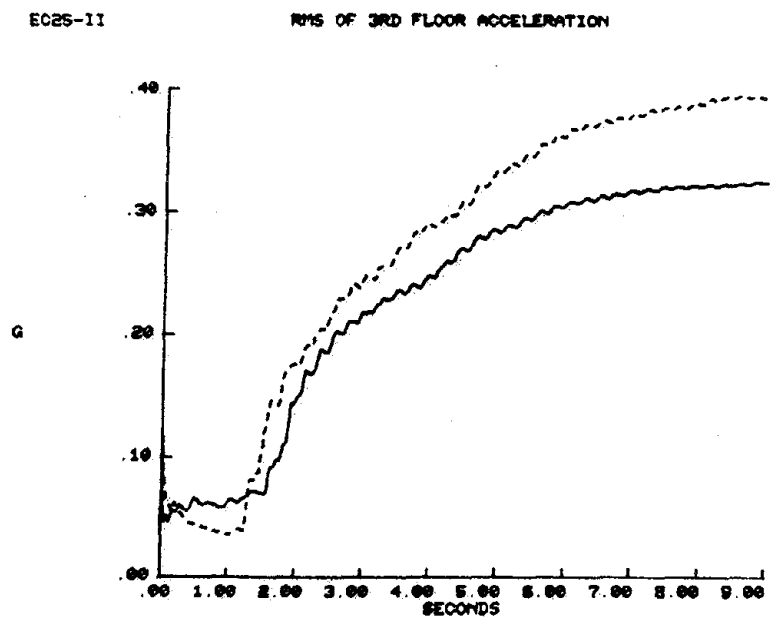
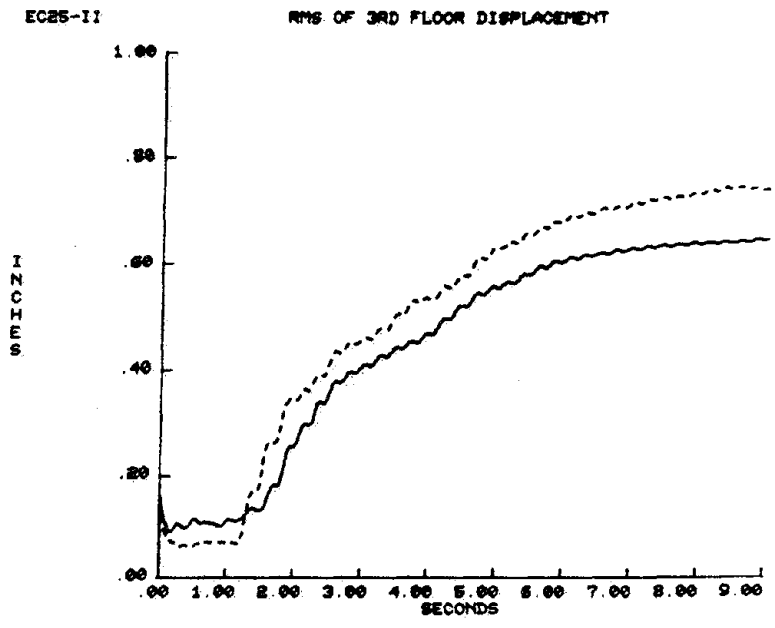


Figure 4.50 EC25 -- RMS of 3rd Floor Motions

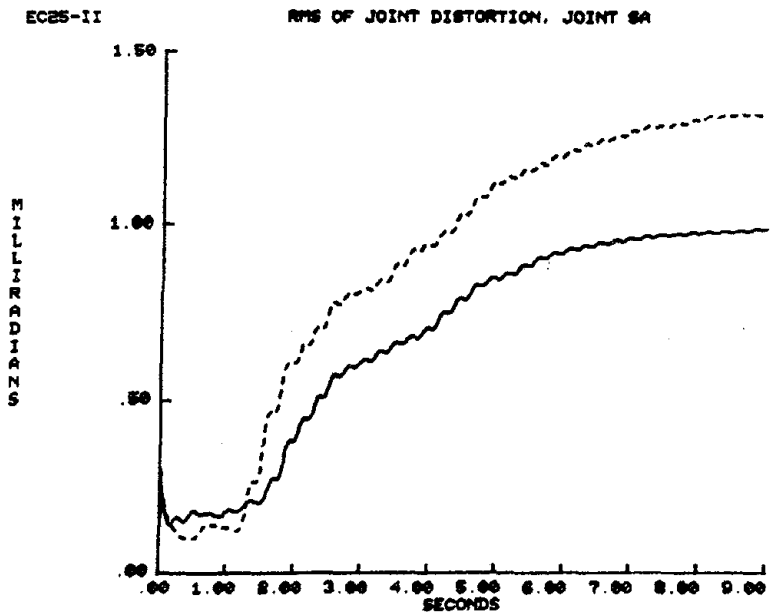
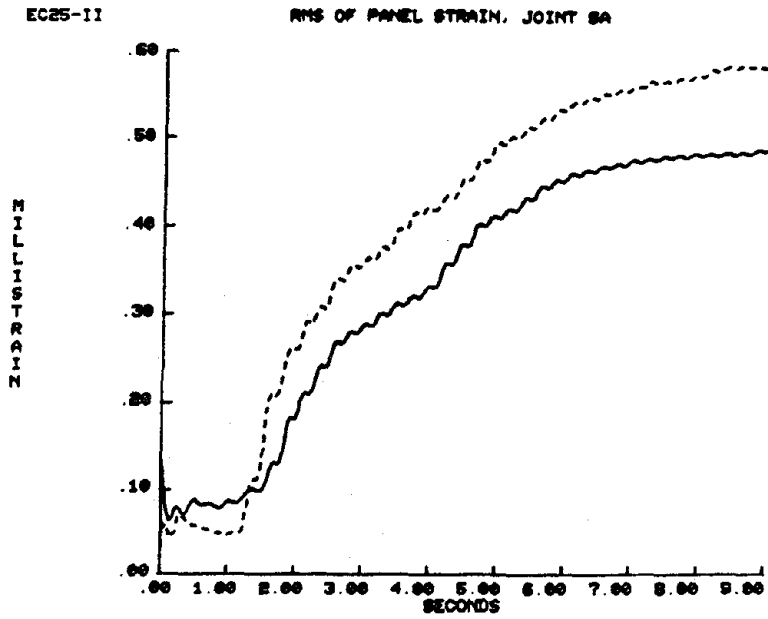
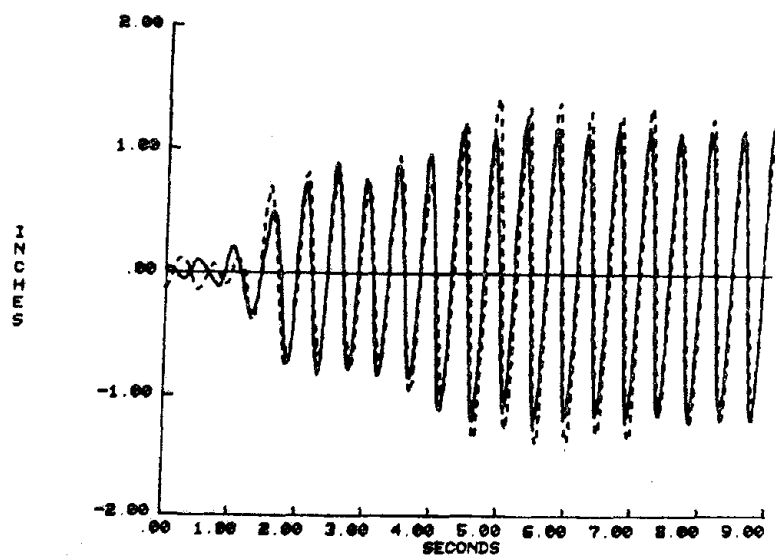


Figure 4.51 EC25 -- RMS of Joint SA Panel Deformation

EC25-II

ELASTIC 1 DOF DISPL. RESPONSE - ANALYTICAL



EC25-II

ELASTIC 1 DOF ACCEL. RESPONSE - ANALYTICAL

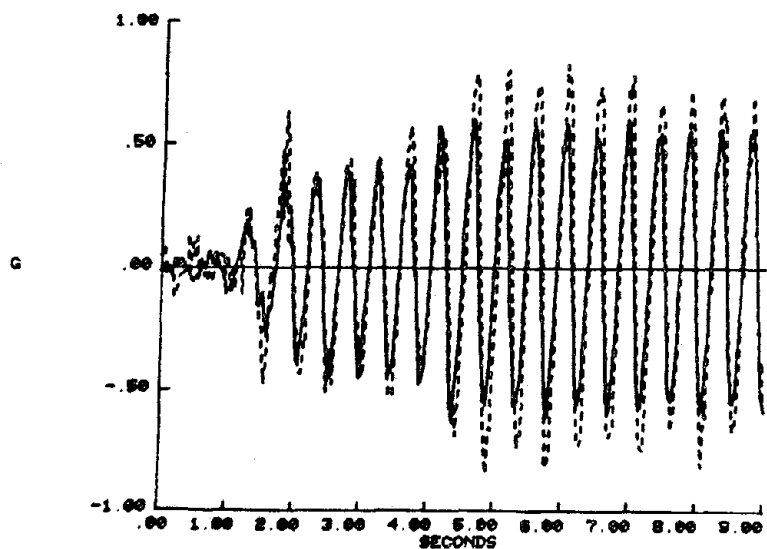


Figure 4.52 EC25 -- Analytic Elastic Response

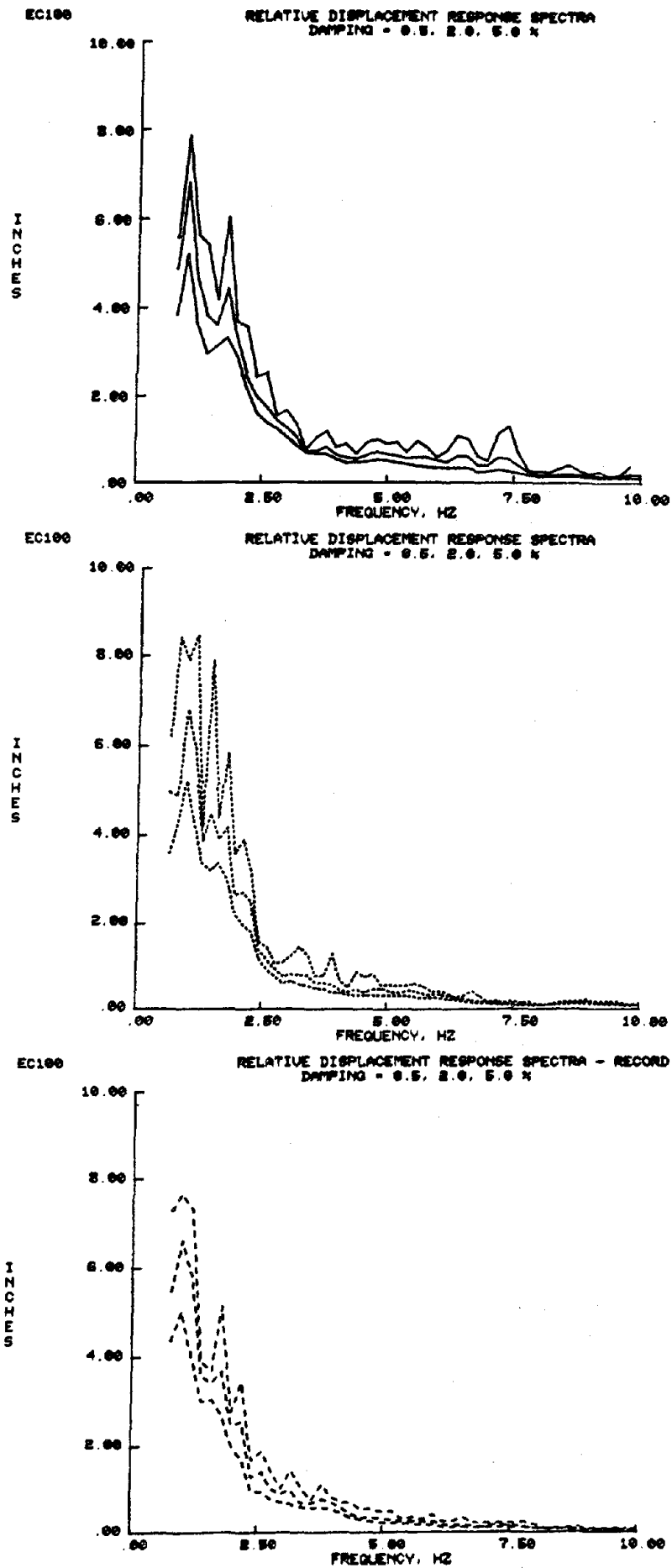
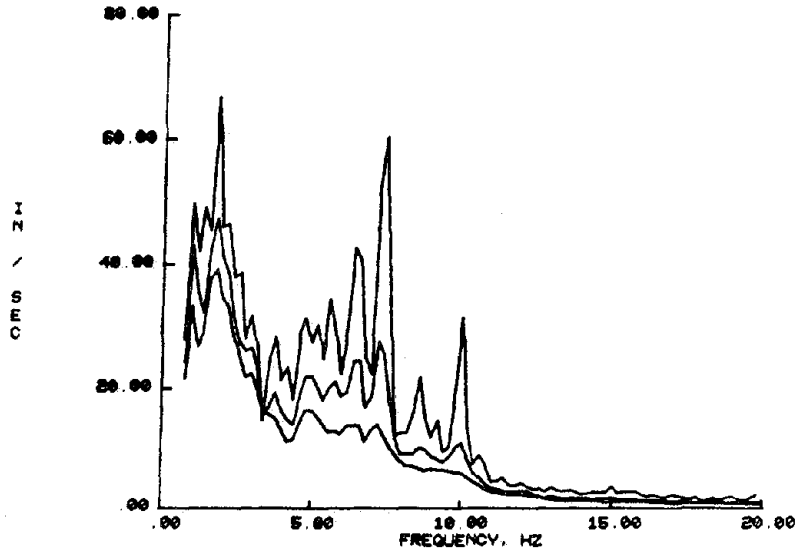


Figure 4.53 EC100 -- Relative Displacement Response Spectra from Table and Input Record Accelerations

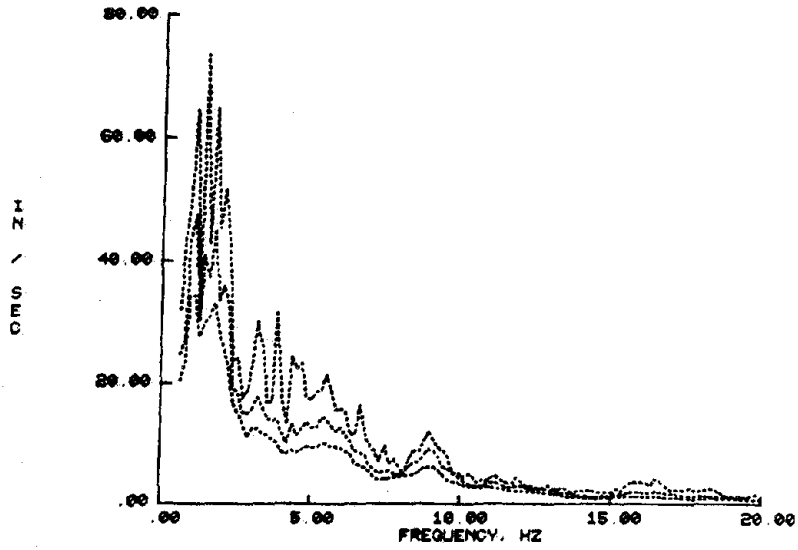
EC100

RELATIVE VELOCITY RESPONSE SPECTRA
DAMPING = 0.5, 2.0, 5.0 %



EC100

RELATIVE VELOCITY RESPONSE SPECTRA
DAMPING = 0.5, 2.0, 5.0 %



EC100

RELATIVE VELOCITY RESPONSE SPECTRA - RECORD
DAMPING = 0.5, 2.0, 5.0 %

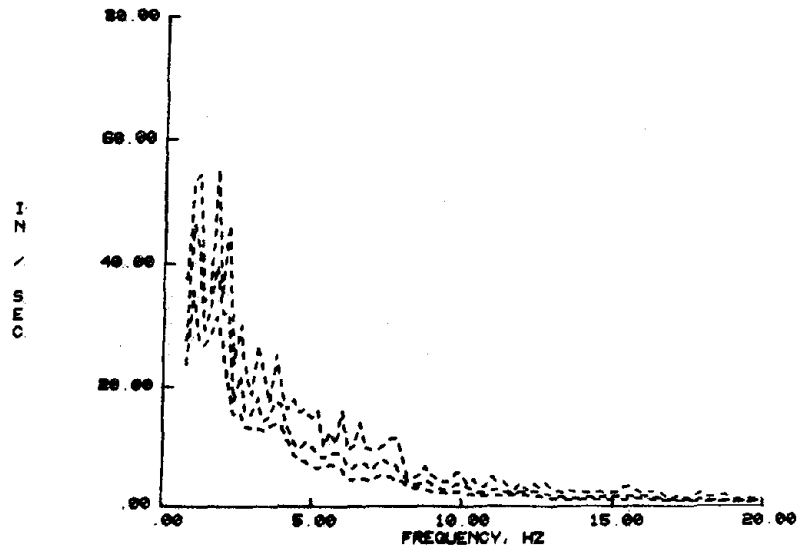


Figure 4.54 EC100 -- Relative Velocity Response Spectra from Table and Input Record Accelerations

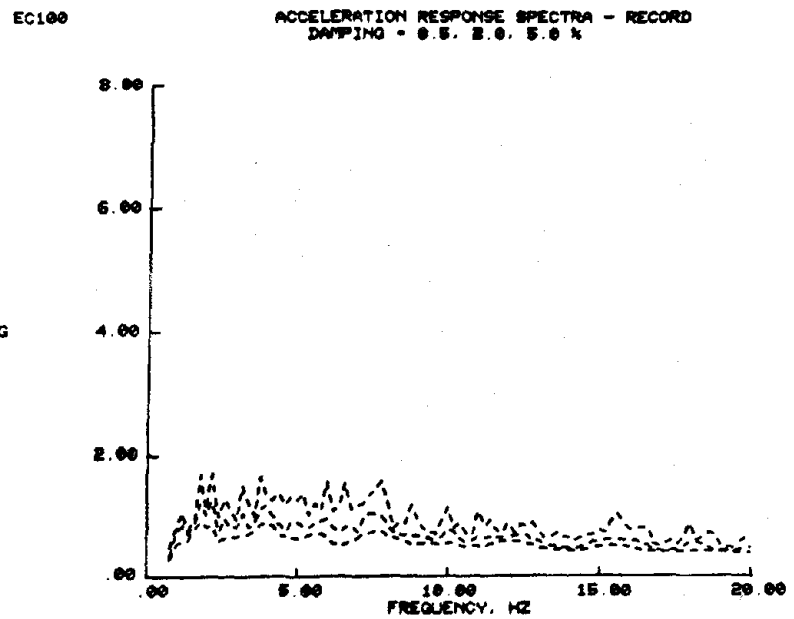
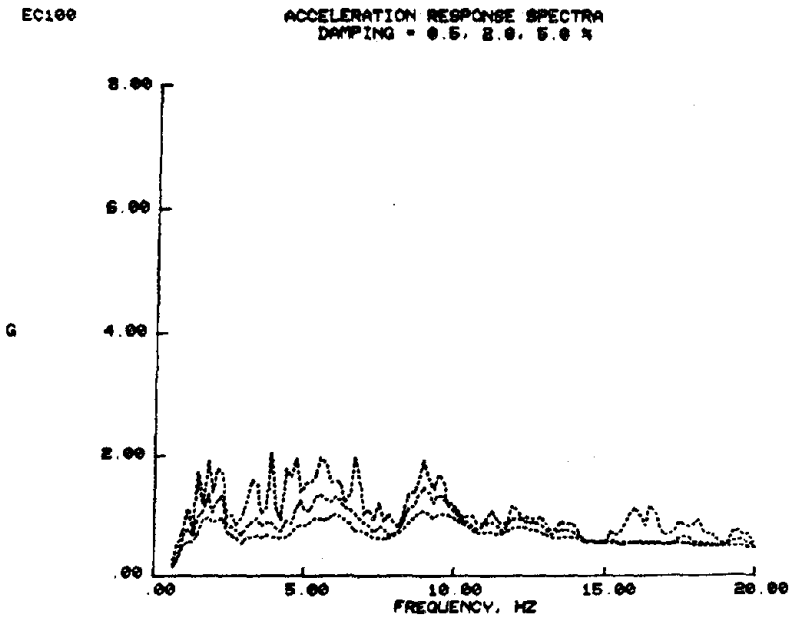
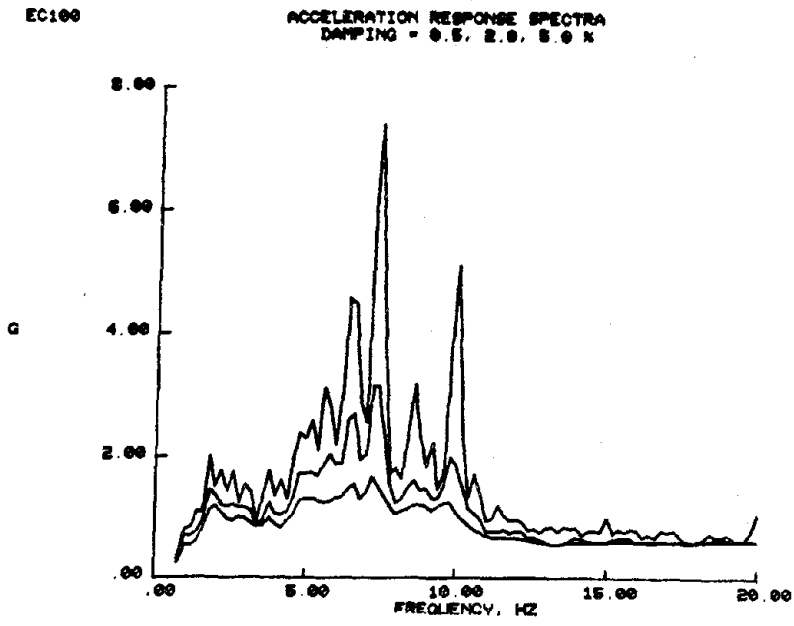
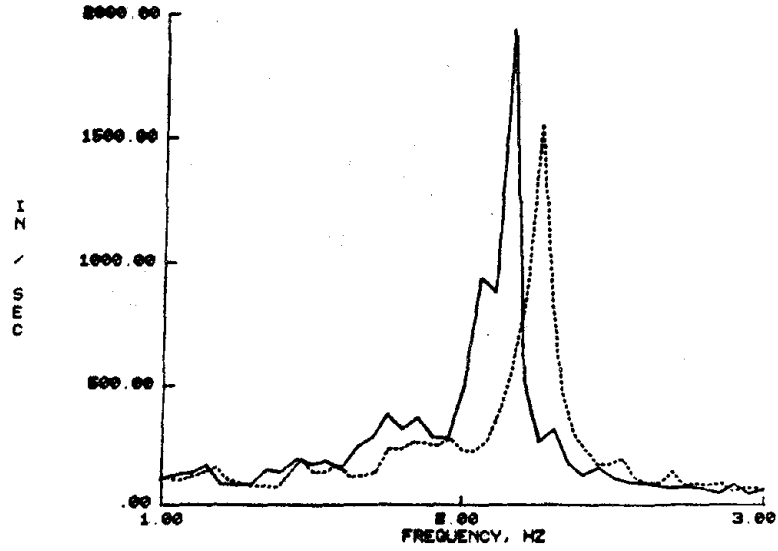


Figure 4.55 EC100 -- Absolute Acceleration Response Spectra from Table and Input Record Accelerations

EC100 SUM OF END FLOOR ACCELERATION, 1ST MODE, DAMPING = 0.0



EC100 SUM OF END FLOOR ACCELERATION, 2ND MODE, DAMPING = 0.0

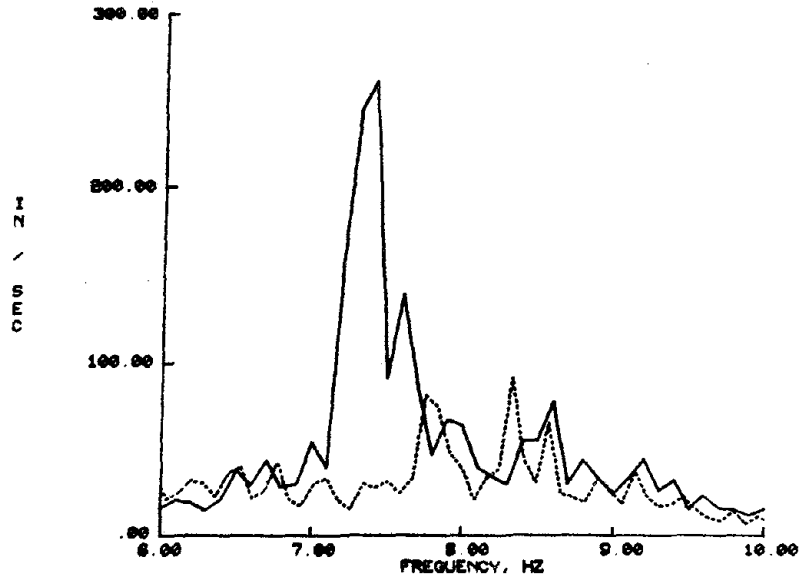


Figure 4.56 EC100 -- Test Structure Floor Response Spectra

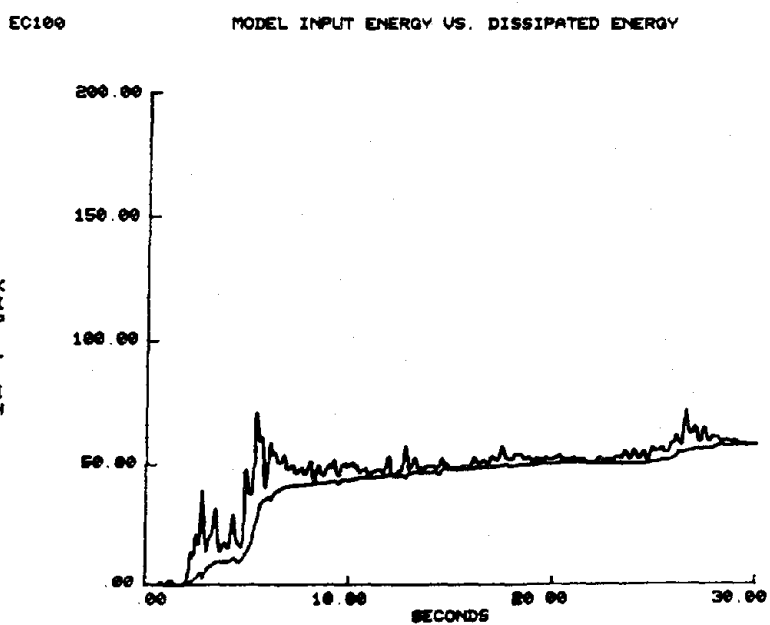
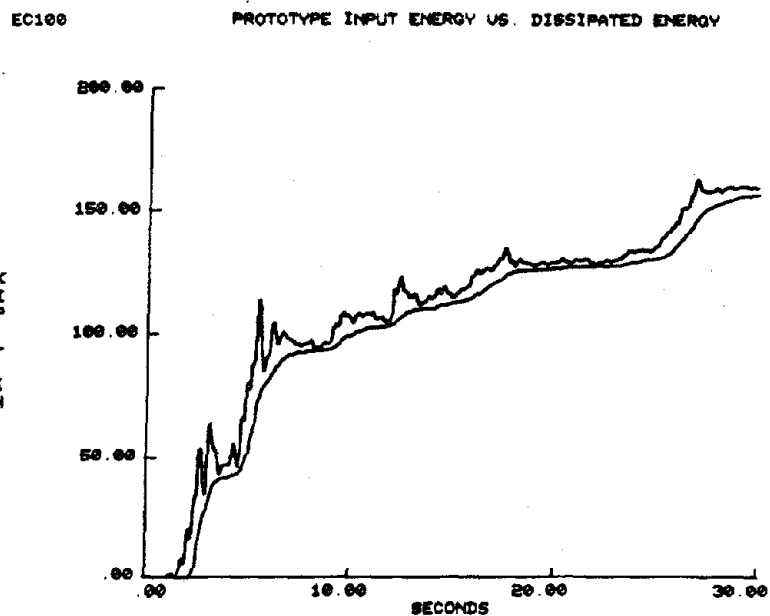
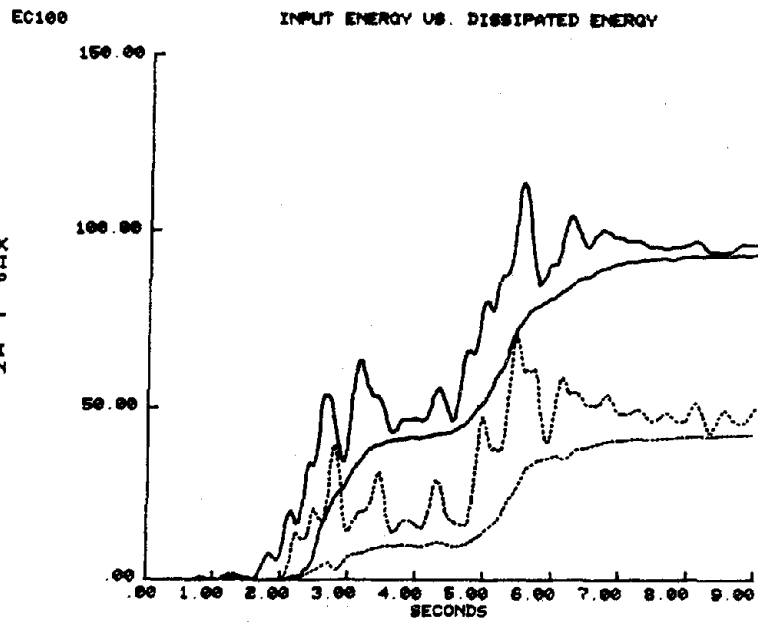


Figure 4.57 EC100 -- Input and Dissipated Energy

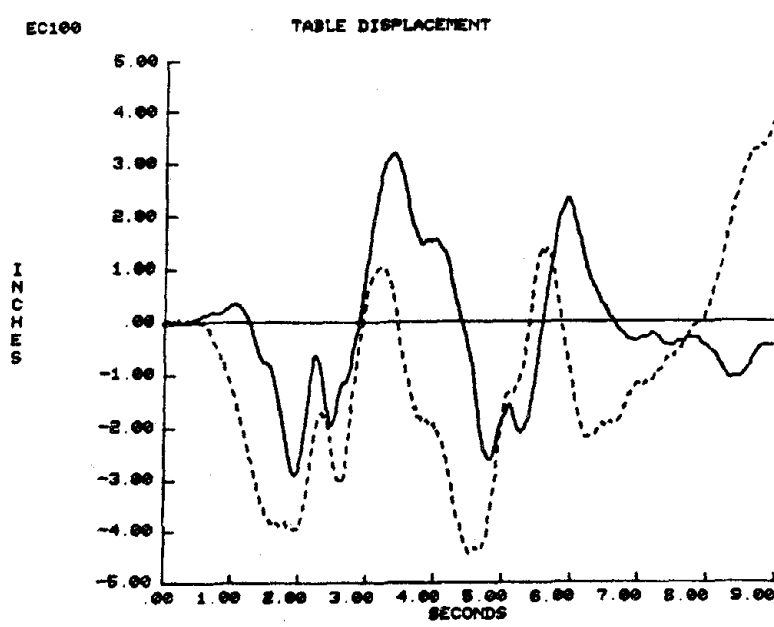
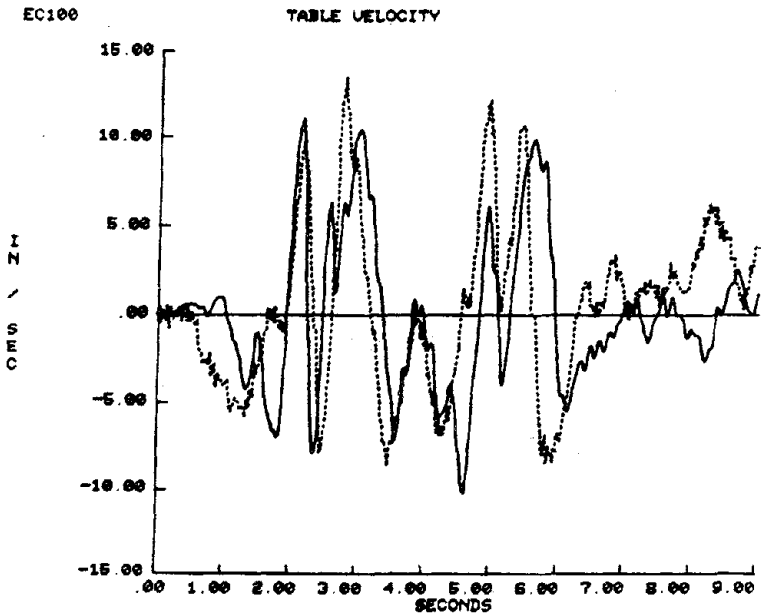
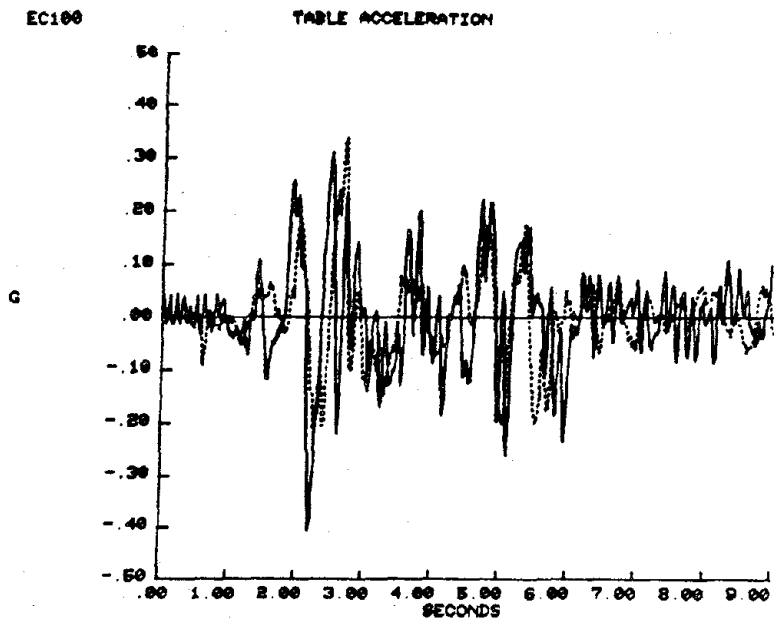
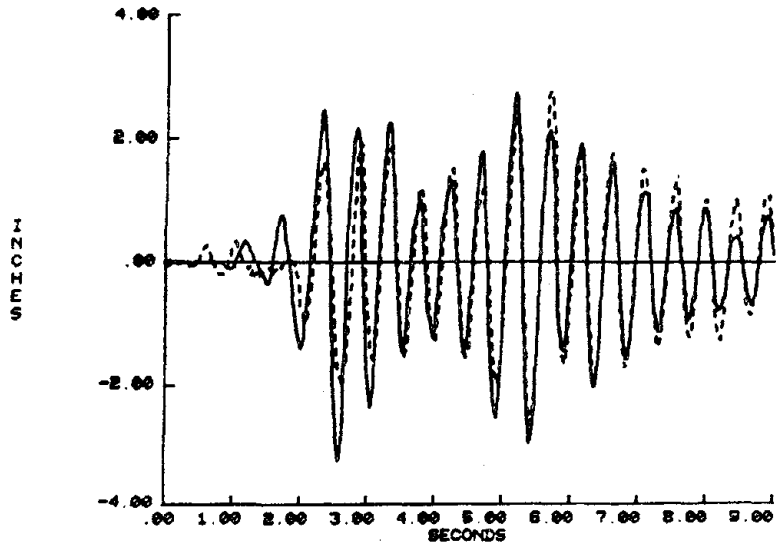


Figure 4.58 EC100 -- Shake Table Motion

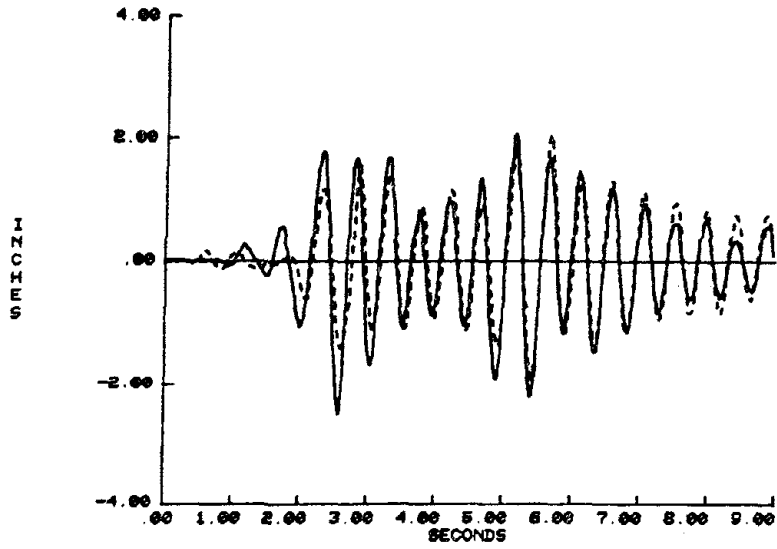
EC100

3RD FLOOR RELATIVE DISPLACEMENT



EC100

2ND FLOOR RELATIVE DISPLACEMENT



EC100

1ST FLOOR RELATIVE DISPLACEMENT

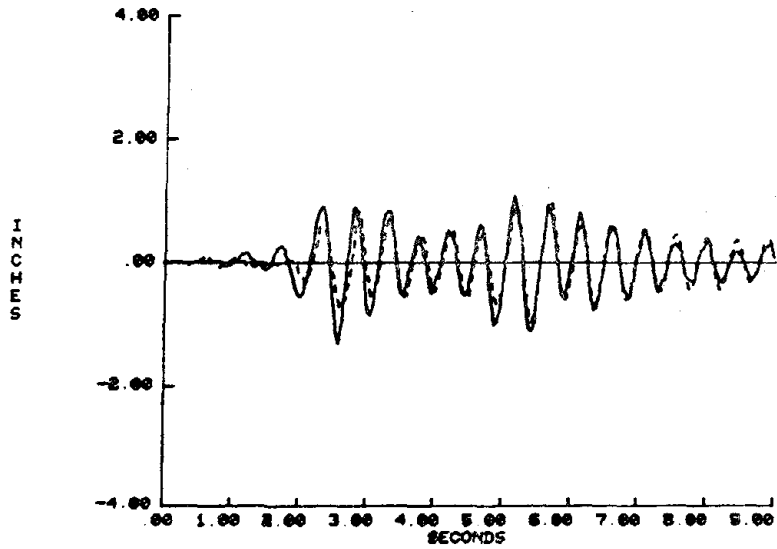


Figure 4.59 EC100 -- Floor Displacements

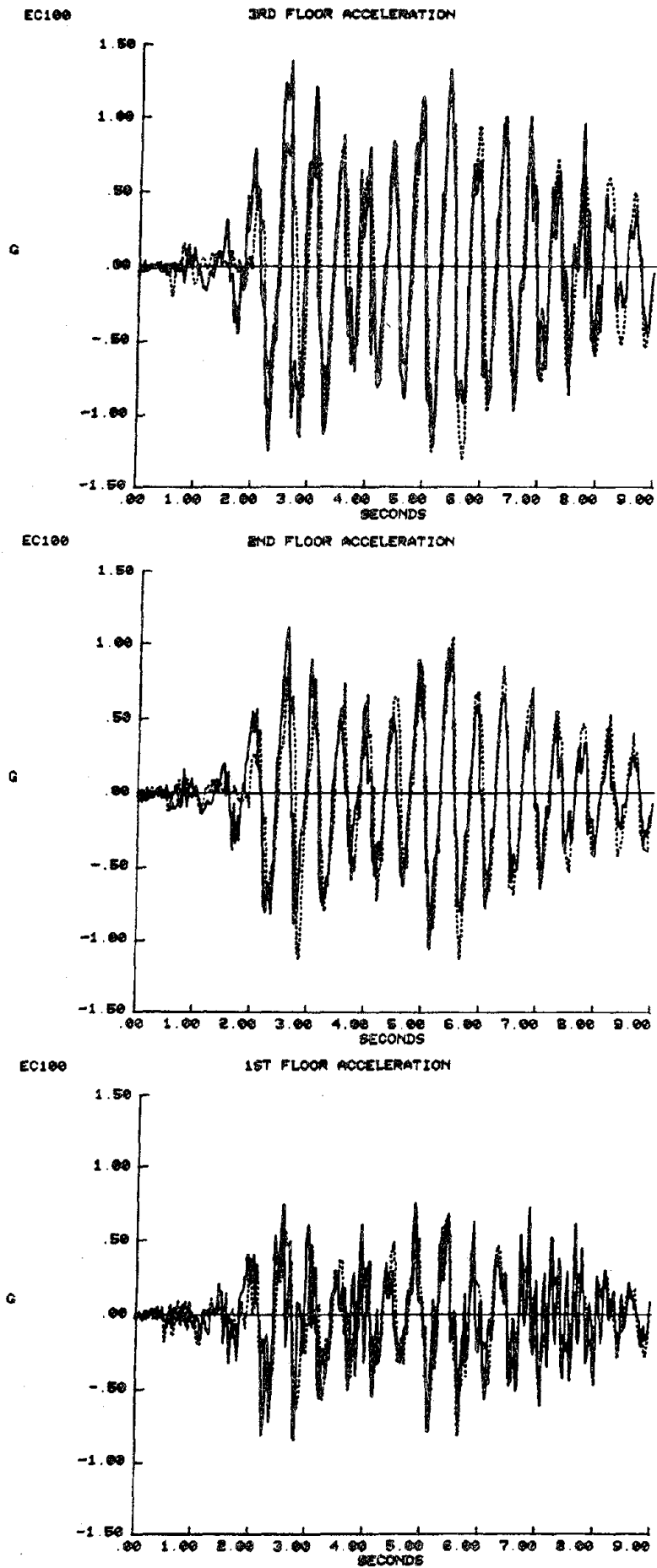


Figure 4.60 EC100 -- Floor Accelerations

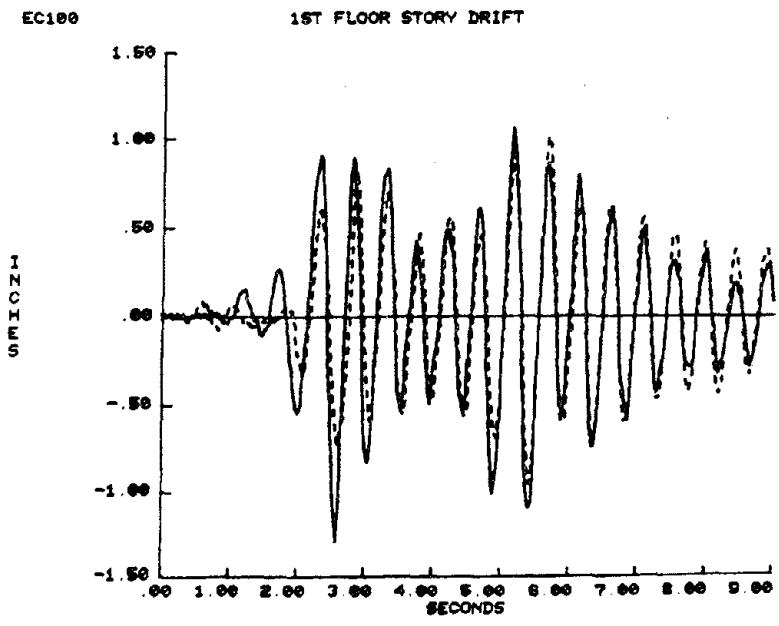
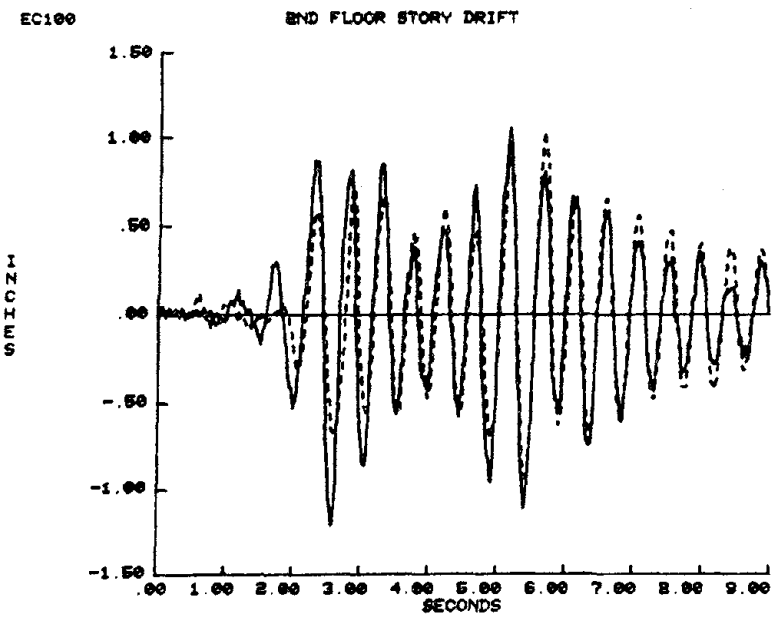
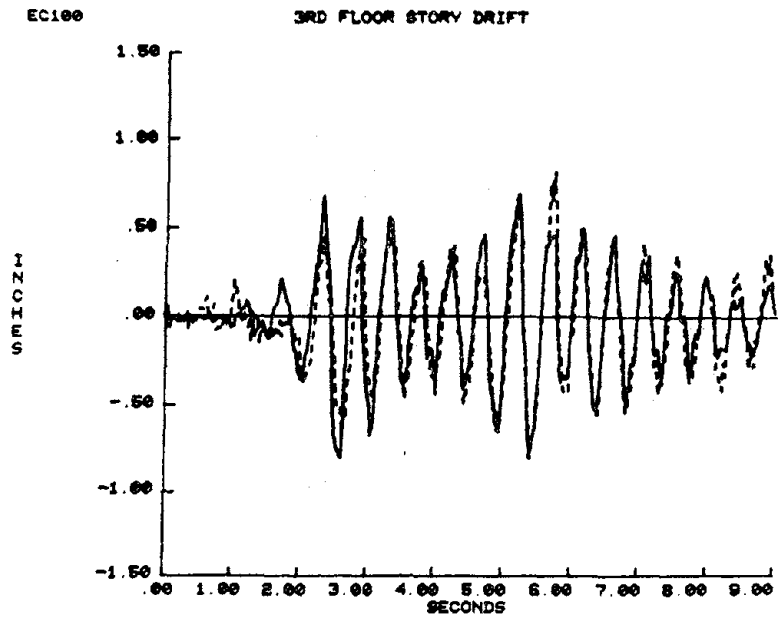


Figure 4.61 EC100 -- Story Drift

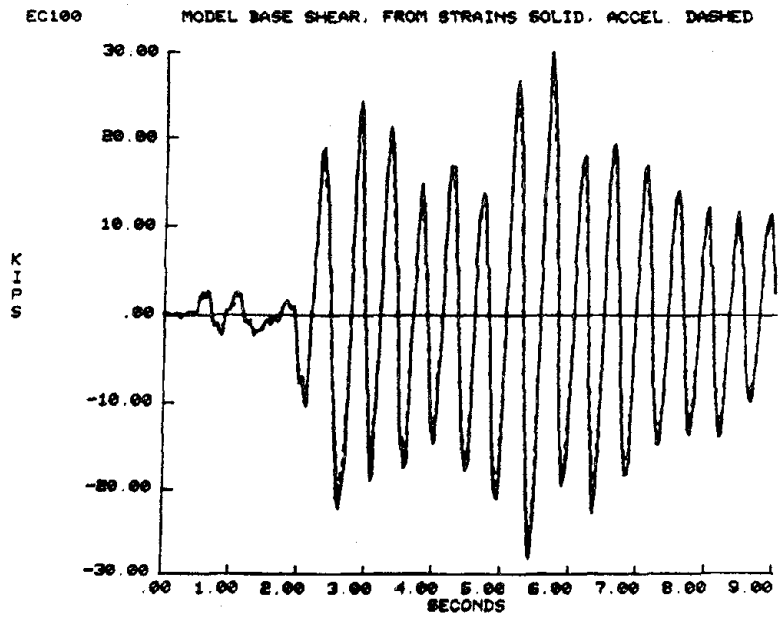
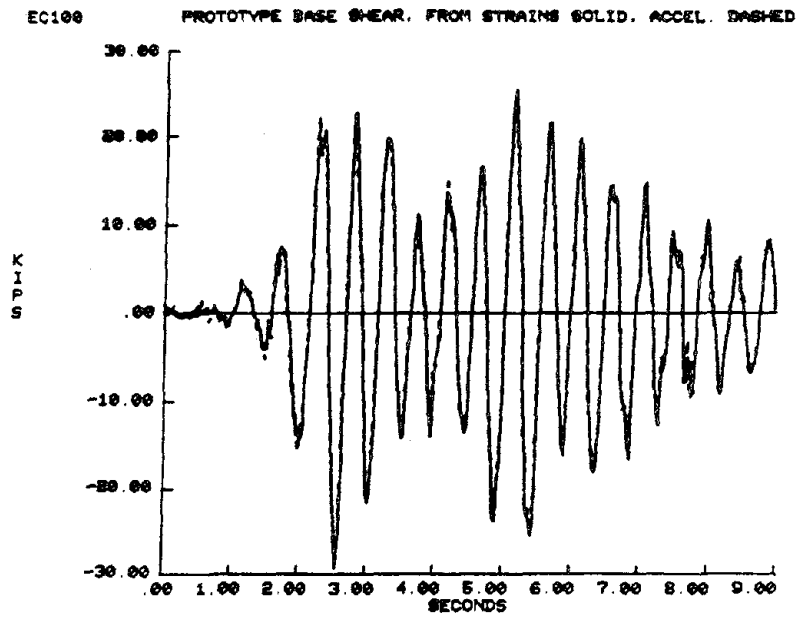


Figure 4.62 EC100 -- Base Shear from Strain Gages vs. Accelerometers

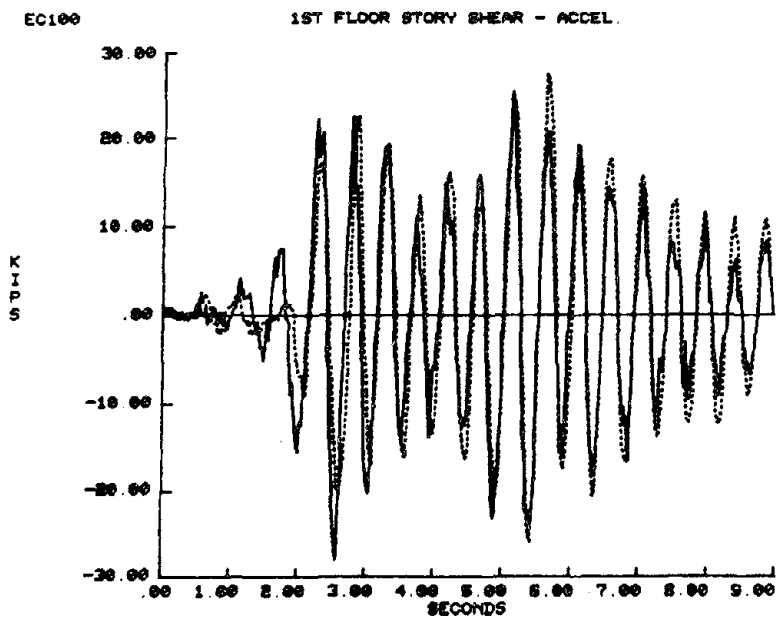
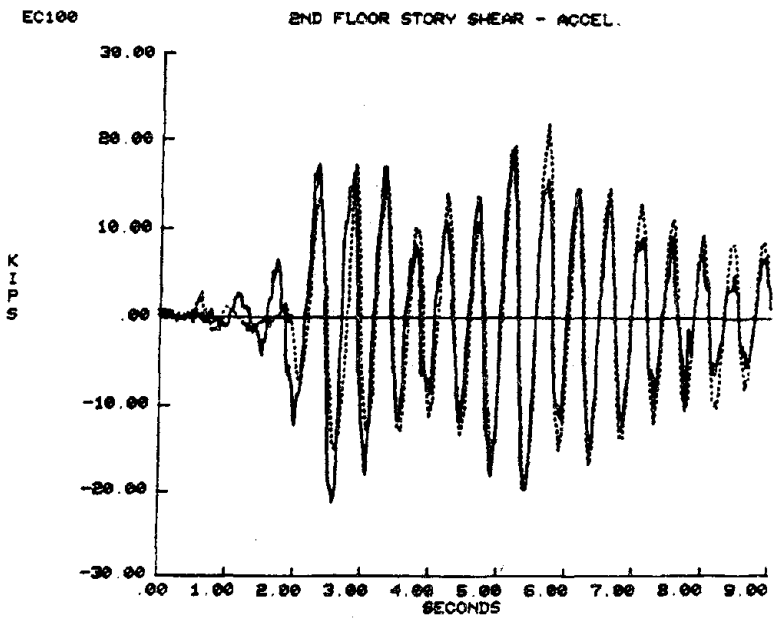
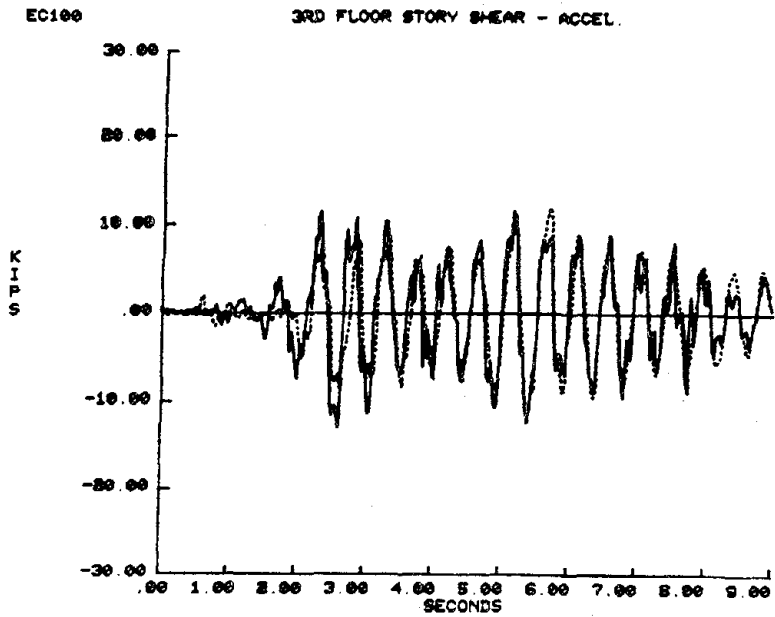
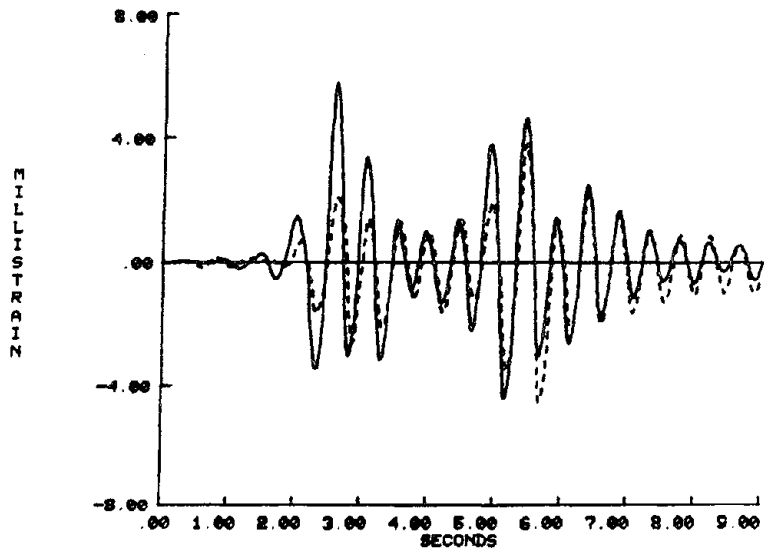


Figure 4.63 EC100 -- Story Shear

EC100

1ST FLOOR PANEL STRAIN, JOINT SA



EC100

1ST FLOOR JOINT DISTORTION, JOINT SA

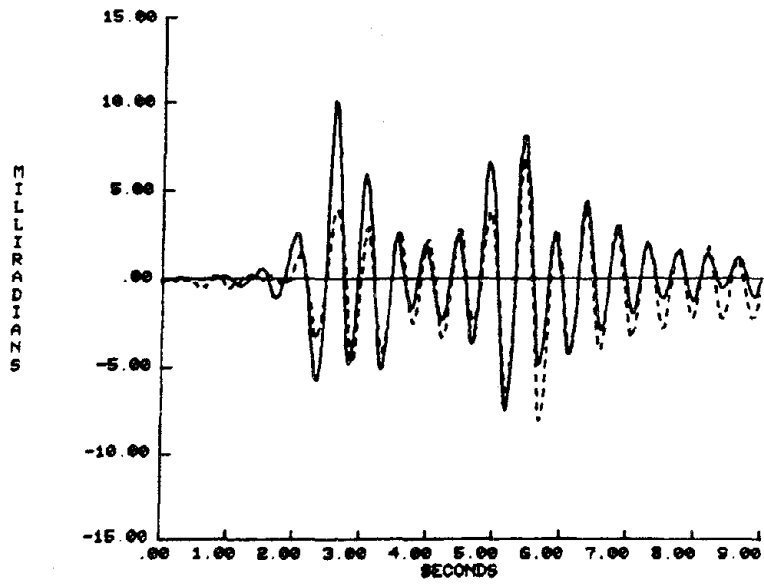
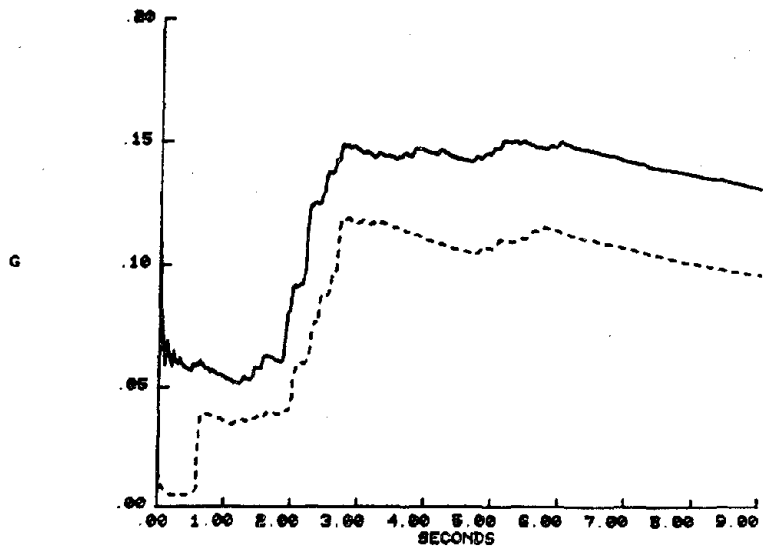


Figure 4.64 EC100 -- Joint Panel Deformations

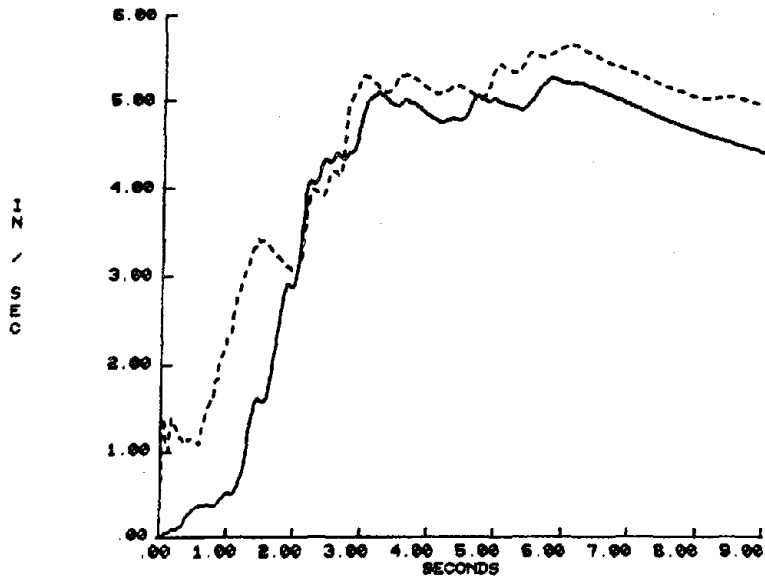
EC100

RMS OF TABLE ACCELERATION



EC100

RMS OF TABLE VELOCITY



EC100

RMS OF TABLE DISPLACEMENT

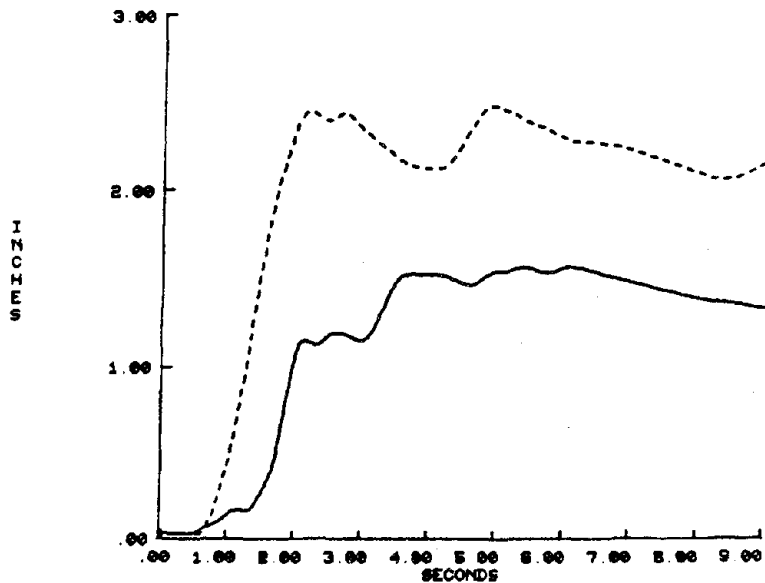


Figure 4.65 EC100 -- RMS of Shake Table Motion

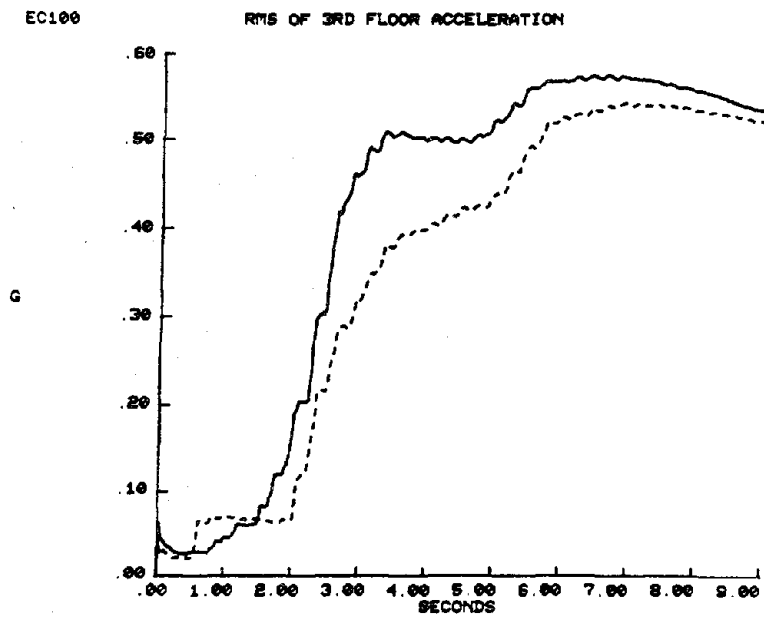
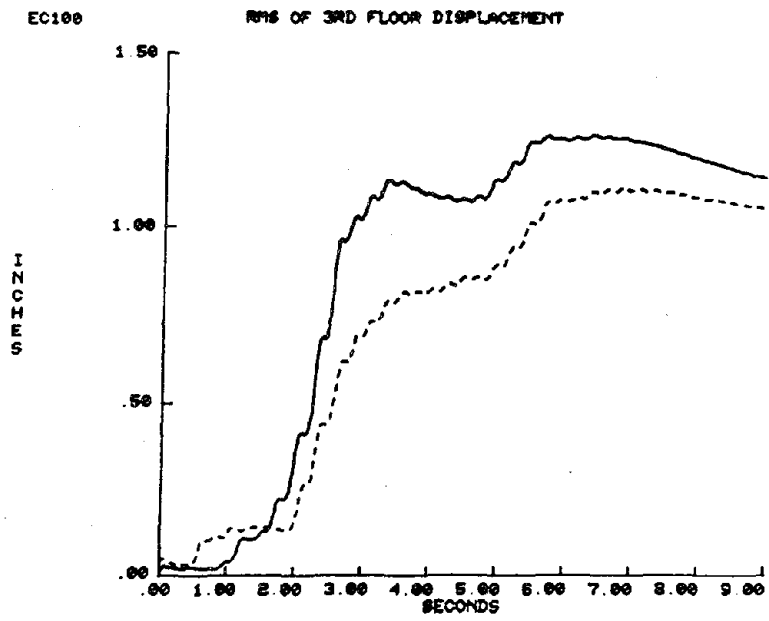


Figure 4.66 EC100 -- RMS of 3rd Floor Motions

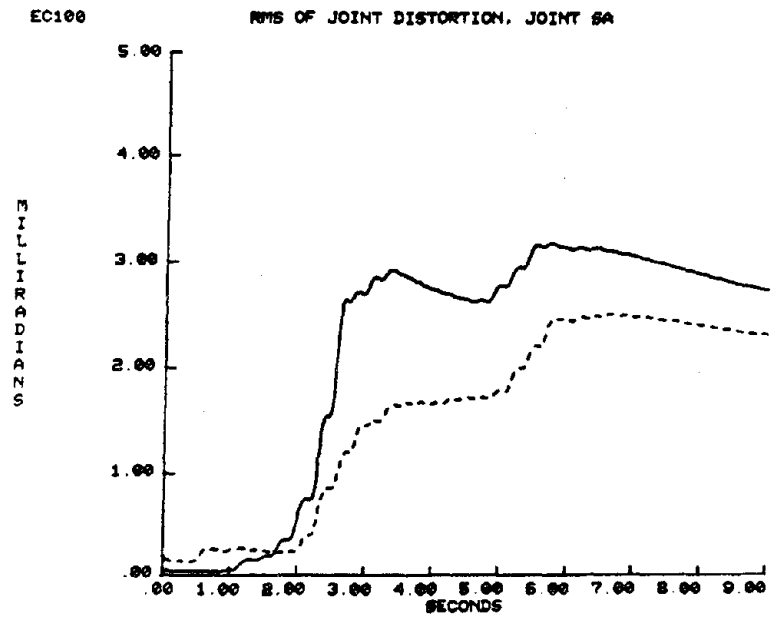
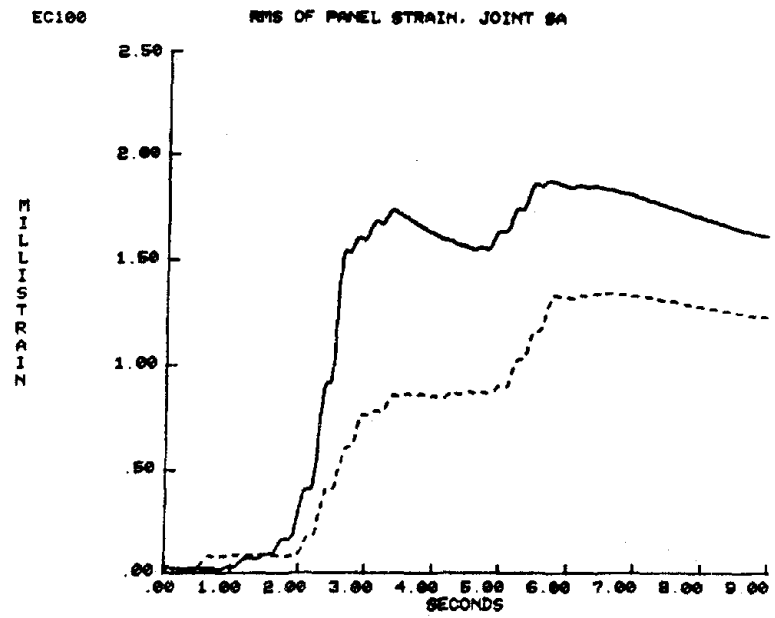


Figure 4.67 EC100 -- RMS of Joint SA Panel Deformation

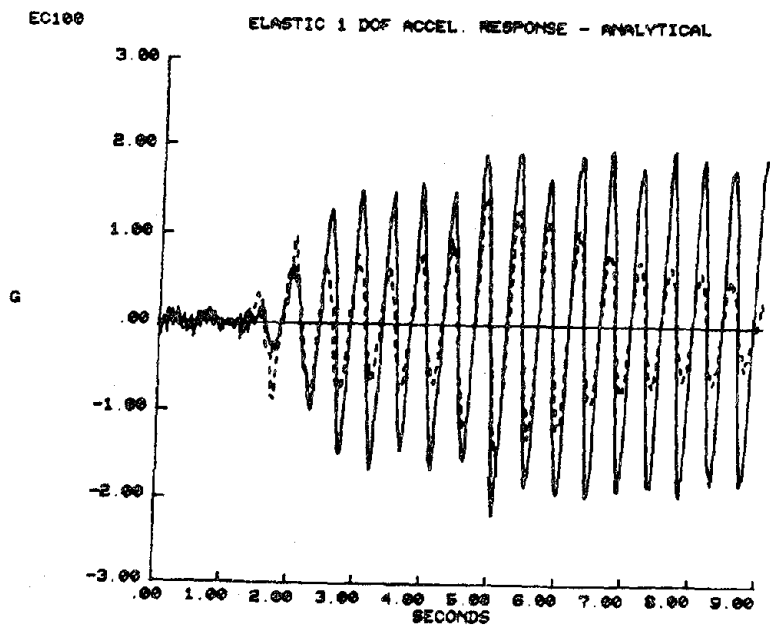
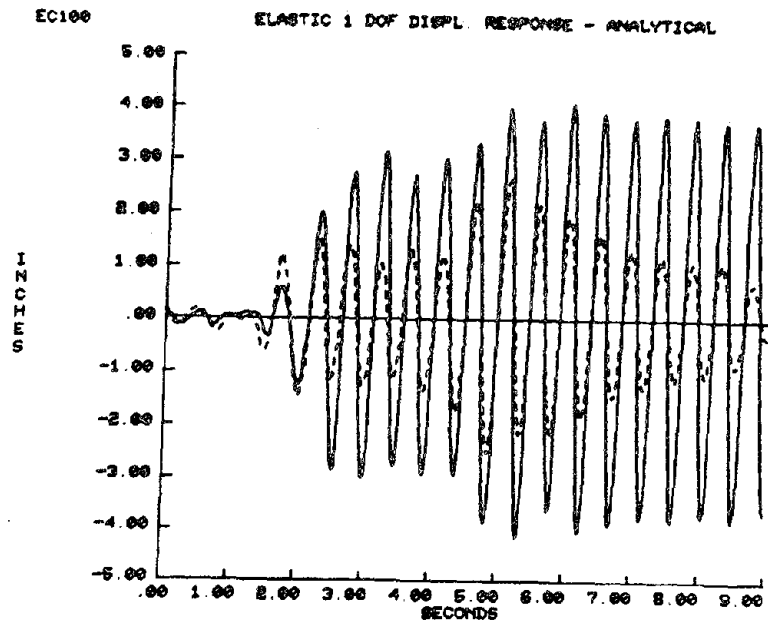


Figure 4.68 EC100 -- Analytic Elastic Response

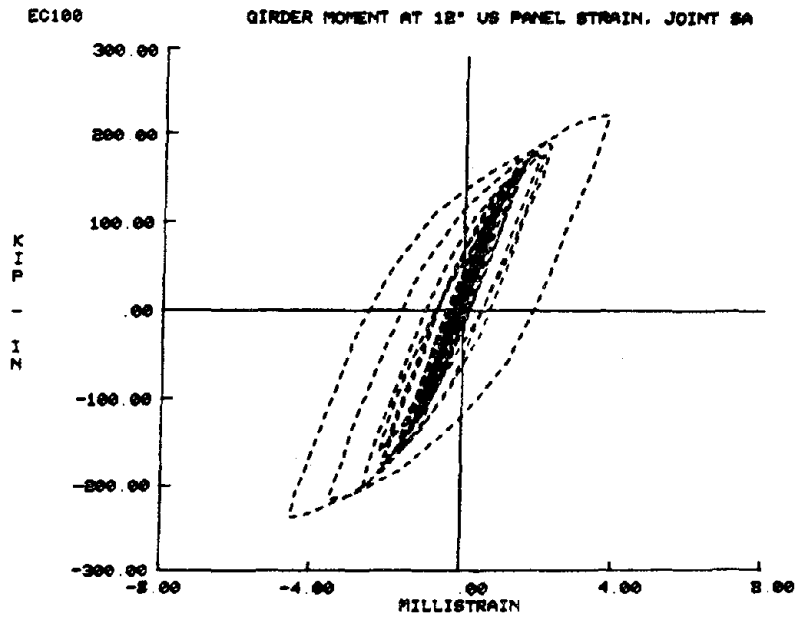
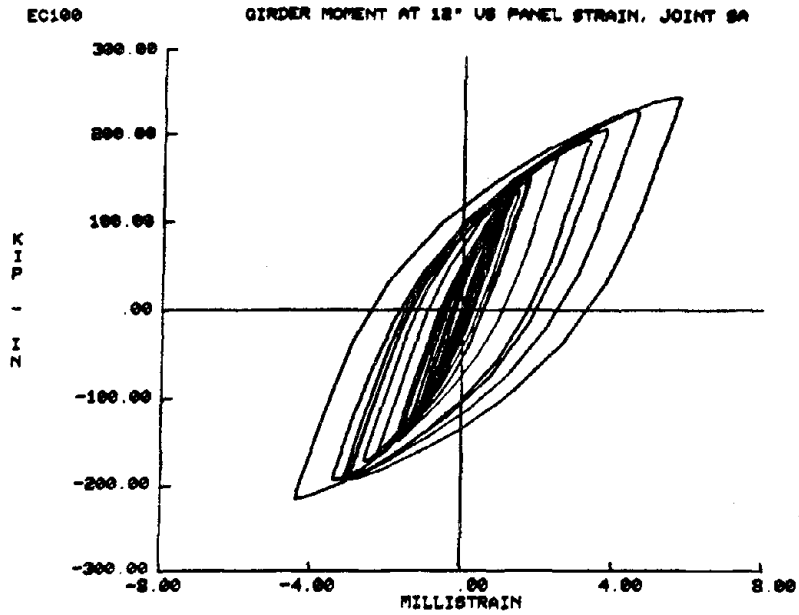


Figure 4.69 EC100 -- Girder Gage Moment vs. Panel 45° Strain--
Joint SA

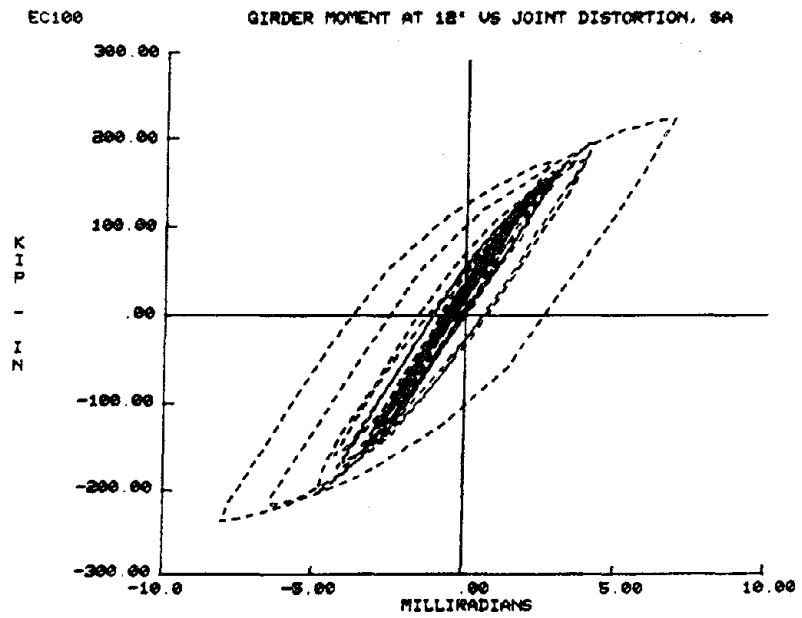
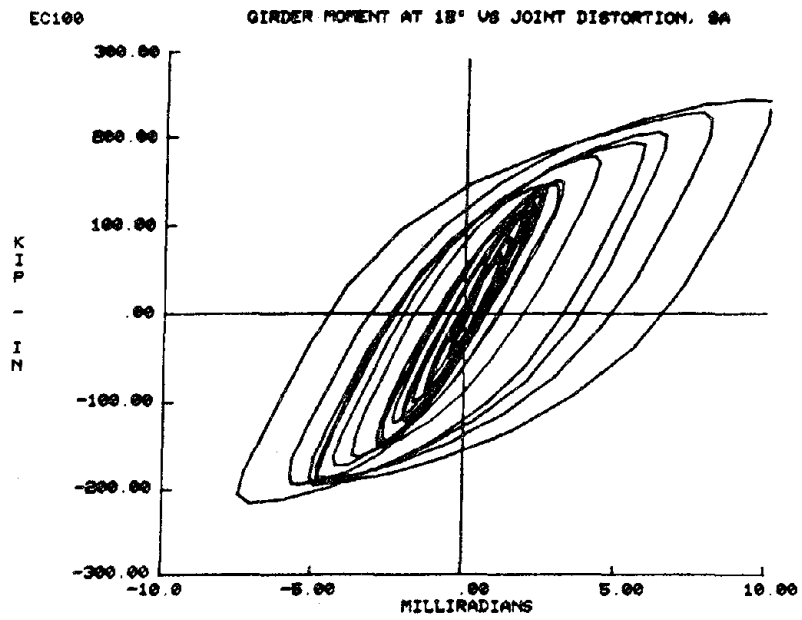


Figure 4.70 EC100 -- Girder Gage Moment vs. Panel Shear Distortion--
Joint SA

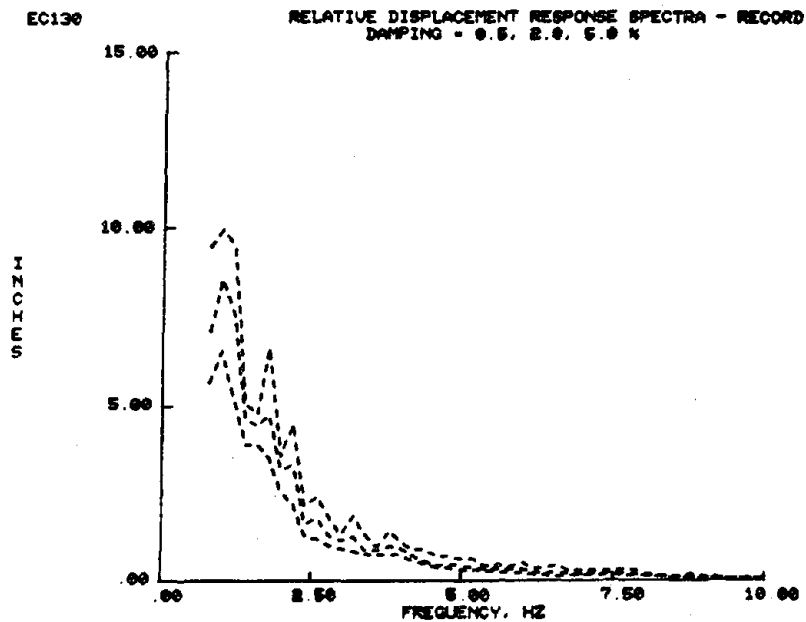
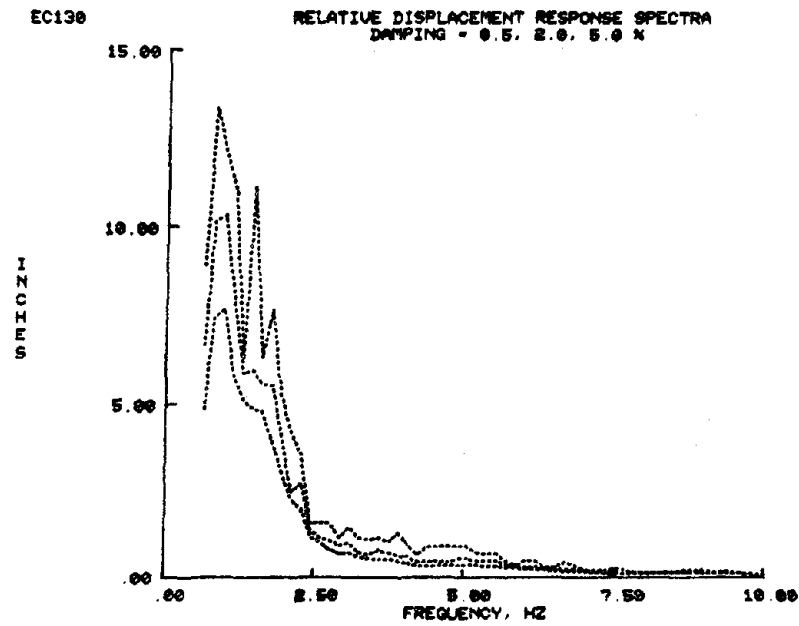
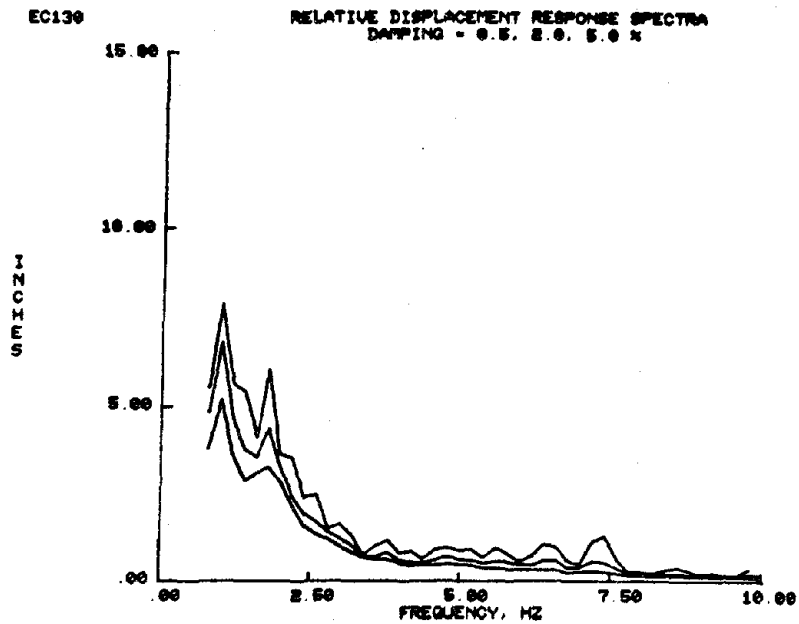


Figure 4.71 EC130 -- Relative Displacement Response Spectra from Table and Input Record Accelerations

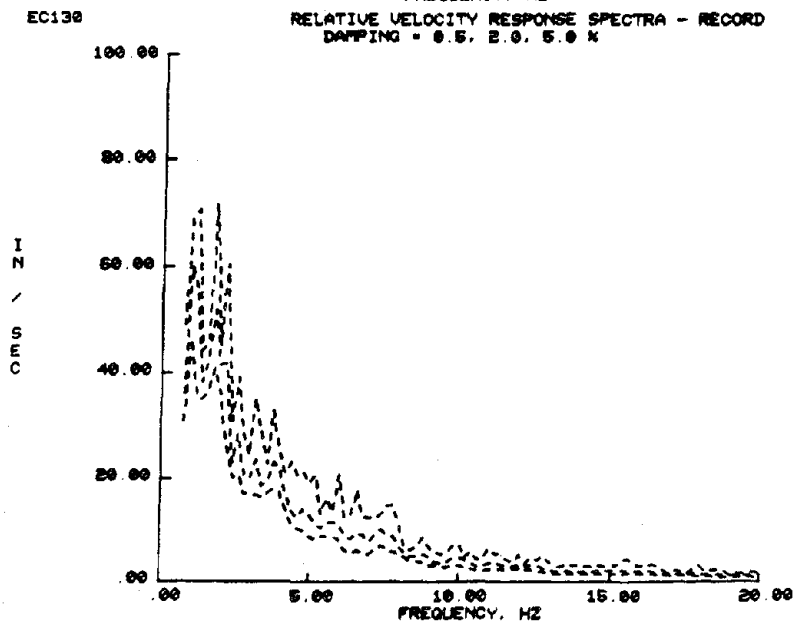
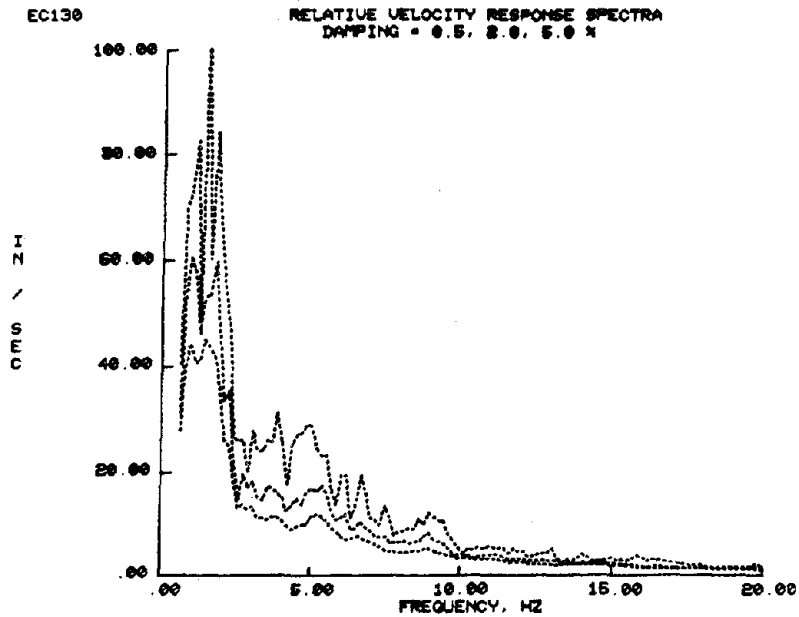
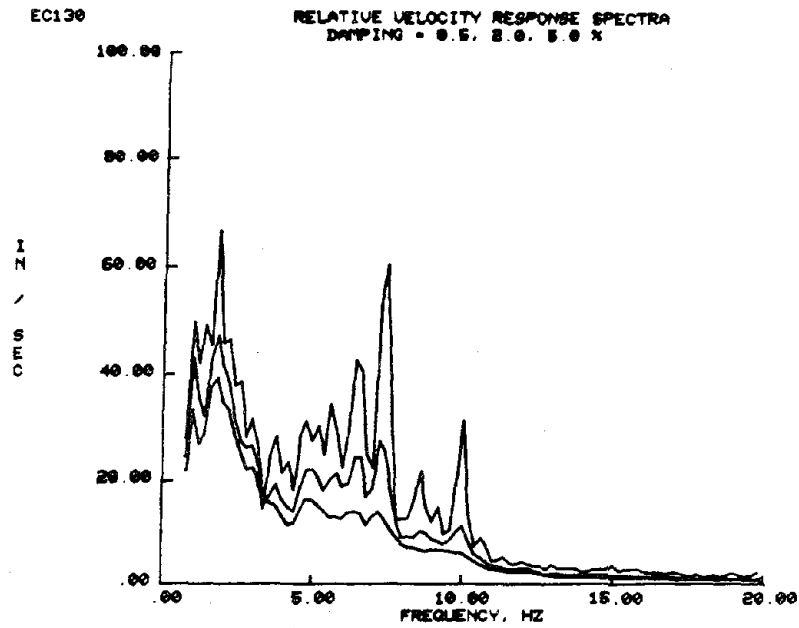
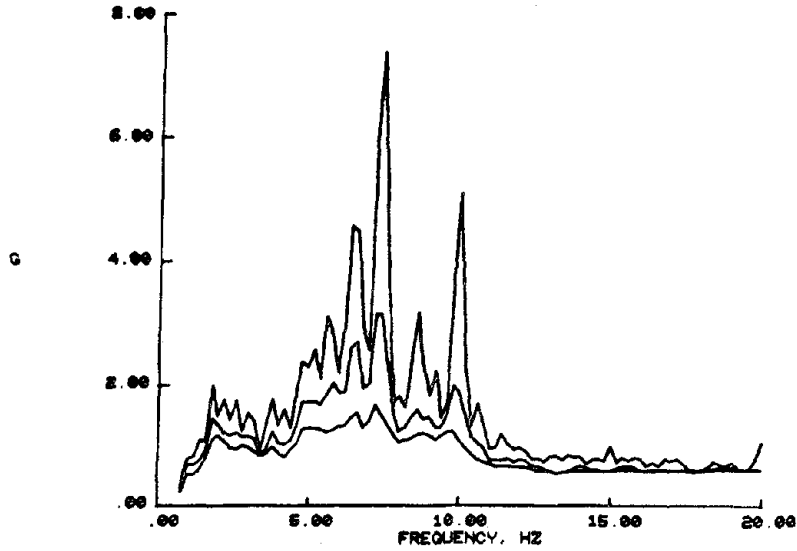


Figure 4.72 EC130 -- Relative Velocity Response Spectra from Table and Input Record Accelerations

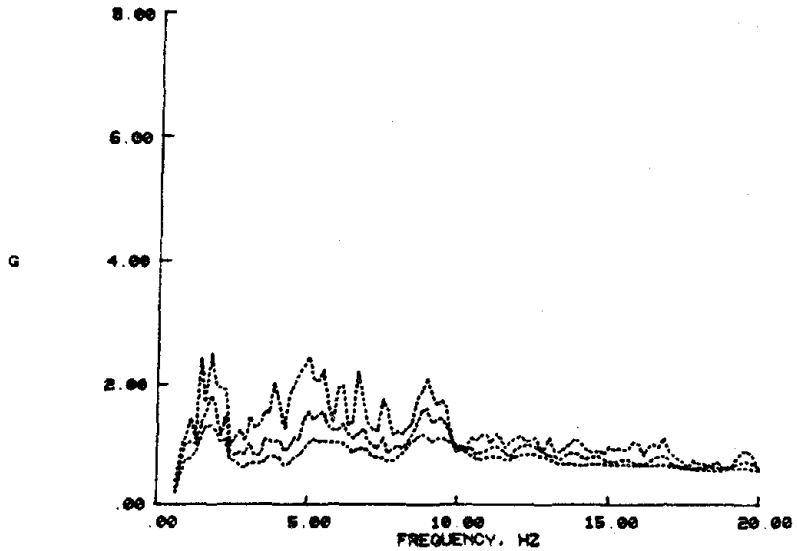
EC130

ACCELERATION RESPONSE SPECTRA
DAMPING = 0.5, 2.0, 5.0 %



EC130

ACCELERATION RESPONSE SPECTRA
DAMPING = 0.5, 2.0, 5.0 %



EC130

ACCELERATION RESPONSE SPECTRA - RECORD
DAMPING = 0.5, 2.0, 5.0 %

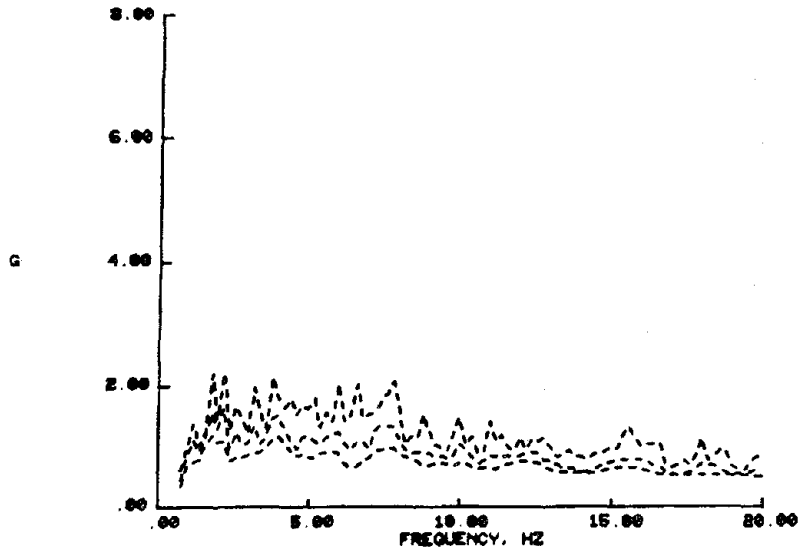


Figure 4.73 EC130 -- Absolute Acceleration Response Spectra from Table and Input Record Accelerations

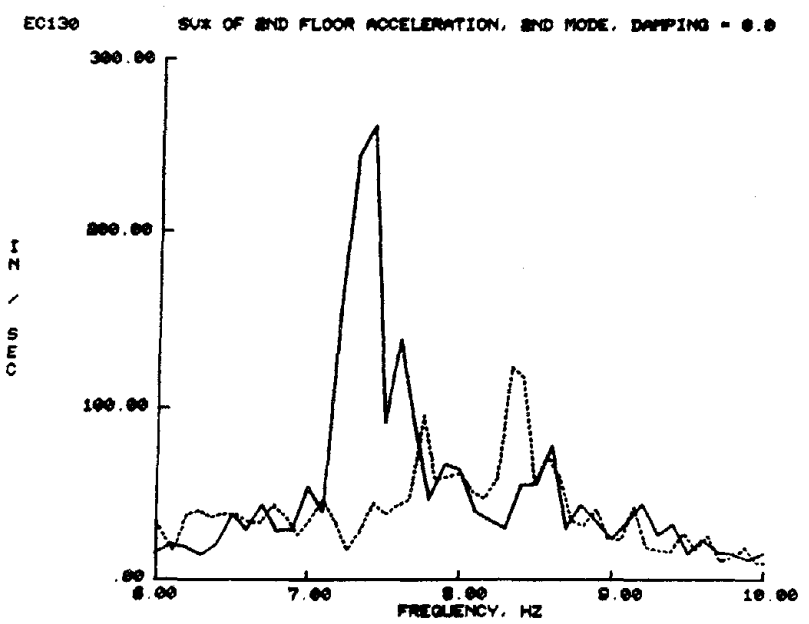
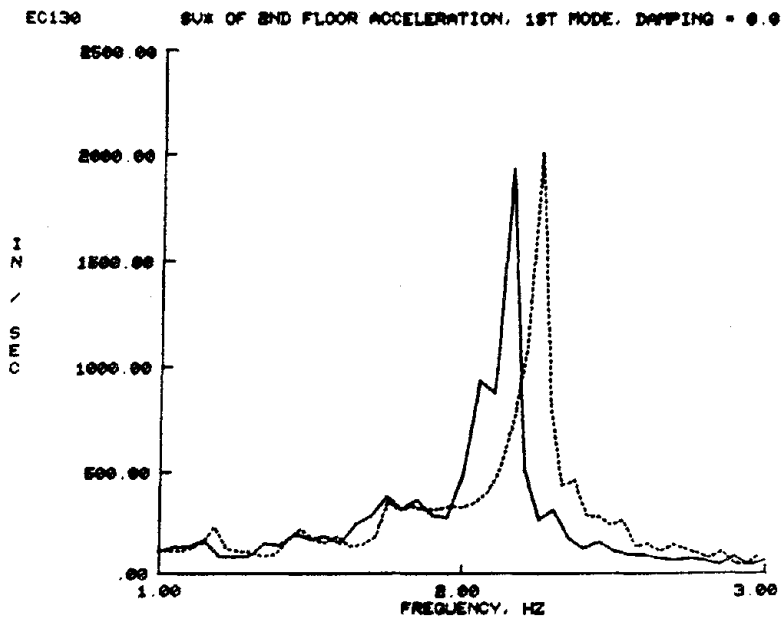


Figure 4.74 EC130 -- Test Structure Floor Response Spectra

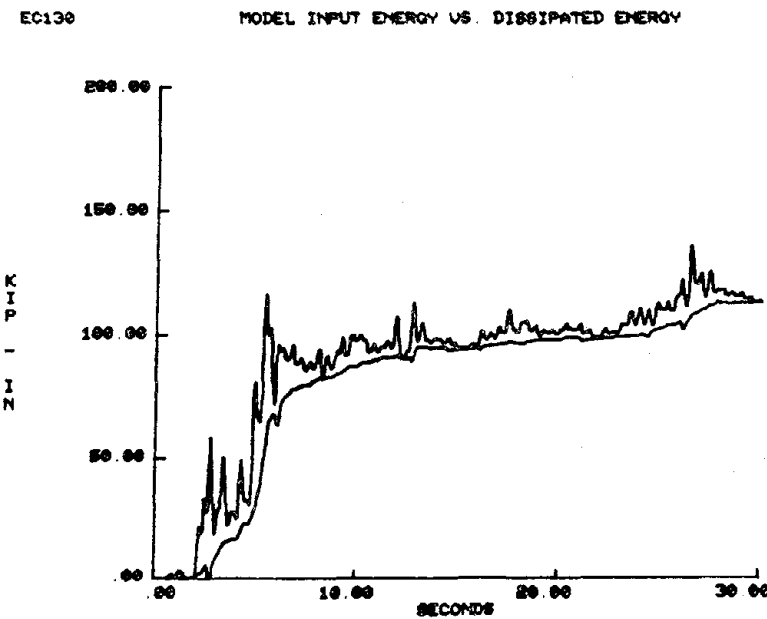
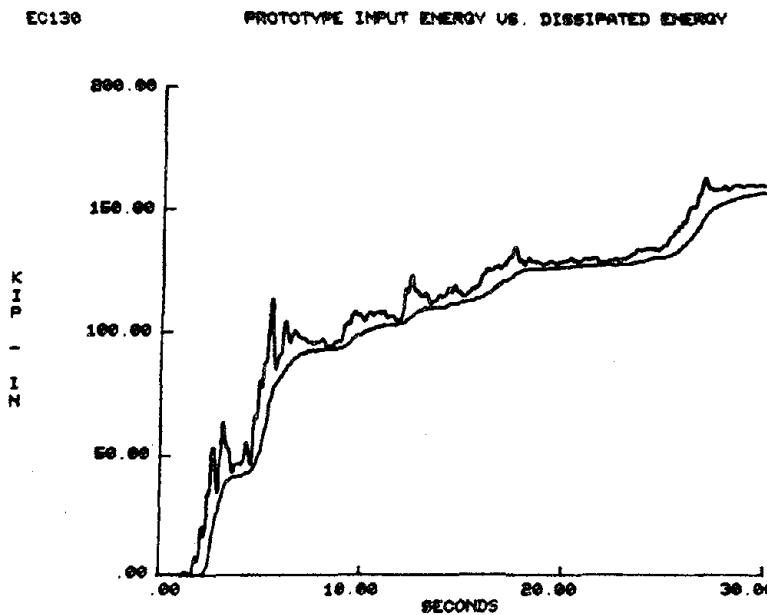
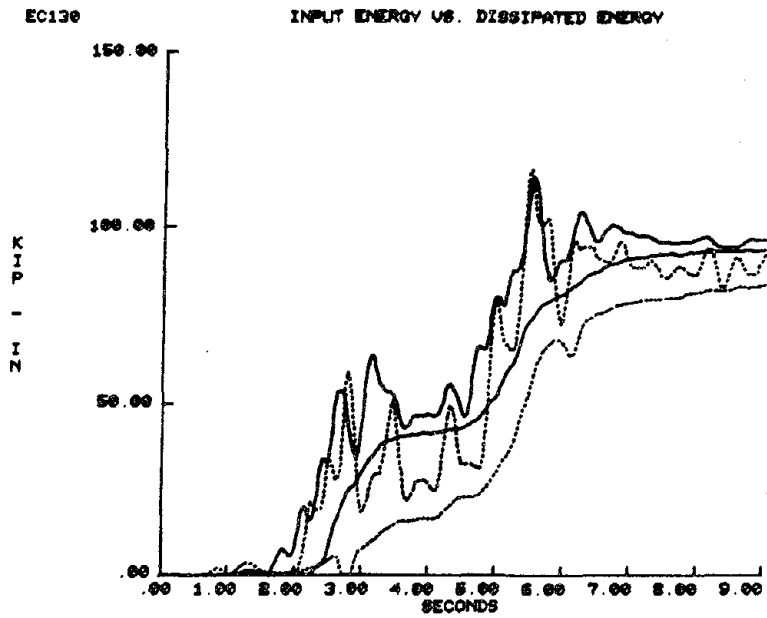


Figure 4.75 EC130 -- Input and Dissipated Energy

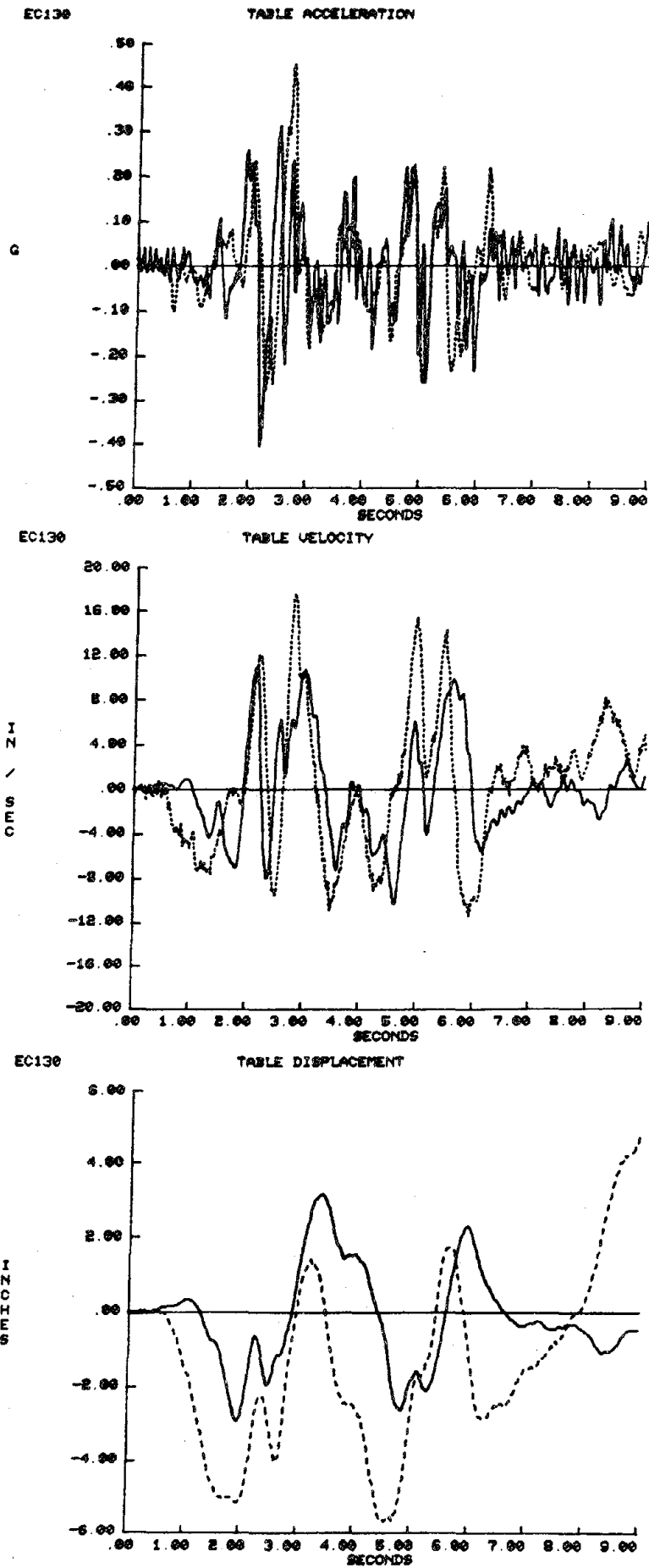
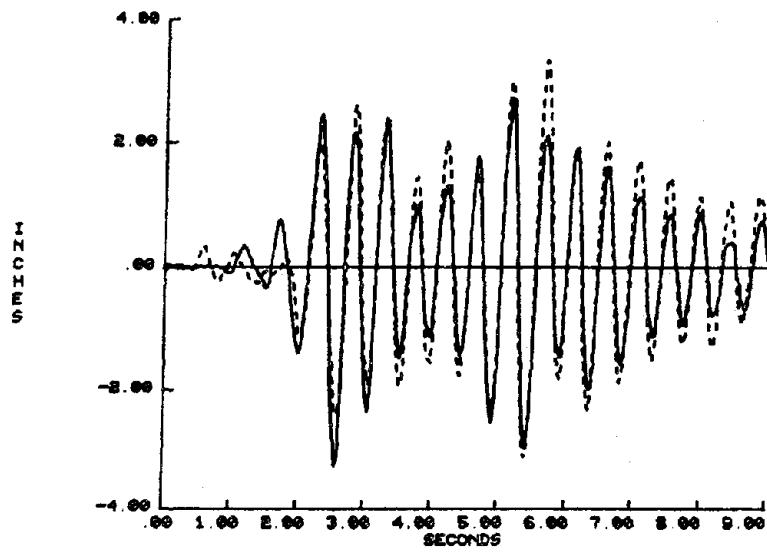


Figure 4.76 EC130 -- Shake Table Motion

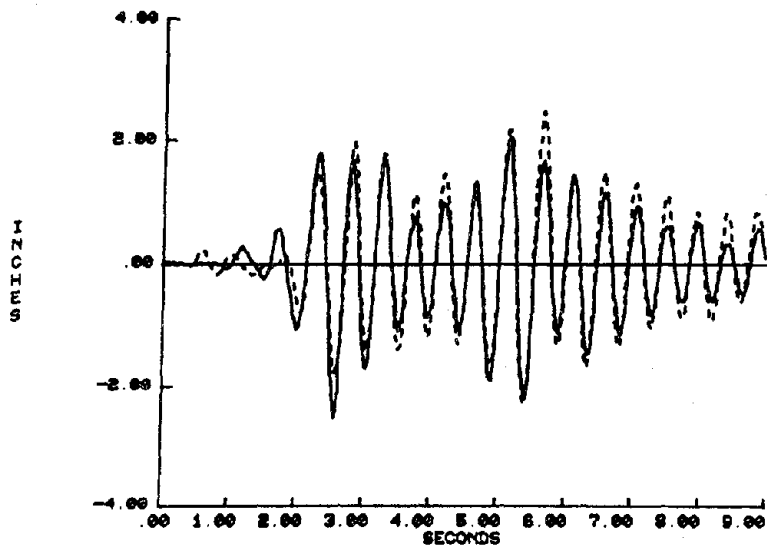
EC130

3RD FLOOR RELATIVE DISPLACEMENT



EC130

2ND FLOOR RELATIVE DISPLACEMENT



EC130

1ST FLOOR RELATIVE DISPLACEMENT

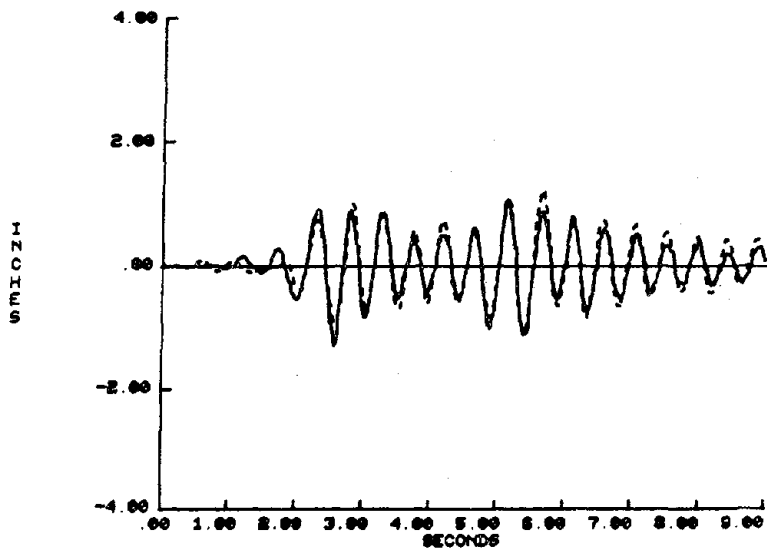


Figure 4.77 EC130 -- Floor Displacements

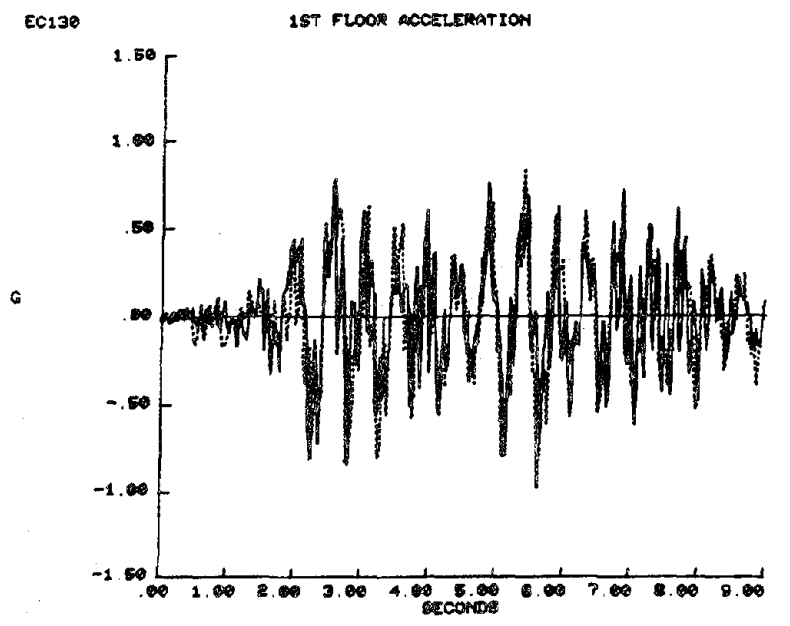
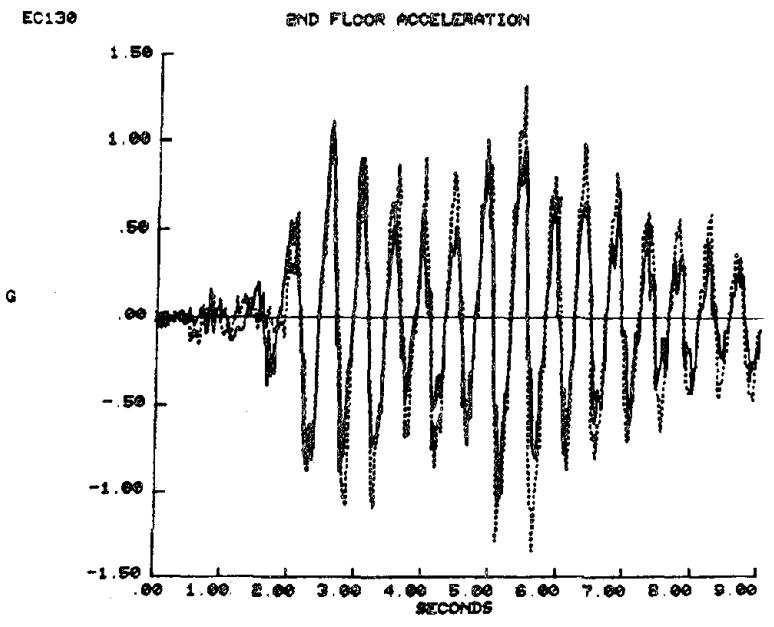
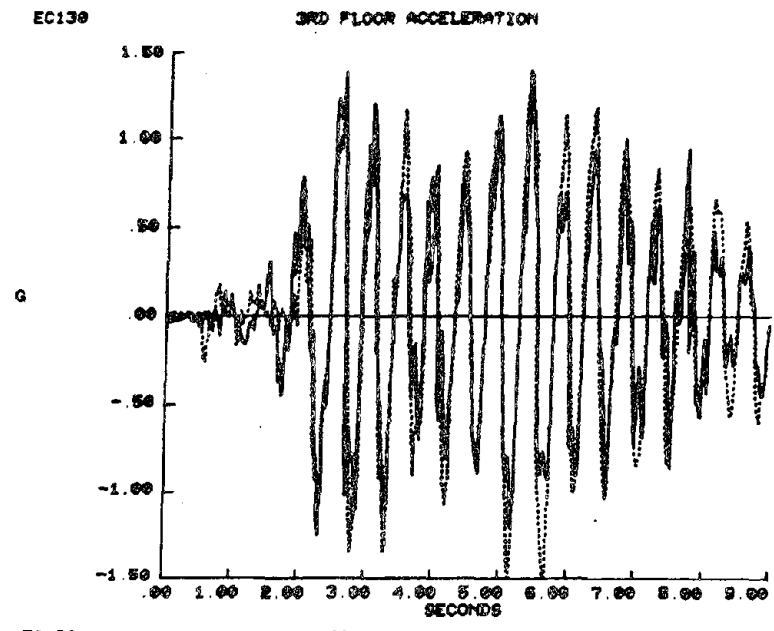


Figure 4.78 EC130 -- Floor Accelerations

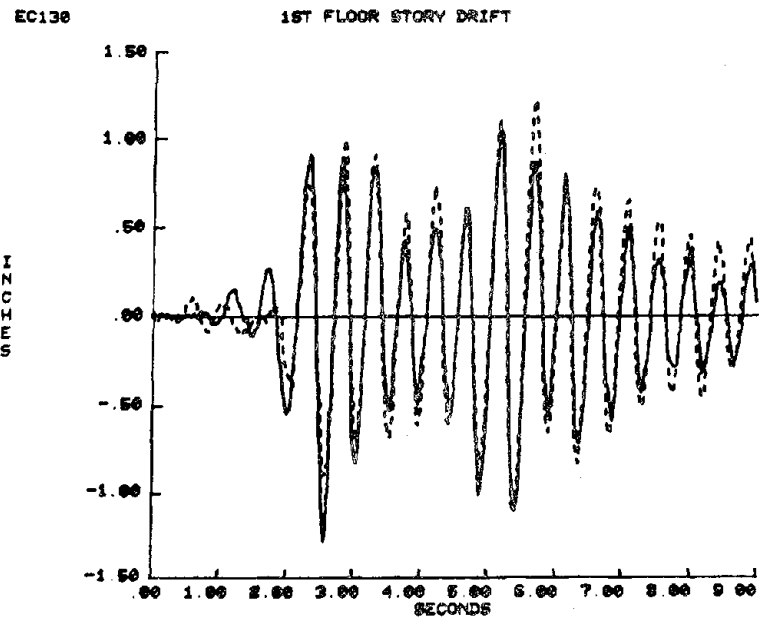
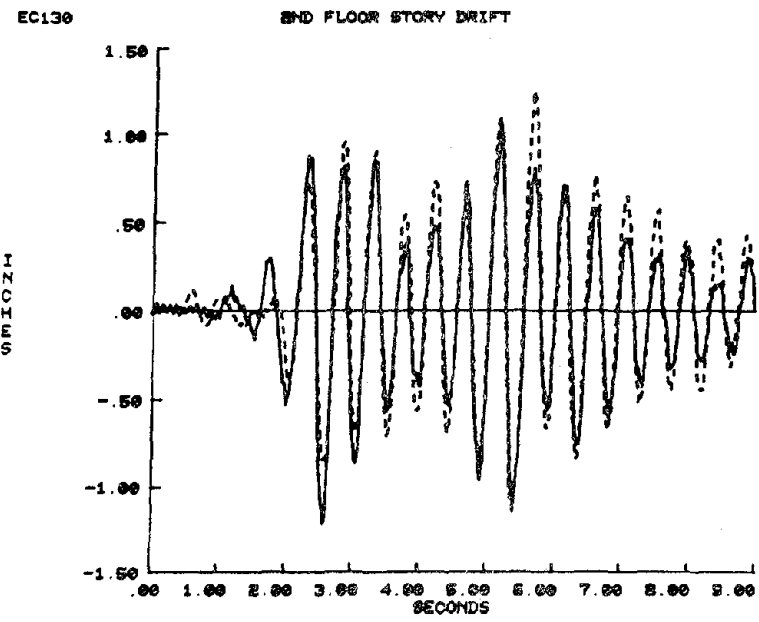
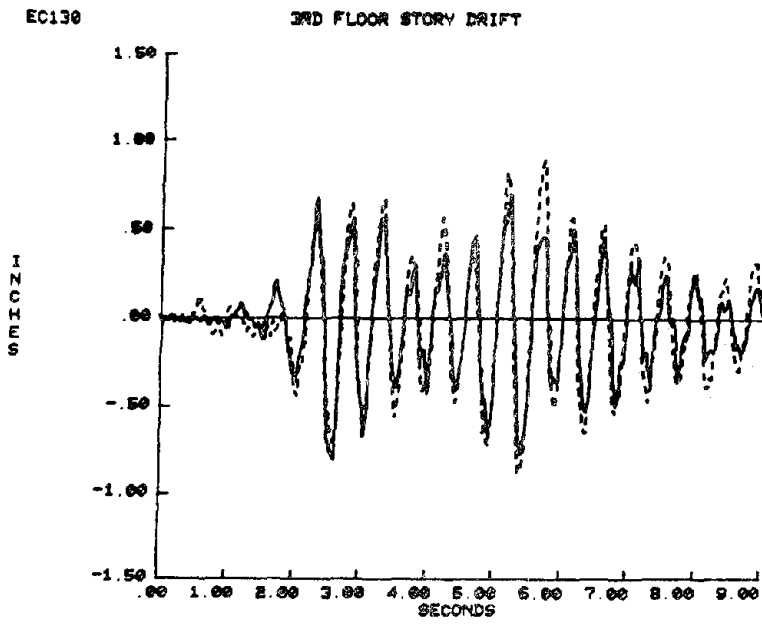
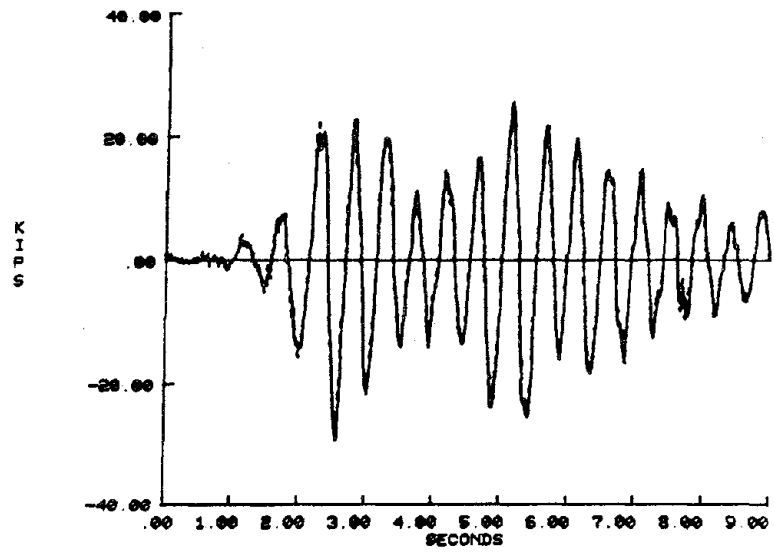


Figure 4.79 EC130 -- Story Drift

EC130 PROTOTYPE BASE SHEAR. FROM STRAINS SOLID. ACCEL. DASHED



EC130 MODEL BASE SHEAR. FROM STRAINS SOLID. ACCEL. DASHED

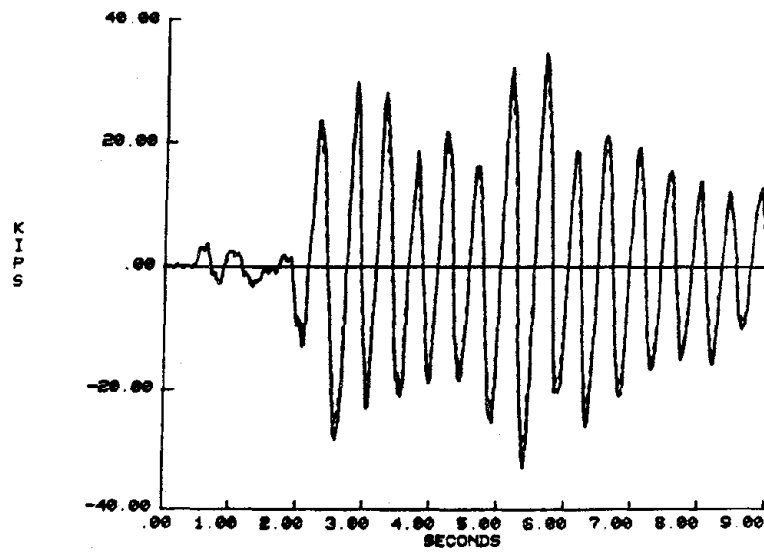
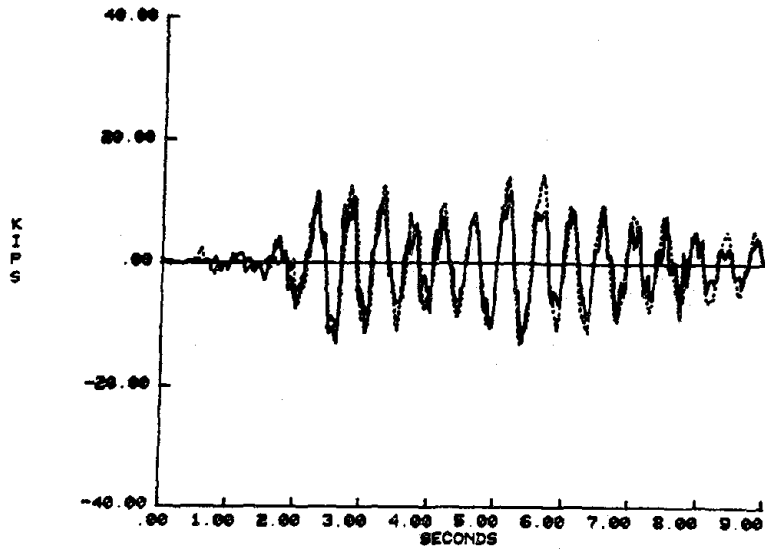


Figure 4.80 EC130 -- Base Shear from Strain Gages vs. Accelerometers

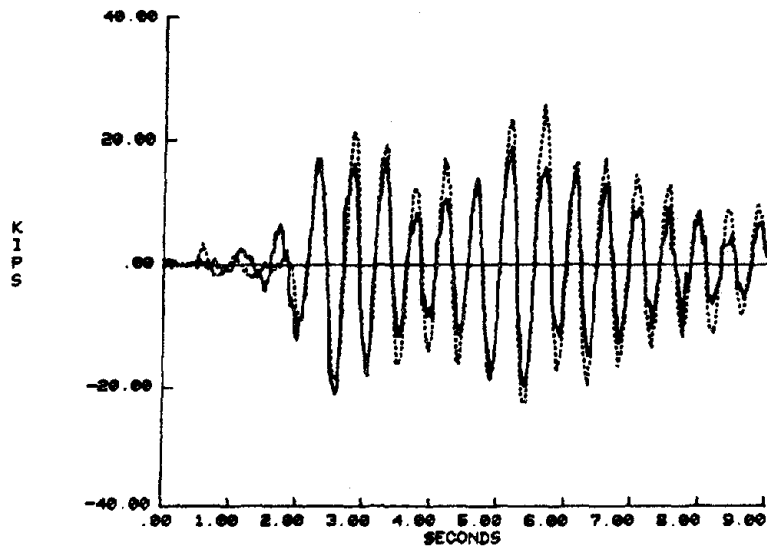
EC130

3RD FLOOR STORY SHEAR - ACCEL.



EC130

2ND FLOOR STORY SHEAR - ACCEL.



EC130

1ST FLOOR STORY SHEAR - ACCEL.

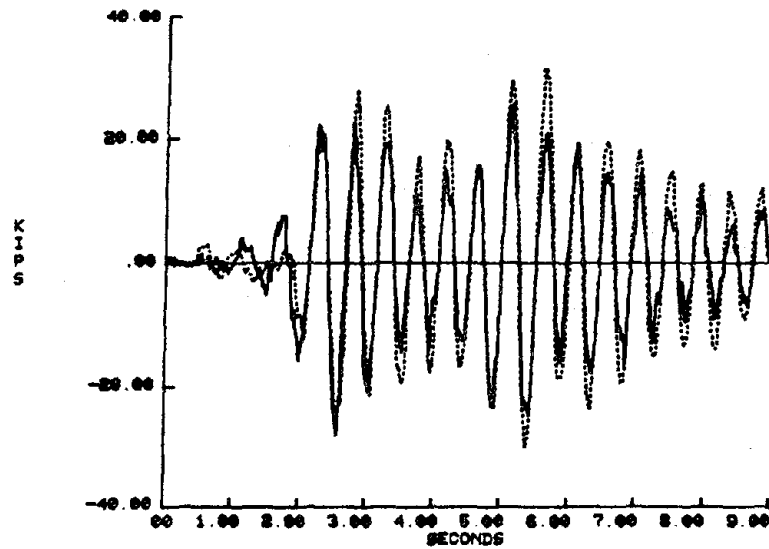
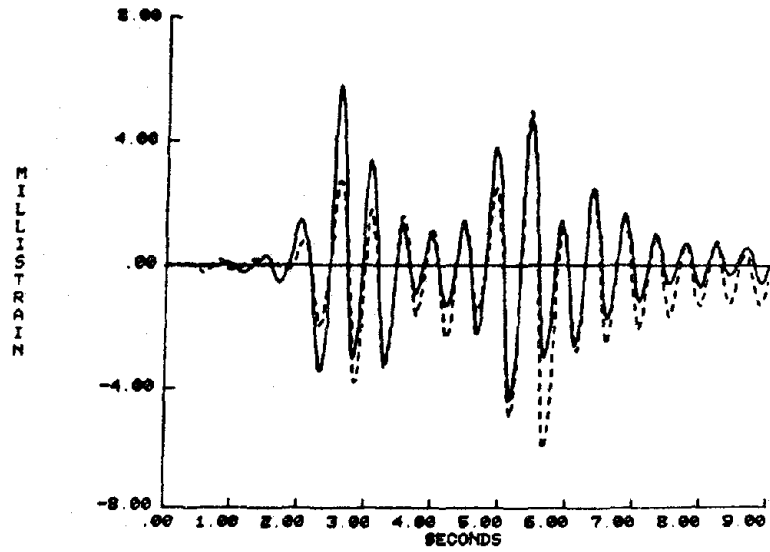


Figure 4.81 EC130 -- Story Shear

EC130

1ST FLOOR PANEL STRAIN, JOINT SA



EC130

1ST FLOOR JOINT DISTORTION, JOINT SA

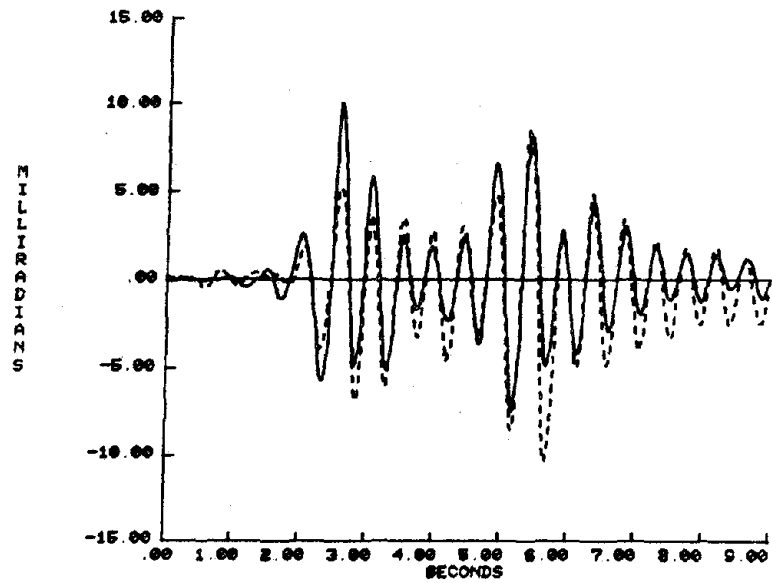
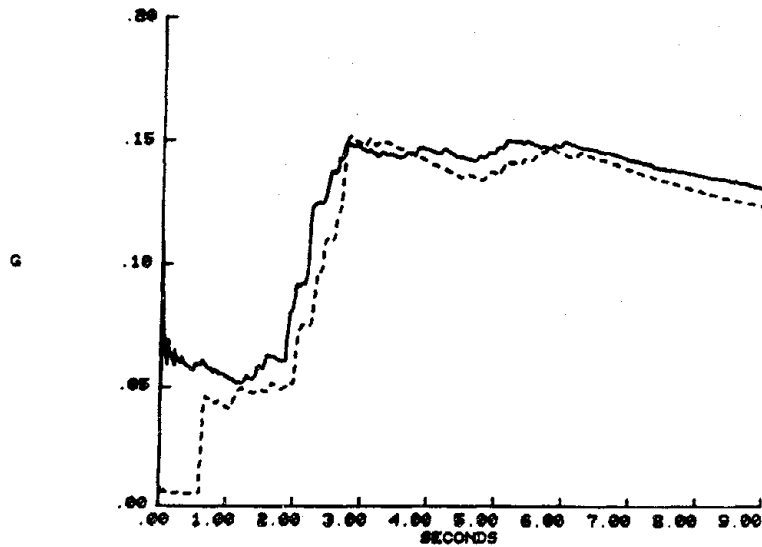


Figure 4.82 EC130 -- Joint Panel Deformations

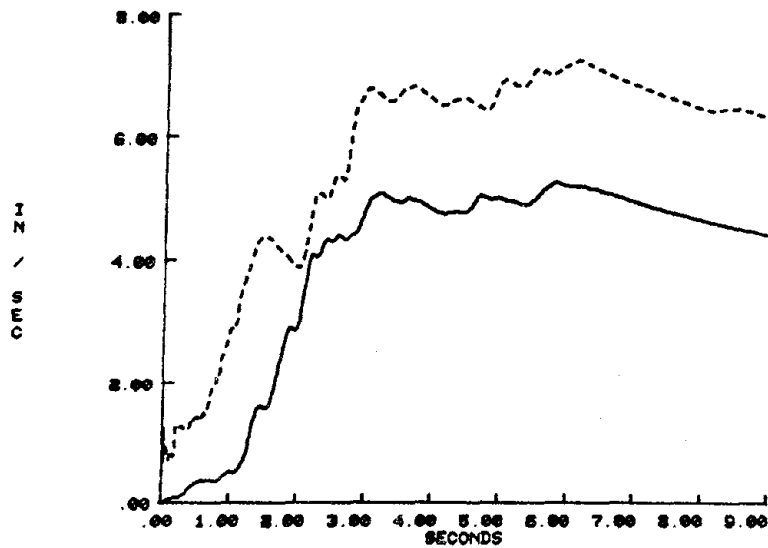
EC130

RMS OF TABLE ACCELERATION



EC130

RMS OF TABLE VELOCITY



EC130

RMS OF TABLE DISPLACEMENT

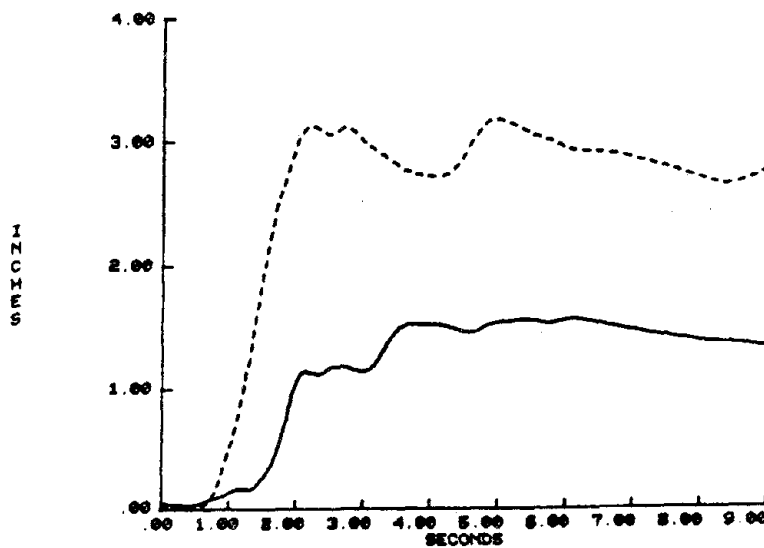


Figure 4.83 EC130 -- RMS of Shake Table Motion

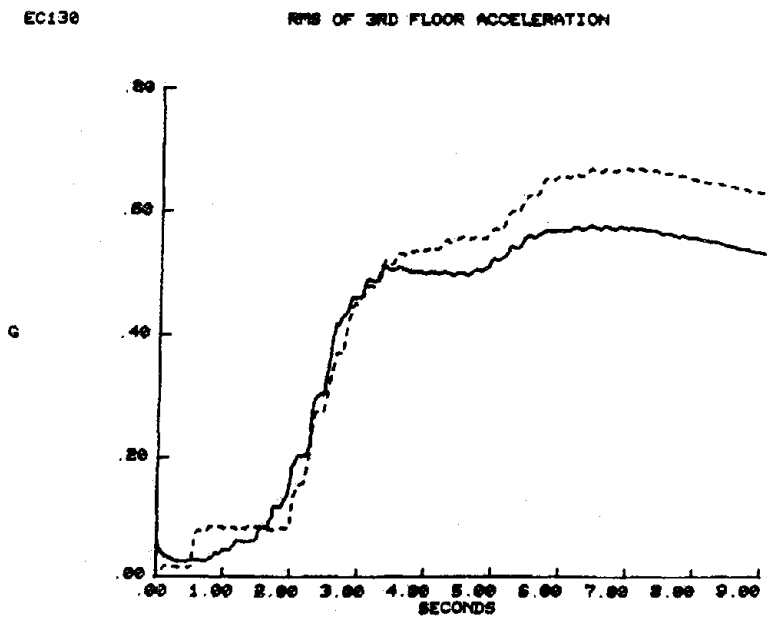
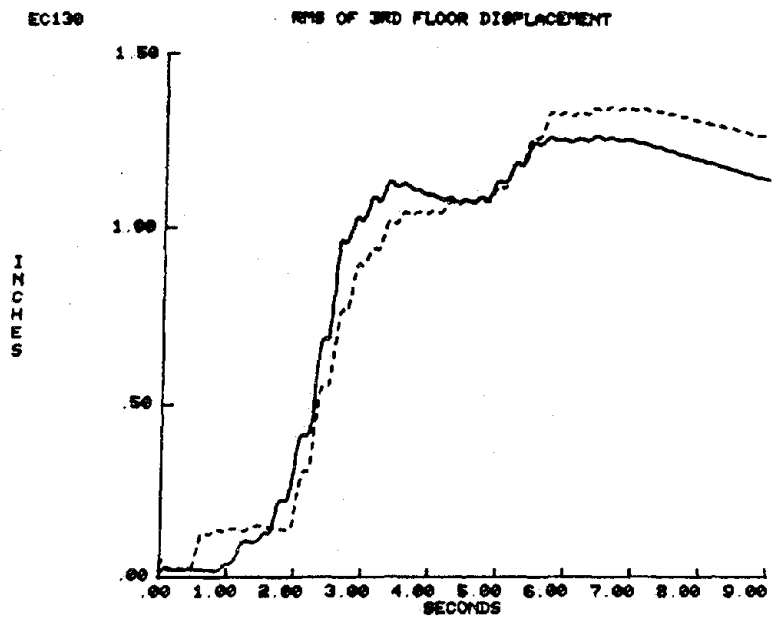


Figure 4.84 EC130 -- RMS of 3rd Floor Motions

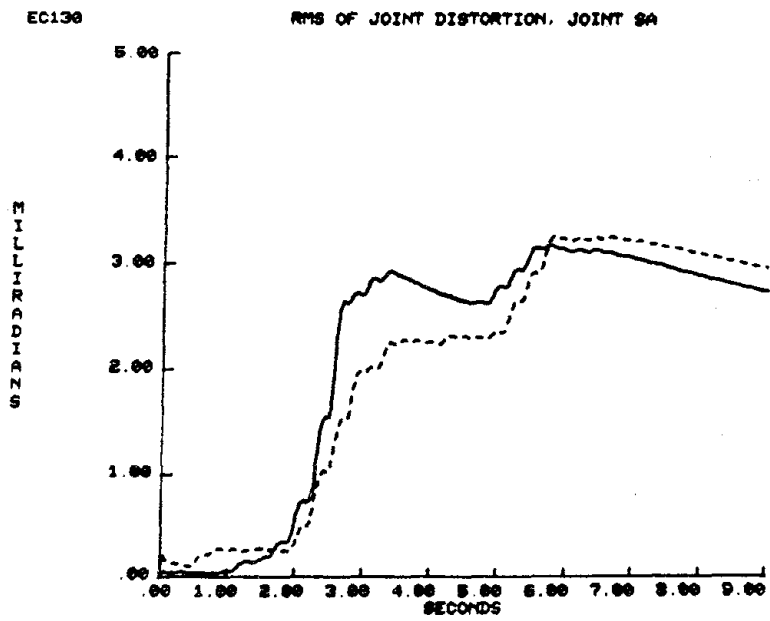
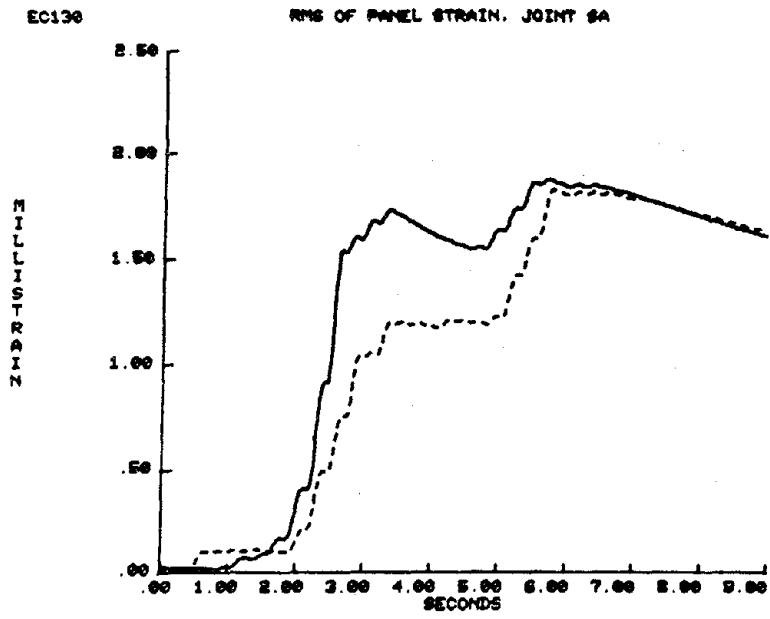


Figure 4.85 EC130 -- RMS of Joint SA Panel Deformation

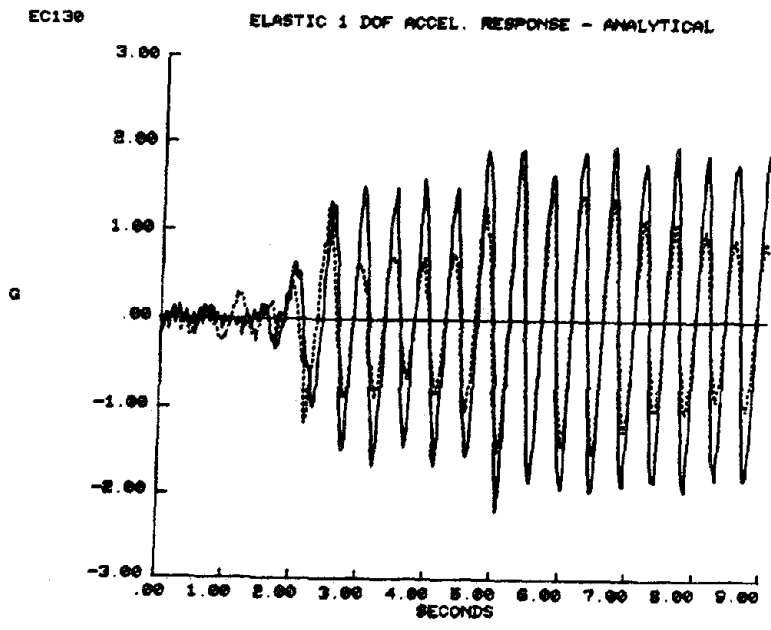
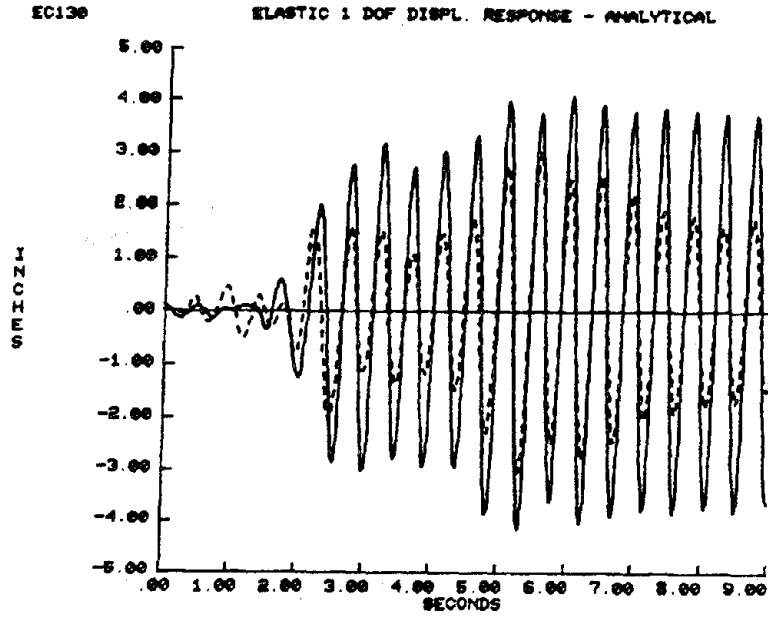


Figure 4.86 EC130 -- Analytic Elastic Response

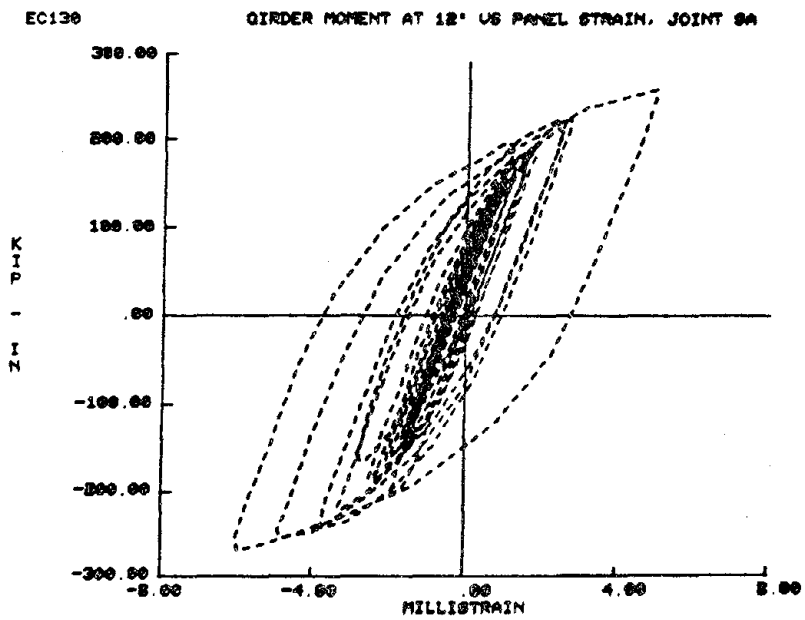
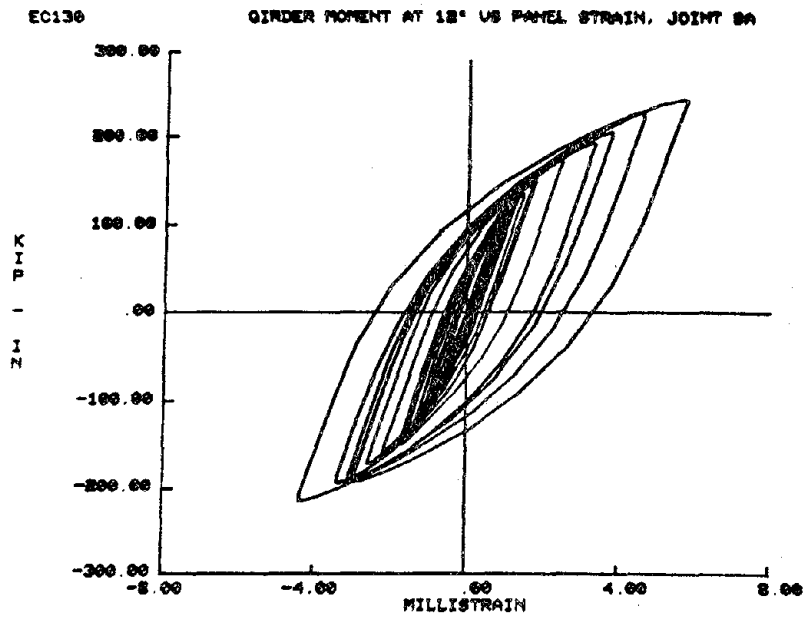


Figure 4.87 EC130 -- Girder Gage Moment vs. Panel 45° Strain--
Joint SA

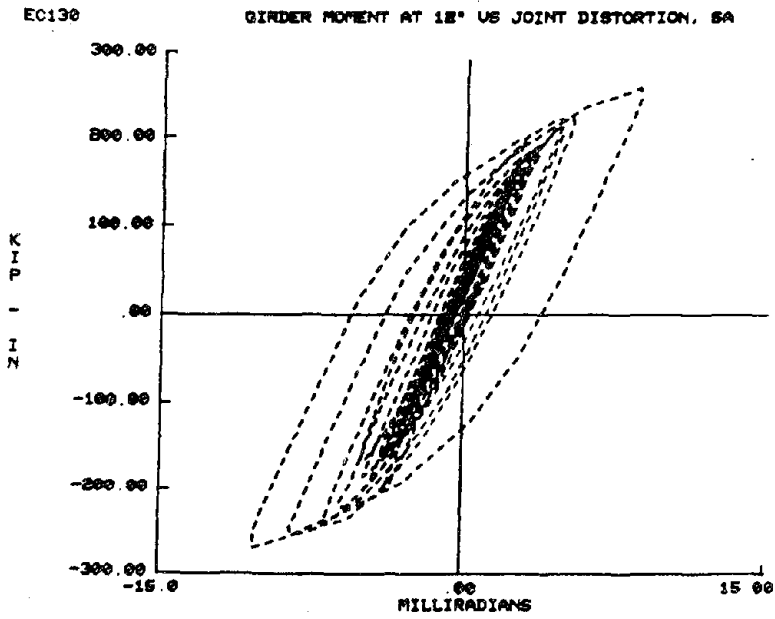
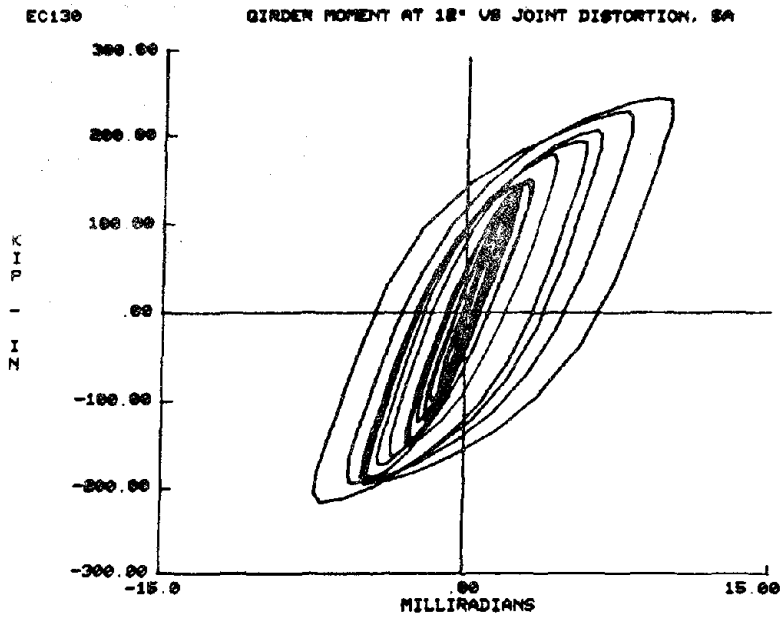


Figure 4.88 EC130 -- Girder Gage Moment vs. Panel Shear Distortion--
Joint SA

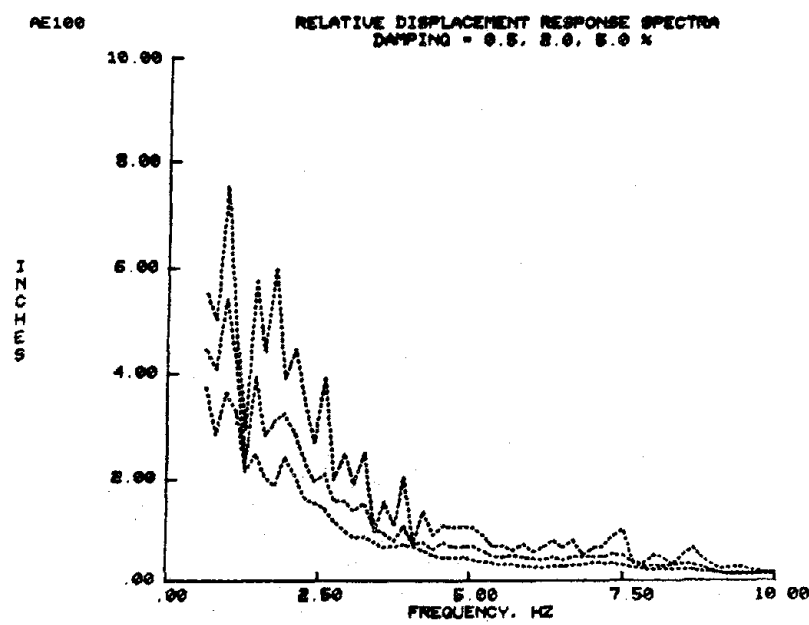
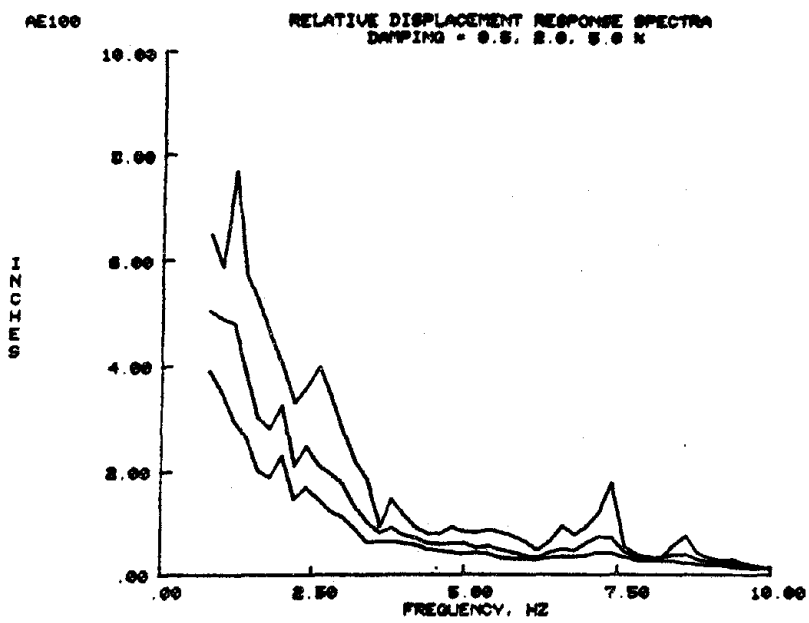


Figure 4.89 AE100 -- Relative Displacement Response Spectra from Shake Table Accelerations

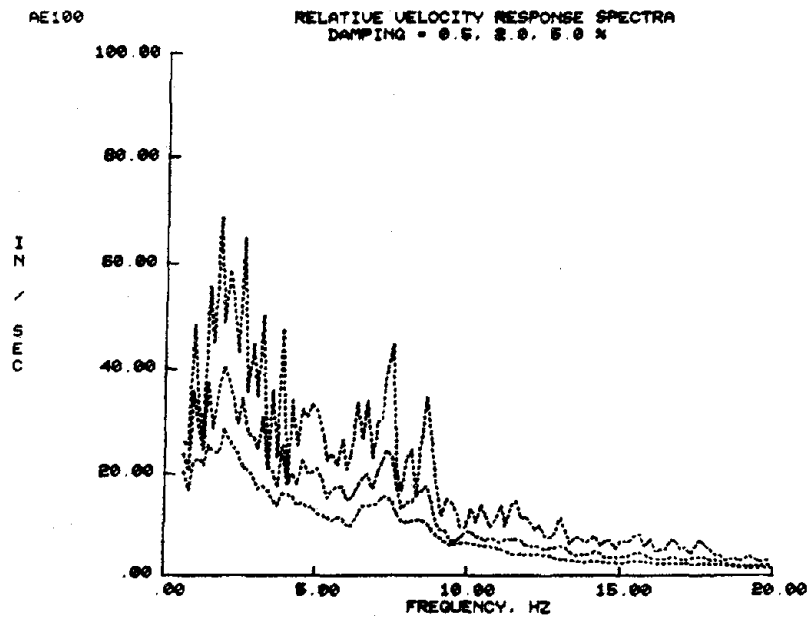
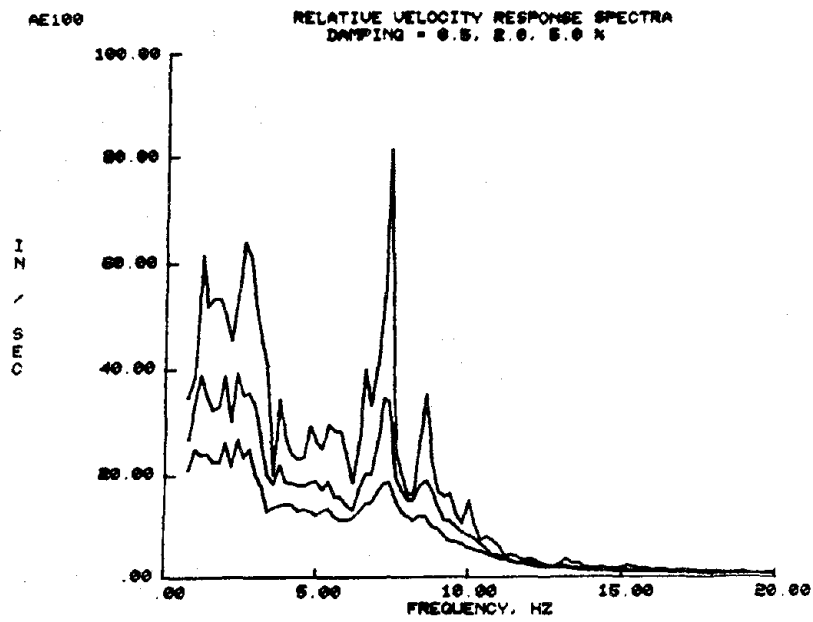


Figure 4.90 AE100 -- Relative Velocity Response Spectra from Shake Table Accelerations

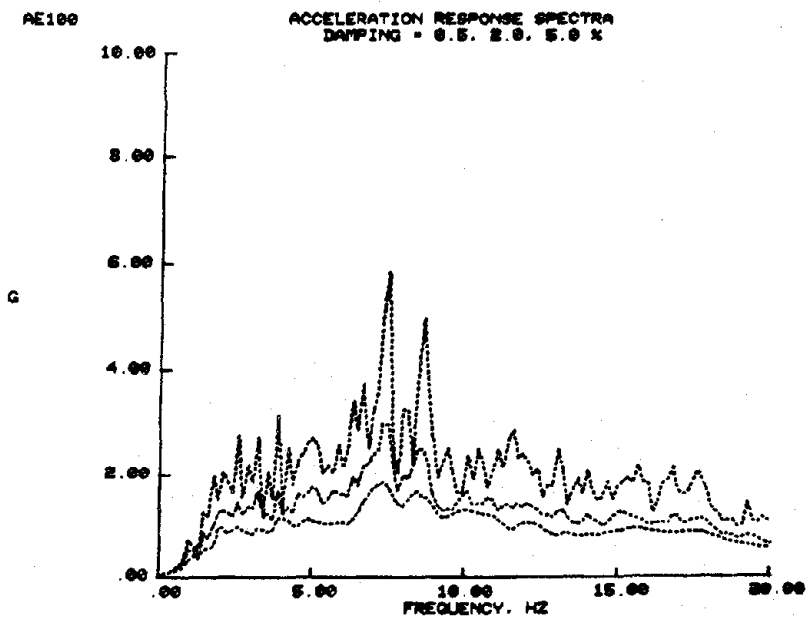
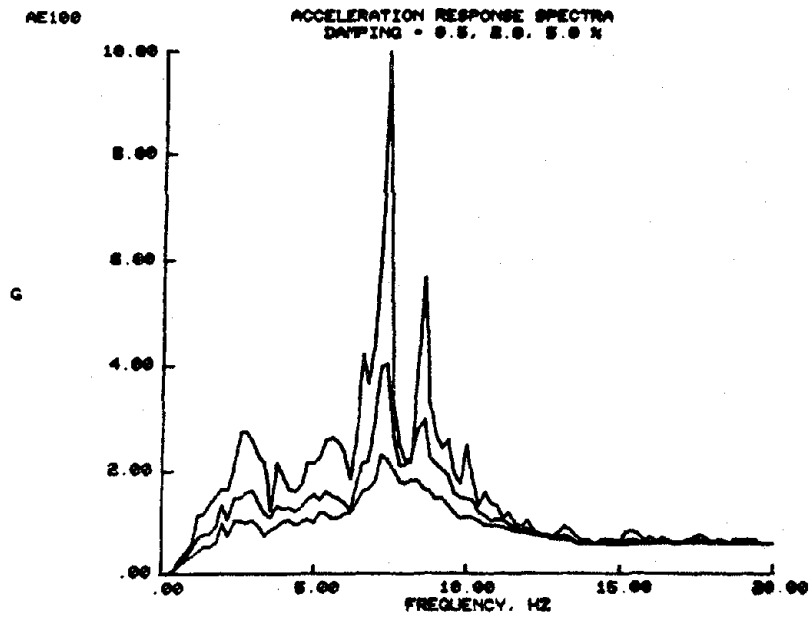


Figure 4.91 AE100 -- Absolute Acceleration Response Spectra from Shake Table Accelerations

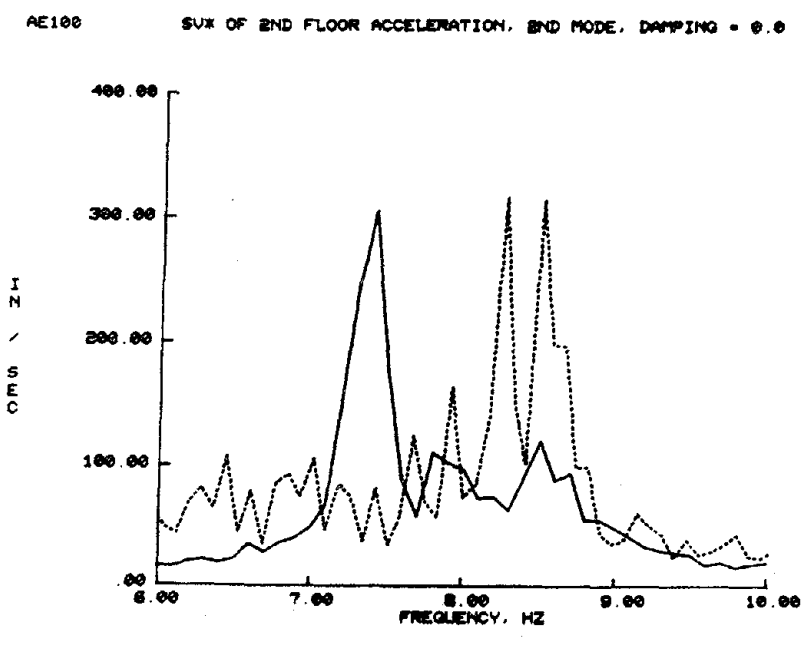
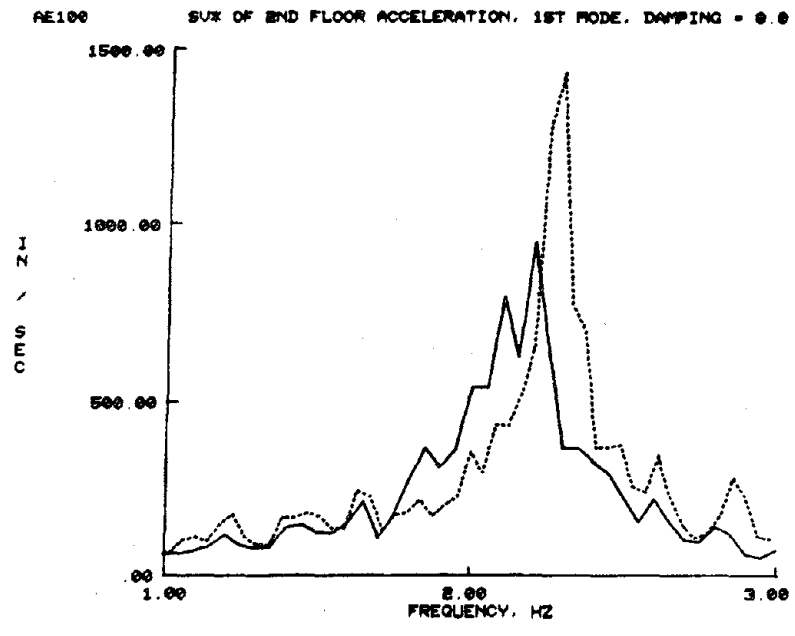


Figure 4.92 AE100 -- Test Structure Floor Response Spectra

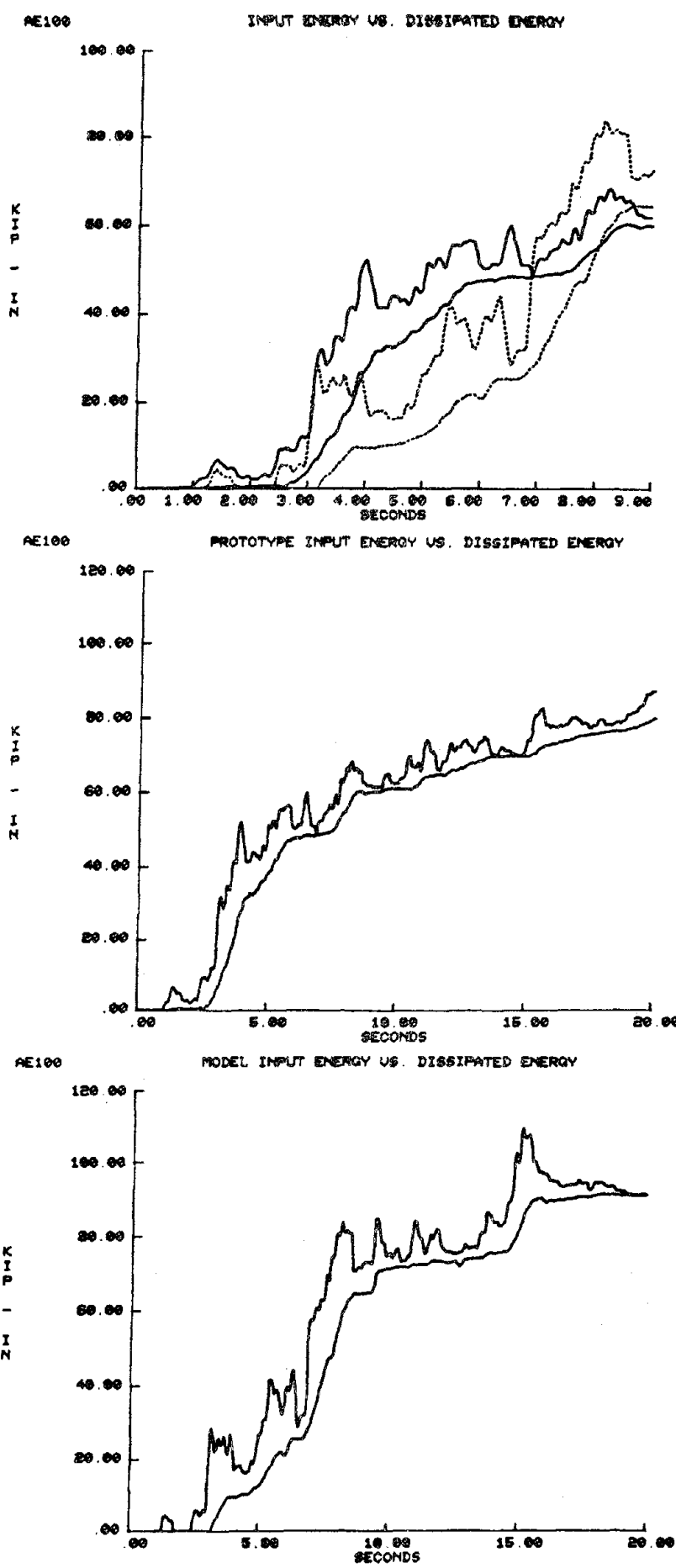
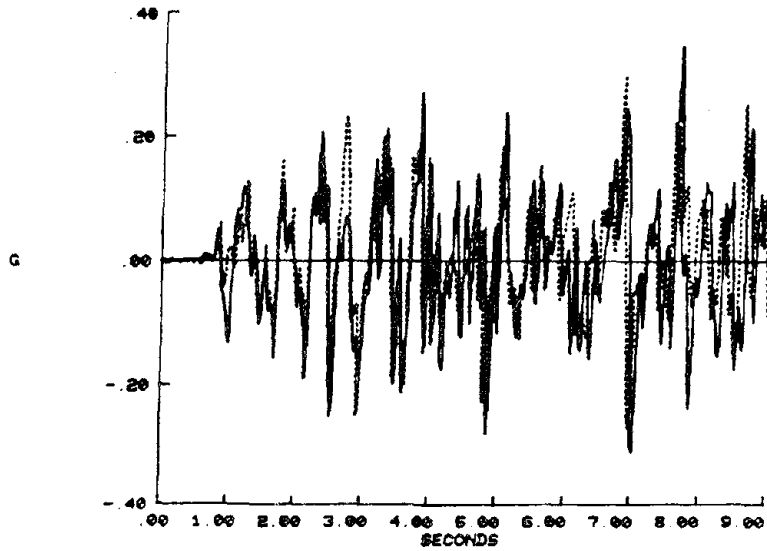


Figure 4.93 AE100 -- Input and Dissipated Energy

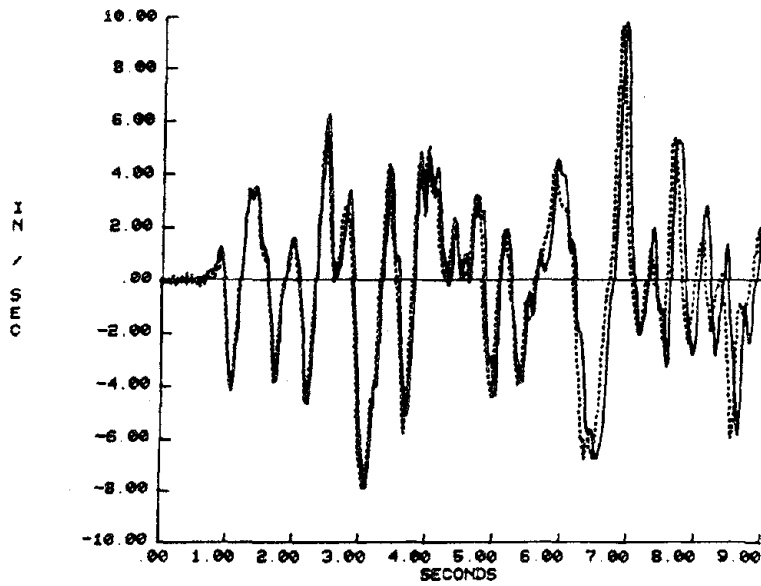
AE100

TABLE ACCELERATION



AE100

TABLE VELOCITY



AE100

TABLE DISPLACEMENT

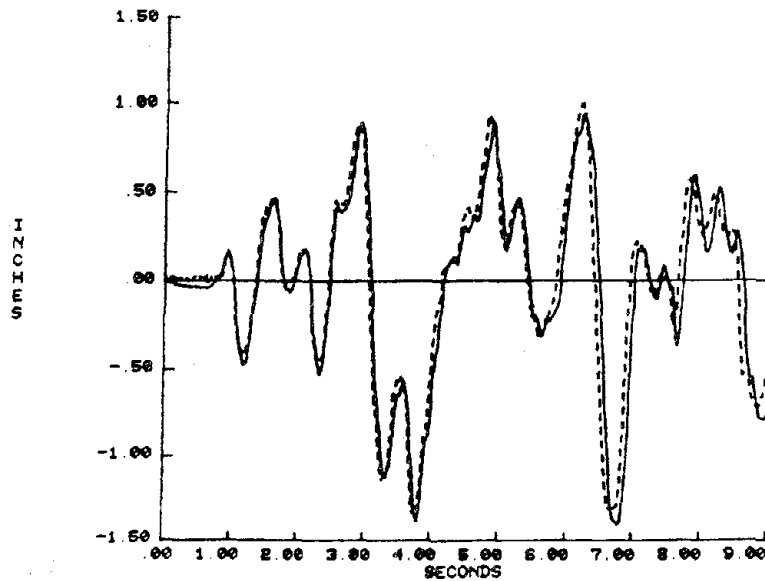


Figure 4.94 AE100 -- Shake Table Motion

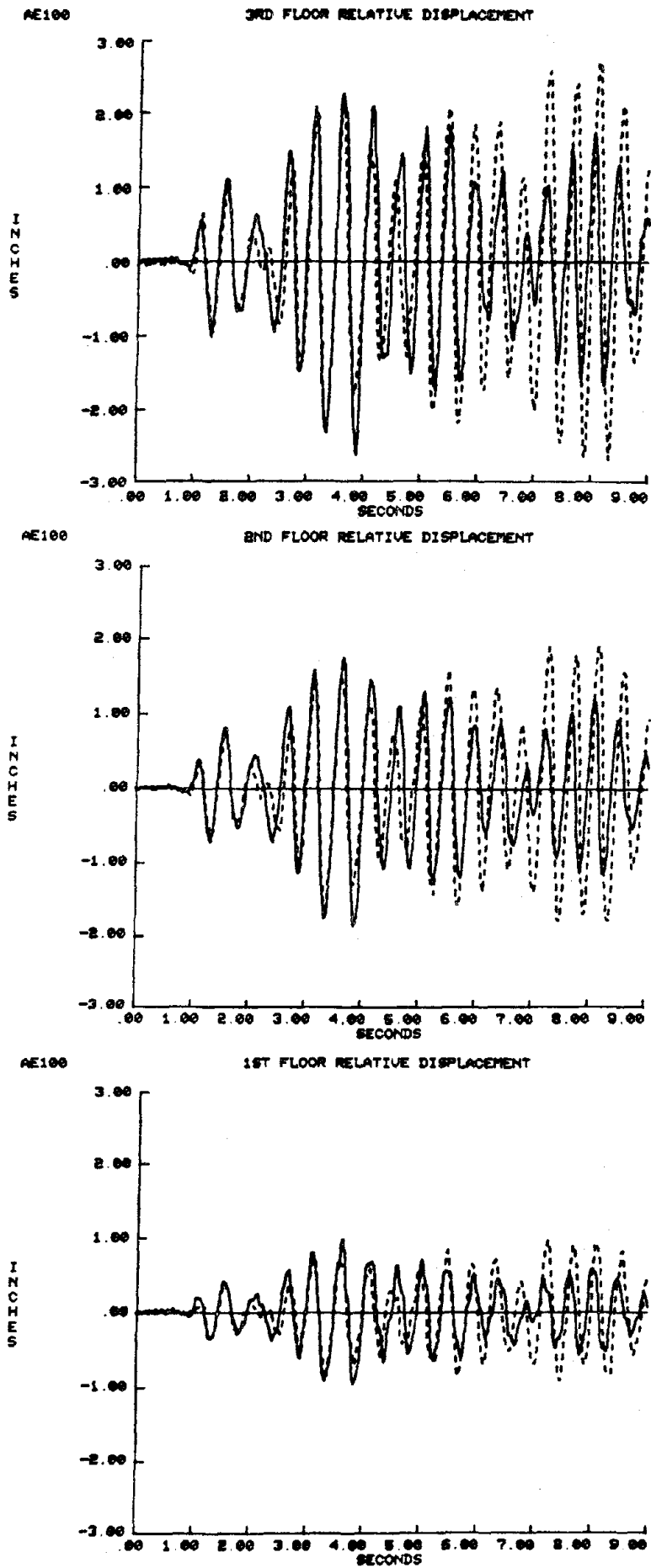
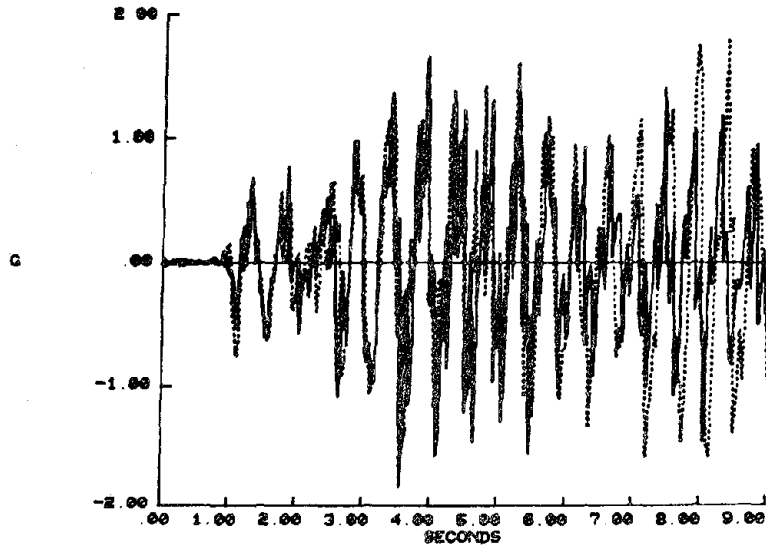


Figure 4.95 AE100 -- Floor Displacements

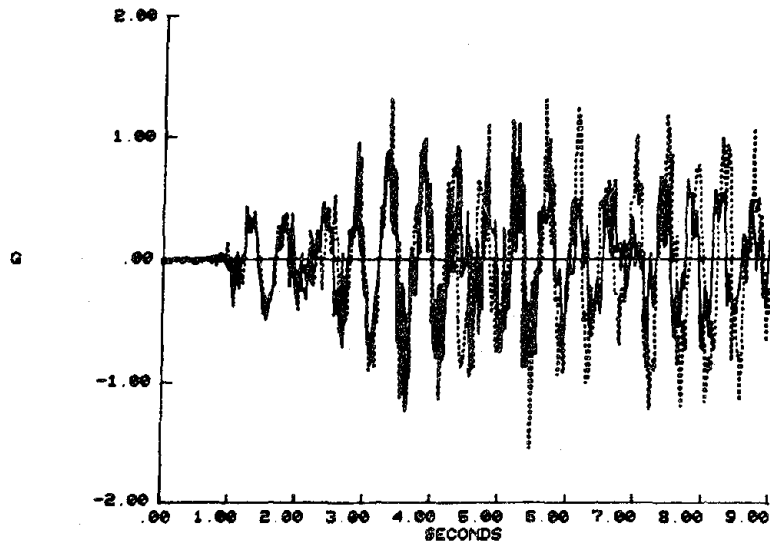
AE100

3RD FLOOR ACCELERATION



AE100

END FLOOR ACCELERATION



AE100

1ST FLOOR ACCELERATION

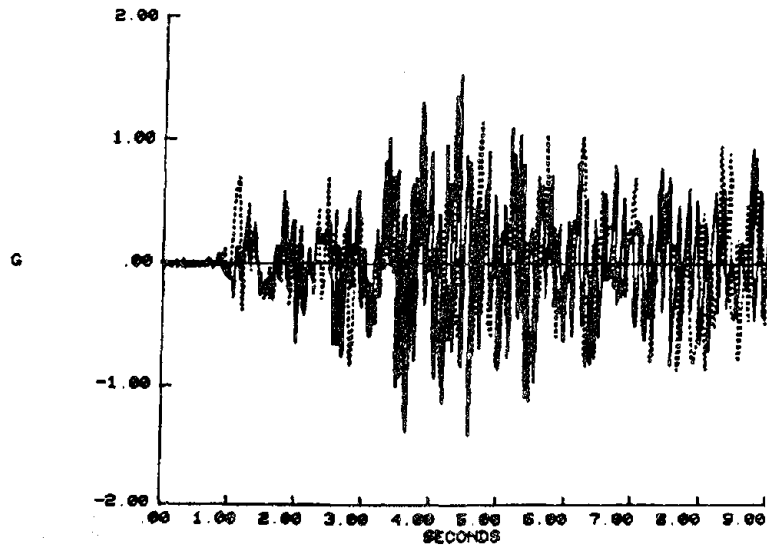


Figure 4.96 AE100 -- Floor Accelerations

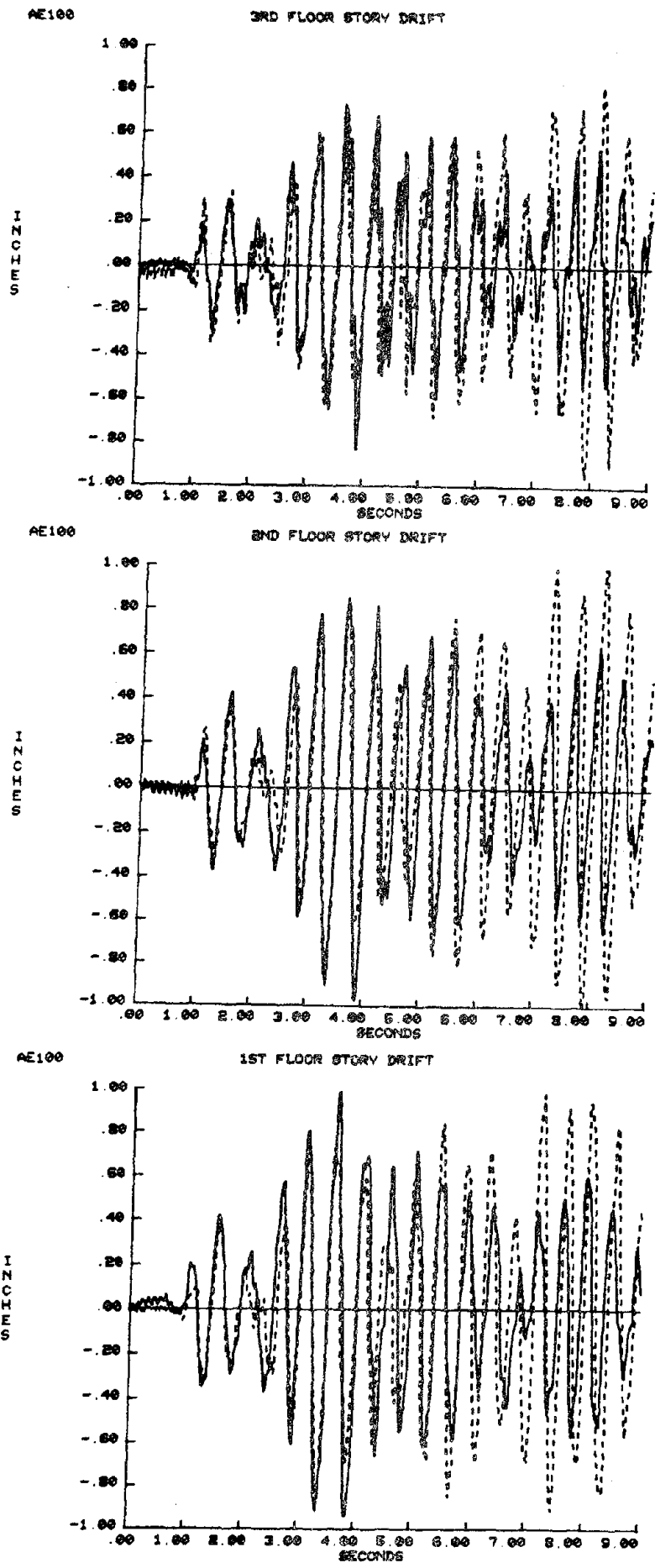


Figure 4.97 AE100 -- Story Drift

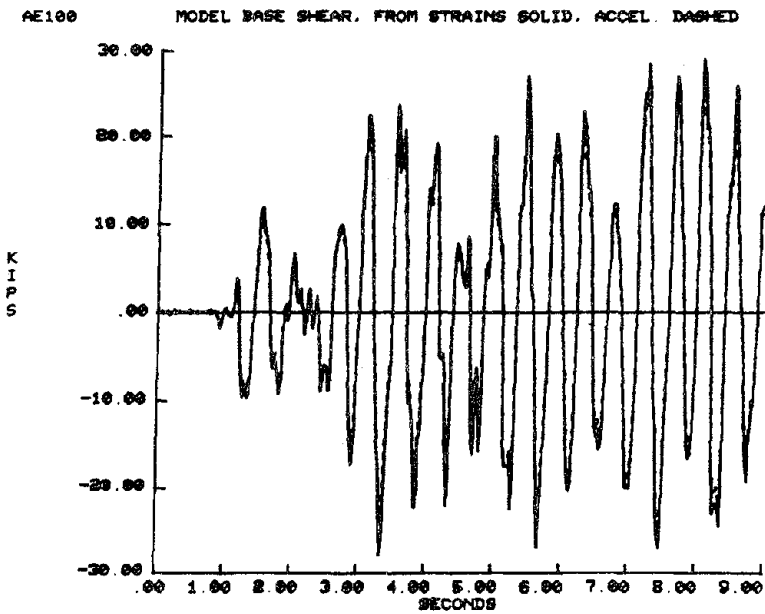
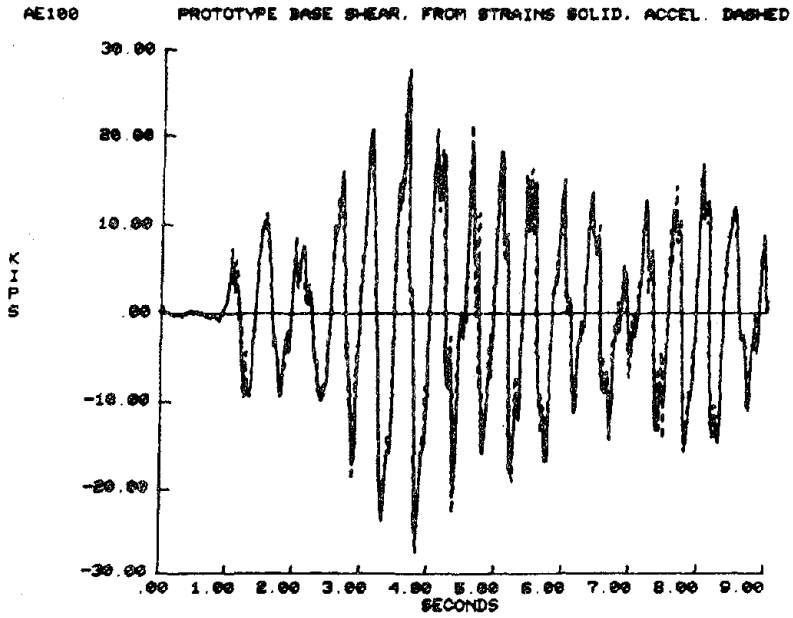


Figure 4.98 AE100 -- Base Shear from Strain Gages vs. Accelerometers

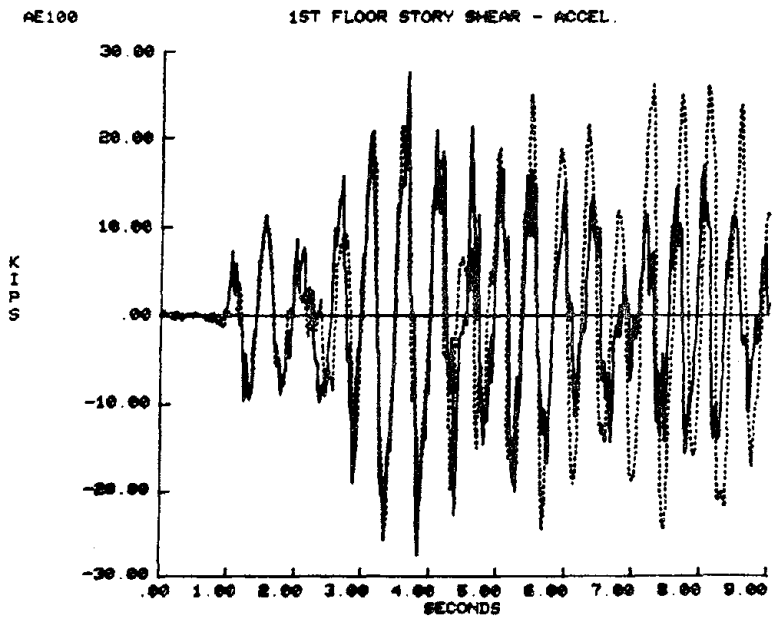
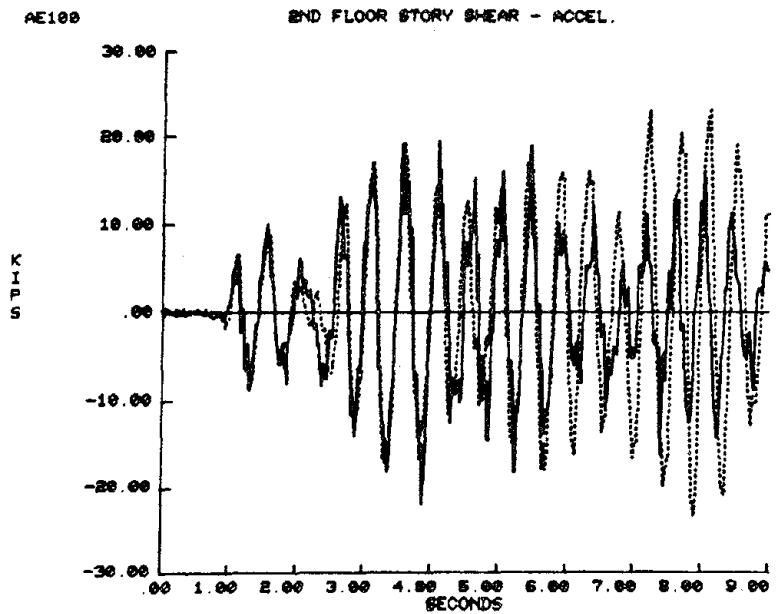
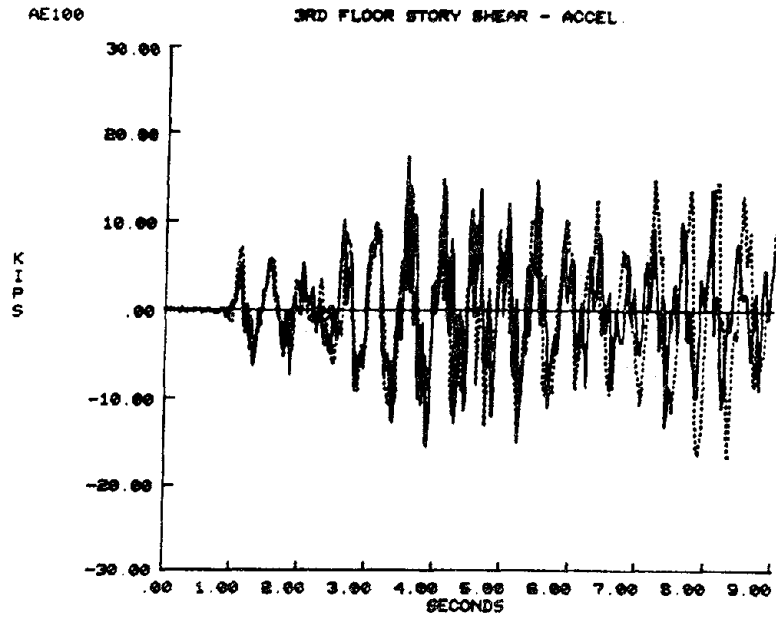


Figure 4.99 AE100 -- Story Shear

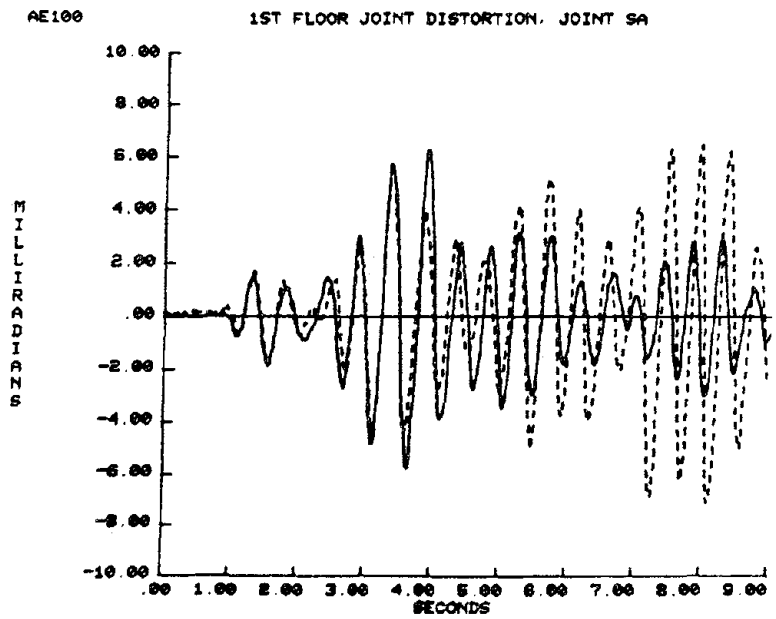
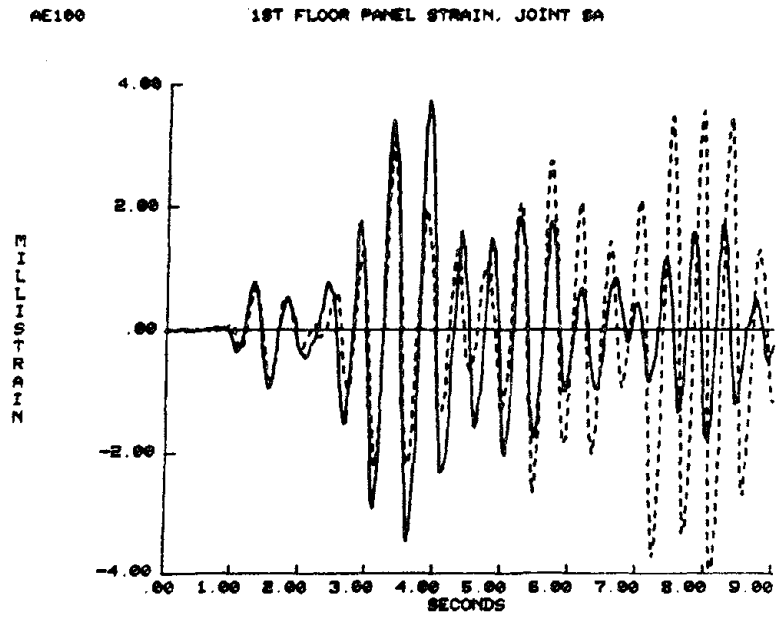
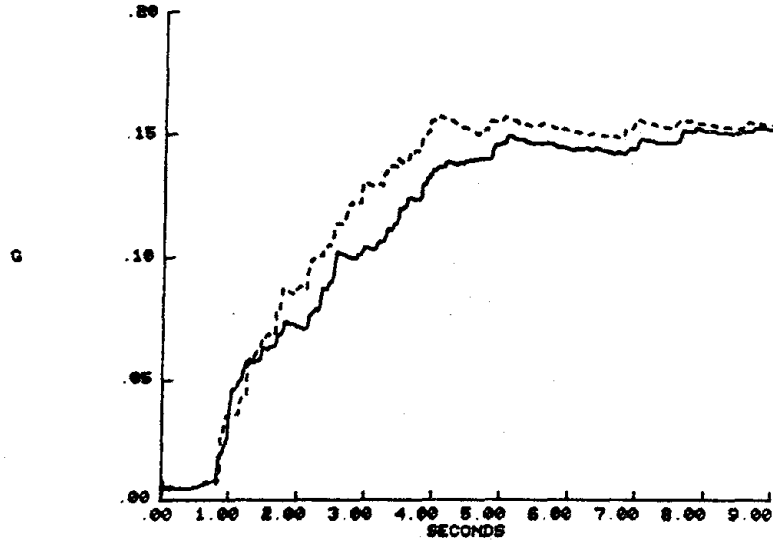


Figure 4.100 AE100 -- Joint Panel Deformations

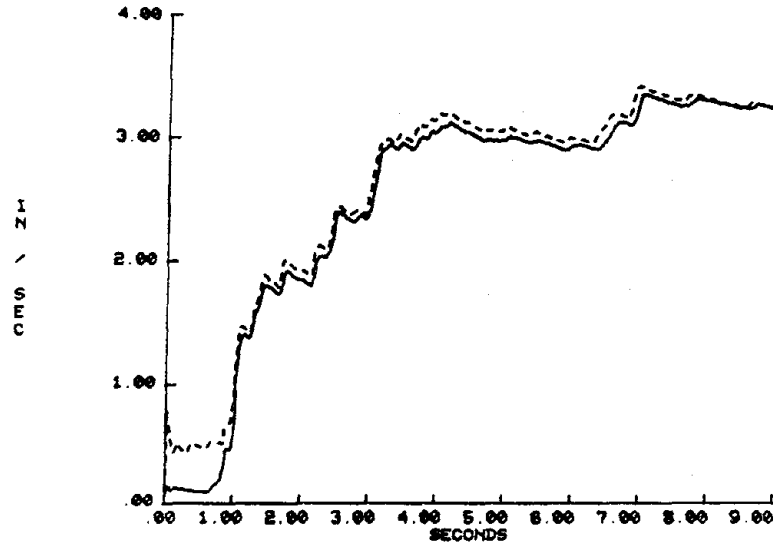
AE100

RMS OF TABLE ACCELERATION



AE100

RMS OF TABLE VELOCITY



AE100

RMS OF TABLE DISPLACEMENT

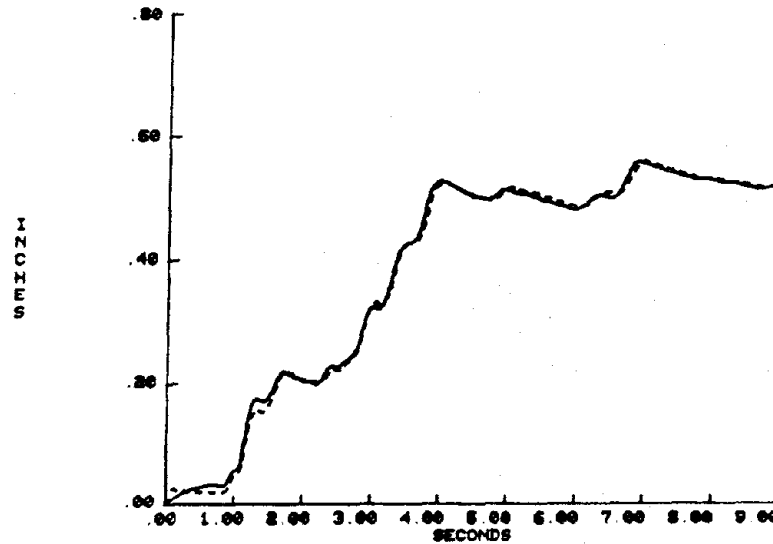


Figure 4.101 AE100 -- RMS of Shake Table Motion

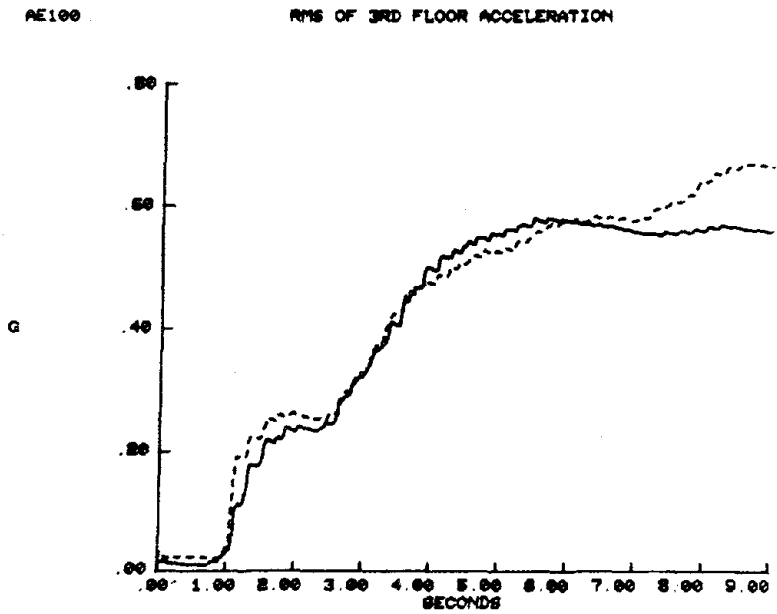
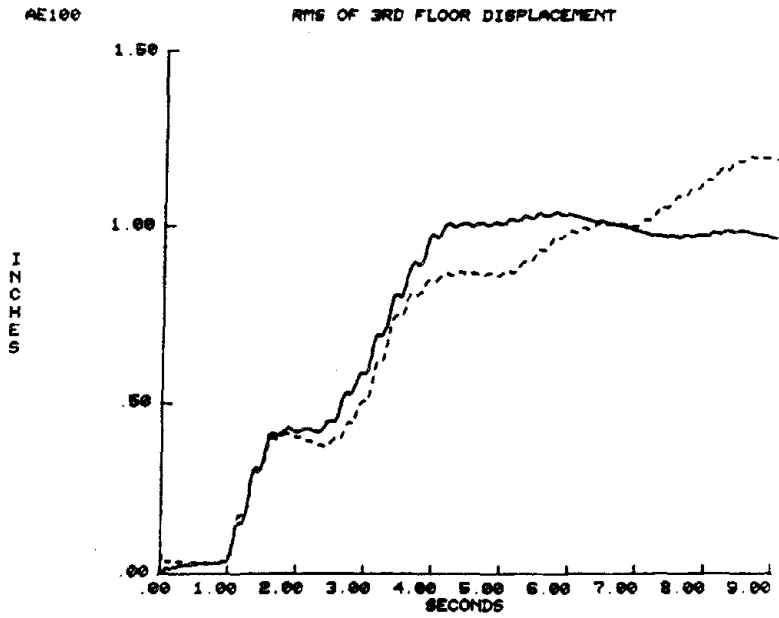


Figure 4.102 AE100 -- RMS of 3rd Floor Motions

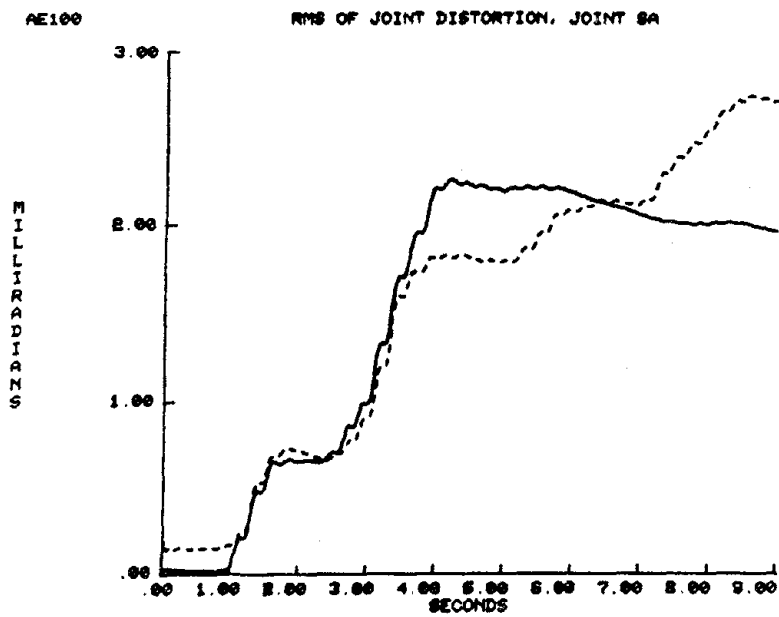
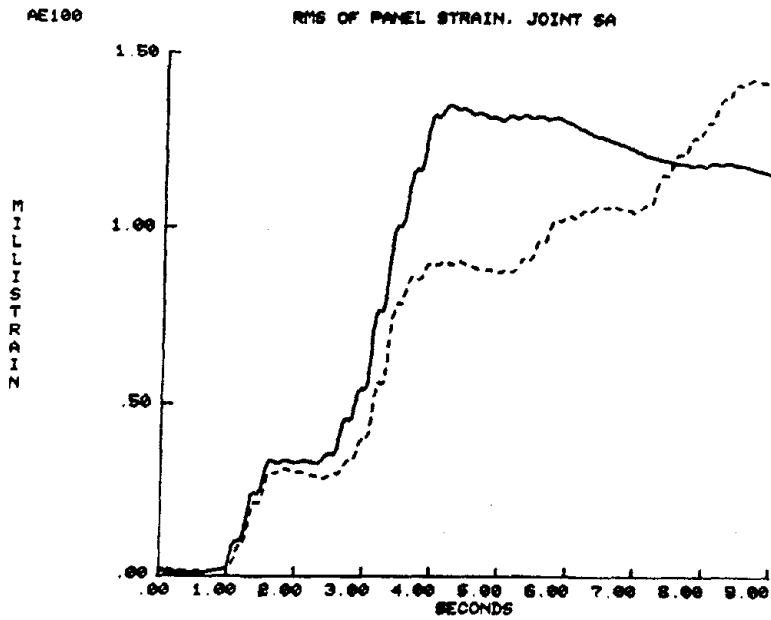
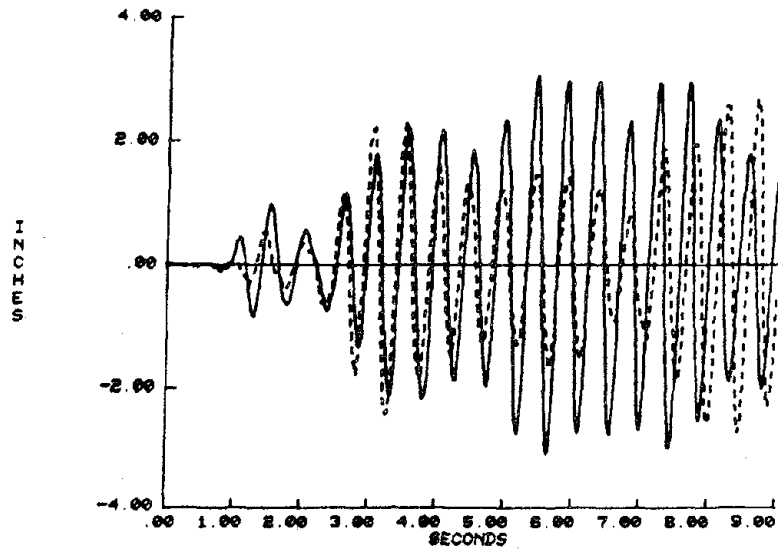


Figure 4.103 AE100 -- RMS of Joint SA Panel Deformation

AE100

ELASTIC 1 DOF DISPL. RESPONSE - ANALYTICAL



AE100

ELASTIC 1 DOF ACCEL. RESPONSE - ANALYTICAL

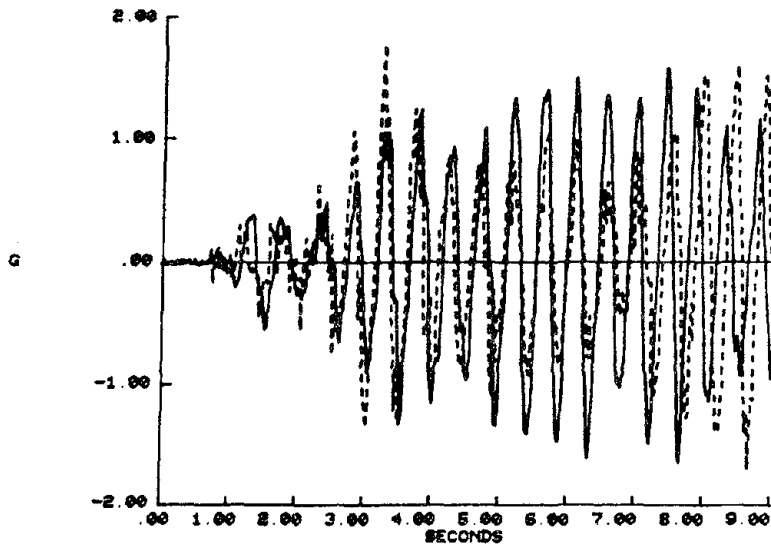


Figure 4.104 AE100 -- Analytic Elastic Response

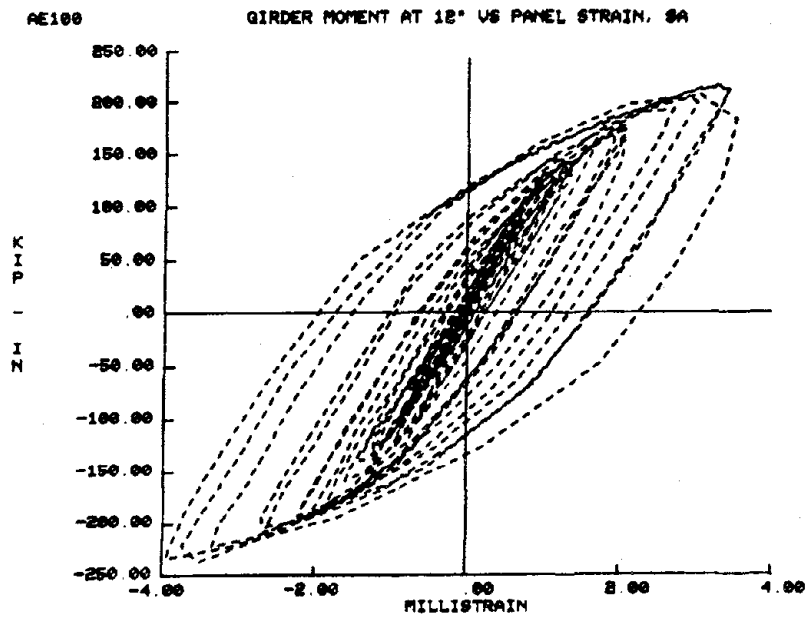
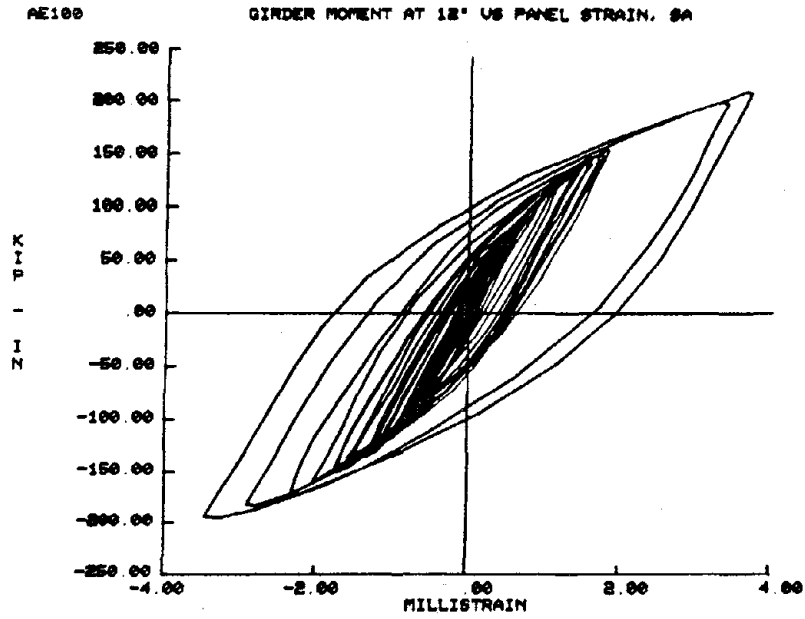


Figure 4.105 AE100 -- Girder Gage Moment vs. Panel 45° Strain--
Joint SA

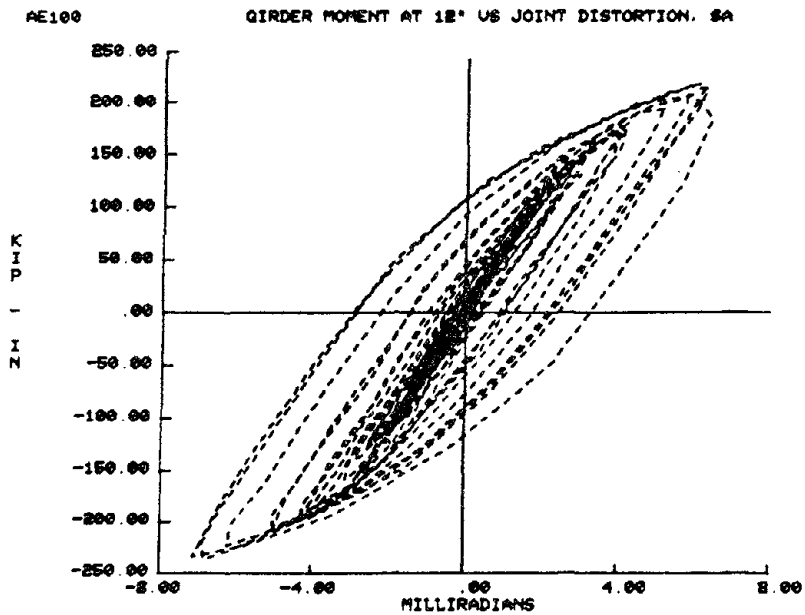
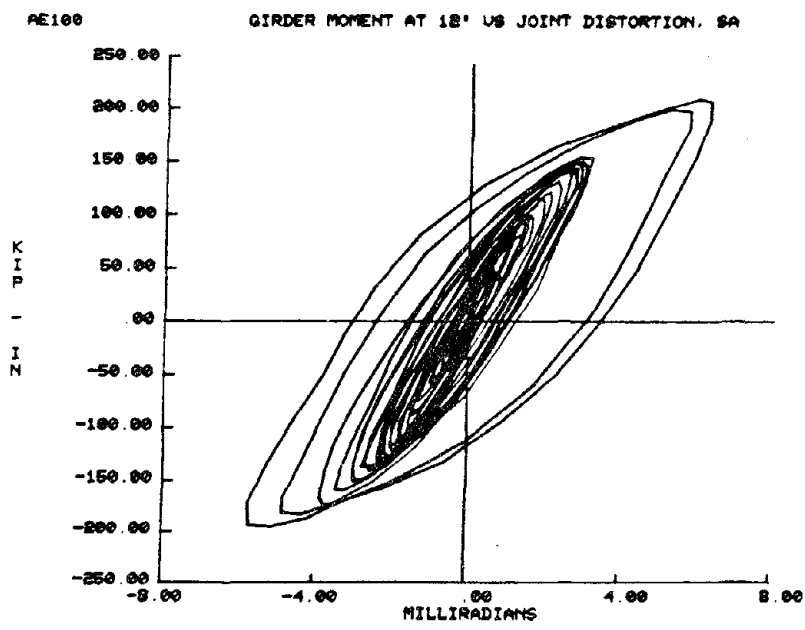


Figure 4.106 AE100 -- Girder Gage Moment vs. Panel Shear Distortion--
Joint SA

Chapter 5

SUMMARY AND CONCLUSIONS

An extensive dynamic test system and well developed methodologies for design, fabrication, testing and analysis are required to enable accurate simulation, at small model scales, of inelastic structural response to earthquake motion.

The primary task of the experimental facility is to permit the reproduction of seismic input as well as accurate measurement and analysis of those parameters whose influence is of importance to the earthquake response behavior of the prototype structure. The specific nature of model analysis, i.e., scaling of physical parameters such as time and displacement, will create unique testing demands. Not only will the test system be required to determine properties of a small-scale model but also of structural materials and components to enable complete definition of the physical model.

There are five basic components of an experimental system for dynamic model studies which must be incorporated into an integrated test system.

1. Earthquake Simulator: Model testing on a shake table permits comprehensive evaluation of structural response to dynamic input motion. The use of a minicomputer with digital-to-analog conversion capabilities enables reproduction of virtually any desired waveform within the capacities of the earthquake simulator.

Certain performance criteria must be established to ensure adequate duplication of the input motion by the earthquake simulator. Any distortions of the desired table response should not be of such a severity as to alter the observed essential response characteristics of a small-scale model from those expected for the prototype structure. Adequate table reproduction

is also essential to provide accurate comparisons with results from analytical studies and experimental investigations performed on other simulator systems. Methods of evaluating the adequacy of a simulator system are discussed in this report.

Shake table actuator force capacity must be sufficient to permit, within the frequency range of interest, the reproduction of maximum input accelerations. At these accelerations the actuator must provide sufficient force to drive the shake table mass as well as to resist the dynamic feedback (base shear) from the structure. The use of performance spectra for rigidly coupled payloads can be misleading.

2. Material and Component Test System: Preliminary material and component tests serve to define mechanical and structural properties for model-prototype response correlation, verify the adequacy of fabrication techniques and evaluate and calibrate instrumentation. Thus, the material and component test system must be suitable for well-controlled, high-rate testing to accurately define properties essential to a model test, such as rate and size effects.

3. Instrumentation: Since an evaluation of inelastic behavior is essential to studies of structural response to earthquakes, the instrumentation system must be capable of sensing yield levels in critical components and of providing information on ductility demands and energy dissipation characteristics. Various electronic transducers are commercially available to provide measurement of these important response parameters. However, certain custom instrumentation design may be needed due to the small size of model structures, requiring adaption of available sensors to perform a specific measurement. Instrumentation must be highly sensitive and of such a design that it does not influence dynamic characteristics, such as damping.

4. Data Acquisition: The high resolution, high rate, multi-channel requirements for a data acquisition system suitable for dynamic model studies can be satisfied by a digital computer with analog-to-digital conversion capabilities. Peripheral storage devices may be used to provide necessary storage space for the large volume of data produced by a dynamic model test. Data block scans should be essentially instantaneous to minimize phase shifts between successive channel samples. The data acquisition system software can be designed to interact with a tape recorded earthquake simulator input command signal, permitting an automatic mode of test control with maximum testing efficiency.

5. Data Reduction and Display: The initial task of data reduction involves conversion of raw data to actual physical parameters and other preliminary manipulation of the data such as interpolation, filtering and time shifting. Development of a comprehensive computer program library enables a complete evaluation of test results through time and frequency domain analysis. Appraisal of experimental results is best accomplished through visual presentation of test data and derived quantities through digital plotting capabilities.

A comprehensive experimental study on a small-scale model was performed in this research study to illustrate the application of model analysis to problems in earthquake engineering and to evaluate the accuracy in predicting the prototype response. This study also provided a basis for evaluation of the dynamic test system and for experimental procedures.

In order to enable accurate evaluation of model replication a well defined prototype with documented response behavior was required. For that reason, a three-story, single bay steel-frame structure previously tested at the Earthquake Engineering Research Center, U. C., Berkeley was used as a prototype for a 1:6 scale dynamic model. The most important

aspects of this model study and several conclusions are summarized in the following paragraphs.

The primary task in the design of a replica model is to simulate all aspects of the prototype design which may contribute to the earthquake response characteristics. One adequate modeling method which is applicable to a great number of building structures where gravity effects must be included is artificial mass simulation (AMS). Such modeling involves the addition of structurally uncoupled mass to augment the density of the model structure. Thus, model structural material can be chosen without regard for mass density scaling. In this study, structural steel was used as the model material.

Methods applicable to fabrication of model sections from structural steel include joining of plate elements by gluing, soldering or welding and forming of structural shapes by machining, rolling or extrusion from bar stock. Of these methods, machining is most suited for highly stressed primary elements and permits fabrication of model elements to length scales of λ_r approximately equal to 1:20. Extrusion, followed by heat treatment, or rolling may be feasible for models where many identical members must be produced.

Structural connections can be considered to be of two basic types. Primary connections are highly stressed and require connection media of similar strength and ductility as the prototype material. Connections stressed considerably below yield levels can be classified as secondary connections. Heliarc welding and bolting are applicable to primary connections while bolting, silver-soldering and gluing are feasible for secondary connections. Experience with TIG heliarc welded structural joints indicate that weld sizes in small-scale models will often be larger than required by geometric scaling.

Tolerances for model fabrication can be defined by appropriate geometric scaling of standard tolerances for building structures. It may be necessary to heat treat the finished structural frames to satisfy these tolerances and to eliminate high initial stresses due to the fabrication procedures. Thus, duplication of the prototype initial stress state is extremely difficult, if not impossible, with these methods.

Distortion of non-essential prototype elements in the model may be used to simplify model construction provided that no noticeable effect on the adequacy of simulation is produced. For instance, in this model study rectangular sections were utilized for secondary beam elements while wide-flange sections were used for the prototype structure.

The results of the AMS model test series provided accurate simulation of the prototype structure in terms of global and local response parameters. The nature of inelastic response was duplicated in the small-scale model as characterized by yielding of the joint panel zones in shear.

The oversized welds in the joint stiffeners of the model structure contributed to an approximately 10% increase in yield strength and to higher inelastic stiffness of the joints when compared to prototype results. Strain-rate effects were of less importance for model to prototype correlation but may be of more influence at smaller model scales.

Discrepancies in initial stress states can have a bearing on initial inelastic test results. In the case of the AMS model, high initial forces produced by aligning of the column base plates and welding to the earthquake simulator platform contributed to yielding of the model structure at a lower dynamic input intensity than was observed for the prototype. However, after initial yielding a redistribution of internal forces eliminated this effect in later inelastic tests.

Dynamic tests illustrate that the reproduction capability of an

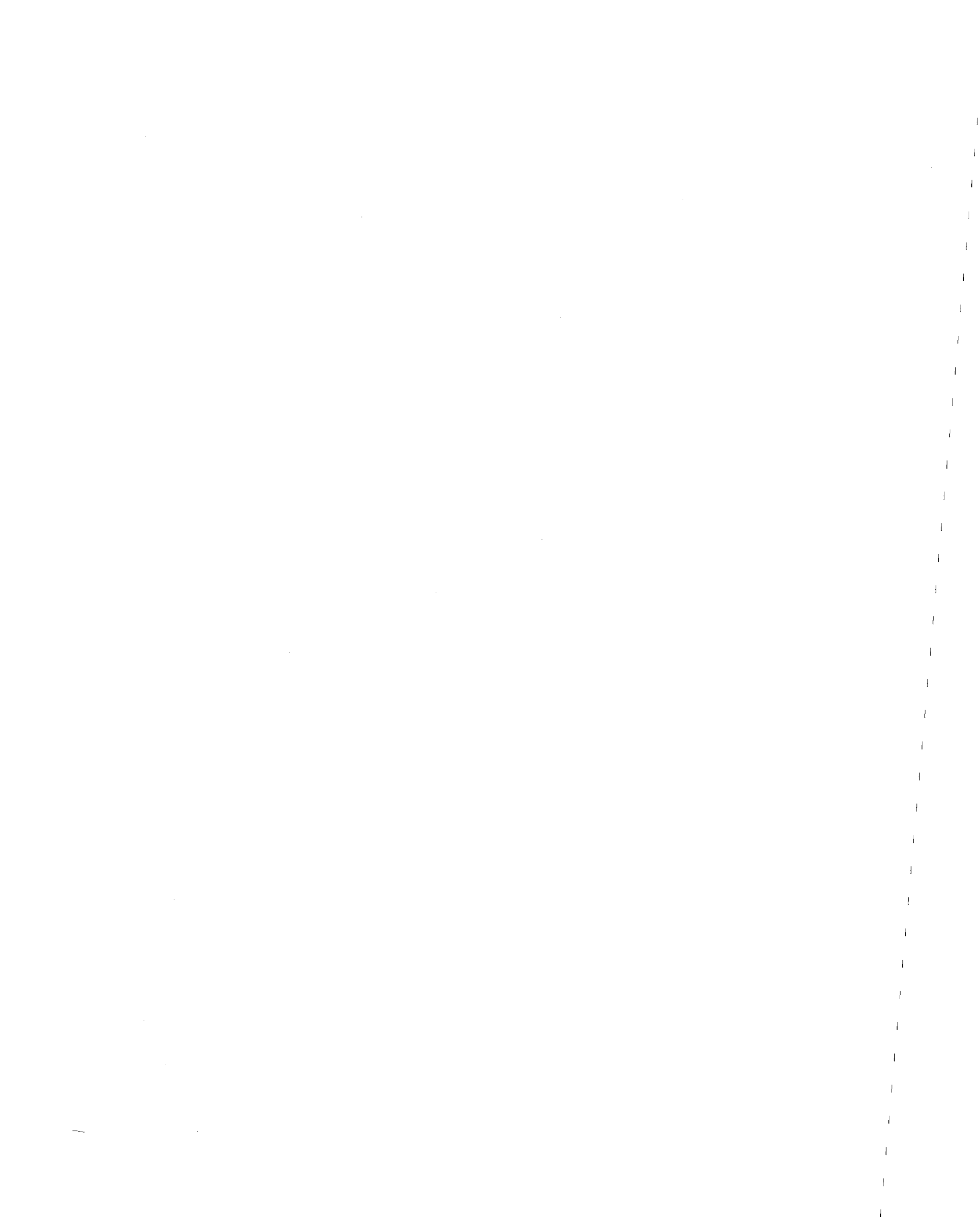
earthquake simulator has a great influence on the apparent correlation of model and prototype results. In particular, a structure responding elastically is extremely sensitive to local fluctuation of the table motion spectrum. This problem may be of less importance for high intensity inelastic tests, however sufficient energy must be transferred to the structure at the elastic level before the threshold required to produce inelastic action can be reached. Once inelastic action does occur, this dependence on a narrow range of input frequency is considerably reduced.

Tests of models with artificial mass simulation are suitable for many types of structural systems, particularly those which can be approximated by lumped mass systems (building systems with large floor masses). The capability of using prototype material as the modeling material makes this procedure of model analysis particularly useful for application to reinforced concrete structures. Also, materials other than prototype materials may be used when modeling steel frame structures to avoid exceedence of earthquake simulator capacities.

Future research concerning the use of small-scale replica models for reproducing earthquake response of building structures is needed on models which are more representative of actual buildings. The ability of a small-scale model to reproduce the effects of floor diaphragms, infill walls, nonstructural elements and other common characteristics of building structures should be explored.

As experimental modeling is felt to be primarily applicable to complex structures where confidence in analytical methods is not fully established, the extension of model analysis to multistory, multibay structures with complex geometry should be developed. For such structures, alternative methods of element fabrication, namely rolling and extrusion, may be utilized for

production of similar structural elements. Procedures must be developed to enable simulation of the prototype initial stress state as this phenomenon may have a considerable influence on the dynamic response of a structural system. Rate and size effects will become more predominant at smaller model scales, requiring definition of these parameters through extensive material and component testing.



REFERENCES

1. Abrahamson, G. R., Florence, A. L. and Colton, J. D., "Scale Modeling in Structural Dynamics Involving Plastic Deformation and Fracture," SRI International, Menlo Park, April 1976.
2. Antebi, J., Smith, H. D., Sharma, S. D. and Harris, H. G., "Evaluation of Techniques for Constructing Model Structural Elements," Research Report R-62-15, Department of Civil Engineering, Massachusetts Institute of Technology, May 1962.
3. Bendat, J. and Piersol, A., Random Data: Analysis and Measurement Procedures, Wiley, N.Y., 1971.
4. Breen, J. E., "Fabrication and Tests of Structural Models," Proceedings, ASCE, V. 94, ST 6, June 1968.
5. Castoldi, A., "New Techniques of Model Investigation of the Seismic Behavior of Large Structures," ISMES Publication No. 56, Bergamo, Italy, April 1973.
6. Castoldi, A. and Casirati, M., "Experimental Techniques for the Dynamic Analysis of Complex Structures," ISMES Publication No. 74, Bergamo, Italy, Feb. 1976.
7. Clough, R. W. and Huckelbridge, A. A., "Preliminary Experimental Study of Seismic Uplift of a Steel Frame," EERC Report No. 77-22, Berkeley, California, 1977.
8. Clough, R. W., Rea, D., Tang, D. and Watabe, M., "Earthquake Simulator Test for a Three Story Steel Frame Structure," Proceedings, 5th World Conference on Earthquake Engineering, Vol. I, Rome, Italy, June 1973.
9. Clough, R. W. and Tang, D. T., "Earthquake Simulator Study of a Steel Frame Structure, Vol. I: Experimental Results," EERC Report No. 75-6, Berkeley, California, 1975.
10. Clough, R. W. and Hidalgo, P., "Design of a Shaking Table Test for a Reinforced Concrete Frame Structure," Proceedings, 5th World Conference on Earthquake Engineering, Vol. I, Rome, Italy, June 1973.
11. Conte, S. and de Boor, C., Elementary Numerical Analysis, McGraw-Hill, N.Y., 1972.
12. Crandall, S., ed., Random Vibrations, Massachusetts Institute of Technology Press, 1958.
13. Dove, R. C. and Adams, P. H., Experimental Stress Analysis and Motion Measurement, Charles E. Merrill Publishing Co., Columbus, Ohio, 1964.

14. "Earthquake Environmental Simulation," Final Report and Proceedings of a Workshop on Simulation of Earthquake Effects on Structures, in San Francisco, Sept. 1973, published by National Academy of Engineering, 1974.
15. Harris, H. G., Pahl, P. J. and Sharma, S. D., "Dynamic Studies of Structures by Means of Models," Research Report R-63-23, Department of Civil Engineering, Massachusetts Institute of Technology, Sept. 1962.
16. Hidalgo, P. and Clough, R. W., "Earthquake Simulator Study of a Reinforced Concrete Frame," EERC Report No. 74-13, Berkeley, California, 1974.
17. Hossdorf, H., Model Analysis of Structures, Van Nostrand Reinhold Co., New York, 1971.
18. Housner, G. and Jennings, P., "Generation of Artificial Earthquakes," Proceedings, ASCE, Engr. Mech. Div., Vol. 90, EMI, Feb. 1964.
19. Ives, K. D., "Considerations for Instrumentation of Typical Dynamic Tests," Experimental Mechanics, 13, 5. May 1973.
20. Krawinkler, H., Bertero, V. V. and Popov, E. P., "Shear Behavior of Steel Frame Joints," ASCE, Structural Division, ST 11, Nov. 1975.
21. Krawinkler, H., Mills, R. S., Moncarz, P. D., "Scale Modeling and Testing of Structures for Reproducing Response to Earthquake Excitation," John A. Blume Earthquake Engineering Center, Stanford University, May 1978.
22. Lauretta, E., "Dynamic Behavior of Large Structures Studied by Means of Models," Prelim. Publication, 7th Congress, IABSE, Rio de Janeiro, Aug. 1964.
23. Lauretta, E., and Castoldi, A., "Earthquake Simulation by a Shake Table," 4th World Conference on Earthquake Engineering, Santiago, Chile, 1969.
24. Lionberger, S. R. and Weaver, W., Jr., "Dynamic Response of Frames with Non-Rigid Connections," Journal of the Engineering Mechanics Division, ASCE, Vol. 95, No. EMI, February 1969.
25. Litle, W. A., Foster, D. C., Oakes, D., Falcone, P. A. and Reiner, R. B., "Structural Behavior of Small-Scale Steel Models," Steel Research for Construction, Bulletin No. 10, AISI, April 1968.
26. Manjoine, M. J., "Influence of Rate of Strain and Temperature on Yield Stresses of Mild Steel," Journal of Applied Mechanics, Vol. II, No. 4, December 1944.
27. Manual of Steel Construction, American Institute of Steel Construction, N.Y., 1973.

28. Mills, R. S. and Krawinkler, H., "The Use of Minicomputers for Control and Data Handling in Dynamic Tests," Proceedings, International Instrumentation Symposium, Instrument Society of America, Anaheim, Calif., May 1979.
29. Newland, D., An Introduction to Random Vibrations and Spectral Analysis, Longman, 1975.
30. Oberti, G. and Lauretta, E., "Dynamic Tests on Models of Structures," ISMES Publication No. 19, Bergamo, Italy, June 1962.
31. Okada, H., Takeda, T., Yoshioka, K., Omote, Y. and Nakagawa, K., "Experiments and Research on the Response of Steel Model Structures Subjected to Impact Horizontal Loading and to Simulated Earthquakes," Proceedings, 5th World Conference on Earthquake Engineering, Vol. II, Rome, Italy, June 1973.
32. Penzien, J., Bouwkamp, J. G., Clough, R. W. and Rea, D., "Feasibility Study of Large-Scale Earthquake Simulator Facility, EERC Report No. 67-1, Berkeley, California, 1967.
33. Rea, D. and Penzien, J., "Dynamic Response of a 20 x 20-ft Shaking Table," Paper No. 180, Proceedings, 5th World Conference on Earthquake Engineering, Rome, Italy, June 1973.
34. Richards, C. W., "Size Effect in the Tension Test of Mild Steel," Proceedings, ASTM, 1954.
35. Richards, C. W., "Effect of Size on the Yielding of Mild Steel Beams," Proceedings, ASTM, 1958.
36. Sabnis, G. M., "Instrumentation in Structural Models," State-of-the-Art Report on Structural Concrete Models, edited by M. S. Mirza, Department of Civil Engineering, McGill University, Montreal, Oct. 1972.
37. Scanlan, R. and Sachs, K., "Earthquake Time Histories and Response Spectra," Proceedings, ASCE, Engr. Mech. Div., Vol. 100, EM4, Aug. 1974.
38. Selander, C. E. and Carpenter, L. R., "Application of the Mini-computer in Measurement, Analysis and Control of Structural Testing by BUREC," Preprint No. 2950, ASCE Convention, San Francisco, Oct. 1977.
39. Stephen, R. M., Bouwkamp, J. G., Clough, R. W. and Penzien, J., "Structural Dynamics Testing Facilities at the University of California, Berkeley," EERC Report No. 69-8, Berkeley, California, 1969.
40. Takahashi, Y., Rea, D. and Abedi-Hayati, S., "Effects of Test Specimen Reaction Loads on Shaking Tables," Preprints, 5th World Conference on Earthquake Engineering, Rome, Italy, June 1973.
41. Tang, D. T., "Earthquake Simulator Study of a Steel Frame Structure, Vol. II: Analytical Results," EERC Report No. 75-36, Berkeley, California, 1975.

42. Tsai, N., "Spectrum--Compatible Motions for Design Purposes," Proceedings, ASCE, Engr. Div., Vol. 98, EM2, April 1972.
43. Tsutsumi, H., "Vibration Research in CRIEPI by Means of Shaking Table, Some Recent Earthquake Engineering Research and Practice in Japan, Japanese National Committee, International Assn. for Earthquake Engineering, Tokyo, May 1973.
44. Uniform Building Code, International Conference of Building Officials, Pasadena, CA., 1970.
45. Wiegel, R. L. (ed.), Earthquake Engineering, Prentice-Hall, Inc., Englewood Cliffs, N.J., 1970.
46. Williams, D. and Godden, W. G., "Experimental Model Studies on Seismic Response of High Curved Overcrossings," EERC Report No. 76-18, Berkeley, California, 1976.

Appendix A
NUMERICAL METHODS

Various numerical methods are utilized during processing of test data at the Stanford dynamic test facility. These methods are incorporated into computer algorithms to enable interpolation, integration, differentiation and smoothing of data time history records. This appendix presents a brief description of the procedures used and illustrates their application in a number of typical example problems.

A. 1 Interpolation

In order to partially restore the data lost during acquisition interruptions produced at data dumps it is necessary to apply an interpolation procedure. A third-order algebraic equation of the form,

$$y = ax^3 + bx^2 + cx + d$$

is used to approximate the response history over the interval. Higher order equations tend to be unstable in certain circumstances.

A graphical representation of the procedure is shown in Figure A.1. The ordinate and first derivative on either side of the dump interval are used to define the interpolation function. In order to simplify the formulation the time scale is normalized to produce a unit dump interval. The term n is derived from the sampling interval t_p and the duration of the data dump interruption, t_d . Since the system clock operates independently of the data transfer procedure the dump time is always an integer multiple of the sampling interval, i.e.,

$$t_d = nt_p \quad n \geq 1$$

where $n = 1$ indicates that no data were lost at the dump transfer.

The formulation of the equation coefficients is as follows:

$$a = 2(y_1 - y_2) + y'_1 + y'_2$$

$$b = \frac{1}{2}(y'_2 - y'_1 - 3a)$$

$$c = y'_1$$

$$d = y_1$$

where the derivatives are approximated by finite differences,

$$y'_1 = (y_1 - y_0)/n$$

$$y'_2 = (y_3 - y_2)/n$$

The function is then evaluated over the interval of 0 to 1 at normalized time increments of $1/n$, producing $n-1$ interpolation values at each dump occurrence.

Since the data acquisition system does not always recover in time for the first data scan after a transfer interval the initial scan subsequent to a dump is often in error. Thus, the computer interpolation algorithm neglects the first data point after a dump interval, provided points were lost at the interruption, actually producing n interpolations at each data dump.

A. 2 Integration and Differentiation

A procedure similar to that used for interpolation is utilized for integration and differentiation of data time histories. The operand is approximated by a multiple-order algebraic equation, enabling the respective analytical operation to be performed. For integration a third-order equation is used while a fourth-order curve is applied for derivatives.

The formulation for a typical integration interval is illustrated in Figure A.2. The third-order equation is defined by the four ordinate

values, y_1 through y_4 , producing the algebraic coefficients

$$a = \frac{1}{6}(-y_1 + 3y_2 - 3y_3 + y_4)$$

$$b = \frac{1}{2}(y_1 - 2y_2 + y_3)$$

$$c = \frac{1}{6}(-2y_1 - 3y_2 + 6y_3 - y_4)$$

$$d = y_2$$

The integral is then constructed by summing the integral increments evaluated over the intervals

$$\Delta x = \begin{cases} -1 \text{ to } 0 & \text{for the 2nd data point} \\ 1 \text{ to } 2 & \text{for the last data point} \\ 0 \text{ to } 1 & \text{for all others (see Figure A.2)} \end{cases}$$

with the initial integral point assigned a zero value.

The formulation is simplified by normalizing the time axis through division by the sampling interval, t_p , producing the final integration formulas,

$$\int_0^1 y \, dx = \frac{t_p}{12}(3a + 4b + 6c + 12d)$$

$$\int_{-1}^0 y \, dx = \frac{t_p}{12}(-3a + 4b - 6c + 12d)$$

$$\int_1^2 y \, dx = \frac{t_p}{12}(45a + 28b + 18c + 12d)$$

The fourth-order formulation,

$$y = ax^4 + bx^3 + cx^2 + dx + e$$

used to determine derivatives of time histories is shown in Figure A.3.

The derivative of the time normalized function is defined by

$$y' = \frac{1}{t_p}(4ax^3 + 3bx^2 + 2cx + d)$$

where

$$a = \frac{1}{24}(y_4 - 4y_3 + 6y_2 - 4y_1 + y_0)$$

$$b = \frac{1}{6}(y_3 - 3y_2 + 3y_1 - y_0) - 6a$$

$$c = \frac{1}{2}(y_2 - 2y_1 + y_0) - 7a - 3b$$

$$d = y_1 - y_0 - a - b - c$$

and the derivative is evaluated at

$$x = \begin{cases} 0 & \text{for the 1st data point} \\ 1 & \text{for the 2nd data point} \\ 3 & \text{for the next to last data point} \\ 4 & \text{for the last data point} \\ 2 & \text{for all others} \end{cases}$$

A. 3 Smoothing

A simple weighted averaging routine is used to smooth data records. Five points are utilized to give an averaged estimate of any given point, y_i , as defined by,

$$y_i \text{ (smoothed)} = \frac{[a(y_{i-2} + y_{i+2}) + b(y_{i-1} + y_{i+1}) + cy_i]}{[2(a + b) + c]}$$

where the coefficients a , b and c are specified by the user to produce the desired degree of smoothing.

A. 4 Examples

The results obtained from application of the interpolation procedure to four specific examples are shown in Figures A. 4 through A. 7.

For this study, a sinusoidal wave with constant amplitude and period T was sampled by the data acquisition system at time intervals t_p so that various dump durations t_d were produced. The parameters which define these examples are given in Table A.1. By presenting these data transfer characteristics in a nondimensional form, the results may be applied to any similar sinusoidal wave form, such as the response of a small-scale model. The number of required interpolations presented, NI , neglects the requirement of an additional interpolation point at the data read subsequent to a dump, as was discussed previously.

Table A.1
INTERPOLATION EXAMPLE

Example No.	t_p/T %	t_d/T %	NI $=t_d/t_p - 1$
1	5	30	5
2	5	55	10
3	2	20	9
4	2	42	20

As can be seen, reasonable results are obtained for the specific examples presented. However, for cases where the dump time is greater than 50% of the predominant period of the response significant errors will be produced. Also, this procedure is not capable of restoring transient signals which may have existed during the transfer interval. Care must be taken to minimize the data acquisition interruption with respect to the anticipated frequency content of an actual dynamic experiment. The signal to noise ratio should be maximized to prevent the high frequency content of the noise from adversely affecting the interpolation procedure.

The numerical calculation of integrals and derivatives is

illustrated in Figures A.8 and A.9. Both figures utilize the El Centro 1940 N-S component. In Figure A.8, the measured shake table accelerations are compared to the acceleration record obtained by differentiation of the table displacement response. The time history and relative velocity response spectrum plots illustrate that the differentiation process amplifies high-frequency noise present in the displacement record, as would be expected. However, if low-pass numerical filtering is used or if only single derivatives are required, as is often the case, accurate results are attainable.

The effectiveness of the integration process is shown in Figure A.9, where the USGS record of the El Centro acceleration history is compared to the acceleration signal calculated from the second derivative of the displacement record, which was obtained by double integration of the USGS acceleration record. Except for slight attenuation of higher frequencies, the acceleration record and the numerically derived history are essentially the same. This result indicates the complementary nature of the integration and differentiation processes, as the integration method utilizes a third-order algebraic equation and a fourth-order formulation is used for derivatives. Since, for many applications, successive differentiation and integration is required, such as for energy calculations, very accurate results are possible.

The filtering characteristics of the smoothing algorithm are illustrated in Figures A.10 and A.11. In Figure A.10, sample results obtained by smoothing of a noise signal with various coefficients are shown. The smoothing coefficient notation is $(a, b, c; n)$, where a , b and c are as defined previously and n is the number of smoothing iterations utilized.

The normalized relative velocity response spectra in Figure A.11, illustrate frequency attenuation characteristics for a wide range of

smoothing coefficients. The amplitude of the spectra were normalized by the amplitude of the unsmoothed spectrum, while frequency was also normalized so that the spectra could be applied for general use. For a specific problem with data time intervals t_p the following equation should be used to convert from the presented to the actual frequency scale,

$$f_{\text{actual}} = f_{\text{spectra}} / t_p \quad (\text{Hz})$$

where t_p is specified in milliseconds. Thus, the spectra indicate the percentage of amplitude attenuation as a function of frequency for a general problem.

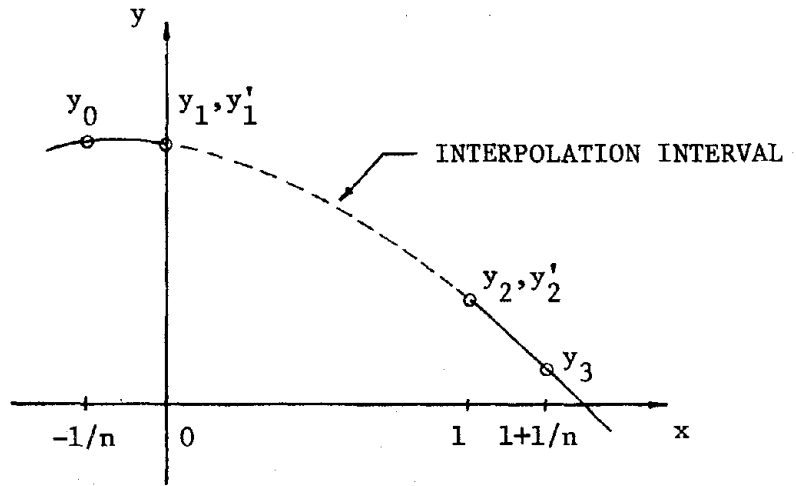


Figure A.1 Interpolation Formulation

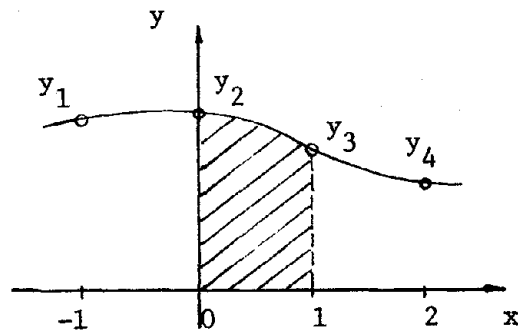


Figure A.2 Integration Formulation

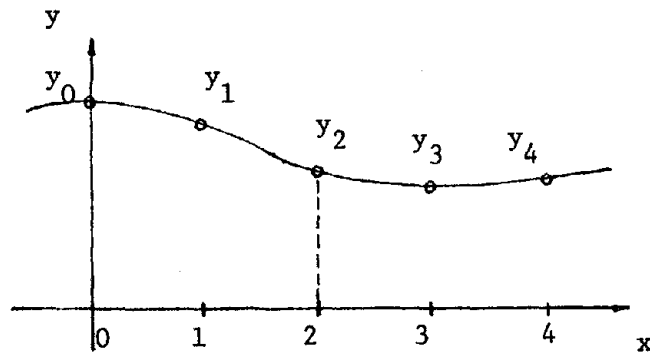


Figure A.3 Differentiation Formulation

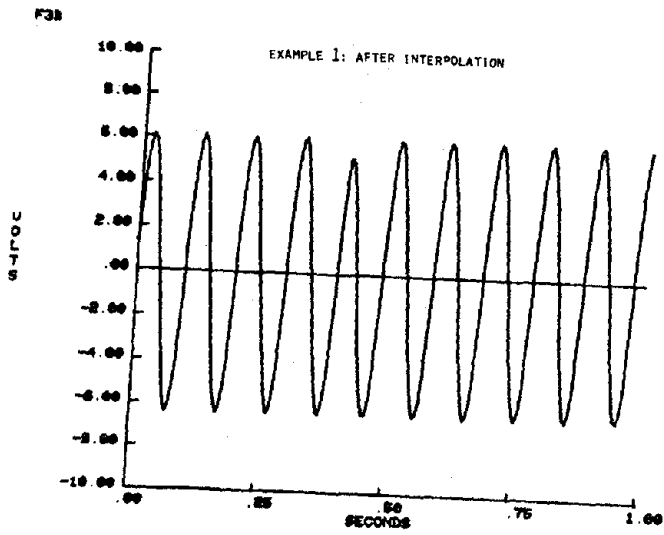
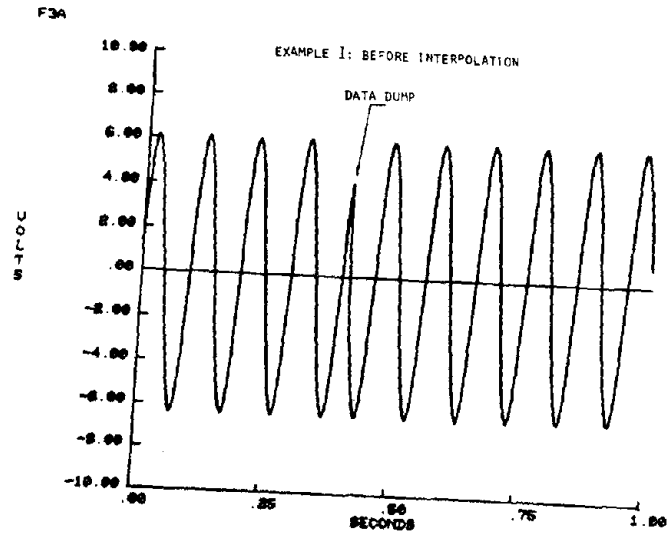


Figure A.4 Interpolation Example 1

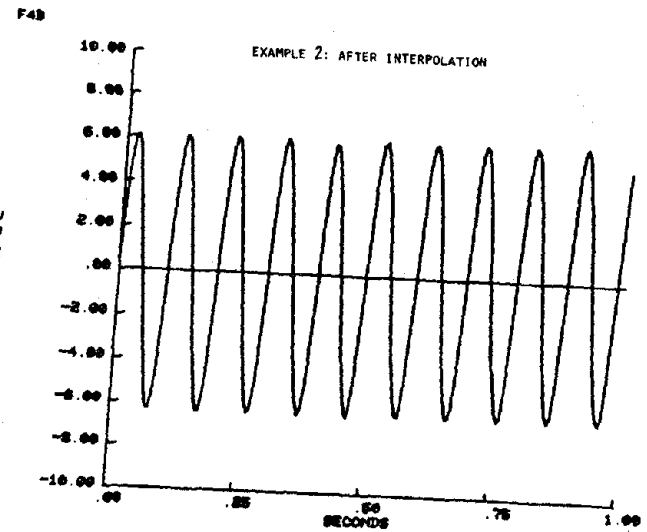
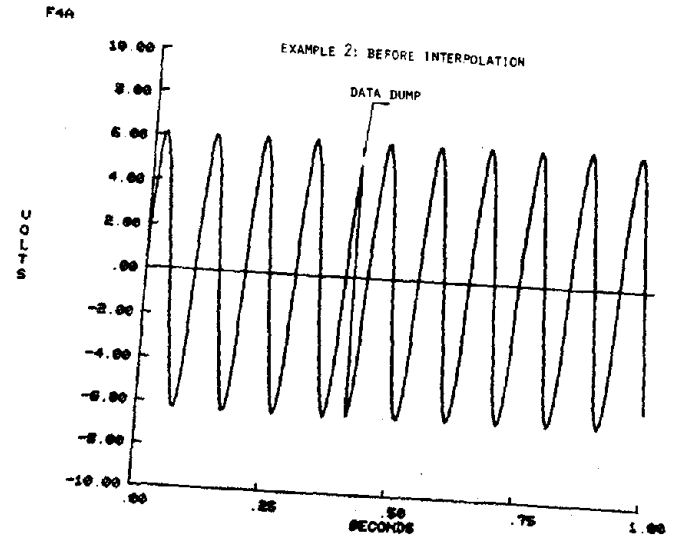


Figure A.5 Interpolation Example 2

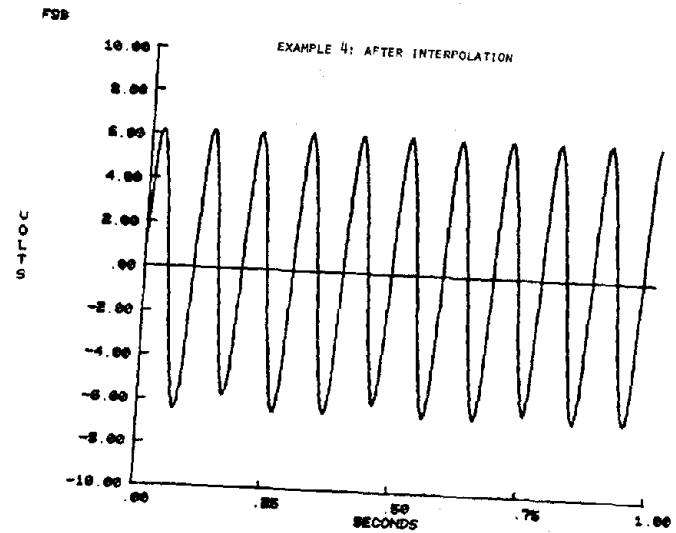
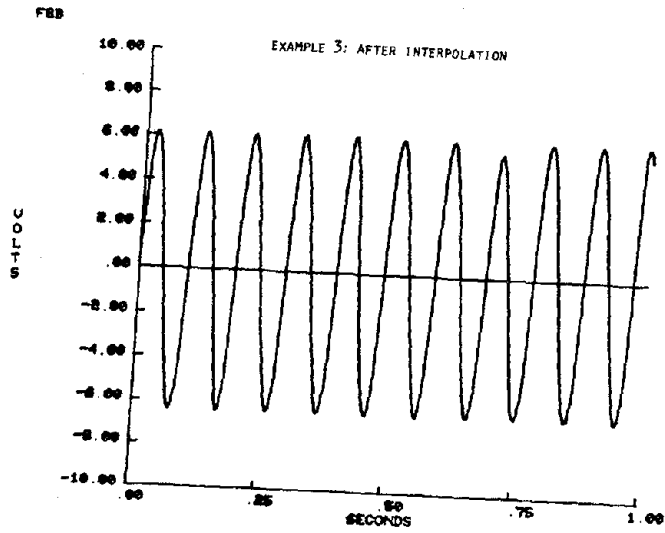
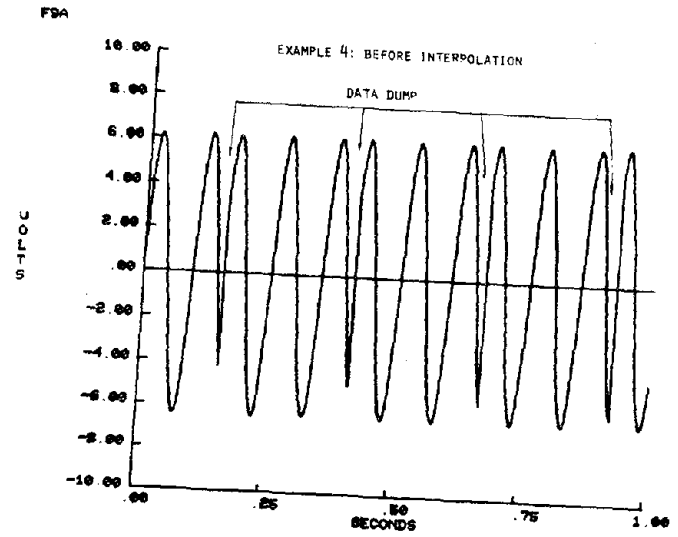
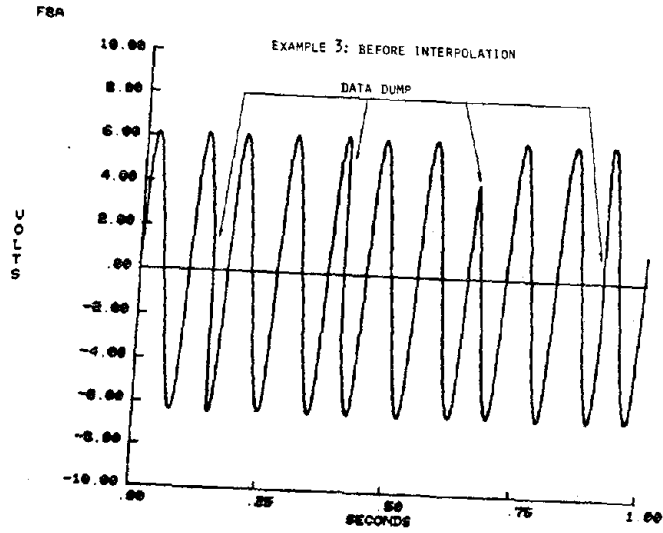
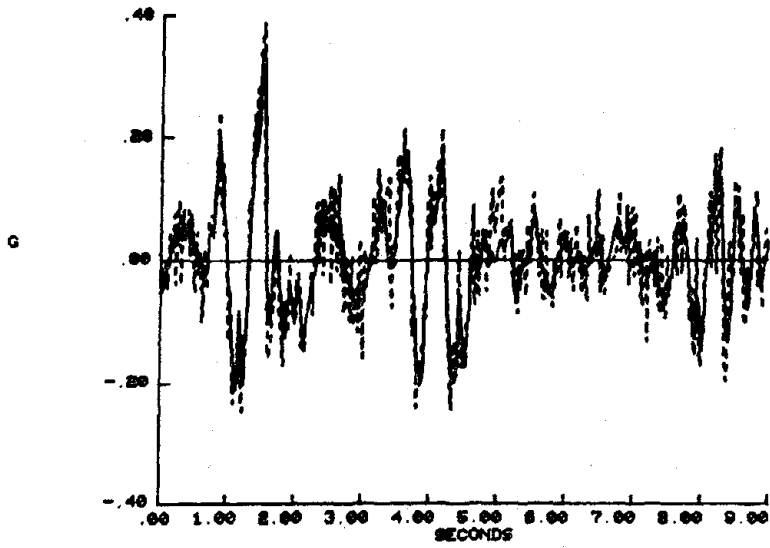


Figure A.6 Interpolation Example 3

Figure A.7 Interpolation Example 4

EC100
1.6.85

EL CENTRO 1940 N-S. MEASURED TABLE ACCEL. SOLID LINE
DBL DERIVATIVE OF DISPL. DASHED LINE



EC100

SUX OF EL CENTRO 1940. FROM TABLE ACCEL. SOLID LINE
DAMPING = 0.1 DBL DERIVATIVE OF DISPL. DASHED

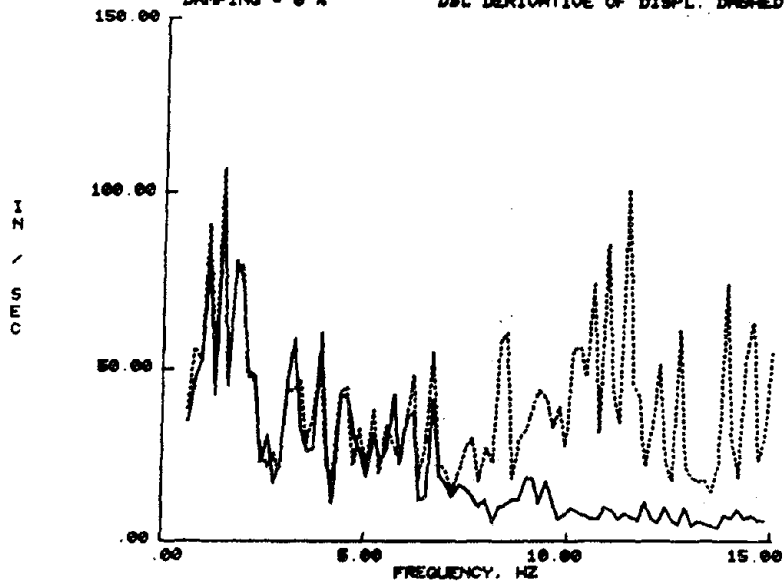


Figure A.8 Derivative Example

EL CENTRO 1940 N-S RECORD SOLID LINE
 DOUBLE DERIVATIVE OF DOUBLE INTEGRAL DASHED LINE

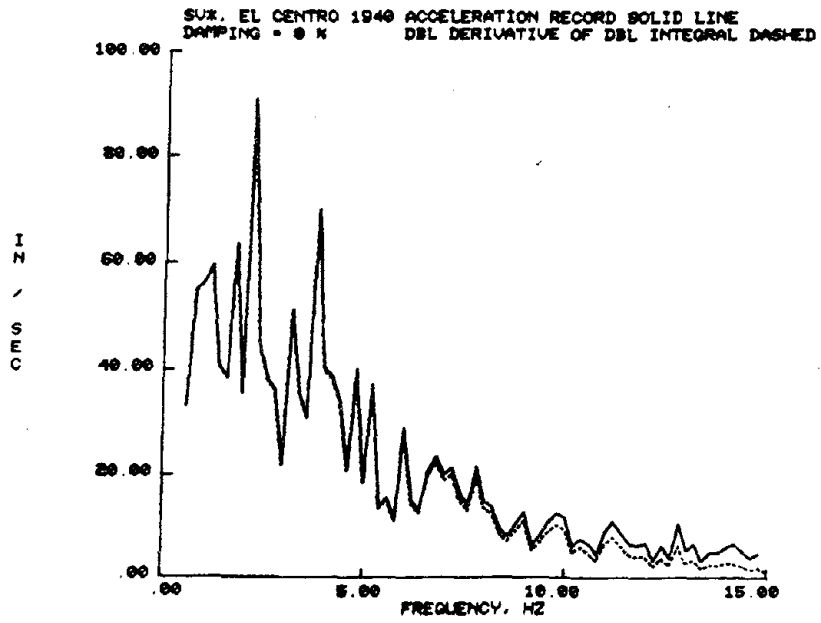
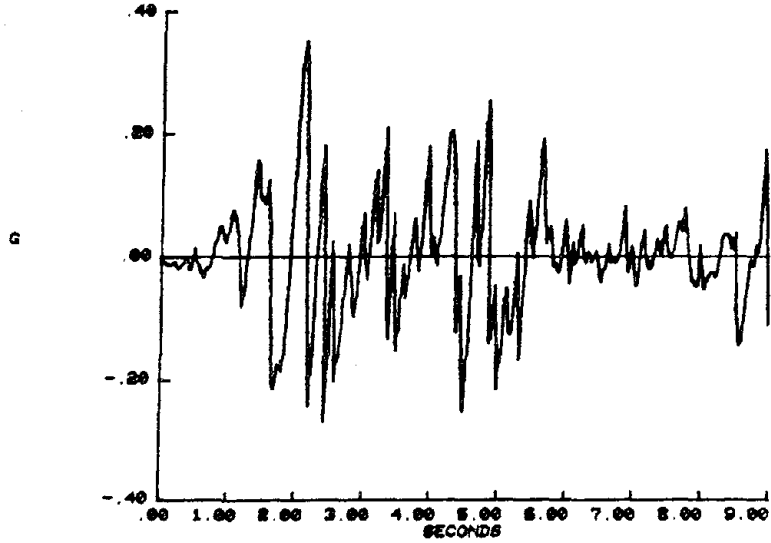


Figure A.9 Derivative and Integral Example

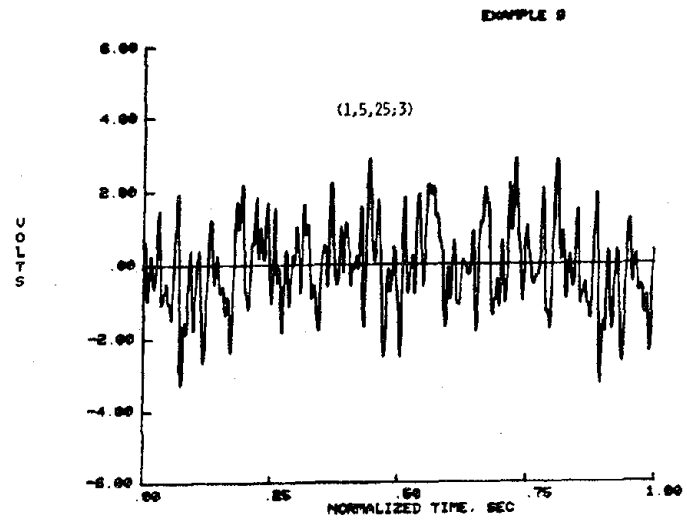
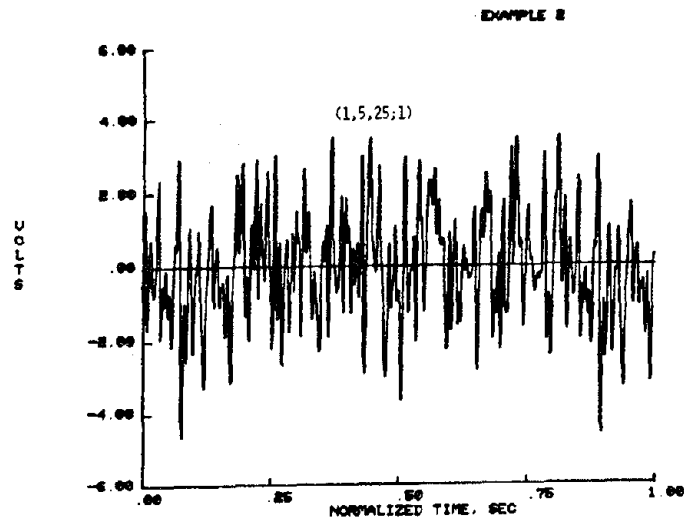
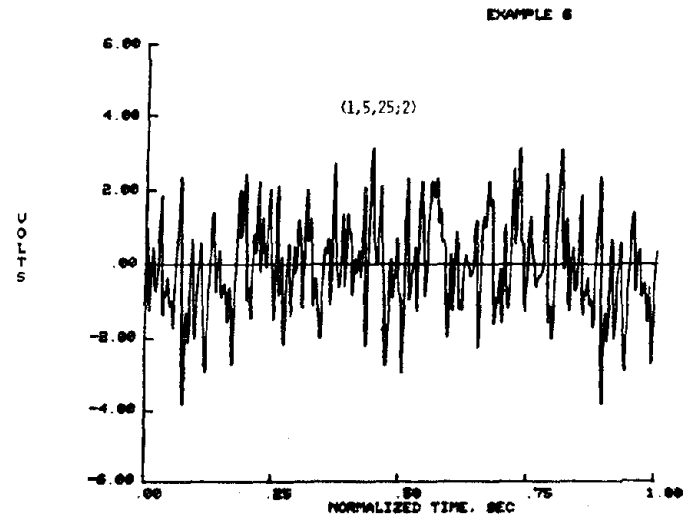
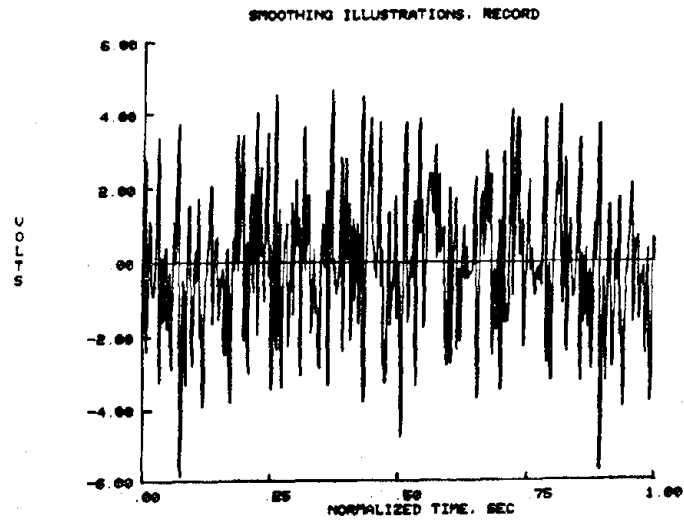


Figure A.10 Smoothing Examples -- Time Histories

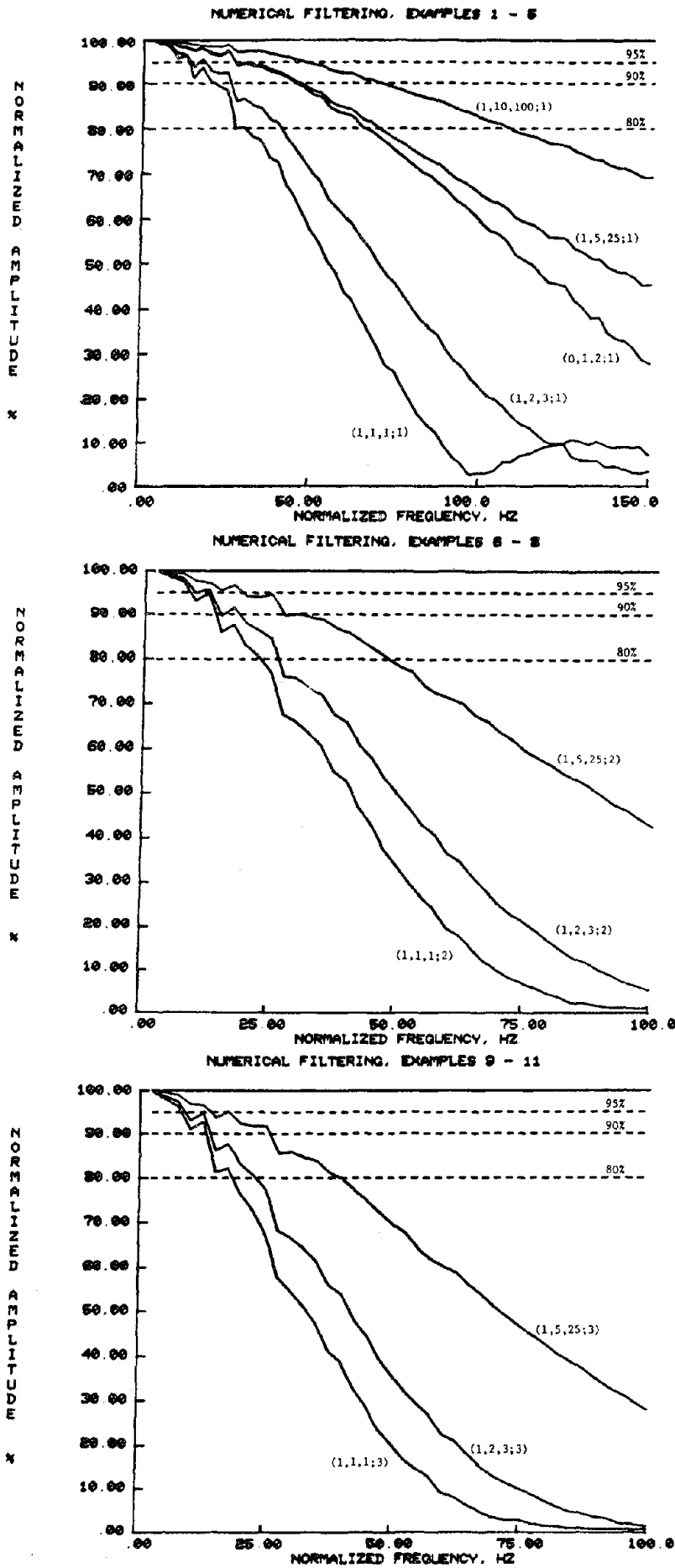


Figure A.11 Smoothing Examples -- Frequency Attenuation

Appendix B

COMPUTER PROGRAMS RELATED TO THE JABEEC TEST SYSTEM

An extensive library of computer programs applicable to dynamic tests has been developed for the laboratory minicomputer system. The programs are designed to interact with the user by prompting for user response and input commands, facilitating general use for test application. Following is an annotated listing of the library as of May, 1979. To indicate respective authors, program names are marked in the form

* by D. Fisher

** by D. Fisher and R. Mills

All programs not so marked are by R. Mills.

ADCTP, ADFST, ADCDT--data acquisition. ADCTP is the general form of the program with storage of raw data on magnetic tape as the test progresses. ADFST permits maximum sampling rates by storing a limited number of points in core, followed by a single transfer to tape subsequent to the test. ADCDT is similar to ADFST, except the results are stored on tape in reduced form.

CALC, CALCD--integration, differentiation and base-line correction of x-increment data files. CALC utilizes core storage providing maximum execution speed but with a limited number of points. CALCD uses disc storage.

DACDC--digital to analog conversion of time history files. An array read from a data disc file is converted to a voltage signal for control of excitation devices (e.g., earthquake simulator).

DATA, DATAF--data reduction. Raw data from magnetic tape are sorted by

channel and converted to the actual physical measurement. Also performs interpolation, time shifting, output of voltage ranges and creation of data disc files. Version DATAF has extended core capabilities.

DATUM--automated subtraction of EERC instrument "zero" files from test files.

DOF1, DOFPT, DOFTB--various analytical formulations for the response of a single degree of freedom system.

DUSER*--reviews current status of the magnetic disc.

EERC--transfers Berkeley EERC data from magnetic tape to Stanford disc storage. Performs conversion of NOVA computer formatted data to HP format.

ELCNTA, ELCNTD--data disc files containing the El Centro 1940 N-S acceleration record and the integrated displacement record.

ENERGY--integration of x-y paired data in the form $\int ydx$. Used for determination of dissipated energy.

EQACC--transfer of USGS earthquake acceleration records from magnetic tape to disc.

FILES*--scans and reports names and status of permanent disc files.

FFT--fast Fourier transform program. Will determine Fourier transform, inverse transform and power spectral density.

FMGFL*--constructs a listing of disc files specified by type or security code in desired format.

JOIN--combines two x-increment files into an x-y form.

LIST--lists USGS tape headings.

LISTP--lists raw or reduced data tape headings.

MATH, MATHD--multiplication, division, addition and subtraction of x-increment data files. MATHD is the disc version.

RSPA--calculation of response spectra with damping and linear or logarithmic frequency increments.

SMOTH--digital smoothing of x-increment or x-y data files.

SPCOP--spectral operations program. Performs conjugate conversion, conjugate multiplication, filtering, conversion to power, phase angle form and normalization by the surface integral of spectrum files produced by FFT and SPCTR.

SPCTR--determination of auto and cross power spectral density functions through segment averaging techniques.

TKPLT**, TKMLT**--Tektronix plot programs. TKPLT is the general form while TKMLT will automatically plot multiple x-increment data files.

TPDK--tape secondary data file storage and recall.

TPLK, TPLOK*--magnetic tape manipulation.

